JOURNAL OF THE

Electrochemical Society

ol. 113, No. 6 June 1966

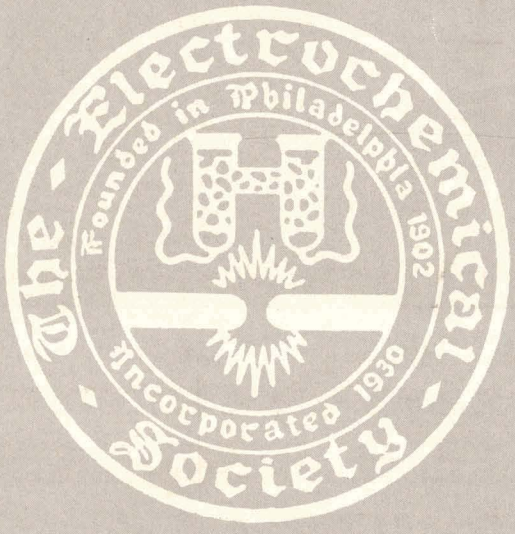

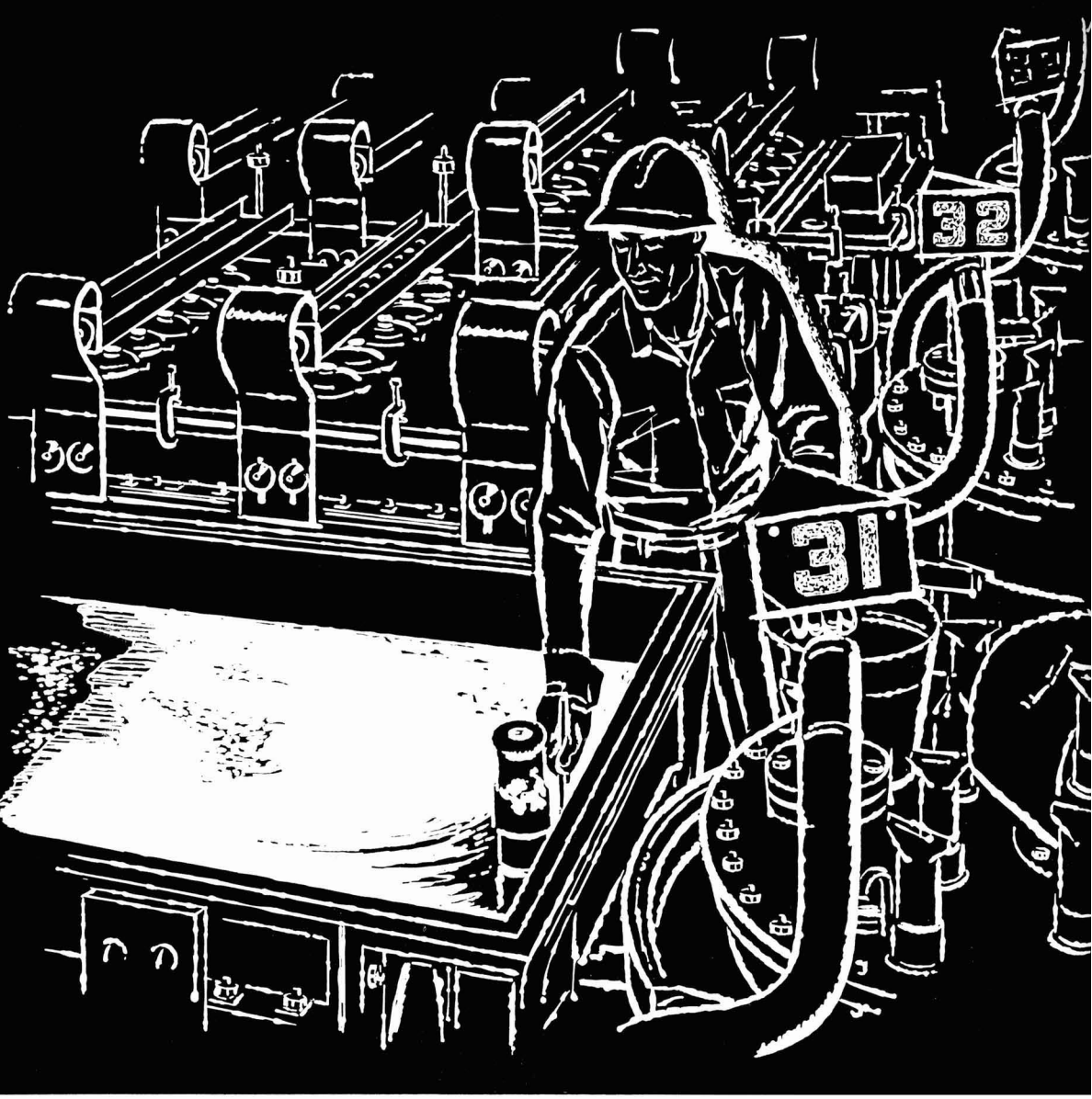

The men who know Olin Mercury Cells best best know the dependability of GLC Anodes

PRODUCTS YOU CAN TRUST
GRAPHITE PRODUCTS
GLC
DIVISION

GREAT LAKES CARBON CORPORATION
18 East 48th Street • New York, N. Y. 10017
OFFICES AND AGENTS FROM COAST-TO-COAST AND AROUND THE WORLD

Great Lakes Carbon Corporation is one of the world's largest manufacturers of graphite for electrochemical and electrothermic processes—and for aerospace, nuclear, metallurgical and other industrial uses.

These two electrometers may look alike, perform almost alike. Both measure virtually every dc parameter. But, one is battery-powered, operates 1500 volts off-ground . . . the other makes more measurements over broader ranges than any other dc instrument.

WHICH ELECTROMETER MEETS YOUR DC MEASUREMENT NEED?

The off-ground capability and 1000-hour battery life of the portable 601 and the extraordinary measuring performance of the line-operated 610B are Keithley features untouched by other electrometers. These instruments precisely measure voltage from extremely high impedance sources, current signals in the picoampere region and ultra-high levels of resistance. They even quantify coulomb charge.

Both the 601 and 610B have only 200 microvolts per hour zero drift. That's 10 times better than other tube-type electrometers. Big, easily read mirror-backed meters feature 1% accuracy. A 0.005% unity-gain output provides impedance matching. And for driving recorders, there's a 1 ma variable-gain output.

For more details or an in-plant demonstration, there's your man from Keithley. Give him a call — or contact us direct.

MODEL 601	MODEL 610B
1 mv f.s. to 10v (10^{14} ohms input resistance)	1 mv f.s. to 100v (10^{14} ohms input resistance)
10^{-14} amp. f.s. to 0.3 amp.	10^{-14} amp. f.s. to 0.3 amp.
100 ohms f.s. to 10^{13} ohms	100 ohms f.s. to 10^{14} ohms
10^{-12} coul. f.s. to 10^{-6} coul.	10^{-12} coul. f.s. to 10^{-5} coul.
only $595	only $565

Write for technical literature on these and other products

KEITHLEY INSTRUMENTS

12415 Euclid Ave. • Cleveland, Ohio 44106 / EUROPE: 14 Ave. Villardin, 1009 Pully, Suisse

June 1966

EDITORIAL

TECHNICAL PAPERS

ELECTROCHEMICAL SOCIETY

VOL. 113 • NO. 6

Manuscripts submitted to the Journal should be sent, in triplicate, to the Editorial Office at 30 East 42 St., New York, N. Y., 10017. They should conform to the revised Instructions to Authors published on pp. 143C-144C of this issue. Manuscripts so submitted become the property of The Electrochemical Society and may not be published elsewhere, in whole or in part, unless permission is requested of and granted by the Editor.

The Electrochemical Society does not maintain a supply of reprints of papers appearing in its Journal. A photoprint copy of any particular paper, however, may be obtained by corresponding direct with the Engineering Societies Library, 345 E. 47 St., New York, N. Y., 10017.

Inquiries re positive microfilm copies of volumes should be addressed to University Microfilms, Inc., 313 N. First St., Ann Arbor, Mich.

Walter J. Johnson, Inc., 111 Fifth Ave., New York, N. Y., 10003, have reprint rights to out-of-print volumes of the Journal, and also have available for sale back volumes and single issues, with the exception of the current calendar year. Anyone interested in securing back copies should correspond direct with them.

Published monthly by The Electrochemical Society, Inc., at 215 Canal St., Manchester, N. H.; **Executive Offices, Editorial Office and Circulation Dept.**, and **Advertising Office** at 30 East 42 St., New York, N. Y., 10017, combining the JOURNAL and TRANSACTIONS OF THE ELECTROCHEMICAL SOCIETY. Statements and opinions given in articles and papers in the JOURNAL OF THE ELECTROCHEMICAL SOCIETY are those of the contributors, and The Electrochemical Society assumes no responsibility for them.

Claims for missing numbers will not be allowed if received more than 60 days from date of mailing plus time normally required for postal delivery of JOURNAL and claim. No claims allowed because of failure to notify the Circulation Dept., The Electrochemical Society, 30 East 42 St., New York, N. Y., 10017, of a change of address, or because copy is "missing from files." Subscription to members as part of membership service; subscription to nonmembers $24.00 plus $1.50 for postage outside U.S. and Canada. Single copies $1.70 to members, $2.25 to nonmembers.

Entered as second-class matter at the Post Office at Manchester N. H., under the act of August 24, 1912. Postage paid at Manchester, N. H.

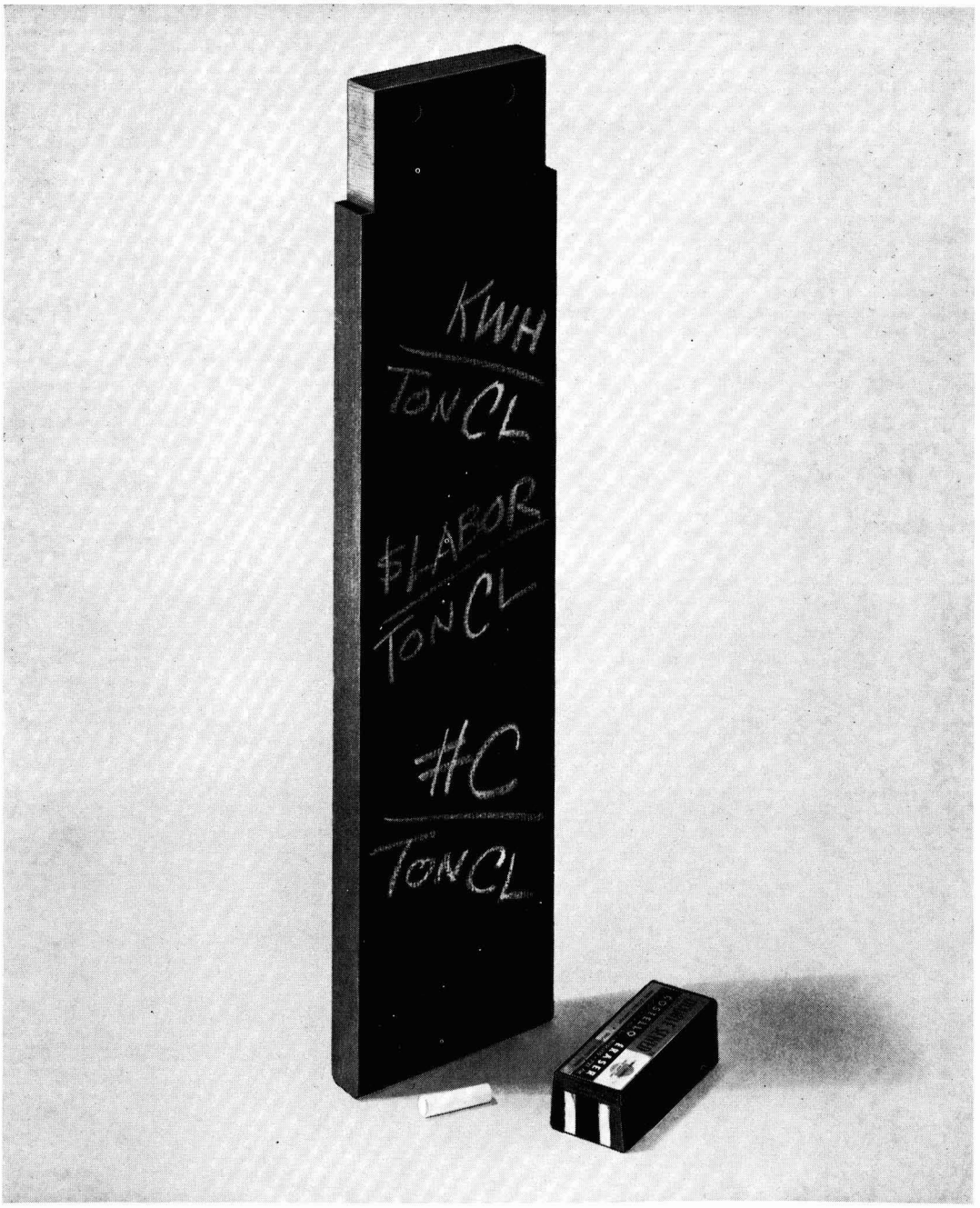

Any way you figure it...

Stackpole GraphAnodes® save you money. That's the way they are made.

When you place your next order for anodes, investigate the savings you could be getting from Stackpole GraphAnodes.® Why not write for the full story today: Stackpole Carbon Company, Carbon Division, St. Marys, Pennsylvania. Phone: 814-781-8463; TWX: 510-693-4511.

STACKPOLE
CARBON DIVISION

EDITORIAL

Journal Page Charge Increase

SOME time ago it was found necessary to institute a page charge in the JOURNAL OF THE ELECTROCHEMICAL SOCIETY. In the time between then and now, costs of publication continue to rise—not only for our JOURNAL but for others in our field. All of us have found it necessary to find additional funds to take care of these rising costs. They can come from membership dues, subscriptions, or page charges. Your Board of Directors, on the advice of the appropriate standing committees, has determined that an increase of $5.00 per page in our charges will provide funds needed now. Other societies have come to similar conclusions regarding the mode of financing increasing costs, although the amounts vary from one organization to another. Even with our increase, our page charges are still quite modest compared with other journals in allied fields. Our experience so far in the acceptance of page charges by authors has been extraordinarily good, in excess of 95%, and it should always be remembered that a paper is accepted for publication *before* the author is asked to accept the page charge.

When the page charge was instituted for the JOURNAL, no similar action was taken for the then very new ELECTROCHEMICAL TECHNOLOGY. It was felt that this journal needed to establish itself before it could assume the load of a page charge. There is no doubt now that ELECTROCHEMICAL TECHNOLOGY can stand on its own feet with regard to the flow of papers of high caliber. If proof is needed, the growing subscription list and the acceptance of the publication as a medium of communication by highly qualified authors will provide it. Your Board of Directors, on the advice of the Publication Committee and with the endorsement of the Finance Committee, has decided to institute a page charge for ELECTROCHEMICAL TECHNOLOGY. Because publication costs are substantially the same as for the JOURNAL, we have determined that the charge should be the same, that is $40.00 per page with 10% discount to members and to employees of sustaining member companies.

A constant problem in scientific and technical communication is the time that elapses between submission of a paper and its appearance in print. Some of the interval cannot be avoided, for proper review and editing takes time. The funds anticipated from the new page charges will provide a basis for minimizing delays in publishing.

Both of these actions become effective October 1, 1966, but papers submitted prior to that date will not be affected by these actions no matter what the date of their final acceptance. Let us emphasize again that acceptance of the page charge is entirely voluntary and is not a factor in the acceptance of any paper for publication. All reviewing and type setting are carried out before an authorization for the page charge is submitted to the author for acceptance.

HAROLD J. READ, President
The Electrochemical Society

CHARLES L. FAUST, Chairman
Publication Committee

Monographs of The Electrochemical Society

ECS Series

The following are books developed and sponsored by The Electrochemical Society and published by John Wiley & Sons, Inc., 605 Third Ave., New York, N. Y. 10016. Members of The Electrochemical Society can receive a 33 1/3% discount by ordering volumes from Society Headquarters, 30 East 42 St., New York, N. Y. 10017. Book and invoice will be mailed by John Wiley & Sons. Nonmembers (including subscribers) should order direct from Wiley.

Corrosion Handbook. Edited by Herbert H. Uhlig. Published 1948, 1188 pages, **$16.00.**

Modern Electroplating, Second Edition. Edited by Frederick A. Lowenheim. Published 1963, 769 pages, **$16.00.**

Abstracts of the Literature on Semiconducting and Luminescent Materials and Their Applications. Compiled by Battelle Memorial Institute. **Vol. I, 1953 Issue**—published 1955, 169 pages, **$5.00** (soft cover); **Vol. II, 1954 Issue**—published 1955, 200 pages, **$5.00** (soft cover); **Vol. III, 1955 Issue**—Edited by E. Paskell, published 1957, 322 pages, **$10.00** (hard cover); **Vol. IV, 1956 Issue**—Edited by E. Paskell, published 1959, 456 pages, **$12.00** (hard cover); **Vol. V, 1957 Issue**—Edited by C. S. Peet, published 1960, 499 pages, **$12.00** (hard cover); **Vol. VI, 1958 Issue**—Edited by J. J. Bulloff and C. S. Peet, published 1961, 528 pages, **$14.00** (hard cover); **Vol. VII, 1959 Issue**—Edited by J. J. Bulloff and C. S. Peet, published 1962 728 pages, **$20.00** (hard cover).

Electrochemistry in Biology and Medicine. Edited by Theodore Shedlovsky. Published 1955, 369 pages, **$11.50.**

Vapor Plating (The Formation of Metallic and Refractory Coating by Vapor Deposition), by C. F. Powell, I. E. Campbell, and B. W. Gonser. Published 1955, 158 pages, **$6.00.**

High-Temperature Technology (Materials, Methods, and Measurements). Edited by I. E. Campbell. Published 1956, 526 pages, **$15.00.** (Out of print; new edition in course of preparation.)

Stress Corrosion Cracking and Embrittlement. Edited by W. D. Robertson. Published 1956, 202 pages, **$7.50.**

Arcs in Inert Atmospheres and Vacuum. Edited by W. E. Kuhn. Published 1956, 188 pages, **$7.50.** (Papers Presented at the Symposium on Arcs in Inert Atmospheres and Vacuum of the Electrothermics and Metallurgy Division of The Electrochemical Society, April 30 and May 1, 1956, San Francisco, Calif.)

The Structure of Electrolytic Solutions. Edited by Walter J. Hamer. Published 1959, 441 pages, **$18.50.** (Based on a Symposium held in Washington, D. C., in May 1957, Sponsored by The Electrochemical Society, New York, and The National Science Foundation, Washington, D. C.)

Mechanical Properties of Intermetallic Compounds. Edited by J. H. Westbrook. Published 1959, 435 pages, **$9.50.** (A Symposium, Sponsored by the Electrothermics and Metallurgy Division of The Electrochemical Society, May 4, 5, and 6, 1959, Philadelphia, Pa.)

The Surface Chemistry of Metals and Semiconductors. Edited by Harry C. Gatos, with the assistance of J. W. Faust, Jr., and W. J. La Fleur. Published 1960, 526 pages, **$12.50.** [Proceedings of an International Symposium Sponsored Jointly by the Office of Naval Research and The Electrochemical Society, Inc. (Corrosion and Electronics Divisions), October 19, 20, and 21, 1959, Columbus, Ohio.]

Transactions of the Symposium on Electrode Processes. Edited by Ernest Yeager. Published 1961, 374 pages, **$20.00.** (The papers and discussions of the Symposium on Electrode Processes, Sponsored jointly by the U. S. Air Force, Office of Scientific Research, and The Electrochemical Society, Inc., Philadelphia, Pa., May 1959.)

Iodide Metals and Metal Iodides, by Robert F. Rolsten. Published 1961, 441 pages, **$17.50.**

Ultrafine Particles, Editor-in-Chief—William E. Kuhn. Published 1963, 561 pages, **$15.00.**

First International Conference on Electron and Ion Beam Science and Technology. Edited by R. Bakish. Published 1965, 945 pages, **$24.50.** (Sponsored by the Electrothermics and Metallurgy Division of The Electrochemical Society and the Metallurgy Society of AIME.)

The Electron Microprobe. Edited by T. D. McKinley, K. F. J. Heinrich, and D. B. Wittry. Published 1966, 1035 pages, **$27.50.** (Proceedings of the Symposium sponsored by the Electrothermics and Metallurgy Division of The Electrochemical Society, October 1964, Washington, D. C.)

Chemical Physics of Ionic Solutions. Edited by B. E. Conway and R. G. Barradas. Published 1966, 622 pages. **$25.00** (Papers Presented at the International Symposium of The Electrochemical Society, May 4-6, 1964, Toronto, Canada.)

Other ECS Publications

Vacuum Metallurgy, third printing, 1958, Edited by J. M. Blocher, Jr.; 216 pages; **$5.00,** less a 20% discount to ECS members only. Available from Electrochemical Society Headquarters, 30 East 42 St., New York, N. Y. 10017. (Papers Presented at the Vacuum Metallurgy Symposium of the Electrothermics and Metallurgy Division of The Electrochemical Society held in Boston, Mass., October 6 and 7, 1954.)

Rhenium. Edited by B. W. Gonser. Published by Elsevier Publishng Co., 1962; 225 pages; **$11.00** (Papers Presented at the Symposium on Rhenium of the Electrothermics and Metallurgy Division of The Electrochemical Society, May 3 and 4, 1960, Chicago, Ill.) ECS Members can obtain a 30% discount by sending their orders directly to Society Headquarters, 30 East 42 St., New York, N. Y. 10017. Remittance, made payable to American Elsevier Publishing Co., 52 Vanderbilt Ave., New York, N. Y. 10017 should accompany the order. Nonmembers must order direct from the publisher.

Iron Ore Reduction. Edited by R. R. Rogers. Published by Pergamon Press Ltd., New York and London, 1962; 359 pages; **$12.50.** (Proceedings of a Symposium on the Electrothermics and Metallurgy Division of The Electrochemical Society, held in Chicago, Ill., May 3-5, 1960.) Send all orders to The Macmillan Co., 60 Fifth Ave., New York, N. Y.

A Stable High-Valency Nickel Oxide

P. Bro and D. Cogley

Laboratory for Physical Science, P. R. Mallory & Co., Inc., Burlington, Massachusetts

ABSTRACT

A high-valency amorphous nickel oxide prepared by the hypochlorite oxidation of nickel nitrate exhibited a mixture of oxidation states characterized by a mean nickel valency of approximately 3.5. The high-valency amorphous oxide was stable in strongly alkaline solutions, but it decomposed rapidly below pH 9. The oxide discharged efficiently when used as a cathode in an alkaline primary cell.

The existence of high-valency amorphous nickel oxides is well established (1), but there has been some discussion regarding the nature of the excess nickel valency in such oxides. The high valency has been attributed to the presence of a tetravalent nickel ion (2) and to superficial oxygen (3). The recent magnetic studies of Labat (4) provide convincing evidence for the existence of a tetravalent nickel.

Data in the literature (5, 6) indicate that high-valency nickel oxides decompose readily, but recent work of Tuomi (7) shows that it is not necessarily so. The data given by Tuomi imply a reasonable stability of tetravalent nickel prepared electrochemically under suitable conditions.

We were interested in exploring the use of a high-valency amorphous nickel oxide as a cathode material for primary cells, but before such use could be considered, it would be necessary to establish whether the high valence state could be stabilized and whether it could be exploited faradaically. Both of these questions can be answered affirmatively, and we report here the work which led to these conclusions.

Experimental Techniques

A laboratory evaluation was conducted of the various methods for preparing high-valency nickel oxide. First among them was the anodic oxidation of mixtures of divalent nickel hydroxide and carbon with a CMC binder in concentrated base at room temperature on a nickel screen. The electrochemical method was unsatisfactory because of the poor adhesion of the oxide to the conductor and because of analytical complications due to the oxides of carbon and the presence of nickel. These considerations notwithstanding, Tuomi (7) obtained satisfactory results with the electrochemical method. Among the chemical methods, the hypochlorite oxidation was found to be most convenient and we used it. It is interesting to note that, although this method has been known for many years (8), it apparently was not recognized that it could yield a stable high-valency oxide.

Preparative procedures.—All the reagents, except the technical grade hypochlorite, were analytical grade chemicals, and the specific preparative conditions were varied as shown in Table I. The sequence of the operations was the same in all cases. The solution of nickel nitrate was added dropwise to the solution of the alkaline hypochlorite during approximately ½ hr. When the nickel oxide precipitate had settled the supernatant liquid was removed by siphoning, and the precipitate was washed twice with fresh base. The oxide was stored under base in a polyethylene container at 25.0°C.

No interferences would be expected by the nitrate shuttle discussed by Casey *et al.* (9), since no reducing agents were present. The anion effects would have to be considered in assembled cells.

The possibility was considered that the oxidative capacity of the nickel oxide might be caused, at least in part, by hypochlorite inclusions in the precipitate. Analyses of the dissolved precipitate for chloride ions showed any such inclusions to be negligible.

In order to evaluate the variability of the entire sequence of the preparative operations and the analyses, a set of three oxides were prepared separately under identical conditions similar to those used in run 4 with the results shown below:

Preparation	Oxidation state
a	3.49
b	3.50
c	3.48

It may be seen that the oxides could be prepared reproducibly with a variability of ±0.01 in the average nickel valency.

The results shown in Table I indicated that the oxidation state of the nickel did not change markedly with the preparative conditions. The values were all within the range of 3.33-3.61. Attempts to prepare higher valency oxides with an oxidation state approaching four were successful in a restricted sense. In the presence of an excess oxidant, under conditions similar to those of run 4, oxidation states between 3.95 and 4.00 were obtained. However, these high valency oxides decomposed rapidly to the lower valency compounds (*ca.* 3.5 oxidation state) as the hypochlorite concentration decreased. The hypochlorite concentration decreased due to the decomposition of hypochlorite in the presence of high-valency nickel oxide. The decomposition of the oxide and the hypo-

Table I. Preparative conditions

Run	Temperature, °C	Oxidant	$Ni(NO_3)_2$ solution	Valency
1	−5	800 ml 0.67M NaOCl 1.0M KOH	200 ml 0.67M	3.54
2	−5	600 ml 0.40M NaOCl 10M KOH	200 ml 0.52M	3.5
3	0	800 ml 0.34M NaOCl 6.45M KOH	200 ml 0.17M	3.52
4	25	800 ml 0.34M NaOCl 6.45M KOH	200 ml 0.17M	3.49
5	40	800 ml 0.34M NaOCl 6.45M KOH	200 ml 0.17M	3.45
6	25	800 ml 0.34M NaOCl 6.45M KOH	200 ml 0.17M	3.46
7	25	800 ml 0.25M NaOCl 4.0M LiOH	200 ml 0.17M	3.60
8*	40	800 ml 0.34M NaOCl sat'd KOH	200 ml 0.17M	3.61
10**	25	200 ml 2.2M Br_2 6.45M KOH	15 ml 2.26M	3.33
11	25	200 ml 6M KOCl sat'd KOH	15 ml 2.26M	3.43
12	25	10400 ml 0.34M NaOCl 6M KOH 6.5M KOH 1M KCl	2600 ml 0.17M	3.46

* Product reoxidized repeatedly with 1M $K_2S_2O_8$ at 25°C.
** Product reoxidized with 0.9M Br_2 in 500 ml 5M KOH at 25°C.

chlorite was accompanied by a noticeable gas evolution. The decomposition reaction between the valence states of approximately 4.0 and 3.5 was not investigated beyond these summary observations.

Chemical analyses.—The oxidation state of the nickel was obtained by iodometric titrations and concurrent polarographic analyses for nickel (Metrohm, Polarecord Model E261). Since the procedures deviated from conventional practice, they will be given in some detail. Two to ten milliliters of slurried nickel oxide in base were added to 35 ml 20% KI with stirring. The *p*H of the solution was adjusted by the slow addition of 2M H_2SO_4 to bring the solution to *p*H 3 and to hold it there for *ca.* 3 min. Then, more H_2SO_4 was added to give a solution of *p*H 1.5, and within 1 min 25 or 50 ml of the solution was transferred to a beaker containing 15 ml H_2O, 5 ml 2M H_2SO_4, and thyodene indicator. The free iodine was titrated with 0.1*N* $Na_2S_2O_3$ to a colorless end point.

The preceding steps were selected from several alternate schemes which were evaluated. The nickel oxide had to be added to an alkaline KI solution, contrary to standard iodometric practice, to avoid losses due to the escape of oxygen which occurs in acid solutions. Calibration tests showed that the results were unaffected by the initial alkalinity provided the titrations were conducted in acid solutions under conditions which prevented air oxidation of iodide. At *p*H values above 2, the nickel oxide was incompletely reduced, and at *p*H values less than 1, air oxidation became noticeable. Therefore, the titrations were done at *p*H 1.5. The iodometric calibration runs agreed with one another within 0.3%.

The nickel content of the oxide was determined by analyzing 1-5 ml of the *p*H 1.5 solution polarographically in 20 ml 1M NH_4Cl, 1M NH_4OH at 40°C. A 0.008% solution of CMC was found to be a satisfactory suppressor. The use of the elevated temperature was dictated by the suppressor requirements. The polarographic method was calibrated against a standard nickel solution prepared from the pure metal, and the calibration runs were reproducible within 0.5%. All of the analytical results reported in this paper represent average values obtained from four determinations for each set of conditions, except for the values given in Fig. 1 where single determinations were made.

Stability of the Oxide

The preparative work had established that a high-valency nickel oxide could be prepared reproducibly. Accordingly, a series of experiments was initiated to investigate the relative stability of the oxide under various conditions.

Sample No. 1, Table I, which had been prepared and stored at —5°C in 1M KOH was analyzed periodically. No change was observed in the oxidation state of the nickel; it remained at a value of 3.54 during the period of observation, 105 days. Thus, the high-valency oxide was stable at —5°C in 1M KOH. Sample No. 7, prepared at 25°C, showed no decomposition during the two days it was examined at 25°C, and sample No. 8, prepared at 40°C, showed no decomposition during the three days it was tested at 40°C. These and similar tests on the other specimens indicated that the high-valency oxides were stable at room temperature in 1M or more concentrated, strong base.

A large batch of high valency oxide, run 12, Table I, was prepared to provide a single source of specimens for a study of the effect of solution *p*H on the stability of the oxide. The oxide was prepared at 25°C and stored at the same temperature under 10^{-3}M KOH. Small portions of nickel oxide suspensions were introduced with stirring into large volumes of buffers with *p*H values down to *p*H 6.0 at 25°C, and samples were withdrawn after a period of three days for analyses. Results are shown in Fig. 1. It may be seen that the oxide had decomposed appreciably in the solutions with a *p*H less than *p*H 9 and that it was relatively stable in the high *p*H solutions. Some decomposition had occurred in the high *p*H solutions, since the nickel valency had decreased from 3.46 for the freshly prepared oxide to a value of 3.34 for the three day old sample in dilute base.

Decomposition of the Oxide

The existence of a *p*H range in which the high-valency oxide decomposed at an appreciable rate allowed measurements to be made of the influence of temperature and *p*H on the rate of the decomposition reaction. The rate measurements were made, using the procedures already described, and the time intervals between the *p*H adjustment of the suspensions and the addition of the suspensions to the iodide solutions were taken to be the reaction intervals. The nickel oxide suspensions were taken from the same master batch to insure an identical starting material for comparison purposes.

The decomposition rates of the high-valency oxide in a *p*H 6.0, 2M phosphate buffer are shown in Fig. 2 for three different temperatures between —1° and 55°C. The results are again expressed in terms of the mean oxidation state of the nickel. It may be seen that the decomposition curves exhibited an induction period at —1° and 15°C, but not at 55°C. Furthermore, the reaction rates increased markedly with the temperature.

The influence of the *p*H of the solutions on the rate of the decomposition reaction was investigated at 25°C in MacIlvaine buffers between *p*H 4.0 and *p*H 6.0. Results are shown in Fig. 3. The rate of the reaction increased markedly as the acidity of the solutions increased, and the reactions proceeded practically to the divalent nickel state. The *p*H effect was studied on a fresh batch of high-valency oxide, and the data indicated that the fresh oxide was more reactive than the aged oxide. In the *p*H 6 phosphate

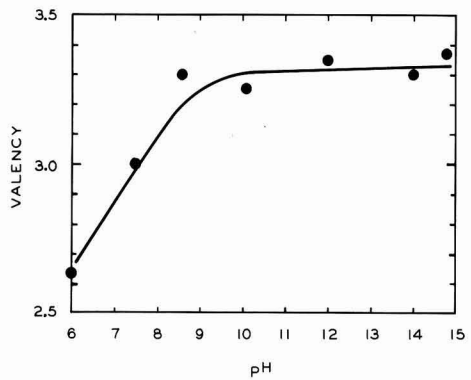

Fig. 1. The *p*H effect on the stability of high-valency nickel oxide

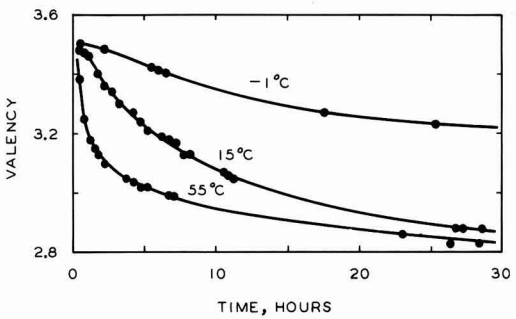

Fig. 2 Decomposition rate of nickel oxide at *p*H 6.0 in a 2M phosphate buffer, aged oxide.

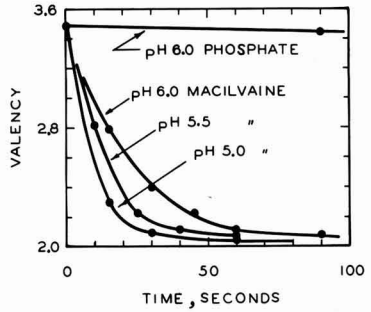

Fig. 3. Influence of pH and buffer type on the decomposition rate of nickel oxide, fresh oxide.

buffer, the valency of the fresh oxide changed by 0.78 units at 25°C during the first 3.9 hr of reaction time, whereas the valency of the aged oxide changed by only 0.53 units at 55°C during the same period, the higher temperature of the latter notwithstanding. A comparison of the *p*H 6 phosphate and *p*H 6 MacIlvaine data in Fig. 3 shows the decomposition reaction to be much faster in the MacIlvaine buffer, which indicates a specific buffer effect.

Cathodic Utilization of the Oxide

Some of the electrochemical characteristics of the high-valency oxide were evaluated by discharging the oxide in conventional primary cell configurations *vs.* zinc anodes in 40% KOH containing 6% ZnO. The desiccated oxide was blended with 5 w/o graphite and pressed into circular pellets approximately 0.25 cm thick with a diameter of 1.3 cm under a pressure of 30,000 psi. The discharge curve of such a cell is shown in Fig. 4. It had an open-circuit voltage of 1.75v, and it exhibited a fairly flat discharge curve. The cell voltage remained at an average value of 1.5v for drain rates in the range of 5-7 ma/cm^2. Polarization characteristics of the cell are shown in Fig. 5 for various discharge levels. It polarized severely at deep discharge levels for current densities in excess of 10 ma/cm^2. However, the cell was not optimized to give a good discharge behavior.

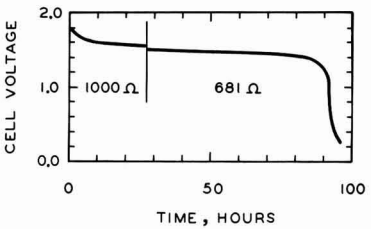

Fig. 4. Discharge curve of high-valency nickel oxide/zinc cell, two load conditions.

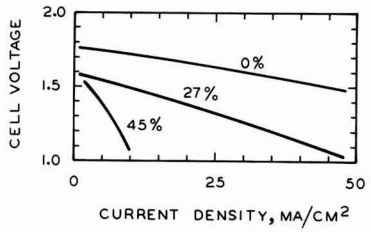

Fig. 5. Polarization characteristics of the cell at various depths of discharge.

An analysis of the discharged cathode showed that the nickel had been reduced to an oxidation state of 2.41. The failure of the cathode to discharge to a valence state of 2.0 may be attributed to an excessive polarization under the conditions of the experiment. The charge withdrawn from the cell was equivalent to a valence change of 0.91, which corresponded to an initial oxidation state of 3.32. The nickel in the wet starting material had a valency of 3.49, but experiments had shown that drying of the high-valency oxide tended to decrease its oxidation state. The dried, charged cathodes had not been analyzed.

Discussion of the Results

The high-valency nickel oxide has been described in terms of the mean oxidation state of the nickel. In an attempt to define the chemical species more precisely, we examined the x-ray diffraction patterns of the oxides in various valence states between 2.2 and 3.5 (Norelco X-Ray Diffraction Unit). In no case did we observe any lines except those due to the cellophane tape used to mount the sample, which prevented a comparison on a structural basis of our material with that of other investigators. Electron microscopic observations (Hitachi HU-11) of the oxide after it had been washed in water and ethanol failed to disclose any discrete crystals at a magnification of 30,000X. The alcohol rinse was used to prevent the introduction of any water into the electron microscope, and it was accompanied by the decomposition of the oxide to the divalent state. Distinct electron diffraction patterns were obtained of the decomposed oxide, which showed it to be a crystalline material. There is a possibility that the material may be composed of very thin crystalline flakes, less than 30Å thick and as large as 1000Å in diameter, which would be transparent to the electron beam except when viewed on edge. It would appear, therefore, that no definitive statements can be made on the basis of our data regarding the exact chemical nature and physical structure of the reaction products resulting from either the oxidation or the reduction reactions.

The highest mean oxidation state obtained in reproducible experiments was 3.6 (except as noted below), and there is a question whether or not this state represented an equilibrium composition of the oxide. It is conceivable that the solid phase contained tri- and tetravalent nickel in equilibrium proportions. However, large surface area states do not normally represent equilibrium states. They may be expected to undergo morphological changes to reduce their surface free energy. Thus, we are led to consider the oxidation product as a metastable entity, and there are no apparent reasons why a mean nickel valency of 3.6 should represent the highest attainable oxidation state for the oxide. We did obtain specimens with mean oxidation states between 3.95 and 4.00, but they could not be maintained in these high valence states unless an excess of the oxidant was present. There are reasons for believing, therefore, that higher valency oxides may be synthesized and stabilized.

No stable tri- or tetravalent nickel ions have been reported in aqueous media; the only stable aqueous nickel ion being divalent (10). It would seem, therefore, that the oxidation reaction must be a heterogeneous reaction, and two requirements must be met for the successful synthesis of very high-valency oxides: (*i*) an adequate concentration of the oxidant must be maintained at the reaction site, and (*ii*) the oxidized surface must be protected from reaction with water by the further precipitation and concomitant oxidation of nickel hydroxide on top of previously oxidized nickel. Thus, there would seem to be a need for detailed investigations of the precipitation kinetics and the morphology of nickel oxides to provide a basis for the selection of the best conditions for the synthesis of high valency nickel oxides. The observations of Okada *et al.* (11) on the

formation of amorphous divalent nickel hydroxide provide a useful basis for further studies.

The observed stability of the high-valency oxide in strongly alkaline solutions agreed with the results obtained by Tuomi (7) who found that the high-valency alpha nickel oxide could be formed readily in concentrated KOH or NaOH but not in dilute alkali solutions and with the results of Conway and Bourgault (12) on a series of oxides having a lower valency than the oxides studied by us.

An analysis of the kinetic form of our rate data was precluded by the inadequacy of the available information. In addition to the absence of an identification of the reaction species, the surface area of the oxides and the concentration of the nickelous ions in solution in the electrolyte occluded in the amorphous precipitate were unknown. The two latter quantities are experimentally inaccessible. Surface areas measured by gas adsorption techniques would be invalid because area changes take place during the dehydration of the specimens. The use of solution adsorption isotherms (13) may prove useful for these materials in the future. Insofar as the analysis of the residual valence state of the oxide is concerned, there is no chemical method available for distinguishing between the nickel in solution in the occluded electrolyte and the nickel in the solid oxide which is sufficiently rapid to be used for kinetic measurements. To the extent that it is possible to determine the true composition of the solid phase and the adjacent solution, it should be possible to obtain mechanistically meaningful data on the decomposition reaction. A detailed analysis of the reaction mechanism using the methodology of Conway and Bourgault (14) would be valuable.

The coincidence of the *p*H range of oxide instability with the *p*H range of solubility of divalent nickel in equilibrium with solid $Ni(OH)_2$ (10) suggested that the decomposition reaction proceeded *via* a dissolution step. Supporting evidence for such a conjecture comes from the observation that the MacIlvaine buffer enhanced the decomposition rate significantly. This buffer contains citrate ions, which are known to complex with divalent nickel (15). Therefore, the solubility of $Ni(OH)_2$ would be greater in citrate buffers than in pure phosphate buffers, and an enhanced decomposition rate would be expected in the citrate buffer, if the mechanism involved the reaction between a high-valency surface ion and a solution species to give a low-valency surface oxide. The transport of reagents and/or products through the divalent surface oxide would control the rate of the reaction, and the removal of the divalent oxide by means of complexation would lead to an increase in the decomposition rate.

The explanation for the differences observed in the reaction rates of fresh (fast) and aged (slow) oxides under comparable conditions must remain conjectural in the absence of a defined morphology of the oxide. An assumption which appears reasonable is that the aged oxide had rearranged to provide a smaller exposed surface area, or that the oxide had rearranged on aging to a configuration with an increased activation energy for one of the solid-state reaction steps involved in the decomposition process. It is also possible that the aged oxide had acquired a thicker surface layer of divalent oxide. However, if this were the case, an accompanying substantial decrease should have been observed in the mean nickel valency, which was not the case.

The rate curves obtained on the aged oxide in the *p*H 6 phosphate buffer at the low temperatures exhibited an initial induction period, an intermediate fast reaction period, and a final slow reaction period. This behavior is consistent with the conjecture that the oxides had acquired an inhibiting surface film. While still present, the film would prevent the decomposition reaction from proceeding very rapidly. Its dissolution would lead to an acceleration in the rate of the reaction because of the increase in the reactive surface area. As the reaction products would accumulate in the interior of the porous structures, the rates would decrease and become mass transfer controlled. The differences in the reaction rates during the intermediate reaction period at the various temperatures would, therefore, be due to the influence of the temperature on the rate of dissolution of low-valency surface oxide. The mass transfer controlled rates would be expected to be relatively insensitive to temperature, as observed. The fresh oxides did not exhibit any induction periods probably because of their larger surface areas, or because of the absence of an effective low-valency surface layer.

The cathodic behavior of the high-valency oxide showed that the high oxidation state of the chemically prepared material was available for electrochemical reduction. This agrees with observations on nickel-cadmium cells where some excess capacity can be obtained by discharging the cells immediately after charging. In the case of secondary cells, however, the excess capacity disappears in a few hours.

The open-circuit potential of the high-valency oxide-zinc primary cell corresponded to that expected for the system in concentrated KOH on the basis of the values given by Latimer (16). Since the high-valency oxide did discharge and since no significant potential arrests were observed above the trivalent nickel potential, it would appear that the high valence state did have a potential close to that of trivalent nickel. However, the assignment of an exact and a thermodynamically meaningful potential to the high-valency material must await the required definitive studies.

If the closeness of the discharge potentials of the trivalent and the higher valency oxides holds for their reversible half-cell potentials as well, the equilibrium constants of the reactions leading to the formation of trivalent and tetravalent nickel would be correspondingly close. Therefore, since the formation of trivalent oxide is thermodynamically favored, so would be the formation of tetravalent nickel. The observed, apparent limitations in the value of the mean valence state of nickel suggest that the reaction of tetravalent nickel with water is kinetically favored over that of trivalent nickel. This is in agreement with our conjecture that the synthesis of the high-valency oxide is limited by kinetic rather than thermodynamic factors. Therefore, it is to be expected that nickel oxides with valencies above 3.6 may be prepared provided the proper oxidation conditions can be established based on detailed information on the kinetics of the precipitation and decomposition reactions of the nickel oxides.

Conclusions

Investigations of the high-valency amorphous nickel oxides showed that they could be prepared reproducibly at room temperature with a mean oxidation state of 3.6 for the nickel. The oxides were stable at room temperature and at lower temperatures in strongly alkaline solutions but decomposed at *p*H values below *p*H 14. Between *p*H 9 and *p*H 14 the decomposition reaction was very slow; below *p*H 9 it became very fast.

The results indicated that the degree of oxidation of the nickel was kinetically as well as thermodynamically controlled, and it is believed that it may be possible to prepare nickel oxides with mean valencies in excess of 3.6.

Primary cell cathodes prepared from the high-valency material exhibited a good utilization of the high oxidation state of nickel.

Acknowledgment

The authors are indebted to J. Epstein for the electrochemical measurements; they wish to express their appreciation to the management of P. R. Mallory & Co., Inc., for permission to publish this report.

Manuscript received Nov. 22, 1965; revised manuscript received Feb. 21, 1966.

Any discussion of this paper will appear in a Discussion Section to be published in the December 1966 JOURNAL.

REFERENCES

1. J. Labat, *J. Chim. Phys.*, **60**, 1253 (1963).
2. O. Glemser and J. Einerhand, *Z. anorg. u. allgem. Chem.*, **261**, 26 (1950).
3. L. Dede and H. Zieriacks, *Z. Anal. Chem.*, **124**, 25 (1942). Quoted by (1).
4. J. Labat, *Ann. Chim.*, **9**, 400 (1964).
5. O. R. Howell, *J. Chem. Soc.*, **123**, 1772 (1923).
6. E. Jones and W. F. K. Wynne-Jones, *Trans. Faraday Soc.*, **52**, 1260 (1956).
7. D. Tuomi, *This Journal*, **112**, 1 (1965).
8. J. Besson in P. Pascal, "Nouveau Traite de Chimie Minerale," Vol. 17, p. 742-59, Masson & Cie, Paris (1963).
9. E. J. Casey, A. R. Dubois, P. E. Lake, and W. J. Moroz, *This Journal*, **112**, 371 (1965).
10. M. Pourbaix, "Atlas D'Équilibres Electrochimiques," Gauthier-Villars & Cie., Paris (1963).
11. T. Okada, T. Shiraishi, and K. Watanabe, *J. Chem. Soc. Jap. Ind. Chem. Soc.*, **51**, 129 (1948).
12. B. E. Conway and P. L. Bourgault, *Can. J. Chem.*, **40**, 1690 (1962).
13. D. H. Everett, *Trans. Faraday Soc.*, **60**, 1803 (1964).
14. B. E. Conway and P. L. Bourgault, *Can. J. Chem.*, **37**, 292 (1959).
15. L. G. Sillen and A. E. Martell, "Stability Constants of Metal-Ion Complexes," The Chemical Society, London (1964).
16. W. M. Latimer, "The Oxidation States of the Elements and Their Potentials in Aqueous Solutions," Prentice-Hall, Inc., New York (1952).

Equilibrium Pressures of Oxygen over Oxides of Lead at Various Temperatures

Earl M. Otto

National Bureau of Standards, Washington, D. C.

ABSTRACT

PbO_2 apparently requires four stages of decomposition to reach PbO. Based on thermogravimetric studies the intermediate products appear to be $5PbO_2 \cdot 4PbO$, $4PbO_2 \cdot 5PbO$, and Pb_3O_4. Although the first three stages seem irreversible, they too come to a steady state in decomposition, but no recombination takes place. $\Delta H°$ and $\Delta S°$ values have been calculated for the four stages.

Thermal decomposition of lead dioxide has been studied by a number of investigators with the emphasis being placed on the composition and the crystal structure of the dioxide and the lower oxides that were formed. Earliest work indicated that an intermediate product of Pb_2O_3 is formed (1) (1878). Later, Moles and Vitoria (2) (1929), Renker (3) (1936), and Baroni (4) (1938) agreed that no other substance than Pb_2O_3 is formed before Pb_3O_4 appears. When the mathematical error of Baroni was corrected showing the formula of the oxide to be $PbO_{1.6}$, more investigation and speculation began. Clark and Rowan (5) (1941) refer to the oxide as Pb_5O_8. Holtermann and Laffitte (6) (1937) ascribed the formula Pb_7O_{11}. However, LeBlanc and Eberius (7) (1932) had stated that the structure of PbO_2 persists to $PbO_{1.66}$ and had ascribed the formula Pb_3O_5 to an intermediate product. They also reasoned that Pb_2O_3 is formed. A few years later Bystrom (8) (1945) and Katz (9) (1950) showed that two intermediate oxides were indicated and these were termed $\alpha\, PbO_x$ and $\beta\, PbO_y$, the former having a monoclinic crystal structure of nonstoichiometric composition where x is somewhat more than 1.5 and the latter having an orthorhombic crystal structure of nonstoichiometric composition where y is less than 1.5 and approximating 1.4. Recently Butler and Copp (10) (1956), and Anderson and Sterns (11) (1959) have confirmed the existence of two intermediate oxides, the latter authors proposing the formulas $Pb_{12}O_{19}$ and $Pb_{12}O_{17}$.

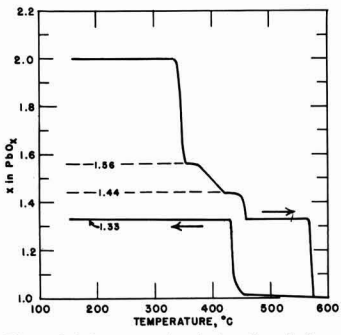

Fig. 1. Thermal balance study of the dissociation of PbO_2 to PbO and reoxidation to Pb_3O_4. Influence of temperature on the value of x in PbO_x, calculated from weight loss.

Very little study has been made of the equilibrium pressures of oxygen over the various oxides of lead. LeChatelier (12) (1897) Reinders and Hamburger (13) (1914) separately determined oxygen pressures over $PbO\text{-}Pb_3O_4$; the two sets of data did not show much agreement.

In view of the lack of pO_2-oxide temperature equilibrium data for the oxides of lead it was thought desirable to conduct the present investigation.

Experimental

Preliminary to the study of oxygen pressures over the PbO_2 and the lower oxides a thermal balance was constructed and used to get indications as to the approximate temperatures at which decompositions in air could be expected. Figure 1 shows that weight loss began before a temperature of 330° was reached and that at about 360° the weight became constant and the formula of the oxide was calculated to be approximately $PbO_{1.56}$. At 420° another level was reached, and calculations indicated the oxide to be approximately $PbO_{1.44}$. At 450° further decomposition began and continued to 460°, at which stage the oxide was $PbO_{1.33}$. (This material is the well-known "red lead," Pb_3O_4.) The final decomposition was reached at 570°, and the product was $PbO_{1.00}$. On cooling the PbO slowly in air, oxygen was consumed starting at about 450° and forming $PbO_{1.33}$. No further reoxidation was observed. The time of decomposition, from PbO_2 to PbO was seven days. This whole experiment was repeated twice, and the results were essentially the

same. Anderson and Sterns suggested that the formation of lower oxides is a result of nucleation and growth. The above mentioned values of x in PbO_x appear to indicate that nine molecules of PbO_2 are involved in the formation of each unit. Thus the products formed are postulated to be $5PbO_2 \cdot 4PbO$, $4PbO_2 \cdot 5PbO$, and $3PbO_2 \cdot 6PbO$. (The last substance may break down forming $PbO_2 \cdot 2PbO$, which is the same as Pb_3O_4.) Further evidence of a nine molecule unit is supplied by Anderson and Sterns for they say that acid leaching of one intermediate oxide gave $PbO_{1.886} \cdot 0.16H_2O$. The product in this case could be represented by $8PbO_2 \cdot PbO$.

The apparatus used for the pressure studies was similar to that previously employed by the author (14, 15) in studies of the Mn_2O_3-Mn_3O_4 and MnO_2-Mn_2O_3 equilibria. Both Fisher, and Baker and Adamson analytical grades of PbO_2 were used in the investigations. Five furnaces, four sets of manometers, and one 300-psi gauge were involved. Each furnace had its own constant temperature cabinet. Essentially the procedure consisted in heating *in vacuo* a sample of PbO_2 in a bulb contained in a crucible furnace until the evolved oxygen, having passed through the silica gel desiccant, began to change the mercury levels in the manometers. The temperature was stabilized and the pO_2 was allowed to become steady. Time for reaching a steady pressure sometimes was hundreds of hours and sometimes less than 5 hr, depending on the stage of dissociation. In one instance in the last stage the build-up in pO_2 from near vacuum to one third equilibrium pressure required less than 2 min. After a steady state was established the temperature or pressure or both were altered and a new steady state sought. After the first stage of dissociation was satisfactorily studied the investigation was extended to the second and third stages. Only one sample of PbO_2 was carried to the fourth stage because the equilibria of the last stage were so quickly attained and because commercially produced (analytical reagent grade) Pb_3O_4 could be used.

Except for the last stage of decomposition no recombination was ever observed when a somewhat higher than steady-state pressure of oxygen was provided to the partially dissociated oxides. The Pb_3O_4-PbO-O_2 reaction was readily reversible and equilibrium attainable in either direction.

The data obtained are shown in Table I and Fig. 2 to 5. The only available data from the literature are included in Fig. 4. The present data on Pb_3O_4-PbO are in good agreement with those of Reinders and Hamburger.

Table I. Dissociation of PbO_2 temperature-pressure steady-state data

Steady state hr to:	hr at:	Temperature, °C	Pressure, atm
		First stage	
168	144	254.2	0.0787
120	120	258.6	0.1467
1960	270	267.2	0.4600
360	144	269.7	0.5256
1632	120	277.4	1.1910
2300	300	285.2	2.258
168	24	286.2	3.401
288	144	287.2	3.016
96	72	287.9	4.238
48	24	298.8	10.88
		Second stage	
360	240	318.5	0.1521
120	48	335.8	0.4369
120	64	357.1	1.4067
360	120	363.4	2.186
		Third stage	
72	24	348.1	0.2174
264	24	354.0	0.3299
240	66	364.0	0.5339
360	480	382.3	1.2593
*		Fourth stage	
16	0	484.1	0.0416
60	0	487.2	0.0474
24	0	524.5	0.1395
19	24	538.8	0.2250
60	0	547.2	0.2938
24	24	547.5	0.2984
5	4	561.2	0.4127
16	96	563.6	0.4277
10	15	564.5	0.4669
16	0	569.2	0.5195
22	48	601.9	1.2466
24	0	603.6	1.2785
40	0	606.2	1.3321
7	16	609.6	1.4522
12	10	627.5	2.3511
8	0	632.0	2.5355
24	0	632.9	2.6376
48	72	634.8	2.6505
20	0	638.4	2.8176

* Minimum time to steady state was not observed. These were the periods that were convenient to the investigator.

Treatment of Data

The straight lines shown in Fig. 2, 3, and 4, drawn for the new experimental data, form the basis for determining values for the thermodynamic functions ΔH° and ΔS°, on the assumption that steady pressures were true equilibrium pressures. The equations for the straight lines, fitted to the experimental point by sight, were put in the form of

$$\Delta H^\circ/T - \Delta S^\circ = \Delta G^\circ/T = -4.5756 \log pO_2$$

The resolved values for the four stages of dissociation are, precisely applicable only for the mean temperatures, as follows:[1]

Proposed equation	Temperature range, °C	ΔH° kcal mol^{-1} O_2	ΔS° cal deg^{-1} mol^{-1} O_2
$9/2PbO_2 \rightarrow 1/2(5PbO_2 \cdot 4PbO) + O_2$	270 ± 30	66.4	121.0
$2(5PbO_2 \cdot 4PbO) \rightarrow 2(4PbO_2 \cdot 5PbO) + O_2$	345 ± 25	44.2	70.9
$2(4PbO_2 \cdot 5PbO) \rightarrow 6PbO_2O_4 + O_2$	367 ± 17	39.9	61.4
$2Pb_3O_4 \rightarrow 6PbO$ (yellow) $+ O_2$	560 ± 80	37.5	43.2

Excepting for the Pb_3O_4-PbO stage these values cannot be converted from the experimental temperatures to 298°K, since heat capacities, heat contents, and entropy changes are unknown for the intermediate oxides and are estimated or partially known for PbO_2 and Pb_3O_4. Considering the first three stages as one, the equation becomes $3PbO_2 \rightarrow Pb_3O_4 + O_2$. Using the

[1] One thermochemical calorie = 4.1840 joules.

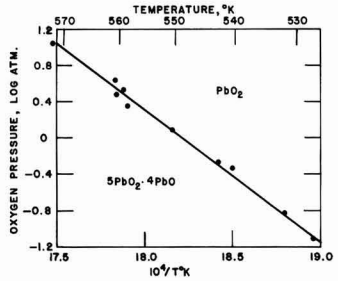

Fig. 2. Dissociation of PbO_2. First stage. Pressure-temperature relationship at steady state.

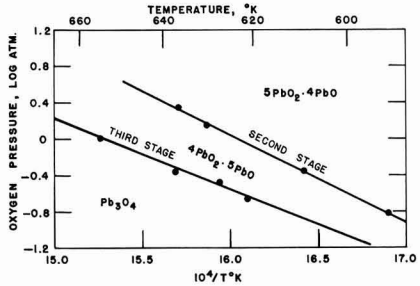

Fig. 3. Dissociation of PbO_2. Second and third stages. Pressure-temperature relationship at steady state.

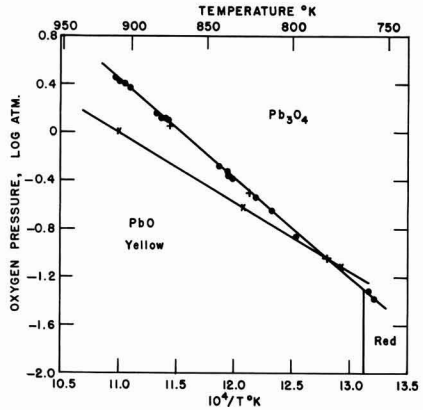

Fig. 4. Dissociation of PbO_2. Fourth stage. (Identical with first stage of dissociation of Pb_3O_4.) Half of the equilibrium points obtained in forward direction and half in the reverse. ● Present work; × LeChatelier; + Reinders and Hamburger.

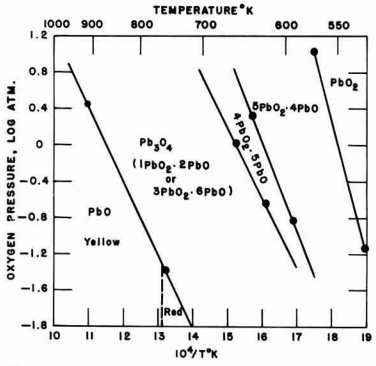

Fig. 5. Dissociation of PbO_2. All four stages. Pressure-temperature relationship at equilibrium. Dots mark the limits of experimental investigation.

Cp values given by Kelley (16) the $\Delta(H_T-H_{298})$ and $\Delta(S_T-S_{298})$ were obtained, where T = 585°K (a rough average of the temperatures of the first three reactions). These are −1.7 kcal/mol O_2 and −2.7 cal/deg, respectively. When these are added to the ΔH° and ΔS° values for the sum of the three reactions, one obtains ΔH°_{298} = 56.6 kcal and ΔS°_{298} = 100 cal/deg. From these ΔG° is calculated to be +26.8 kcal. Taking ΔG°_f of PbO_2 to be −52.0 kcal the ΔG°_f of Pb_3O_4 becomes −129.2 kcal.

The Pb_3O_4-PbO-O_2 system was readily brought to equilibrium and the Cp equation for PbO is well established. It does have to be assumed that the Cp value for Pb_3O_4 at 298°K is usable up to 1000°K. For the reaction $2Pb_3O_4 \rightarrow 6PbO + O_2$ at the mean temperature of 833°K ΔH°_{833} = 37.5 kcal/mol O_2 and ΔS°_{833} = 43.2 cal/deg.

From the Cp equations the calculated value of $\Delta(H_{833}-H_{298})$ becomes +7.1 and $\Delta(S_{833}-S_{298})$ becomes +21.1, thus making ΔH°_{298} = 44.6 kcal/mol and ΔS°_{298} = 64.3 cal/deg. From these two figures ΔG°_{298} is found to be 25.4 kcal. On the selection of ΔG°_f of PbO as −45.2 kcal ΔG°_f of Pb_3O_4 then becomes −148.3 kcal.

The resulting values for Pb_3O_4 may now be compared with those from the literature.

	$\Delta G^\circ_f Pb_3O_4$ kcal
From cell data for $Pb_3O_4 + 2HgO = 3PbO_2 + 2Hg$	
Chartier (17)	−148.4
Andrews and Brown (18)	−146.0
From cell data for $3PbO + HgO = Pb_3O_4 + Hg$	
Andrews and Brown (18)	−142.5
From present work $3PbO_2 = Pb_3O_4 + O_2$	−129.2
From present work $2Pb_3O_4 = 6PbO + O_2$	−148.3

Note: In the above considerations selected values were

$$\Delta G^\circ_f PbO_2 = -52.0 \text{ kcal and } \Delta G^\circ_f PbO = -45.2 \text{ kcal}$$

The results are surprisingly good, considering the lack of precise thermodynamic data for some of the oxides of lead and considering the fact that steady-state pressures were obtained in only one direction for the first three stages of dissociation.

Manuscript received Nov. 9, 1965; revised manuscript received Feb. 11, 1966. This paper was presented at the Buffalo Meeting, Oct. 10-14, 1965.

Any discussion of this paper will appear in a Discussion Section to be published in the December 1966 JOURNAL.

REFERENCES

1. Debray, *Compt. rend. Paris*, **86**, 813 (1878).
2. Moles and Vitoria, *An. Fis. Quim.*, **27**, 52 (1929).
3. Renker, *Bull. Soc. Chim. France*, **3**, 981 (1936).
4. Baroni, *Gazz. Chim. Ital.*, **68**, 387 (1938).
5. Clark and Rowan, *J. Am. Chem. Soc.*, **63**, 1305 (1941).
6. Holtermann and Laffitte, *Compt. rend. Paris*, **204**, 1813 (1937). Also Holtermann, *Ann. Chim. Paris*, **14**, 121 (1940).
7. LeBlanc and Eberius, *Z. Physik. Chem.*, **A160**, 69 (1932).
8. Bystrom, *Ark. Kemi. Mineralog. Geol.*, **20A**, No. 11 (1945).
9. Katz, *Ann. Chim. Paris*, **5**, 5 (1950).
10. Butler and Copp, *J. Chem. Soc.*, 725 (**1956**).
11. Anderson and Sterns, *J. Inorg. Nucl. Chem.*, **11**, 272 (1959).
12. LeChatelier, *Bull. Soc. Chim. France*, **17**, 791 (1897).
13. Reinders and Hamburger, *Z. Anorg. Chem.*, **89**, 71 (1914).
14. E. M. Otto, *This Journal*, **111**, 88 (1964).
15. E. M. Otto, *ibid.*, **112**, 367 (1965).
16. K. K. Kelley, *U. S. Bur. Mines Bull. 584* (1960).
17. Chartier, *Compt. rend. Paris*, **256**, 1976 (1963).
18. Andrews and Brown, *J. Am. Chem. Soc.*, **56**, 388 (1934).

Oxidation of Copper Single Crystals in Aqueous Solutions of Inorganic Salts

III. Kinetics of Oxidation in $Cu(OAc)_2$ Solution

W. W. Porterfield and G. T. Miller, Jr.[1]

Department of Chemistry, Hampden-Sydney College, Hampden-Sydney, Virginia

ABSTRACT

The kinetics of formation of Cu_2O on the three principal (low-index) faces of Cu metal monocrystals are reported and correlated with the surface microtopography. A novel technique is described for the determination of surface areas of small metal samples. Over extended periods of time the relative rates of oxide formation are found to be: (100)>(111)>(110); the forms of the rate curves, however, differ markedly. The specific forms of the rate curves on the three faces are accounted for by a proposed mechanism in which the rate-controlling step is the drift velocity of positive holes through the Cu_2O film. This mechanism also correctly indicates the microtopography on the basis of the previously observed epitaxial relationships.

This is the third in a series of papers describing the oxidation of copper metal in solutions of copper(II) salts. The first two papers (1, 2) dealt with the topography of the copper(I) oxide film formed in such oxidations and are indispensable to an understanding of the data reported here. The present work attempts to describe the kinetics of the oxide growth and to begin, at least, the inference of a mechanism for the oxidation process.

Benard (3) has an excellent summary, with critical comments, of experimental techniques for the determination of oxide film thickness on metal surfaces. Of the methods he describes, the coulometric was chosen because of its experimental simplicity. This method is well established (4-8) but requires some comment in two respects. First, even though the electropolishing technique enables the worker to assume that the metal surface area is equal to the gross area of the specimen, the measurement of area continues to be a problem with this method; in this case, the problem was accentuated by the small areas available when using monocrystalline specimens. A procedure was devised, which is described below, that enabled the measurement of surface areas within an error of 1%; in this work the error was on the order of 0.1 mm^2. It is felt that this may be of use to other workers using coulometric techniques on small specimens. Second, as Evans (9) has made clear, the phenomenon of metal corrosion is, to a substantial extent, inherently irreproducible. It is therefore necessary to indicate clearly the extent to which irreproducibility affects conclusions to be drawn from irreproducible data. Unfortunately, many previous workers have not made such an indication. It should be noted, then, that the error bars shown in Fig. 2, 3, and 4 represent 2σ, the standard deviation for measurements displaying Gaussian scatter about an unknown true value.

The previous studies, in parts I and II of this series, of the topography of oxide films as a function of the anion and as a function of time show clearly that in this system, as in others, there is a marked difference in the behavior of the three principal crystal faces. It seemed likely, then, that the coulometric study of oxide formation, performed on individual crystal faces and interpreted in conjunction with the known variations of topography with time, would yield important evidence bearing on the mechanism of the oxide growth. This appears to be true, although much further experimentation will be required to conclusively demonstrate a detailed mechanism.

Experimental

99.999% copper monocrystals were used throughout this series of experiments (Virginia Institute for Scientific Research, Richmond, Virginia). Flats were cut on these crystals to expose the (100), (110), and (111) faces individually. The orientation of these faces was maintained within 2° [1° for the (100) face] by Laue back-reflection x-ray photography after every fourth mechanical polishing [every second mechanical polishing for the (100) face]. The crystals were mechanically polished through 4/0 Buehler paper, then electropolished in an unstirred phosphoric acid bath and washed, finally, in water of approximately 1.2×10^6 ohms resistivity. The flats were dried in a stream of Seaford grade nitrogen (Southern Oxygen Company, Washington, D.C.; maximum impurity limits 30 ppm total) before immersion in the corroding solution. The only solutions used in this study were $0.0500N$ $Cu(C_2H_3O_2)_2$, made up from Fisher copper(II) acetate dihydrate, used as received from lot number 731759. Oxidation patterns from this lot were found to remain unchanged upon repeated recrystallization, whereas other lot numbers gave patterns which only approached that from this lot after two or three recrystallizations. Solutions were adjusted to a pH of 4.300 ± 0.005 before each oxidation. All solutions were thermostatted at 30.0°C before and during the corrosion process, since a study of the effect of temperature on the corrosion process, to be undertaken shortly, is expected to reveal marked temperature dependence. After oxidation for stipulated times, each crystal was dried and the spherical sides of the crystal, together with the edges of the flat face, were masked by painting with the electrically insulating lacquer Miccrostop (Michigan Chrome and Chemical Company, Detroit, Michigan). Coulometric measurement of the oxide on the area remaining was made in the apparatus shown in Fig. 1, after appropriate deaeration. The electrical potential of the crystal against an Ag/AgCl electrode was recorded on a Bausch and Lomb VOM-5 recorder. The exposed area of the flat was calculated by stripping the masking lacquer from the crystal, photographing the flat by using a Polaroid film pack at 6X on a Reichert metallurgical microscope, and measuring the photographed area with a planimeter. Equivalent copper(I) oxide film thickness could then be calculated on the assumptions that: (*i*) film density was equal to that of the bulk oxide; (*ii*) current efficiency was 1.000; and (*iii*) the oxide formed a film of uniform thickness. A discussion of the influence of departures from these assumptions upon reproducibility follows below; here it might be noted that the error bars in Fig. 2, 3, and 4 are roughly between 5 and 10% of the indicated mean.

With respect to the first assumption, lattice parameter measurements for films on the major faces of copper [(10) and references therein] indicate a linear expansion of 1-2% normal to the surface, but an offsetting compression in the surface plane. The unit cell volume is that of the bulk oxide, and the density

[1] Present address: Department of Chemistry, St. Andrews Presbyterian College, Laurinburg, North Carolina.

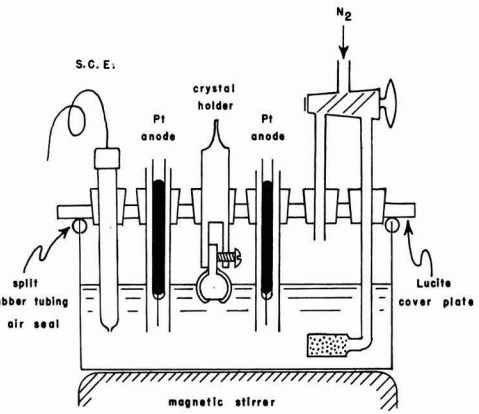

Fig. 1. Apparatus for coulometric oxide determination. Crystal holder is shown with a masked crystal in place.

will thus be unaffected. The validity of the second assumption is more difficult to establish. Studies comparing oxygen uptake (in gaseous oxidation) with coulometric values suggest an efficiency of at least 0.90 (11), and studies of current efficiency as a function of current density (micro-amperes/cm^2) for the Fe-Fe_3O_4-Fe_2O_3 system (7) suggest the same approximate figure under our experimental conditions. Of course, this is not a comparable system, but the order of magnitude of current density is perhaps suggestive. In any event, only the absolute determination of deposited oxide mass would suffer from this type of error; the rate curves would retain their general form and relative magnitudes. However, substantial scatter could arise from this source. Finally, the assumption of a uniform oxide film requires severe qualification. The rather rugged microtopography revealed in the electron micrographs (1, 2) indicates that interpretation of the coulometric data as thicknesses of oxide films is illusory. Clearly, the only appropriate interpretation is that of a gross average, that is, deposited oxide mass per unit area. This figure is used in each case.

Results and Discussion

Figures 2, 3, and 4 show the oxide growth rates on the three low-index faces of copper metal crystals, as determined in this study. Figure 5 indicates the marked differences between the faces. In Fig. 2, 3, and 4 the notation is as follows: (*i*) The error bars, as previously stated, are 2σ long. (*ii*) The arithmetic mean of all determinations is indicated by a crossbar. It must be remembered, however, that the arithmetic mean is the most probable value only for a Gaussian error distribution. It is not certain that this is the true distribution in corrosion measurements. (*iii*) The mode is indicated by a heavy dot. Evans (9) has suggested that, given the irreproducible nature of the measurements, the mode may be the most significant quantity. (*iv*) The number of measurements at a given time of immersion is indicated over the error bar. (*v*) To provide a more meaningful interpretation, the right-hand scale in these figures is given as deposited copper(I) oxide mass per unit area (micrograms per square centimeter). However, the convenient comparison of this work with other film-thickness studies requires that the data also be presented as equivalent average thickness in Angstrom units. It must be remembered that these thicknesses are rather fictional; that both vertical and lateral growth are occurring, and to different extents on different crystal faces of the metal.

It was anticipated from preliminary experiments that the oxide growth would be quite rapid; Fig. 2, 3, and 4 confirm this. Indeed, the growth on all three faces is so fast that it does not seem possible for the

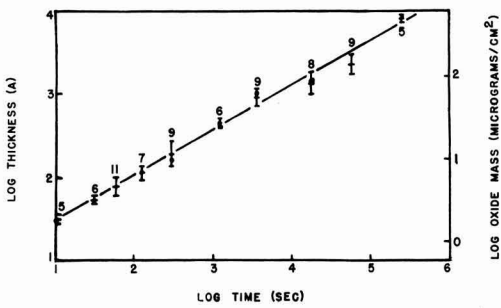

Fig. 2. Kinetic data for oxide growth on the (100) face of the Cu metal crystal. Reciprocal slope is 1.86.

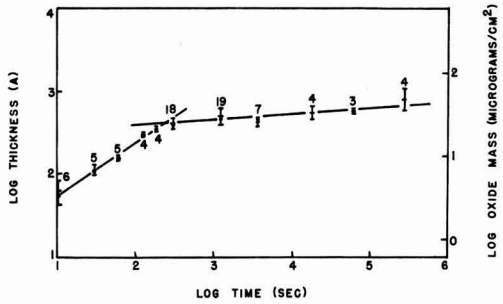

Fig. 3. Kinetic data for oxide growth on the (110) face of the Cu metal crystal. Reciprocal slope of initial rise is 1.57.

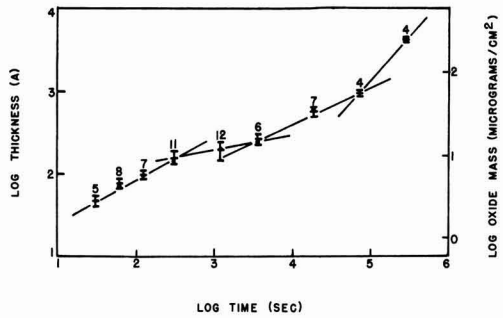

Fig. 4. Kinetic data for oxide growth on the (111) face of the Cu metal crystal. Reciprocal slope of initial rise is 1.99.

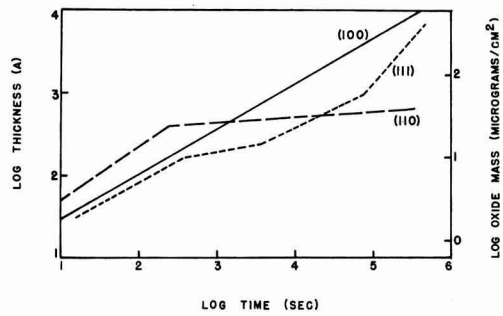

Fig. 5. Comparative kinetic behavior for oxide growth on the three principal metal crystal faces.

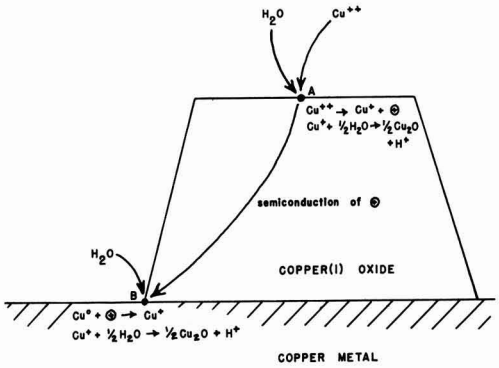

Fig. 6. Schematic representation of proposed mechanism

rate-determining step to be the diffusion of copper atoms through the oxide film, which is almost immeasurably slow at 30°C, the temperature of the reaction. Thus it seems likely that a significant amount of Cu(I) in the oxide film must originate from the Cu(II) in solution. Furthermore, if atomic (or ionic) diffusion is ruled out, any Cu(I) in the oxide originating from the metal must be obtained from a location where the oxide is either quite thin or nonexistent.

Figure 6 diagrammatically indicates a mechanism which appears to satisfy these requirements. Copper(II) ions from solution are adsorbed onto existing copper(I) oxide nuclei which are in contact with bulk copper metal. This adsorption may be assumed to occur preferentially on the close-packed faces of the oxide (not necessarily on the close-packed faces of the metal). After adsorption each ion donates a positive charge to the copper(I) oxide, becoming a Cu(I) ion. This ion may react immediately with the solution's oxygen-supplying species (at point A) or may migrate some distance across the surface of the Cu_2O polyhedron before reacting to form additional Cu_2O. The mean migration distance will be governed by the ratio of the migration velocity to the rate of reaction with the oxygen-supplying species in solution. The copper(I) oxide, functioning as a p-type semiconductor, conducts the positive hole to a point at which the three phases Cu_2O, Cu°, and solution are all present (such as point B in Fig. 6). Here a copper atom acquires the positive charge, becoming a copper(I) ion, and reacts with the solution to form more Cu_2O. The same migration considerations apply at point B as at point A. The mechanism may be summarized as follows:

(*i*) diffusion of Cu(II) species and adsorption on the oxide surface

(*ii*) $Cu^{2+} \rightarrow Cu^+ + \oplus$ (cathodic reaction at A)
(*iii*) $Cu^+ + \frac{1}{2}H_2O \rightarrow \frac{1}{2}\underline{Cu_2O} + H^+$
(*iv*) movement of $\oplus$ from A to B
(*v*) $\oplus + Cu^\circ \rightarrow Cu^+$ (anodic reaction at B)
(*vi*) $Cu^+ + \frac{1}{2}H_2O \rightarrow \frac{1}{2}\underline{Cu_2O} + H^+$

The net cathodic and anodic processes are, respectively the sum of (*ii*), (*iii*) and (*v*), (*vi*):

$$Cu^{2+} + \tfrac{1}{2}H_2O \rightarrow \tfrac{1}{2}\underline{Cu_2O} + H^+ + \oplus \qquad (E_c)$$

$$Cu^\circ + \tfrac{1}{2}H_2O + \oplus \rightarrow \tfrac{1}{2}\underline{Cu_2O} + H^+ \qquad (E_a)$$

$$Cu^{2+} + Cu^\circ + H_2O \rightarrow \underline{Cu_2O} + 2H^+ \qquad (E_{net})$$

It must be noted that steps (*v*) and (*vi*) of such a mechanism require that the oxidizing solution be in contact with the oxide-metal interface for growth to occur, since the solution must provide the oxygen for the lattice, otherwise the oxide cannot continue to remove positive holes from its surface. The crevices visible in the earlier electron micrographs (1) would appear to provide just such a solution contact. Possible sources of oxygen would be free H_2O, the aquo complex of Cu(II), CH_3COO^-, or dissolved O_2. (H_2O is used as an example in the equations above.) Exploratory experiments using BF_4^- anion and dissolved O_2 removal indicate that probably neither the anion nor dissolved O_2 provides the oxygen.

In examining the rate curves it will be shown below that the adequacy of the proposed mechanism depends on the assumption that adsorption of the copper(II) species on the Cu_2O surface occurs preferentially on the most closely packed surface of the oxide. This is intuitively reasonable but by no means necessary. It may be that another mechanism could be devised which would not require this feature, but its nature is not immediately obvious.

The forms of the three rate curves (Fig. 2, 3, and 4) must be examined separately with respect to the proposed mechanism because of their strikingly different natures (Fig. 5).

Oxide growth on the (100) face occurs by an apparently uniform mechanism over an extended period of time (Fig. 2). It might be noted in passing that on the logarithmic scale employed here the age of the universe would not fill a double-page spread of this Journal! The mathematical form of the growth law, as determined from the inverse slope of the log-log plot, is very roughly parabolic (exponent 1.86). The parabolic law might be expected if the positive hole draft velocity were the rate-determining step: $d(Th)/dt = K\mu$, where Th represents oxide thickness and μ the drift velocity. Drift velocity is proportional to electric field strength, which in this case is decreasing with increasing thickness, so that

$$\mu = K'/Th$$

Then

$$d(Th)/dt = KK'/Th, \text{ and } (Th)^2 = K''t$$

The steady growth is also consistent with the topography of the oxide on the (100) face (polyhedra), since the crevices between the polyhedra would permit the necessary uninterrupted solution contact with the metal-oxide interface.

The (110) face is quite different. Oxide grows on it somewhat faster than on the (100) face initially (exponent 1.57), but only for the first three or four minutes. Growth then stops almost completely. Some justification for this may be found in the electron micrographs of the (110) face, which reveal an unusually smooth oxide film (1). Apparently lateral growth fills the crevices between oxide nuclei in this orientation, thereby preventing solution contact with the oxide-metal interface and providing effective protection for the metal. The very slow growth which continues to occur may be due to a few unfilled crevices or to positive hole conduction to exposed oxide-metal interfaces on adjacent faces of different orientation. It is interesting to observe that the initial growth on this face is faster than that on the (100) face; one would not expect this either from metal-atom packing considerations or by analogy with the high-temperature dry oxidation of copper (12).

Upon consideration of the probable modes of deposition of the copper(II) ions, however, the relative rates may be rationalized. The epitaxial relationships displayed in this system are as follows (13): the (100) copper face requires the growth of the (111) Cu_2O face parallel to it; the (110) metal face, the (110) oxide face; the (111) metal face, the (111) oxide face. Then, following the assumption of preferential adsorption on the close-packed face, the (100) and (111) metal faces will both tend to adsorb copper(II) ions on the top of the nuclei, thereby producing the vertical growth governed by the parabolic law; but the (110) metal face, having the thermodynamically more stable (close-packed) (111) faces on the slant sides of the nuclei, will tend to adsorb on the sides. In this case the growth will be predominantly lateral, with

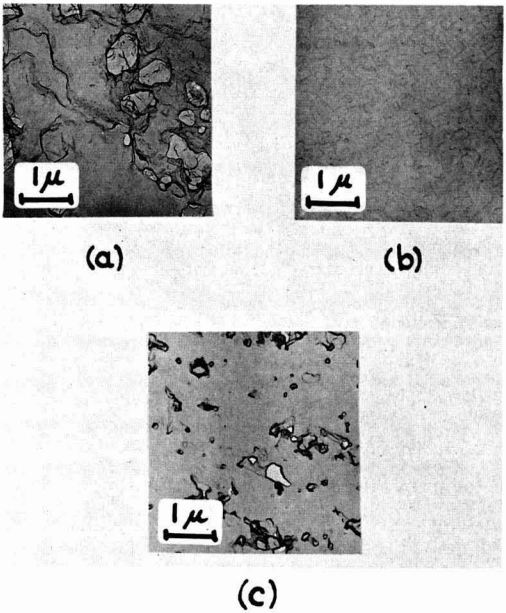

Fig. 7. Microtopography of oxide growth on three principal metal crystal faces after 72 hr (2.6×10^5 sec). (a) (100); (b) (110); (c) (111).

the vertical thickness changing only rather slowly. The drift velocity, μ, will be essentially constant, and the oxide growth will occur by a linear law. To the extent, then, that lateral growth predominates over vertical growth, the exponent in the growth law will be reduced from 2 toward 1. The faster growth on the (110) face, characterized by the lower exponent, is thus consistent with the orientation of close-packed faces produced by epitaxy, as is the almost complete cessation of growth after complete coverage has been achieved. The slight lowering of the exponent for the (100) face (from the hypothetical 2.00 to the observed 1.86) is perhaps also due to appreciable lateral growth.

Growth of oxide on the (111) face is also, initially, approximately parabolic (exponent 1.99). After five to ten minutes, however, a slackening of rate occurs like that on the (110) face. The electron micrographs at this time (1) corroborate this, since the surface appears to be reasonably uniformly covered, with few crevices to allow solution access to the positive hole sink. The rate soon increases again to approximately the parabolic value, and after quite a long time increases to nearly a linear rate (exponent 1.0). The increase appears to be due to etching of the oxide film, which would provide renewed solution access to the metal.

Etching is indicated by the electron micrographs shown in Fig. 7 for the three faces after 72 hr. These electron micrographs were obtained as part of the series described in part I (1). The conditions of polishing, washing, and microscopy are described therein. Note that the etching appears to be more pronounced on the (100) and (111) faces than on the more or less permanently protected (110) face. Photomicrographs (a) and (c) of Fig. 7 indicate that etching probably occurs to roughly the same extent for the oxide on the 100 and 111 metal faces. However, the patterns of etching are not at all similar and it is difficult to compare the two faces' kinetic behavior on this basis. Close examination of Fig. 2 suggests that there may be a slackening of oxidation rate (around 10^4 sec) like that seen clearly in Fig. 4, but the reproducibility of the data is simply inadequate to allow a confident interpretation in this way. After a crevice had opened by etching it would presumably remain open, since further nucleation on the bare metal could not occur due to the surface tension differential between a new nucleus and the large polyhedra.

A consideration of etching brings up the question of the importance of the effect of *p*H on the growth process proposed in the mechanism outlined above, which produces H^+ at localized sites. Although the bulk *p*H remained essentially constant during each experiment, local *p*H changes could profoundly affect the topography. Careful observations of the *p*H changes during the reaction and its *p*H dependence are presently being made and will be reported on in a subsequent part of this series.

The present measurements provide only a possible interpretation of the growth laws and topography of the principal faces; the proposed mechanism assumes existing nuclei and does not suggest any features of the nucleation process. Preliminary results from the *p*H study which is underway indicate that the nucleation is quite sensitive to small *p*H changes. Other studies are contemplated which might yield more information on nucleation and confirm or reject the proposed growth mechanism. It must also be pointed out that this study does not account for the persistence of well-defined oxide polyhedra on the (100) face and their merging on the other two faces (1). It is felt that this is a feature more of the nucleation process than of the growth process, and may be due to the symmetry mismatching in epitaxy.

Acknowledgments

The authors are deeply indebted to Dr. K. R. Lawless of the Department of Materials Science of the University of Virginia for the generous use of specialized equipment, and to Dr. Lawless and Dr. J. W. Mitchell of the Department of Physics of the University of Virginia for helpful discussions. Students at this college who participated in this project and to whom a great deal of credit is due are: P. R. Anderson, A. T. Elliott, L. E. Hightower, D. W. Mason, D. J. McKittrick, E. B. Noland, L. F. Towers, and W. F. Wright. This research was supported by National Science Foundation Undergraduate Science Education grants and by PHS Research grants DE-01893-02 and DE-01893-03, National Institute of Dental Research, Public Health Service.

Manuscript received Nov. 29, 1965; revised manuscript received March 3, 1966.

Any discussion of this paper will appear in a Discussion Section to be published in the December 1966 JOURNAL.

REFERENCES

1. C. E. Guthrow, Jr., and G. T. Miller, Jr., *This Journal*, **113**, 415 (1966).
2. R. W. Topham and G. T. Miller, Jr., *ibid.*, **113**, 421 (1966).
3. J. Benard, "L'Oxydation des Metaux," pp. 97 ff, Gauthier-Villars et Cie., Paris (1962).
4. U. R. Evans and H. A. Miley, *Nature*, **139**, 283 (1937).
5. J. A. Allen, *Trans. Faraday Soc.*, **48**, 273 (1952).
6. G. R. Hill, *This Journal*, **100**, 345 (1953).
7. H. G. Oswin and M. Cohen, *ibid.*, **104**, 9 (1957).
8. R. H. Lambert and D. J. Trevoy, *ibid.*, **105**, 18 (1958).
9. U. R. Evans, "The Corrosion and Oxidation of Metals," Chap. XXII, Edward Arnold Ltd., London (1960).
10. J. V. Cathcart and G. F. Petersen, "Studies of Thin Oxide Films on Copper Crystals with an Ellipsometer," Proc. Symp. on Ellipsometry in Measuremen of Surfaces and Thin Films, Washington (1963).
11. K. R. Lawless, Private commmunication.
12. F. W. Young, J. V. Cathcart, and A. T. Gwathmey, *Acta Met.*, **4**, 145 (1956).
13. K. R. Lawless and G. Tyler Miller, Jr., *Acta Cryst.*, **12**, 594 (1959).

Effect of Plastic Deformation on the Anodic Dissolution of Iron in Acids

Z. A. Foroulis

Esso Research and Engineering Company, Florham Park, New Jersey

ABSTRACT

The effect of plastic deformation, introduced by cold-rolling, on the anodic dissolution of iron was investigated using short-time galvanostatic transients in deaerated HCl, H_2SO_4, and $HClO_4$ at 25°C. Cold-rolling was found to have no effect on the anodic Tafel polarization parameters of iron. Anodic Tafel lines in 1*N* HCl have slopes of about 60 mv; the slope is reduced at higher polarizing potentials. For 1*N* H_2SO_4 and 1*N* $HClO_4$ the slopes were about 40 mv and 35 mv, respectively. The results indicate that the dissolution kinetics of iron is controlled by charge transfer, and any effect on the kinetics of iron dissolution, due to surface topography, is not observed. The variation of the anodic Tafel polarization parameters with the nature of the acid anion is explained by specific adsorption of anions on the iron surface in competition with OH^-. The decrease in polarization of iron in HCl solutions at higher polarizing currents ($i > 10^{-2}$ amp cm^{-2}) indicates that adsorbed Cl^- may directly participate in the dissolution process depending on the potential region of polarization.

The published work relating to the influence of mechanical stress on the electrode behavior of metals in aqueous media is contradictory. It is well established that stresses within the elastic range change the potential reversibly by less than 1 mv (1, 2). It is in the range of plastic deformation and its effect on the anodic polarization and corrosion that many investigators have reported conflicting results and interpretations (3-10). It is clear, then, that this problem should be reexamined. This paper reports the results of a laboratory study on the effect of cold-rolling on the anodic polarization behavior of iron in acidic environments, using short-time galvanostatic transients.

Experimental

The cell used for electrochemical measurements consists basically of three compartments; the inner two compartments each approximately 100 ml in volume are removable and fitted through ground glass joints to the center compartment; these compartments contain one auxiliary platinum electrode each and could be deaerated in the same manner as the large center compartment. Electrical communication is achieved by means of fine glass fritted discs. The test electrode was introduced through the center compartment by means of two eccentric joints so that the distance between the test electrode and the top of the Luggin capillary could be adjusted. The tip of the Luggin capillary, about 1 mm OD, was placed about 1 to 2 mm from the electrode, so that screening effects and IR corrections were negligible (11). Additional features of the cell include a capillary stopcock for withdrawing known quantities of solution for analysis, a hydrogen bypass arrangement, and a salt bridge with a Luggin capillary filled with same solution as the cell. Greaseless ground glass joints were used to avoid possible contamination from lubricant.

The electrodes about 2-3 cm^2 total exposed area were cut from remelted (in a helium atmosphere) electrolytic iron castings. The analysis of the iron was 0.009%C, 0.003% N, < 0.003% S, < 0.004% O, < 0.001% Cu, < 0.001% Ni. The castings were cold-rolled in the direction of the long axis by successive passes to a final reduction in thicknesses 20, 40, 50, 60, and 70%. After cold-rolling the specimens were aged at R.T. for about two years. Before cold-rolling, the castings were homogenized in a purified helium atmosphere at 1050°C for about 48 hr. All the reported results were obtained with electrodes made from the above remelted electrolytic iron. The electrode assembly was similar to the one described earlier (12). Surfaces were abraded through 4-0 emery paper, pickled in same solution as the test solution to remove effects of abrading, rinsed thoroughly in double distilled water, and immediately placed in the solution.

Solutions were prepared using reagent grade acids and double distilled water, one distillation of the latter being carried out in dilute alkaline potassium permanganate. The following test solutions were used, 1*N* HCl, 1*N* H_2SO_4, and 1*N* $HClO_4$. Solutions were deaerated by bubbling prepurified hydrogen through the solution for at least 24 hr prior to a run and over the solution during the run. Additional purification of the high-purity commercial hydrogen was done by passing it successively through copper turnings heated at 500°C, ruthenium catalyst at 350°C, and palladium catalyst at R. T. The solutions were preelectrolyzed between platinum electrodes for about 24 hr at about 1.5 ma. Preelectrolyses were carried out at a potential below that corresponding to appreciable evolution of H_2 to avoid significant change of *p*H in the solution. Potentials were measured against a SCE using a vacuum tube millivoltmeter (high impedance). Constant current was obtained through an appropriate assembly of decay resistance units from a high d-c voltage source ($R_{ext} >> R_{cell}$). Figure 1 shows

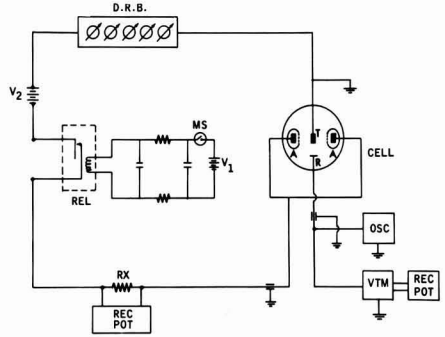

Fig. 1. Experimental setup for polarization measurements. D.R.B., current controlling decay-resistance box; R_x, current measuring resistance; MS, microswitch activating the relay; VTM, high impedance vacuum tube voltmeter; REC. POT., recording potentiometer; REL, relay; V_1, relay driving voltage; V_2, applied d-c voltage; T, test electrode; R, reference electrode; A, auxiliary electrodes (Pt), enclosed in removable compartments fitted with fritted glass disks.

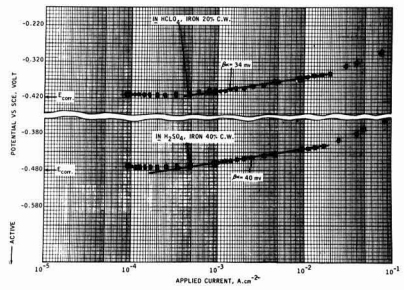

Fig. 2. Anodic polarization of iron in acids (H_2 sat'd), 25°C

the experimental arrangement which is similar to the one reported earlier (13).

In making a run, each electrode was immersed in solution and after a stable corrosion potential was measured, solution samples were withdrawn for Fe^{++} analysis, and immediately after that anodic polarizations were conducted by applying short-time galvanostatic transients. The electrode was subjected to a series of short-time anodic pulses (from 10 to 15 sec in duration) at various increasing current densities. In a few instances, the potential/time transients were recorded photographically on the oscilloscope screen and enlarged several times. The polarization curves were established by plotting the steady-state potential *vs.* the applied current density. Similar polarization curves were established at various decreasing current densities.

Results

The time of sweep for the anodic galvanostatic transients was determined by the time necessary to reach steady-state and was about 10-15 sec. The analysis of galvanostatic transients and their advantages for polarization studies were discussed earlier in the literature (13-15). The applied current density range was about 5×10^{-5} to 1×10^{-1} amp cm^{-2}.

In H_2SO_4 and $HClO_4$ solutions after each pulse the electrode potential returned to the steady-state corrosion potential usually within a few seconds so that further pulses were applied almost continuously ("continuous" polarization). The polarization curves traced with increasing and decreasing current density coincide (Fig. 2). In this figure are shown anodic polarization curves for iron in deaerated sulfuric and perchloric acids. The upper curve is for iron (cold-rolled to 20% reduction in thickness) in 1*N* $HClO_4$. The lower curve is for iron (cold-rolled to 40% reduction in thickness) in 1*N* H_2SO_4.

In the HCl solutions a much longer time of recovery was necessary after each pulse before the electrode potential returned to the steady-state corrosion potential so that further pulses were applied only after sufficient time had elapsed for the electrode potential to return to the steady-state corrosion potential ("interrupted" polarization). When "continuous" polarization was applied in HCl solutions, hysteresis was observed between the ascending and the descending polarization curves (lower curve in Fig. 3). In Fig. 3 are shown anodic polarization curves of iron (cold-rolled to 20% reduction in thickness) in 1*N* HCl. The upper curve was determined by interrupted polarization. The lower curve was determined by continuous polarization, and a hysteresis was observed between the ascending and descending polarization curves.

Cold-rolling was found to have no effect on the anodic Tafel polarization parameters of iron. The anodic Tafel lines in 1*N* HCl have slopes β_{Fe} of about 60 ± 8 mv at c.d. 10^{-4} to 10^{-2} amp cm^{-2}, and are the same for both the annealed and cold-rolled iron as shown in Fig. 4. Tafel slopes in HCl solutions were determined from the ascending polarization curves established by continuous polarization. Interrupted polarization gave identical Tafel slopes.

Figure 5 shows the dependence of the anodic Tafel slopes at c.d. 6×10^{-4} to 2×10^{-2} amp cm^{-2} for iron dissolution on the degree of cold-rolling for H_2SO_4, $HClO_4$ acids. A slope of about 40 ± 10 mv was found for 1*N* H_2SO_4 and about 35 ± 8 mv for 1*N* $HClO_4$. In both acids the slopes were the same for the annealed as well as the cold-rolled specimens.

At current densities higher than 10^{-2} amp cm^{-2}, the Tafel slope in HCl is reduced to about 40 mv or lower, but the reproducibility of the slope in this region of polarization was poor and in many runs a slope of zero was observed. As can be seen from Fig. 3 in HCl, iron does not polarize significantly at anodic current higher than 10^{-2} amp cm^{-2}. In $HClO_4$ and H_2SO_4, at c.d. 2×10^{-2} to 10^{-1} amp cm^{-2} or higher, polarization of iron deviates from the Tafel line and increases appreciably. This deviation is probably due to IR contribution and in particular to concentration polarization due to diffusion limited mass transport

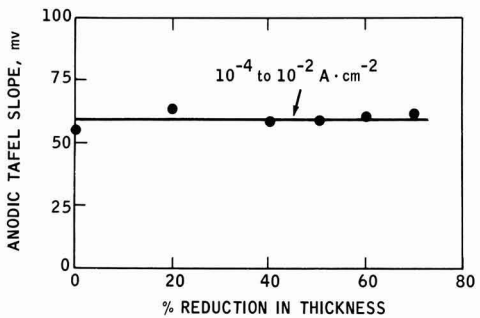

Fig. 4. Dependence of anodic Tafel slope for iron dissolution in 1*N* HCl on the degree of cold-rolling.

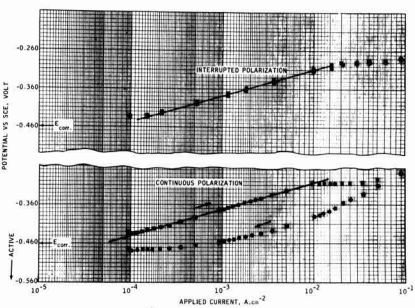

Fig. 3. Anodic polarization of iron, 20% C.W., in 1*N* HCl (H_2 sat'd), 25°C.

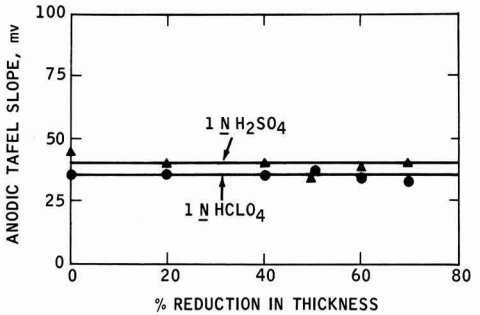

Fig. 5. Dependence of anodic Tafel slope for iron dissolution in acids on the degree of cold-rolling.

of OH^- at the iron surface sites. It is, therefore, rather apparent that the significant decrease in polarizability of iron in HCl at c.d. higher than 10^{-2} amp cm^{-2} is associated with chloride ions which directly participate in the dissolution process by adsorption and eventual complex formation with the iron surface atoms.

Exchange current densities for the anodic dissolution of iron ($i_{o,Fe}$) were determined by extrapolation of the Tafel lines to the reversible potential of iron in each solution tested. The concentration of Fe^{++} in each solution was determined by colorimetric analysis prior to each polarization using the orthophenanthroline colorimetric method (16). Reversible potentials were calculated using the Nernst equation and the activity of Fe^{++} in solution. Activity coefficients were calculated from the Debye-Hückel theory using equation (17)

$$\log f = -\frac{0.358\, Z^2\, \Gamma^{1/2}}{1 + 10^8\, \alpha\, 0.2325\, \Gamma^{1/2}} \qquad [1]$$

where f is the rational activity coefficient for Fe^{2+}, α is the effective diameter of the hydrated Fe^{2+} ($\alpha = 6 \times 10^{-8}$ cm), Z is the charge on each Fe^{2+} in solution, and $\Gamma = 2\, I(m)$ where $I(m) = \sum_i m_i Z_i^2$ is the ionic strength of the solution taking into consideration all the ionic components of the solution. The activity coefficients were calculated because of the lack of experimental data on activity coefficients of Fe^{2+} in HCl solutions. The error in $i_{o,Fe}$ introduced by calculating the activity coefficients by use of Eq. [1] is small in comparison with that produced by small errors in the experimentally determined Tafel slopes.

As can be seen from Table I, for any particular acid solution the $i_{o,Fe}$ was found to be independent of the degree of cold-rolling. However, it varied substantially with the nature of the acid anion and was of the order of 10^{-11} amp cm^{-2} for 1*N* HCl, 10^{-13} for 1*N* H_2SO_4, and 10^{-16} for 1*N* $HClO_4$. The experimental analyses for Fe^{2+} in solution for a typical set of runs, together with the calculated activities and reversible potentials ($E_{Fe,Fe2+}$) are given in Table I.

Anodic polarization ($E_{meas'd} - E_{corr}$) at 10 ma cm^{-2} determined for iron in various solutions from the polarization curves as a function of per cent reduction in thickness by cold-rolling is given in Fig. 6. Figure 6 shows that the anodic polarization at 10 ma cm^{-2} is the same for the annealed iron as well as iron cold-rolled down to 70% reduction in thickness. However, the anodic polarization depends on the acid anion and is about 145 mv in 1*N* HCl, about 65 mv in 1*N* H_2SO_4, and about 52 mv in 1*N* $HClO_4$. Similar independence of the anodic polarization on the degree of cold-rolling was observed at an applied current of 2 ma cm^{-2}.

Table I. Dependence of exchange current for iron dissolution in acids on the degree of cold-rolling

Acid	% Thickness reduction by cold-rolling	Exchange current $i_{o,Fe}$, amp/cm²	Fe^{2+} Concentration M	Fe^{2+} Activity M	$E_{rever.}$, calc, V
1*N* HCl	Annealed	7.9×10^{-12}	198×10^{-5}	4.1×10^{-6}	−0.600
1*N* HCl	20	6.3×10^{-11}	1.5×10^{-5}	3.1×10^{-6}	−0.603
1*N* HCl	40	1×10^{-11}	3.5×10^{-5}	7.3×10^{-6}	−0.592
1*N* HCl	50	5×10^{-12}	2.37×10^{-5}	4.9×10^{-6}	−0.597
1*N* HCl	60	1.6×10^{-11}	2.67×10^{-5}	5.5×10^{-6}	−0.595
1*N* HCl	70	7.9×10^{-11}	1.98×10^{-5}	4.1×10^{-6}	−0.599
1*N* H_2SO_4	Annealed	1.2×10^{-13}	2.04×10^{-5}	3.8×10^{-6}	−0.600
1*N* H_2SO_4	20	2.5×10^{-13}	1.35×10^{-5}	2.5×10^{-6}	−0.606
1*N* H_2SO_4	40	2.5×10^{-13}	3.27×10^{-5}	6.08×10^{-6}	−0.594
1*N* H_2SO_4	50	1×10^{-13}	1.26×10^{-5}	2.34×10^{-6}	−0.607
1*N* H_2SO_4	60	1.2×10^{-14}	2.0×10^{-5}	3.7×10^{-6}	−0.601
1*N* H_2SO_4	70	6.3×10^{-14}	1.84×10^{-5}	3.42×10^{-6}	−0.602
1*N* $HClO_4$	Annealed	3.1×10^{-16}	2.2×10^{-5}	4.6×10^{-6}	−0.599
1*N* $HClO_4$	20	7.9×10^{-16}	1.9×10^{-5}	3.9×10^{-6}	−0.600
1*N* $HClO_4$	40	6.3×10^{-17}	2.03×10^{-5}	4.2×10^{-6}	−0.598
1*N* $HClO_4$	50	1.6×10^{-16}	1.55×10^{-5}	3.21×10^{-6}	−0.603
1*N* $HClO_4$	60	5×10^{-17}	3.45×10^{-5}	7.13×10^{-6}	−0.592
1*N* $HClO_4$	70	1×10^{-16}	2.51×10^{-5}	5.2×10^{-6}	−0.596

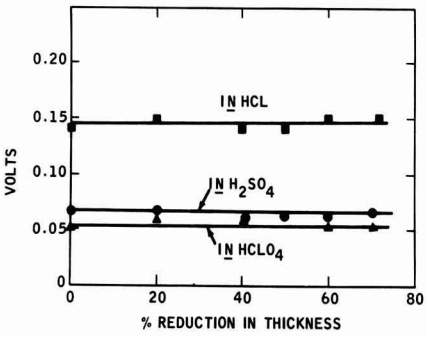

Fig. 6. Dependence of anodic polarization ($E_{meas'd} - E_{corr}$) at 10 ma/cm² for iron dissolution in acids on the degree of cold-rolling, 25°C.

Discussion

It is well known that an equilibrium metal surface is characterized by a distribution of steps each having a large population of kinks. The nonequilibrium metal surface has, in addition, a large distribution of steps arising from dislocations having a component of the Burger's vector normal to the surface and numerous other steps arising from the mechanism of growth of that particular surface.

An annealed polycrystalline iron specimen is bounded by numerous such surfaces of various crystallographic orientations, which are separated by ordinary high angle grain boundaries of rather high surface energy. Cold-rolling such an iron specimen introduces numerous dislocation loops which are arrayed in their slip planes. They are prevented from retreating into their sources when the deforming force is no longer applied by formation of jogs as a result of intersection with other dislocations, by becoming "locked" by interaction with other dislocations, because their source may have moved out of the slip plane in which the loops have originated, or because parts of the loops may have emerged at a free surface or into a grain boundary. During severe deformation, arrays of dislocations are produced on several intersecting sets of slip planes, so that numerous parts of dislocation loops are emerging at a free surface. Severe cold-working is known to increase the density of dislocations from perhaps 10^8 for annealed iron to 10^{12} dislocations/cm² (18).

Another major effect of deformation is on the orientations of the grains. It is known that the deformation of a randomly oriented polycrystalline specimen results in material with a preferred orientation, the grains tending to approximate progressively to one or more well-defined orientations. Cold-rolling of iron produces a preferred orientation of the (001) crystal face parallel to the rolling plane (19). In addition to a high content of dislocations, cold-rolling produces a considerable excess of vacancies as a result of the movement of jogs in directions that do not correspond to slip. However, it is expected the excess vacancies anneal during the long R.T. aging of our specimens after cold-rolling.

Let us now consider the dissolution of a specimen bounded by such surfaces in contact with an electrolyte. At temperatures below the critical temperature of surface roughening (20) such surfaces are expected to be characterized by large numbers of equilibrium and nonequilibrium steps and kinks. Consequently, such surfaces have been considered (7) to be able to dissolve at least initially by the lateral motion of such steps in accordance with the crystal growth and dissolution theories (21-23). Jenkins (24) found that under certain conditions the dislocations played a role in the dissolution process of the (100) copper surface at low current densities in deaerated

solutions of acidified $CuSO_4$. He showed that at current densities of about 2 $\mu a/cm^2$ dissolution occurred only from the steps on the surface that result because of the difficulty of preparing a perfect crystal face. At current densities of about 10 $\mu a/cm^2$, pitting attack was observed at dislocations until finally the pits grew in size and a faceted surface resulted. The above experiments were carried out under low overpotential, to which crystal growth and dissolution theories might be applicable. However, during anodic dissolution of iron in acid solutions, the anodic overpotential is much higher, and it probably plays a dominant role in determining the kinetically slow step in the over-all reaction path of anodic iron dissolution.

It is more likely that at the high overpotentials (large driving free energy) necessary to establish the anodic polarization curve for iron homogeneous dissolution occurs anywhere on the surface, and any effect due to surface topography is lost. This is in accord with the present data indicating that, in the three acid solutions used, cold-rolling was found to have no effect on the Tafel parameters ($i_{o,Fe}$, β_{Fe}) for anodic dissolution of iron (Fig. 4 and 5 and Table I), or the anodic polarization (Fig. 6).

In sulfuric acid solution the observed Tafel slope of 40 mv/decade, *i.e.*, $2/3(2.303RT/\mathbf{F})$ in the region of current density 6×10^{-4} to 1.5×10^{-2} amp cm^{-2} is in agreement with results obtained by Bockris *et al.* (13) and more recently by Kelly (25) for iron in acidic sulfate solutions. For the anodic dissolution of iron in sulfuric acid solutions, the mechanism proposed by Bockris *et al.* (13) can be expressed in terms of the following equations.

$$Fe + OH^- \rightleftarrows Fe(OH)_{ads} + e^- \quad [2]$$

$$Fe(OH)_{ads} \rightarrow (FeOH)^+ + e^- \text{ (rate determining)} \quad [3]$$

$$(FeOH)^+ = Fe^{++} + OH^- \quad [4]$$

in which the surface species $Fe(OH)_{ads}$ act as a reaction intermediate.

In 1*N* HCl solution the observed Tafel slope of 60 mv/decade, *i.e.*, $(2.303RT/\mathbf{F})$ during interrupted polarization experiments or during continuous polarization from the ascending curve, in the region of current density 10^{-4} to 10^{-2} amp cm^{-2} is consistent with the following mechanism

$$Fe + OH^- \rightarrow Fe(OH)_{ads} + e^- \text{ (rate-determining)} \quad [5]$$

$$Fe(OH)_{ads} \rightarrow Fe(OH)^+ + e^- \text{ (rate-determining)} \quad [6]$$

$$Fe(OH)^+ \rightleftarrows Fe^{++} + OH^- \quad [7]$$

in which the OH^- competes with the Cl^- for the metal surface sites.

Tafel slopes of 54 mv/decade in chloride solutions were reported by Makrides *et al.* (26), 68 mv/decade by Stern and Roth (27), and 30 mv/decade in HCl ($pH > 1.5$) by Lorenz *et al.* (28). The difference in Tafel slopes obtained by the various investigators can be attributed to the various chloride anion concentrations and the experimental techniques used. Recently, it has been recognized (29) that short-time galvanostatic transients offer many advantages over conventional polarization techniques which often give rise to complex results difficult to interpret.

In 1*N* $HClO_4$ solution the observed Tafel slope of 35 mv/decade, *i.e.*, $(2.303RT/2\mathbf{F})$ is consistent with the following mechanism:

$$Fe + OH^- \rightleftarrows Fe(OH)_{ads} + e \quad [8]$$

$$Fe(OH)_{ads} \rightarrow Fe^{++} + OH^- + e \text{ (rate-determining)} \quad [9]$$

The observed Tafel slope is in agreement with the results of Bonhoeffer and Heusler (30) who found for iron in perchlorate solutions at 20°C a slope of 30 mv/decade.

The observed hysteresis in the anodic polarization of iron in HCl during continuous polarization (Fig. 3) is probably due to adsorption of Cl^- and the eventual complex formation with the iron surface atoms at higher polarizing potentials. This phenomenon will be discussed in more detail in another paper (31). Participation of anions such as Cl^-, Br^-, I^- in the dissolution of cadmium and indium amalgams was proposed by Kolotyrkin (32). Heusler and Cartledge (33) also suggested that the iodide ion participates in the anodic reaction of iron dissolution.

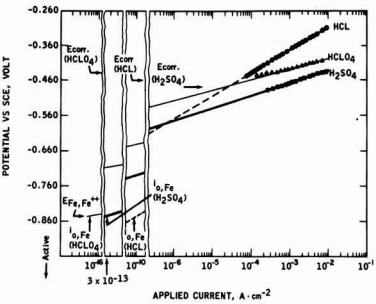

Fig. 7. Anodic polarization curves for iron illustrating the influence of the Tafel slope, β, and the ferrous ions activity in solution, $\alpha_{Fe^{++}}$, on the exchange current, $i_{o,Fe}$, in three acids.

The large variation of the exchange currents for anodic dissolution of iron ($i_{o,Fe}$) with the nature of the acid anion shown in Table I can be realized if one considers the difference in the Tafel slopes for the various acids and the low activity of Fe^{++} in solution, necessitating extrapolation of the Tafel slopes to the fairly active potential of the reversible iron electrode in these solutions ($E_{Fe,Fe^{++}}$) in order to establish the $i_{o,Fe}$. This is shown in Fig. 7. It is also obvious that a small error in the experimentally determined Tafel slopes produces a large error in $i_{o,Fe}$. This explains the large scatter in $i_{o,Fe}$ values observed (Table I) for the same acid.

In determining the reversible electrode potential $E_{Fe,Fe^{++}}$ using the Nernst equation, the same value of the standard electrode potential $E^o_{Fe,Fe^{++}} = -0.440v$ *vs.* SHE was used for both cold-rolled and annealed iron electrodes. This is justified because of the lack of precise data on the effect of cold-rolling on the reversible standard electrode potential of iron, which in any case is very small.[1]

The lack of any effect of cold-rolling on the Tafel polarization parameters of iron dissolution in acids and also the acid anion dependence of this reaction suggest that at high polarizing potentials necessary to establish the anodic polarization curves (large driving free energy) homogeneous dissolution takes place directly from the surface and it is independent of the number of kink sites on the iron surface. The rate of anodic dissolution is kinetically controlled by the charge transfer step. The nature of the rate-determining charge transfer step depends on the nature of the acid anion as can be seen from Eq. [3], [5], [6], and [9].

Recently, Greene and Saltzman (8) reported an increase, with plastic deformation, of the exchange current density for anodic dissolution of iron and steel in 1*N* H_2SO_4. They interpreted their results to indicate that iron dissolves during anodic polarization, preferentially from dislocation sites because of the lower bonding energy of iron atoms at such sites. This explanation, however, is not compatible with the small increase in residual energy (approximately 5 cal/g) of severely cold-worked iron (34), and in

[1] For iron the increase in internal energy by severe cold-working was measured calorimetrically to be about 5 cal/g (34). Neglecting entropy effects, this value of enthalpy change corresponds to a change of potential of about 6 mv (35). However, as shown by Titchener and Bever (34) the change in entropy by cold-working a metal is positive and thus the change of potential due to cold-working, corrected for entropy effects, should be less than 6 mv.

particular with the high overpotentials involved during anodic polarization of iron in 1N H_2SO_4. Our own work, on the other hand, has not shown an effect of plastic deformation on the anodic Tafel polarization parameters. The increase noted by Greene and Saltzman must, therefore, have another explanation. The above authors reported that the specimens (wires) after torsional deformation, by twisting them a number of times, were degreased in benzene, rinsed in water, and dried before testing without additional polishing of the twisted wire surface. It is possible, therefore, that the torsional straining produced an increase of true surface area with accompanying higher exchange current densities.

It remains our conclusion, therefore, that at high overpotentials the anodic iron dissolution is kinetically controlled by the charge transfer step, and it is independent of the number of kink sites introduced by cold work on the iron surface.

Details on the kinetics of anodic dissolution of iron in various acidic environments are not given in the present paper since the purpose of this report is to discuss the effect of cold-rolling on the anodic polarization behavior of iron. However, the kinetics of anodic dissolution of iron will be discussed in detail in another report.

Acknowledgment

The author is grateful to Esso Research and Engineering Company for permission to publish the work. He also acknowledges the skillful assistance of Mr. A. W. Putnoky who conducted the experimental measurements.

Manuscript received Nov. 17, 1965; revised manuscript received March 10, 1966. This paper was presented at the Buffalo Meeting, Oct. 10-14, 1965.

Any discussion of this paper will appear in a Discussion Section to be published in the December 1966 JOURNAL.

REFERENCES

1. G. T. Yang Ling Horne and C. M. Pound, "Physical Metallurgy of Stress-Corrosion Fracture," p. 29, Interscience Publishers Inc., New York (1959).
2. K. Nobe, E. Baum, and F. W. Sayer, *This Journal*, **108**, 97 (1961).
3. H. Gerischer and H. Rickert, *Z. Metallk.*, **46**, 681 (1955).
4. Z. A. Foroulis and H. H. Uhlig, *This Journal*, **111**, 522 (1964).
5. M. T. Simnad and U. R. Evans, *Trans. Faraday Soc.*, **46**, 176 (1950).
6. I. Sekerka and O. Vanicek, *Coll. Czech. Chem. Comm.*, **22**, 705 (1957).
7. T. Hurlen, *Electrochim. Acta*, **7**, 653 (1962).
8. N. D. Greene and G. A. Saltzman, *Corrosion*, **20**, 293t (1964).
9. H. E. Bühler and W. Schwenk, *Z. Metallk.*, **56**, 24 (1965).
10. A. Windfeldt, *Electrochim. Acta*, **9**, 1139 (1964).
11. S. Barnartt, *This Journal*, **99**, 549 (1952); *ibid.*, **106**, 722 (1959).
12. M. Stern and A. C. Makrides, *ibid.*, **107**, 782 (1960).
13. J. O'M. Bockris, D. Drazic, and A. R. Despic, *Electroch. Acta*, **4**, 325 (1961).
14. W. Mehl and J. O'M. Bockris, *J. Chem. Phys.*, **27**, 818 (1957); *Can. J. Chem.*, **37**, 190 (1959).
15. H. Gerischer, *This Journal*, **62**, 256 (1958).
16. E. B. Sandell, "Colorimetric Determination of Traces of Metals," p. 271, Interscience Publishers Inc., New York (1944).
17. B. E. Conway, "Electrochemical Data," p. 102, Elsevier Publishing Co., Amsterdam (1952).
18. L. Darken in "The Physical Chemistry of Metallic Solutions and Intermetallic Compounds," Vol. II. 4G, Nat. Phys. Lab. Symp. No. 9 (London) (1959).
19. "Structure of Metals," C. Barrett, 2nd Ed, p. 446, McGraw-Hill Book Co. (1952).
20. N. Cabrera, The Structure of Crystal Surfaces. *Discussion Faraday Soc.*, **28**, 16 (1959).
21. W. K. Burton, N. Cabrera, and F. C. Frank, *Proc. Roy. Soc.*, **A243**, 299 (1951).
22. M. Fleischmann and H. R. Thirsk, *Electrochim. Acta*, **2**, 22 (1960).
23. T. Hurley, *ibid.*, **8**, 609 (1963).
24. L. H. Jenkins and J. O. Stiegler, *This Journal*, **109**, 467 (1962).
25. E. J. Kelly, *ibid.*, **112**, 124 (1965).
26. A. C. Makrides, N. W. Komodromos, and N. Hackerman, *ibid.*, **102**, 363 (1955).
27. M. Stern and R. M. Roth, *ibid.*, **104**, 390 (1957).
28. W. Lorenz, H. Yamaoka, and H. Fisher, *Ber. Bunsenges. Physik. Chem.*, **67**, 932 (1963).
29. W. Mehl and J. O'M. Bockris, *J. Chem. Phys.*, **27**, 818 (1957); *Can. J. Chem.*, **37**, 190 (1959); H. Gerischer, *This Journal*, **62**, 256 (1958).
30. K. F. Bonhoeffer and K. E. Heusler, *Z. Physik. Chem.*, **8**, 390 (1956).
31. Z. A. Foroulis, *This Journal*, To be submitted for publication.
32. J. M. Kolotyrkin, *ibid.*, **108**, 209 (1961).
33. K. E. Heusler and G. H. Cartledge, *ibid.*, **108**, 731 (1961).
34. A. Titchener and M. Bever, *Prog. in Metal Phys.*, **7**, 247 (1958).
35. Z. A. Foroulis and H. H. Uhlig, *This Journal*, **112**, 1177 (1965).

The Role of the Anion in the Anodic Dissolution of Magnesium

P. F. King[1]

Metallurgical Laboratory, The Dow Metal Products Company, Division of The Dow Chemical Company, Midland, Michigan

ABSTRACT

In a number of aqueous environments the increase in the corrosion rate (i_c) of magnesium with an increase in impressed anodic current (i) is expressed by

$$\frac{d\, i_c}{di} = \tau_a$$

where τ_a is the transport number of the anions of the electrolyte. This adds confirmation to the viewpoint that film damage by anions rather than metal spalling or the production of monovalent magnesium ions is the chief contributor to the current inefficiency observed with magnesium anodes. The same equation holds for the decrease in corrosion rate of magnesium with applied cathodic current in acids, indicating that anion supply to the metal surface is controlling that process, also.

Because of its low equivalent weight and its active potential under load, magnesium has become important as an anode for cathodic protection and in primary cells. However, the full benefit of magnesium's low equivalent weight is not realized. Instead, the anode consumption is substantially greater than that

[1] Present address: Parker Rust Proof Division, Hooker Chemical Corporation, Detroit, Michigan.

calculated from Faraday's law and the formation of divalent magnesium ions as the sole electrode process. This excess metal loss results in an increase in the amount of hydrogen at the anode above that evolved on open circuit in contrast to the decrease observed on other, less active metals. Since the decrease has been known historically as the difference effect (1), the increase as observed with magnesium has long been known as the negative difference effect.

The causes for the coulombic inefficiency of the magnesium anode have been the basis for much research and conjecture. Explanations that have been offered for the inefficiency include: (a) the formation of metastable, monovalent magnesium ions as well as the divalent ions (2-5); (b) the loss of metal by spalling (6-8); and (c) corrosion that is accelerated through damage to the protective film by the impressed current (9, 10).

In an earlier publication, Robinson and King (10) expressed the view that the film damage explanation offered a reasonable and sufficient description of the excess consumption, the steady-state potential, and the transient potential behavior of the magnesium anode. According to this view, the consumption of the anode (i_t) can be represented as the sum of the applied and local action currents (i and i_c^o, respectively) and the excess weight loss caused by the applied current [$f(i)$]

$$i_t = i + f(i) + i_c^o \qquad [1]$$

In many environments, as discussed previously (10), $f(i)$ has been shown to be directly proportional to i, so that for these environments Eq. [1] can be rewritten

$$i_t = i + ki + i_c^o \qquad [2]$$

If we define the excess corrosion rate i_c as

$$i_c = i_t - i \qquad [3]$$

from Eq. [2] we have

$$i_c = ki + i_c^o \qquad [4]$$

and differentiation gives

$$\frac{di_c}{di} = k \qquad [5]$$

We suggested previously that this is true because the number of anions transported to the anode and, therefore, the amount of film damaging soluble magnesium salts at the anode increases linearly with current. Thus, a logical extension of the above reasoning is that k in Eq. [2], [4], and [5] and the anion transport number τ_a should be simply related. Indeed since both are dimensionless numbers, they might be equal. The work to be described here was planned to test this hypothesis.

Experimental Details

The experiments were carried out in the following manner. Primary magnesium was chosen for study because of its relative purity (98.5%), availability, and the unlikelihood, as deduced from the work reported by Robinson and George (11), that impurities have much effect on the efficiency of the magnesium anode at high enough current densities. A 2.5 × 0.5 cm cylindrical primary magnesium anode was mounted in a glass holder as previously described (10) and immersed in a round bottom flask containing additional openings for platinum working electrodes and a capillary reference probe. The latter was used only to insure that the anode had not become passive during the measurements.

The experiments were run at room temperature (20° ± 2°C) in stagnant solutions made from chemically pure salts and distilled water. The experiments in acidic environments were usually of 5-min duration. In salt solutions under anodic drain, times were adjusted to give weight losses of the order of 50 mg. Where currents greater than 100 ma/cm² were required, the anode area was reduced by the use of electroplater's tape. Before use, the specimens were pickled for 1 min in the so-called acetic-nitrate pickle (5% $NaNO_3$, 40% acetic acid, remainder distilled water), thoroughly rinsed and dried before weighing. At the conclusion of electrolysis they were rinsed with distilled water, cleaned until cleaning action stopped at 90°C in 20% chromic acid containing a pinch of $AgNO_3$, rinsed, and once again dried thoroughly before weighing. Where electroplater's tape was used, this final drying took considerable time.

Results and Discussion

In order to test the hypothesis that the constant k in Eq. [2], [4], and [5] is equivalent to the transport number of the anion of the electrolyte under study, the anodic dissolution rate of magnesium was tested at a number of current densities in six electrolytes selected for wide variation in transport properties. The results of these tests are shown in Fig. 1-5. In Fig. 6 results are summarized with the anion transport numbers from the literature (12) compared with the constant k as calculated from Eq. [2]; it should be pointed out that in some cases the literature transport numbers are extrapolated ones. The agreement, while not perfect, is good enough and covers a wide enough range of values to suggest that Eq. [5] may be rewritten

$$\frac{di_c}{di} = \tau_a \qquad [6]$$

a strikingly simple expression, and one which adds additional credence to the theory developed in the earlier publication.

It now becomes apparent why the observed anode efficiency of magnesium almost always lies between 50 and 100% if measurements are made at high enough current densities that the open-circuit corrosion is a trivial portion of the total anode consumption. The efficiency under these conditions is defined as

$$\% \text{ eff} = \frac{i}{i + i_c} \times 100 \qquad [7]$$

or, substituting τ_a for k in Eq. [4] and then combining Eq. [4] and [7] (continuing to neglect i_c^o)

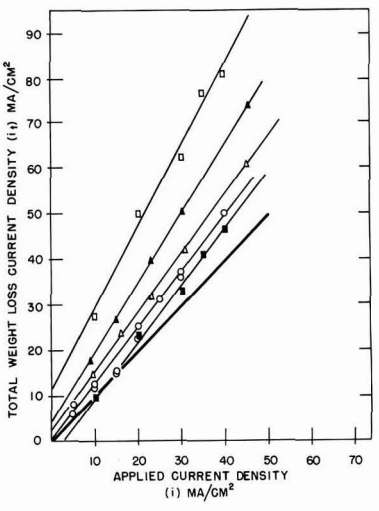

Fig. 1. Weight loss current density as a function of applied anodic current density for primary magnesium in 1N potassium malonate (○); 0.1N LiCl (□); 0.1N $KC_2H_3O_2$ (■); 1N $KCHO_2$ (△); and 2N $MgCl_2$ (▲). The heavy line represents Faraday's law.

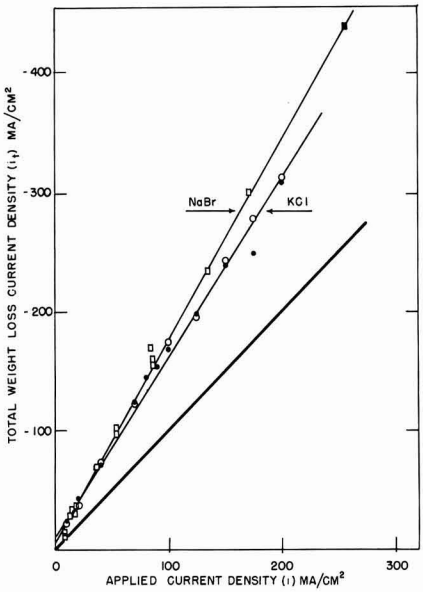

Fig. 2. Weight loss current density as a function of applied anodic current density for primary magnesium in 1*N* NaBr (□); 1*N* KCl (○); and 0.1*N* KCl (●). The heavy line represents Faraday's law.

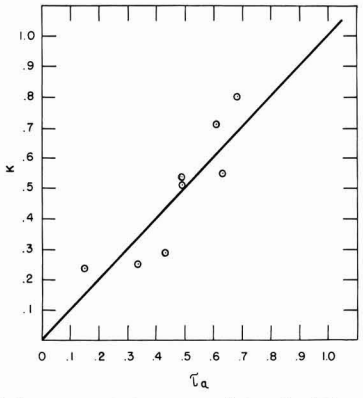

Fig. 3. Comparison of the constant *k* from Eq. [5] with literature τ_a values. The line is theoretical; that is, it assumes $k = \tau_a$.

$$\% \text{ eff} = \frac{i}{i + \tau_a i} \times 100 = \frac{100}{1 + \tau_a} \qquad [8]$$

and since τ_a is bounded by 0 and 1, the efficiency must be bounded by 100 and 50%.

Table I shows a test of Eq. [8] as a method for predicting the limiting efficiencies. The agreement between the measured and the predicted efficiencies suggests that Eq. [8] will be of practical value in the selection of electrolytes.

The results suggest that each anion equivalent which reaches the magnesium surface removes, in some manner, an equivalent of magnesium over and above that which is put into solution by the external anodic current. The exact mechanism by which this occurs is still unclear. However, since the limiting anodic efficiency of magnesium thus appears to bear a quantitative relationship to the electrochemical properties of

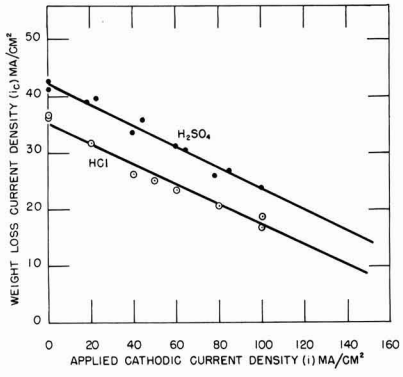

Fig. 4. Weight loss current density as a function of applied cathodic current density for primary magnesium in H_2SO_4 at *p*H 1.1 and in HCl at *p*H 1.1. The lines are drawn with slopes corresponding to τ_a in $H_2SO_4 = 0.18$; τ_a in HCl = 0.17.

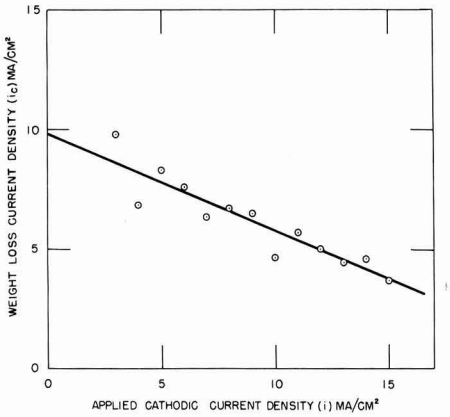

Fig. 5. Weight loss current density as a function of applied cathodic current density for primary magnesium in 1*N* $NaC_2H_3O_2$ containing 0.1*N* $HC_2H_3O_2$.

the environment, it seems unlikely that Mg^+ formation and metal spalling can be an important part of the process. It should be pointed out that there is no doubt that some magnesium spalling does occur. One can sometimes see metal in the anodic corrosion products. If one tries to liberate hydrogen from this corrosion product with acid in these cases, however, one can account for at most only a few per cent of the wasteful corrosion. In addition, only a few per cent of the corrosion product appears to be solid metal by x-ray diffraction examination.

It also appears that τ_a is the appropriate coefficient for the linear reduction of the corrosion rate of magnesium in acids with applied cathodic current which was observed by Coates (13) and Roald and Beck (14). These authors did not attempt to explain this linearity beyond Roald and Beck's comment that

Table I. Comparison of experimental and theoretical efficiency values

Salt	Efficiency calculated from: Concentration, *N*	Efficiency calculated from: Literature transport numbers, %	Experimental efficiency, %
$MgCl_2$	2	61	65
$KCHO_2$	1	70	78
$KC_2H_3O_2$	0.1	75	80
LiCl	0.1	60	56
Potassium malonate	2	87	81
NaBr	1	62	59
KCl	1	67	66
KCl	0.1	67	65

transport within the diffusion layer might be responsible. In contrast to the anodic case where the detailed mechanism remains obscure to the author, a reasonable physical picture of this situation can be proposed.

It is generally agreed (13-16) that on open circuit the dissolution of magnesium is controlled by the diffusion of acid to its surface. The over-all reaction is

$$Mg + 2HA \rightarrow H_2\uparrow + MgA_2$$

where A stands for the anion of a magnesium salt which must be soluble to prevent film growth with concomitant stifling of the reaction. Because preservation of charge requires that both protons and anions diffuse to the surface at the same rate, protons to provide the cathodic reaction and anions to sustain the solubility of magnesium are equally available to sustain dissolution.

If now magnesium reacting with pure aqueous acid is made a cathode, the current carried by protons reaching the magnesium surface will be increased by $\tau_{H+}i$. However, since the applied cathodic current must liberate hydrogen at the cathode at a rate equal to i, it follows that

$$i_c = i_c^o + \tau_{H+}\, i - i = i_c^o - (1 - \tau_{H+})i \qquad [9]$$

Because $(1 - \tau_{H+}) = \tau_a$ for the pure acid, Eq. [9] can be restated as

$$i_c = i_c^o - \tau_a i \qquad [10]$$

which is the same equation one would deduce if anion supply, being reduced by transport away from the surface by cathodic current, were controlling the dissolution rate. That these equations do apply to the present case is shown by Fig. 4, which compares the reduction of i_c by impressed cathodic current for magnesium in dilute H_2SO_4 and dilute HCl at pH 1.1 with lines having slopes of —0.18 and —0.17 corresponding to the respective τ_a values for each acid.

It appears that distinction can be made between the relative importance of proton transport and anion transport by using a buffer wherein the dissociation of the acid is greatly suppressed. Figure 5 shows the results for the dissolution of a magnesium cathode in 0.1*N* HOAc plus 1*N* NaOAc. In this system τ_{H+} should be trivial. Thus, τ_a should be approximately 0.42, which is the transport number for acetate ions in 1*N* NaOAc, while $(1 - \tau_{H+})$ should be very close to unity. The line in Fig. 5 has a slope of —0.41. Therefore, it appears that under impressed cathodic current

$$i_c = i_c^o - \tau_a i > i_c^o - (1 - \tau_{H+})i \qquad [11]$$

This suggests that the rate of supply of anions rather than the rate of supply of protons controls the rate of dissolution of magnesium in acids. A simple rationale for this result is that so long as film growth is thwarted by the formation of soluble reaction products, the reduction of water is able to sustain the rate.

Summary

The excess corrosion of the magnesium anode at currents high with respect to open-circuit corrosion currents appears to be related quantitatively to the rate of arrival of the anions of the electrolyte at the anode surface. That is, the excess corrosion is equal to $\tau_a i$, where τ_a is the transport number of the anion involved and i is the applied anodic current. Thus, the increase in the wasteful corrosion rate with increasing anodic current, di_c/di is simply τ_a.

Correspondingly, in acids the corrosion of magnesium is decreased by cathodic current since anions are thereby transported away from the magnesium surface. The proportionality constant between the applied current and the decrease in corrosion rate again is τ_a.

These observations support the view that anion promoted film-damage and a resultant more or less direct reaction of the underlying magnesium with water is responsible for the nonfaradaic corrosion of the magnesium anode in aqueous environments.

Manuscript received Aug. 20, 1965; revised manuscript received Feb. 20, 1966. This paper was presented at the Buffalo Meeting, Oct. 10-14, 1965.

Any discussion of this paper will appear in a Discussion Section to be published in the December 1966 JOURNAL.

REFERENCES

1. U. R. Evans, "The Corrosion and Oxidation of Metals," p. 321, Edward Arnold (Publishers) Ltd., London (1960).
2. R. L. Petty, A. W. Davidson, and J. Kleinberg, *J. Am. Chem. Soc.*, **76**, 363 (1954).
3. M. D. Rausch, W. E. McEwen, and J. Kleinberg, *Chem. Rev.*, **57**, 417 (1957).
4. A. W. Davidson in "The Encyclopedia of Electrochemistry," p. 49, C. E. Hempel, Editor, Reinhold Publishing Co., New York (1964).
5. W. E. McEwen, *ibid.*, p. 53.
6. M. E. Straumanis, *ibid.*, p. 44.
7. M. E. Straumanis and B. K. Bhatia, *This Journal*, **110**, 357 (1963).
8. W. J. James, M. E. Straumanis, B. K. Bhatia, and J. W. Johnson, *ibid.*, 1117.
9. H. A. Robinson, *Trans. Electrochemical Soc.*, **96**, 499 (1946).
10. J. L. Robinson and P. F. King, *This Journal*, **108**, 36 (1961).
11. H. A. Robinson and P. F. George, *Corrosion*, **10**, 182 (1954).
12. R. Parsons, "Handbook of Electrochemical Constants," Butterworth Scientific Publications, London (1959).
13. G. E. Coates, *J. Inst. Metals*, **71**, 457 (1945).
14. B. Roald and W. Beck, *This Journal*, **98**, 277 (1951).
15. C. V. King and M. M. Braverman, *J. Am. Chem. Soc.*, **54**, 1744 (1932).
16. C. V. King and W. H. Cathcart, *ibid.*, **59**, 63 (1937).

Correction

In the paper "Concentration Gradients at Horizontal Electrodes" by R. N. O'Brien which appeared in the April 1966 issue of the *Journal*, pp. 389-392, the principal formula was printed incorrectly. It should be

$$AC_{(x,t)} = \frac{2\sqrt{Dt/l^2}\, Ilt^-}{nFD}\ \text{ierfc}\ \frac{1 - x/l}{2\sqrt{Dt/l^2}}$$

The Oxidation of GaP and GaAs

M. Rubenstein

Westinghouse Research Laboratories, Pittsburgh, Pennsylvania

ABSTRACT

Thermal oxidation of GaP and GaAs by oxygen has been studied. GaP on oxidation undergoes a violent exothermic reaction at 1130° ± 20°C. The products of the oxidation of GaP are the christobalite form of $GaPO_4$ as a primary product and β-Ga_2O_3 as a secondary product (about 5 w/o). GaAs on oxidation undergoes a mild exothermic reaction at 840° ± 10°C. The products of this reaction are β-Ga_2O_3 as a primary product and the low quartz form of $GaAsO_4$ as a secondary product (about 10 w/o). The $GaAsO_4$ at temperatures higher than 1000°C decomposes to As_2O_5 + β-Ga_2O_3. The above statements are made on the basis of x-ray diffraction data, change in weight data, and wet chemical analyses. On the basis of this data, it is concluded that thermal oxide masking should be readily applicable to GaP and that thermal oxide masking should not be applicable to GaAs.

GaP and GaAs are usually considered very stable compounds, especially with respect to their reactivity toward oxygen. At temperatures less than 800°C this is more or less true. A film might form on the surface at temperatures less than 800°C, but the bulk of the material would not change with respect to weight, crystal structure, or other physical parameters. The thermal oxide masking of GaAs was investigated (1) but was found to be not readily applicable.

Experimental

Oxygen was passed over the sample to be oxidized at a flow rate of about 200 cc/min. A Pt-Pt 10% Rh thermocouple was tied to the quartz boat containing the sample, using a platinum wire insulated from the thermocouple. A hinged split furnace with a 1¼ in. bore accommodated the quartz tube. A variable autotransformer and a Wheelco Capacitrol Model 402 were used to control the temperature. The oxygen was dried using a P_2O_5 packed vertical tower and a CO_2-acetone cold trap.

Weight change determinations were made to the nearest tenth of a milligram. Sample sizes were usually about half a gram. Wet chemical analyses were made on some of the oxidized GaP and GaAs samples. Phosphorus was determined by the precipitation of magnesium ammonium phosphate in the presence of citric acid. This precipitate was ignited, thermally decomposed, and weighed as $Mg_2P_2O_7$. Arsenic was extracted from a 2*N* HCl solution with diethyl-ammonium diethyldithiocarbamate in chloroform. The extracted arsenic was oxidized and determined by the photometric molybdenum blue method.

X-ray diffraction studies were made using a 57.32 mm radius Straumanis-type camera with nickel filtered copper radiation.

Results

GaAs.—If GaAs, on being oxidized by oxygen, produced only β-Ga_2O_3, the weight loss would be 35.20%. If $GaAsO_4$ were the product, there would be a weight gain of 44.25%. When GaAs was heated above 700°C, a weight loss was observed which increased with temperature (see Fig. 1). In the range of temperature between 830°-850°C, an exothermic reaction took place. Between 850° and 965°C the weight loss was 30-32%. At a temperature of 1000°C and higher, there was a total weight loss of about 35.4%.[1] Samples heated for longer periods of time, at temperatures under 830°C, showed larger decreases in weight than samples heated for shorter periods of time, at the same temperature (see Fig. 1, samples heated at 760°C).

X-ray diffraction studies showed that the products of the oxidation of GaAs between 850° and 965°C were primarily β-Ga_2O_3 (3) with a minor constituent of the low quartz form of $GaAsO_4$ (2) (about 10%). Samples heated at temperatures of 1000°C and above showed only β-Ga_2O_3 as a product.

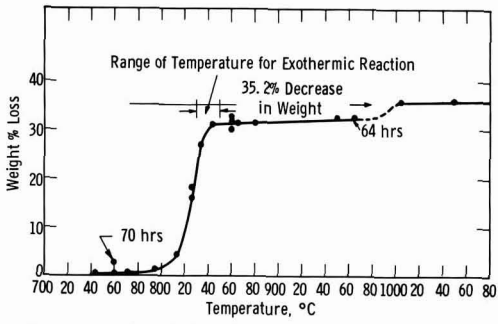

Fig. 1. Oxidation of GaAs in oxygen. Per cent weight loss vs. temperature. All points on this curve are for samples fired for 20 ± 2 hr, except 2 labeled points.

Wet chemical analyses of several samples of oxidized GaAs were performed and the total weight per cent arsenic in the samples was obtained. Assuming that the samples analyzed contained only $GaAsO_4$ and Ga_2O_3, weight per cent values for these two products were calculated from wet analysis data and from weight loss data. These values are presented in Table I-GaAs. The weight percentages of $GaAsO_4$ and Ga_2O_3 obtained from these two independent measurements agree quite well. The total weight loss of sample S14S (Table I) is 35.6%. The theoretical weight loss if all the GaAs were oxidized to β-Ga_2O_3 is 35.2%. Possibly some of the Ga_2O_3 and/or GaAs was vaporized during the oxidizing reaction.

Figure 2 shows photographs of the progressive oxidation with temperature of slices of GaAs. Figure 3 shows how the oxidation proceeds from the surface of a sample. The samples in Fig. 3 were cracked perpendicular to the plane of the plate, and lapped and polished on this cracked edge to give these cross-sectional views.

When a sample of GaAs was oxidized with oxygen to 965°C, there was a loss of volume of 0.66% and the bulk density is 3.58 g/cc. Since the density of GaAs is 5.3216 g/cc (4), the density of the low quartz form of $GaAsO_4$ is 4.20 g/cc (2), and the density of β-Ga_2O_3 is 5.88 g/cc (2), the product of the oxidation of GaAs showed a porosity of 35.6%.

GaP.—If GaP, on being oxidized by oxygen produced only β-Ga_2O_3, there would be a weight loss of

[1] $2GaAsO_4 \rightarrow \beta$-$Ga_2O_3$ + As_2O_5 at 1000°C and at higher temperatures (2).

Table I

GaAs

Sample designation	Temperature, °C	Hr at temperature	Weight % loss	Weight per cent $GaAsO_4$: From weight loss	Weight per cent $GaAsO_4$: From wet analysis	Weight per cent Ga_2O_3: From weight loss	Weight per cent Ga_2O_3: From wet analysis
S14S	1050	20	35.6	0.0	0.1	100	99.9
S12N	950	19	32.2	7.8	9.8	92.2	90.2
S18J	860	22	32.4	7.7	8.1	92.3	91.9
S10F	850	22	29.8	13.9	15.3	86.1	84.7

GaP

Sample designation	Temperature, °C	Hr at temperature	Weight % gain	Weight per cent $GaPO_4$: From weight gain	Weight per cent $GaPO_4$: From wet analysis	Weight per cent Ga_2O_3: From weight gain	Weight per cent Ga_2O_3: From wet analysis
S24N	1110	20	63.2	(99.76)	92.13	(0.24)	7.87
S21H	1130	24	62.3	(99.08)	93.55	(0.92)	6.45
S21J	1150	22	62.5	(99.15)	95.4	(0.85)	4.6

6.92%. If $GaPO_4$ were the only product, then there would be a weight gain of 63.6%. When GaP was heated above 1000°C, a weight increase was observed, increasing slowly with temperature (see Fig. 4) until a range of 1110°-1150°C. In this range a very energetic exothermic reaction took place. The product of the reaction melted.[2] At the beginning of this exothermic reaction, the furnace was opened (for several experiments), and measurements as high as 1700°C were made with an optical pyrometer. It was noted at that time that a small amount of white powder was evolved during this reaction. This powder deposited on the quartz wall nearby which had a temperature in excess of 1100°C. Samples which had undergone the exothermic reaction experienced a weight gain of 62-63%. Heating at higher temperatures (as high as 1250°C) did not cause any further weight change. Samples heated for longer periods of time, at temperatures under 1110°C, showed larger increases in weight than samples heated for shorter periods of time, at the same temperatures (see Fig. 4, samples heated at 1100°C). Figure 5 photographically shows the progressive oxidation with temperature of slices of GaP. The 1120°C sample had gone through the exothermic reaction and the melted product is shown in its quartz boat. Figure 6 is a cross section of the "1100°C, 70 hour" sample of Fig. 5. This sample was cracked perpendicular to the plane of the plate and lapped and polished on this cracked edge to give a cross-section view.

X-ray diffraction studies showed that the products of the oxidation of GaP over the entire range of temperatures were the christobalite form of $GaPO_4$ (2) as a major phase and as a minor phase, β-Ga_2O_3 [5-10 w/o (weight per cent)].

Wet chemical analyses of several samples of oxidized GaP were performed and total weight per cent phosphate in the samples was obtained. Assuming that the samples analyzed contained only $GaPO_4$ and Ga_2O_3, weight per cent values for these two products were calculated from the wet analysis data and the weight gain data, and these values are given in Table I-GaP.

[2] The melting points of β-Ga_2O_3 and the christobalite form of $GaPO_4$ are 1715° ± 15°C (3) and 1670° ± 10°C (2), respectively.

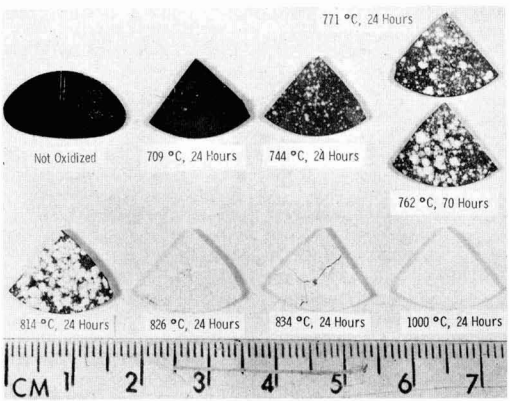

Fig. 2. Photographs of slices of GaAs oxidized in oxygen at various temperatures. Samples oxidized at 834° and 1000°C had undergone the exothermic reaction.

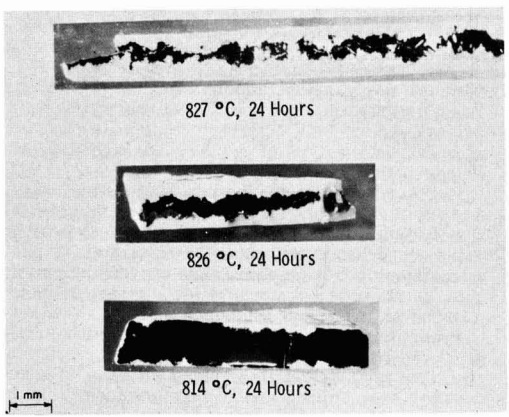

Fig. 3. Cross section of GaAs plates oxidized at three different temperatures.

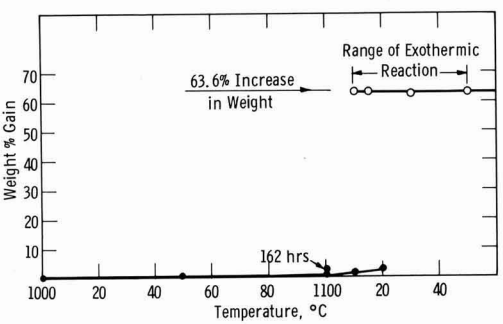

Fig. 4. Oxidation of GaP in oxygen. Per cent weight gain vs. temperature. All points on this curve are for samples fired for 22 ± 2 hr, except the labeled points.

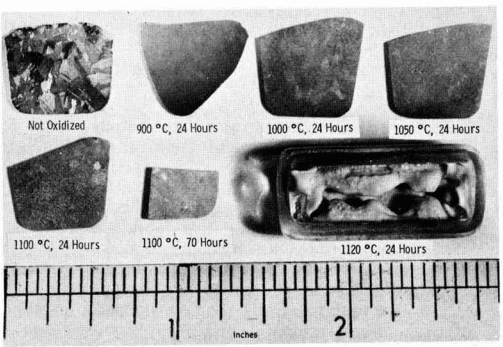

Fig. 5. Photographs of slices of GaP oxidized in oxygen at various temperatures. Sample fired at 1120°C for 24 hr had undergone the violent exothermic reaction.

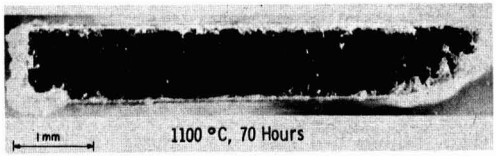

Fig. 6. Cross section of GaP plate oxidized in oxygen. Some sample as 1100°C, 70 hr in Fig. 6.

The values obtained for the weight per cent of $GaPO_4$ and Ga_2O_3 from wet analysis and weight gain data differ markedly. Since β-Ga_2O_3 was observed on the x-ray film for these samples, one can be sure that β-Ga_2O_3 was present in concentrations of at least a few per cent. It is felt that the weight gain measurements are all on the high side. Some of the powder deposited during the reaction was scraped off the wall of the quartz tube and examined by x-ray diffraction. Christobalite $GaPO_4$ with a small amount of β-Ga_2O_3 was identified. Therefore, the weight per cent $GaPO_4$ and β-Ga_2O_3 obtained by wet chemical analysis are considered quite reliable, and the quantitative data for Ga_2O_3 obtained from weight gain data are to be considered too low.

The densities of the christobalite form of $GaPO_4$, GaP, and β-Ga_2O_3 are 3.29 g/cc (2), 4.1304 g/cc (4), and 5.88 g/cc (3). The density of the oxidation product is certainly less than either GaP or β-Ga_2O_3.

Conclusion

The thermal oxidation of GaAs with oxygen produces β-Ga_2O_3 as a primary product and the low quartz form of $GaAsO_4$ as a secondary product. This was demonstrated by x-ray diffraction and quantitatively proved by weight loss determinations and wet chemical analysis. Minden observed that an oxide masking film was not formed when GaAs was thermally oxidized with oxygen. This paper has tried to prove that a low bulk density product composed primarily of β-Ga_2O_3 is formed, but the product is porous (about 35%), and As_2O_3 is driven from the area of the reaction.

The thermal oxidation of GaP with oxygen produced the christobalite form of $GaPO_4$ as a primary product with a secondary product of β-Ga_2O_3. This was demonstrated by x-ray diffraction, indicated by weight loss determinations, and proved by wet chemical analysis. When GaP is thermally oxidized by oxygen, the resulting product is primarily $GaPO_4$. Since this is a lower density material than GaP it spreads over the surface of the GaP and tends to cover the entire surface in much the same manner that an SiO_2 film covers a silicon surface. Only a small amount of a volatile product (P_2O_5) may be produced in this reaction since some β-Ga_2O_3 is formed.

Since this oxidation of GaP takes place slowly at temperatures below 1100°C the thickness of the oxide film can easily be controlled. This paper would like to suggest that thermal oxide masking may be applicable to GaP.

Manuscript received Dec. 23, 1965.

Any discussion of this paper will appear in a Discussion Section to be published in the December 1966 JOURNAL.

REFERENCES

1. H. T. Minden, *This Journal*, **109**, 733 (1962).
2. E. C. Shafer and R. Roy, *J. Am. Ceram. Soc.*, **39**, 330 (1956).
3. R. Roy, V. G. Hill, and E. F. Osborn, *J. Am. Chem. Soc.*, **74**, 719 (1952).
4. Von G. Giesecke and N. Pfister, *Acta Cryst.*, **11**, 369 (1958).

Properties of Anodic Films Formed on Reactively Sputtered Tantalum

D. Gerstenberg

Bell Telephone Laboratories, Incorporated, Murray Hill, New Jersey

ABSTRACT

The technique of reactive sputtering has been used for producing tantalum films with various concentrations of interstitial additives like oxygen, carbon, nitrogen, and hydrogen. A number of compounds between tantalum and these nonmetallic elements also have been deposited. The dielectric properties of anodic films on the tantalum formed in an aqueous solution of citric acid have been related to the composition of the tantalum. It was found that the capacitance density of 130v anodic films remains unaffected by the presence of oxygen and hydrogen, while it decreases as the atomic concentration of nitrogen and carbon in the tantalum increases. The dielectric constant, ϵ, of anodic films on Ta_2N is approximately 50% of the value of anodic Ta_2O_5 formed on pure tantalum.

The properties of sputtered refractory metal films like tantalum, niobium, and titanium are influenced greatly by deliberate addition of reactive gases to an argon sputtering atmosphere (1-4). Nonmetallic additives like oxygen, nitrogen, or carbon are incorporated in these films during the deposition process. At low concentrations, this incorporation takes the form of interstitial solution, and the solubility limits for all three additives appear to be much higher in tantalum and niobium films than in the bulk metals. At higher concentrations a number of compounds like oxides, nitrides, and carbides are formed. The resistivity and the temperature coefficient of resistivity of reactively sputtered refractory metal films depend strongly on the type of gas and the partial pressure at which the films are sputtered.

Reactively sputtered tantalum nitrides and carbides have a much higher resistivity than tantalum, a very low temperature coefficient, and a high thermal stability when deposited on heated substrates. In particular, tantalum nitride films have proven their usefulness as resistive components for integrated circuitry (5) and as individual components (6).

Preliminary results also indicated interesting dielectric properties of anodically formed films on tantalum sputtered with deliberately added nitrogen (7). These results were obtained on anodic films formed on tantalum which, initially, without deliberate addition of

nitrogen consisted of β-tantalum (8). As the atomic concentration of nitrogen is increased in the tantalum films the resulting anodic film has lower capacitance, but equivalent dielectric loss and leakage compared to anodic films formed on pure tantalum films (9). It was also demonstrated that the decrease in capacitance was caused by a change in dielectric constant due to the formation of a tantalum oxynitride. Associated with the decrease in capacitance is a large increase in the cathodic breakdown voltage. The purpose of the present investigation was to study the influence of other nonmetallic elements on the dielectric properties of anodic films formed on reactively sputtered tantalum films. The reactive gases used in this study include oxygen, methane, hydrogen, and nitrogen. Nitrogen has been added to this list because it was desirable to reinvestigate the properties of thin film capacitors fabricated from nitrogen containing tantalum sputtered under conditions which allow deposition of bcc α-tantalum reproducibly.

Experimental

As in the previous investigation (1) the tantalum films were sputtered from a high purity tantalum cathode through a mask on clean 2.5x7.5 cm barium alumina borosilicate glass substrates to a thickness of 4500Å. The distance between cathode and anode was 6.5 cm and the deposition rate about 130 Å/min for tantalum at 0.25 ma/cm^2, 4 kv and an argon pressure of $25\text{x}10^{-3}$ Torr. A removable shield between substrate and cathode allowed equilibrium to be reached in the sputtering atmosphere before starting deposition on the substrate. For outgassing, the mask and the substrate were maintained at 400°C during the presputtering and the subsequent sputtering run. The resistivity of the tantalum films was determined by a four point probe technique immediately after deposition.

The tantalum films were anodized at room temperature in an aqueous solution of 0.01% citric acid at a current density of $5\text{x}10^{-3}$ amp/cm^2. After reaching the desired voltage the anodization was continued for another 30 min allowing the current to decrease to $5\text{x}10^{-6}$ amp/cm^2 which is in the order of the electronic leakage current. The majority of the films were anodized to 130v resulting in oxide films on pure tantalum about 2000Å thick (10). In most cases, the anodization was interrupted to etch the tantalum films electrochemically at weak spots in the oxide in an aluminum chloride in methanol solution, which has proven beneficial in reducing anodic leakage or shorts (11). A number of films were anodized to voltages ranging from 75 to 250v for determining the amount of charge passed during anodization, and the dependence of the capacitance density on the forming voltage. The last step in the capacitor fabrication was the evaporation of the counter electrode structures from a tungsten filament at pressures of $1\text{x}10^{-4}$-$1\text{x}10^{-5}$ Torr. Gold counter electrodes, about 2000Å thick, were evaporated through mechanical masks yielding from 8 to 10 capacitors per substrate with an area of 0.35 cm^2 per capacitor. A General Radio Type 1620A Measuring Assembly was used for the determination of the capacitance and tan δ at 1 kc, and in a number of cases at frequencies ranging from 0.1 to 10 kc.

The structure of the tantalum films sputtered at different reactive gas pressures has been determined by x-ray diffraction analysis of processed slides after the capacitor properties had been evaluated. Since the anodic oxide is x-ray amorphous it does not generate a pattern interfering with the x-ray diffraction pattern obtained from the underlying tantalum film.

Experimental Results and Discussion

Resistivity.—Figure 1 shows how the resistivity of reactively sputtered tantalum films is affected by the type and the partial pressure of the reactive gases added to the argon atmosphere. The tantalum films

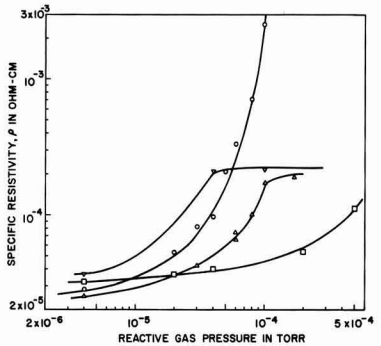

Fig. 1. Specific resistivity of 4500Å tantalum films as a function of the type and reactive gas pressure (measured by four-point probe). Sputtered films: ▽ N_2; △ CH_4; ○ O_2; □ H_2.

which were sputtered without deliberate addition of a reactive gas ($p = 3\text{x}10^{-6}$ Torr) have resistivities, ρ, ranging from 25 to 35 μohm-cm. These values are between 2 and $3\cdot\rho_B$, where ρ_B is the resistivity of pure bulk tantalum, indicating an impurity concentration of less than 3 a/o (atomic per cent) of interstitials like oxygen or nitrogen (1). The deliberate addition of reactive gases increases the resistivity until in the case of nitrogen and methane the curve reaches a plateau region at about 200-250 μohm-cm. These values agree very well with those reported for 1200Å films (1). The curve for tantalum sputtered in a partial oxygen atmosphere shows a sharp rise in resistivity above $6\text{x}10^{-5}$ Torr. The formation of insulating Ta_2O_5 occurs at partial pressures of oxygen of $1.7\text{x}10^{-4}$ Torr and above. The presence of hydrogen in the sputtering atmosphere does not seem to influence the resistivity of the tantalum films very much below 10^{-4} Torr, while in the 10^{-4} Torr range the values increase by about an order of magnitude.

Structure and composition.—The structure of the tantalum films sputtered with various additions of nitrogen, methane, oxygen, and hydrogen is indicated on the upper half of Fig. 2. The tantalum films deposited in a partial nitrogen atmosphere have the same phases Ta_2N and TaN which have been reported before (1). Sputtering of tantalum in a partial methane atmosphere results in the formation of Ta_2C and TaC (12). The phase Ta_2C had not been observed for reactively sputtered tantalum films before (1) either due to the small concentration range of this phase or due

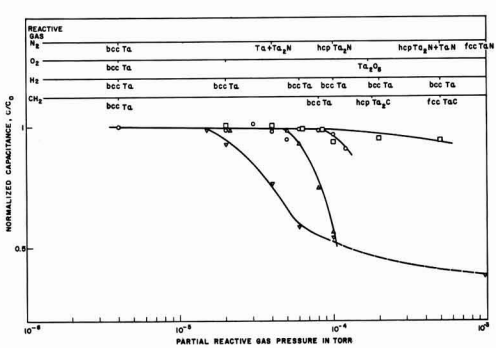

Fig. 2. Structure of the tantalum films and normalized capacitance of the dielectric at 1 kc vs. the type of gas and gas pressure. Capacitors were fabricated by anodization in 0.01% citric acid to 130v and have an area of 0.35 cm^2. C_0 is the capacitance of Ta_2O_5 on pure bcc tantalum films. $C_0 = 0.031$ uF. Sputtered films: same symbols as in Fig. 1.

Table I. Data on tantalum films sputtered in a partial oxygen atmosphere prior to anodization

Partial oxygen pressure P_{O_2} 10^5 Torr	Resistivity $\rho \times 10^6$ ohm-cm	Lattice constant a_o, in Å	Average crystallite diameter in Å*	Concentration** of oxygen in at. %
No O_2	27	3.327	94	—
2	52	3.360	64	3.6
4	97	3.405	52	11.4
6	340	3.430	17	—
8	720	3.46	16	29.5
10	2500	3.50	14	46

* The true average size of the crystallite is probably somewhat larger because of the x-ray line broadening on which this calculation was based might also be caused by strain in the tantalum films.
** Determined by anodization of films using Faraday's law.

to a higher solubility limit for carbon in tantalum at small film thicknesses. The films for the structural determination in the previous study by electron diffraction were only 300Å as compared to about 4000Å for the present films. Only preliminary data with respect to the composition of nitrogen and methane sputtered films are available. It has been established, however, that for both types of films (13, 14) the solubility limits are in the order of 10 to 15 a/o before the x-ray diffraction pattern of a second phase, Ta_2C or Ta_2N, can be observed.

The addition of oxygen to the sputtering atmosphere results in a drastic decrease of the crystallite size while the lattice constant increases as shown in Table I. The drop in crystallite size becomes particularly noticeable between $4x10^{-5}$ and $6x10^{-5}$ Torr probably indicating the formation of small Ta_2O_5 particles. These particles, however, are not large enough to contribute to the x-ray diffraction pattern. The tantalum films sputtered in a partial hydrogen atmosphere do not show a change in structure. This is reasonable in view of the fact the substrate temperature during deposition was about 400°C, too high a temperature for the formation of stable tantalum hydrides (15). It is likely, however, that there is interstitial solution of hydrogen which might occur during deposition or during the cooling period after sputtering.

Capacitance.—The lower half of Fig. 2 shows how the normalized capacitance of 130v anodic films on the reactively sputtered tantalum measured at 1 kc changes with increasing reactive gas pressure. The concentration of the gases in the tantalum is not known for all films, but the preliminary analytical results mentioned in the previous section indicate that the atomic concentration of the reactive gases is directly proportional to the reactive gas pressure in the sputtering atmosphere. The normalized capacitance of the dielectric on tantalum films sputtered with additions of oxygen and hydrogen appears to be affected the least. This result is to be expected for the anodic film formed on tantalum films sputtered in a partial oxygen atmosphere. The drop in capacitance for these films at $1x10^{-4}$ Torr is probably due to the presence of oxide particles prior to anodization resulting in an increased effective thickness for the anodic film. Films sputtered at this pressure contain about 45 a/o of oxygen. Anodic films formed on tantalum containing such high oxygen concentrations also tend to crystallize during anodization.

The incorporation of nitrogen and carbon in the tantalum films results in fairly large decreases in capacitance which are accompanied by a slow change of the interference color of the 130v anodic film. It will be shown in the next section that the lower capacitance for the capacitors formed on nitrogen sputtered films is not due to a variation in oxide thickness but rather due to a decrease in the dielectric constant with increasing nitrogen concentration in the films. The anodization of Ta_2N does not present difficulties; the voltage increases at a constant rate with time during the constant current period, and after reaching voltage the anodization current drops inversely with time (16). The films consisting solely of TaN exhibit gas evolution during the anodization process. They can be anodized to at least 130v but the resulting anodic film has a rather dull appearance. The finished capacitors also have low anodic and cathodic breakdown characteristics. In the case of the carbon containing tantalum, anodization of films sputtered at $1x10^{-4}$ Torr of methane consisting of a mixture of tantalum with a small amount of Ta_2C results in discoloration and low breakdown characteristics for the dielectric. For Ta_2C and TaC films citric and nitric acid act as etchants when a positive voltage is applied to these films.

Coulometric and other measurements.—A number of "pure"[1] tantalum films, and films sputtered at various reactive gas pressures were used for measuring the charge transfer during anodization. The theoretical values for the charge transfer per volt during the conversion of tantalum metal to Ta_2O_5 has been calculated on the basis of a reduction in thickness of the metallic film which is $k_3(Ta) = 6.63$ Å/v (10, 17). This value and the one obtained for converting metallic Ta_2N to the dielectric by anodization, $k_3(Ta_2N) = 4.8$ Å/v, (17, 18), had been determined previously from the increase in resistance of samples due to the reduction of the conducting film thickness by anodization. The number of electronic charges per volt of anodization and per square centimeter of film area, q_{th}, is then according to Faraday's law

for Ta:

$$q_{th} = n \cdot k_3(Ta) \cdot N_{Ta} \cdot e \quad [1]$$

and for Ta_2N:

$$q_{th} = n \cdot k_3(Ta_2N) \cdot N_{Ta_2N} \cdot e \quad [2]$$

where n is the number of charges per tantalum atom, N is the number of tantalum atoms per cubic centimeter of the original film of tantalum or Ta_2N which is equal to the inverse of the volume of the unit cell times the number of tantalum atoms per unit cell, and e is the electronic charge. The resulting q values for tantalum and Ta_2N are, respectively, $q_{th} = 0.287 \cdot 10^{-2}$ coulomb/v cm[2] [2] and $q_{th} = 0.194 \cdot 10^{-2}$ coulomb/v cm^2 for $n = 5$, assuming no changes in valency for the nitrogen atoms during anodization.

The experimental values for q were determined graphically from the plot of the anodizing current as a function of time. A comparison of the theoretical value with the experimental value for tantalum films sputtered without addition of a reactive gas which were anodized to 130 and 250v shows satisfactory agreement (see Table II) indicating about 100% efficiency for the anodization process. The oxygen containing tantalum films show the expected decrease in the q values. In Fig. 3 the resistivity of these films has been plotted as a function of the atomic concentration of oxygen calculated from the q values. Also shown are the resistivity values of 1200Å films *vs.* oxygen concentration de-

[1] Pure films are those sputtered without deliberate addition of a reactive gas.

[2] In a more refined treatment the change in cell parameter due to the presence of intersitial oxygen, etc. would have to be taken into consideration for the calculation of q_{th} of tantalum.

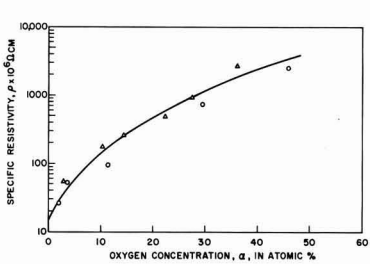

Fig. 3. Resistivity as a function of the atomic concentration of oxygen in reactively sputtered tantalum films: ○ based on the coulometric measurements, 4000Å; △ analyzed by inert gas fusion analysis, 1200Å.

Table II. Results of coulometry experiments on reactively sputtered tantalum films

Gas pressure $p \times 10^{-5}$ Torr	Reactive gas	No. of samples	Anodization voltage, V_A in V	Charge transfer $q \times 10^2$ coulomb/v-cm^2	Structure of the original film
—	None	4	130, 250	0.296 ± 0.012	bcc Ta
2×10^{-5}	O_2	6	130	0.301	bcc Ta + O
4×10^{-5}		4	130	0.258	bcc Ta + O
8×10^{-5}		6	130	0.179	bcc Ta + O
10×10^{-5}		2	130	0.118	bcc Ta + O
10×10^{-5}	N_2	4	100, 150, 200, 250	0.192 ± 0.014	Ta_2N
8×10^{-5}	CH_4	4	100, 150, 200, 250	0.293 ± 0.008	bcc Ta + C
35×10^{-5}	H_2	2	130	0.289	bcc Ta + H

termined by inert gas fusion analysis (1). Both sets of values agree very well suggesting that the coulometric experiments are a convenient method for oxygen analysis of tantalum films if the oxygen is uniformly distributed throughout the tantalum.

The experimentally determined value for the charge transfer during formation of the dielectric on Ta_2N, listed in Table II, is approximately equal to the theoretical value. The calculation of q_{th} for Ta_2N was based on the assumption that the tantalum atoms reacting with oxygen during anodization have five charges. The good agreement between the theoretical and the experimental value, therefore, seems to indicate five oxygen atoms react with each Ta_2N molecule during the formation of the anodic film. This has been confirmed by the gravimetric determination of the mass of the dielectric on Ta_2N formed during anodization. The conversion factor k_3 has not been determined for methane and hydrogen sputtered films. But if we assume that it is close to that of pure bcc tantalum which still is the structure of these reactively sputtered films it can be concluded from the q values that carbon and hydrogen do not participate in the charge transfer during anodization.

The results of capacitance measurements, plotted in Fig. 4 as a function of the anodization voltage, reveal that the inverse capacitance is not a linear function of the voltage which would be expected for a uniform composition of the dielectric. Especially the inverse capacitance of the dielectric film formed on Ta_2N films shows a large deviation from linearity at higher voltages. But the values for the dielectric formed on methane sputtered tantalum films also reveal a nonlinear dependence on voltage. Such a nonlinearity could be attributed to either a nonlinear dependence of the thickness of the dielectric with increasing voltage or a nonuniform distribution of the additives in the original film. Both possibilities have been investigated for the Ta_2N films and the results indicate that these two factors cannot be responsible for the nonlinearity of the inverse capacitance.

For all the Ta_2N films, anodized from 70 to 200v, the step height of the dielectric above the surface of the original Ta_2N film has been measured by Talysurf[3] and it was found to be a linear function of the anodization voltage. The factor for the increase in thickness was found to be $k_2(Ta_2N) = 11.9$ Å/v.

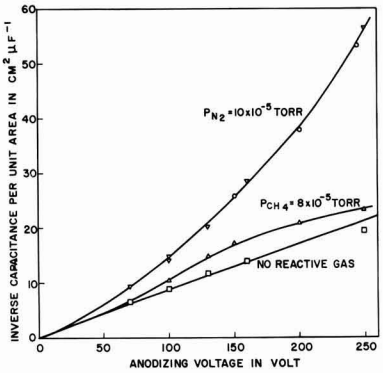

Fig. 4. Inverse capacitance density of capacitors on tantalum films with three different compositions as a function of the formation voltage.

Thus the total thickness of the dielectric formed on Ta_2N films per volt is then $k_3(Ta_2N) + k_2(Ta_2N) = k_1 = 16.7$ Å/v. Similar measurements for pure tantalum films yielded a value of $k_3(Ta) + k_2(Ta) = k_1 = 16.5$ Å/v. These values were used to determine the dielectric constant, ϵ, which is listed in Table III. The table also contains the film thickness of the original films before anodization. Since the anodic films formed on Ta_2N showed a systematic decrease in dielectric constant with increasing anodization voltage which might be due to a nonuniform composition of the Ta_2N, films with only half the original thickness have been anodized to intermediate voltages. The values of the dielectric constant of the anodic films formed on 2200Å Ta_2N films correspond closely with those found for the anodic films on thicker Ta_2N films. These results suggest that the decrease of the dielectric constant for the dielectric on Ta_2N films cannot be explained by a nonuniform distribution of nitrogen in the original film. It might be speculated, however, that the potential applied during anodization might cause migration of nitrogen ions. Such a migration might then result in a nonuniform distribution of the nitrogen in the dielectric.

It is not clear at present whether the increase of the dielectric constant with anodizing voltage obtained for anodic films on pure tantalum (Table III) is systematic and what its causes are. In addition, the average of the dielectric constant, 21.7, is considerably lower than the value reported by Young (19) which is widely used in the literature, but very close to the value recently obtained by Klerer (10).

Finally, the values for the decrease in thickness below the surface of the metallic film, k_2V_A, and the total thickness of the oxide, $(k_2 + k_3)V_A$, have been used for determining the density of the anodic films formed on pure tantalum and Ta_2N films. The density was calculated by combining Eq. [3] and [4]

$$\rho_{Ta_2O_5} = \frac{M_{Ta_2O_5}}{A \cdot (k_2 + k_3) \cdot V_A} \quad [3]$$

$$\rho_{Ta} = \frac{M_{Ta}}{A \cdot k_2 V_A} \quad [4]$$

[3] Taylor-Hobson, Ltd. Model 3 Talysurf with a straight line datum attachment.

Table III. Dielectric constant of anodic films

(a) Original film thickness, t[Å]	On tantalum Anodization voltage, V_A[V]	Dielectric constant, ϵ	(b) Original film thickness, t[Å]	On Ta_2N Anodization voltage, V_A[V]	Dielectric constant, ϵ
4400	70	20.1	4400	70	13.7
4400	100	20.8	4400	100	12.7
4400	130	21.5	2200	100	13.7
4400	160	22.2	4400	130	12.15
4400	250	24.0	2200	150	10.97
	Average	21.7	4400	160	10.50
			2200	200	10.0
			2200	245	8.70
			4400	250	8.34

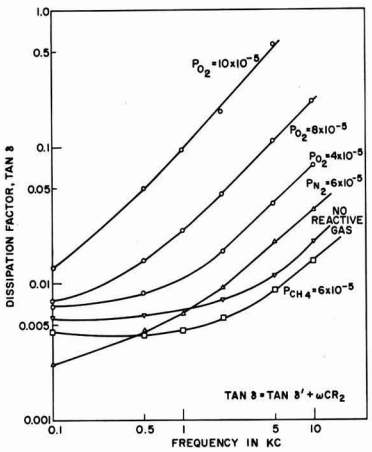

Fig. 5. Plot of the dissipation factor *vs.* frequency for capacitors formed on reactively sputtered tantalum.

to Eq. [5]

$$\rho_{Ta_2O_5} = \frac{M_{Ta_2O_5} \cdot k_2}{M_{Ta} \cdot (k_2 + k_3)} \cdot \rho_{Ta} \qquad [5]$$

where ρ is the density, M is the mass (which can be replaced by the molecular weight in Eq. [5], V_A is the anodizing voltage, and A is the area of the anodized film which both can be eliminated. The resulting value of 8.12 g/cm³ for the density of the Ta_2O_5 formed on pure tantalum is in good agreement with those found by Young (19) and Klerer (10).

For the calculation of the density of the dielectric on Ta_2N films it has been assumed that the dielectric has the stoichiometric composition Ta_2O_5N yielding a density of 5.30 g/cm³. But even if the anodic film contains a nitrogen concentration which is larger or smaller, it would have only a small effect on the molecular weight and, therefore, would change the density of the dielectric very little. Thus the presence of nitrogen in the dielectric formed on Ta_2N appears to result in a structure considerably less dense than that of Ta_2O_5 formed on pure tantalum.

Frequency and temperature characteristics.—The capacitance and the dissipation factor of a number of typical capacitors have been measured at frequencies between 0.1 and 10 kc. The results are summarized in Fig. 5. Since tantalum oxide belongs to a category of dielectrics which show only a small dependence of the dielectric loss on frequency up to very high frequencies, the dissipation factor of the dielectric itself and the loss due to the series resistance of the tantalum film can be separated according to the following equation (20)

$$\tan \delta = \tan \delta' + \omega C R_2 \qquad [6]$$

Where tan δ' is the frequency independent dissipation factor of the dielectric, ω is the angular frequency, C is the capacitance, and R_2 is the series resistance of the tantalum film and the counter electrode.

If the dissipation factor, tan δ, obeys this equation, then when tan δ is plotted against frequency as shown in Fig. 5, tan δ' should predominate at low frequencies and tan δ will vary little with frequency. At higher frequencies ωCR_2 will predominate and the curve will approach a 45° slope. The capacitors made from pure tantalum films appear to fulfill this expectation. There is little change in tan δ from 0.1 to 1 kc, and above 5 kc the curve approaches a 45° slope indicating predomination of ωCR_2. With increasing oxygen concentration, this term predominates at lower and lower frequencies suggesting a steady increase of the R_2 values. An analysis of the data shows that R_2 increases from 8.5 to 810 ohms while tan δ' decreases from 0.0051 to 0.0030 as the partial oxygen pressure used in sputtering is increased to $1x10^{-4}$ Torr. The capacitors made from nitrogen sputtered tantalum films have the lowest tan δ' values.

The R_2 values of the methane sputtered film are even lower than the value of the pure tantalum film although its specific resistivity is six times higher, and the film thickness is the same. The low R_2 value and the initial decrease of tan δ (Fig. 5) probably indicate that tan δ' is dependent on frequency and that the present model is too simple for describing the frequency dependence of tan δ for these films. The capacitors made from carbon containing tantalum films are the only ones showing such a behavior.

The changes in capacitance in the frequency range are between 0.59 and 1.19%, except for the capacitors formed upon oxygen containing tantalum films. They reveal a larger decrease in capacitance at higher frequencies, especially those on films sputtered at $8x10^{-5}$ and $10x10^{-5}$ Torr of oxygen.

Figures 6 and 7 show how the reduced capacitance and dissipation factor of a number of capacitors change with temperature. The measurements were carried out in a dry atmosphere in order to eliminate the influence of moisture on these properties (11). For control purposes the measurements were made while increasing the temperature as well as while decreasing it.

The capacitors fabricated on pure tantalum films (sputtered without deliberate addition of a reactive gas) show the largest changes (Fig. 6). The temperature coefficient of capacitance for these capacitors in

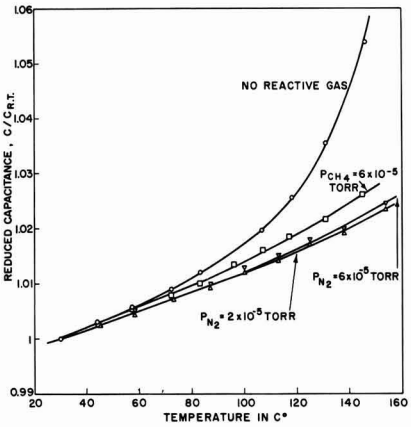

Fig. 6. Capacitance ratio as a function of temperature for capacitors formed on reactively sputtered tantalum.

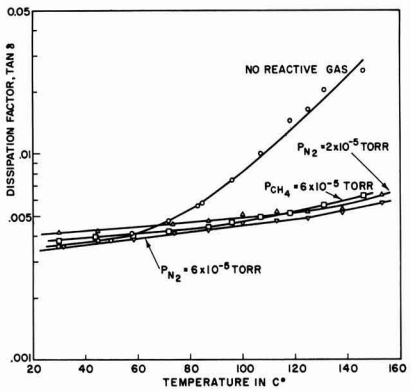

Fig. 7. Dissipation factor as a function of temperature for capacitors formed on reactively sputtered tantalum.

the range of a linear dependence of the capacitance on temperature, up to 60°C, is 220×10^{-6}/°C, below the value reported for tantalum thin film capacitors (8). Between 100° and 150°C these capacitors display a more rapid change with temperature. The capacitors made from reactively sputtered films (containing nitrogen and carbon) have smaller temperature coefficients, between 170×10^{-6} and 190×10^{-6}/°C, and the linear dependence of the capacitance on temperature holds up to higher temperatures. The capacitors made from pure tantalum films also show the largest change in the dissipation factor with temperature which is about an order of magnitude for the temperature range (Fig. 7). The temperature dependence of tan δ is much smaller for the capacitors made on reactively sputtered films.

Conclusions

One of the important results of the present investigation is the observation that the presence of interstitial oxygen, nitrogen, carbon, and hydrogen atoms does not interfere with the formation of anodic films on tantalum when it is deposited by reactive sputtering. The presence of Ta_2C in the tantalum film, however, results in a varied oxide growth so that the anodic film does not show a uniform interference color but rather displays a spectrum of interference colors. The dielectric strength of these anodic films is an order of magnitude lower. Further increase in carbon concentration, when the structure of the films is that of Ta_2C or TaC, inhibits the formation of anodic films in 0.01% citric or 0.01% nitric acid. In the case of the nitrogen containing tantalum the anodic films formed on Ta_2N still show uniform and bright interference colors and the dielectric strength remains high. It does not begin to decrease until the Ta_2N films become mixed with a considerable amount of TaN. There is an anodic reaction in citric acid even for TaN films but the resulting anodic film on TaN has very low dielectric strength. The capacitance density of the anodic films on carbon and nitrogen containing tantalum films decreases with increasing atomic concentration of these additives in the tantalum to less than 50% compared to that of anodic films on pure tantalum. The cause for this decrease in capacitance for nitrogen containing tantalum films could be attributed to a lower dielectric constant of the anodic film. The dielectric on tantalum nitride films also shows a much lower density than that of Ta_2O_5 and its stoichiometric composition can probably be best described as $Ta_2O_5N_x$ where the upper limit for x remains to be determined by analytical techniques. More experimental data are also required for the determination of the dielectric constant and the density of anodic films formed on carbon containing tantalum.

Acknowledgment

The x-ray diffraction analysis of the tantalum films by Mrs. M. H. Read and the Talysurf measurements of film thicknesses by R. Brown are greatly appreciated.

Manuscript received Dec. 30, 1965. This paper was delivered before the San Francisco Meeting, May 9-12, (1965).

Any discussion of this paper will appear in a Discussion Section to be published in the December 1966 JOURNAL.

REFERENCES

1. D. Gerstenberg and C. J. Calbick, *J. Appl. Phys.*, **35**, 402 (1964).
2. D. Gerstenberg and P. M. Hall, *This Journal*, **111**, 936 (1964).
3. D. Gerstenberg, *Ann. Phys.*, **11**, 354 (1963).
4. N. Schwartz, "Transactions of 10th National Vacuum Symposium 1963," p. 325, MacMillan Co., New York (1963).
5. D. Gerstenberg and E. H. Mayer, Proceedings of the 1962 Electronic Components Conference, p. 57.
6. R. W. Berry *et al.*, Proceedings of the 1964 Electronic Components Conference, p. 86.
7. (a) N. Schwartz, M. Gresh, and J. Deaderick, Abstr. No. 15, 1962 Meeting of the Electrochem. Soc., Los Angeles; (b) D. A. McLean, N. Schwartz, and E. D. Tidd, Proc. of the IEEE 52, 1450 (1964).
8. C. Altman and M. H. Read, *Appl. Physics Letters*, **7**, 51 (1965).
9. R. W. Berry and D. J. Sloan, *Proc. IRE*, **47**, 1070 (1959).
10. J. Klerer, *This Journal*, **112**, 896 (1965).
11. N. Schwartz and M. Gresh, *ibid.*, **112**, 295 (1965).
12. V. I. Smirnova and B. F. Ormont, *Dokl. Akad Nauk SSSR*, **96**, 557 (1954).
13. W. G. Guldner, Proceedings of the 1964 Electronic Components Conference, p. 9.
14. W. G. Guldner, Private communication.
15. M. Hansen and K. Andero, "Constitution of Binary Alloys," McGraw-Hill Book Co., New York (1958).
16. W. Ch. van Geel and H. Emmens, *Z. Phys.*, **87**, 220 (1933).
17. D. Gerstenberg, Unpublished results.
18. D. Mills, Private commmunication.
19. L. Young, "Anodic Oxide Films," p. 82, Academic Press, London and New York (1964).
20. D. A. McLean, *This Journal*, **108**, 48 (1961).

The Effect of the Concentration of Hypophosphite Ion on the Magnetic Properties of Chemically Deposited Co-P Films

J. S. Judge, J. R. Morrison, and D. E. Speliotis

Systems Development Division, International Business Machines Corporation, Poughkeepsie, New York

ABSTRACT

Samples of electroless cobalt phosphorus films of various thickness in the region less than 3000Å were prepared from solutions containing different concentrations of hypophosphite ion. These samples were analyzed by x-ray fluorescence and their magnetic characteristics were studied. The per cent phosphorus in the films was found to increase approximately logarithmically as the concentration of hypophosphite was increased. The plating rate increased concomitantly. The saturation magnetic moment and the coercivity were found to depend strongly on the phosphorus content of the films. The coercivities of these films also have a strong dependence on thickness. To a large extent the interaction of these two physical properties of the film determine the magnetic properties observed.

The magnetic properties of films of chemically deposited cobalt-phosphorus have been investigated several times in the past. Fisher and Chilton (1) have reported the preparation of high coercivity deposits as possible media for magnetic recording. The present authors have shown that somewhat thinner deposits exhibit superior recording performance and have reported on their magnetic properties (2, 3). Ransom

Table I. Composition of solution

$CoSO_4$	0.0855M
Na_3 citrate	0.183M
$(NH_4)_2$ H citrate	0.088M
$(NH_4)_2$ SO_4	0.307M

pH = 8.3 (at 85°C)—adjusted with NH_4OH
Temperature = 85°C

and Zentner (4) have shown that low coercivity uniaxial deposits of electroless cobalt can be prepared under somewhat different conditions of deposition. In short, the magnetic properties of chemically deposited cobalt-phosphorus films are critically dependent on the conditions of preparation. The magnetic properties of these deposits are a complicated function of the phosphorus content, crystallite size, and orientation of the deposits which in turn are controlled by the deposition variables, primarily solution composition, pH, and temperature. In this investigation we have restricted ourselves to a study in some detail of the effects of one of the more important variables in solution composition, the concentration of hypophosphite ion.

Preparation

The films were deposited on Mylar[1] substrates which were presensitized with the usual $SnCl_2$-$PdCl_2$ treatments (5). Prior to this, the Mylar substrates had been rendered hydrophilic by immersion into a hot chromic-sulfuric acid solution and then a hot sodium hydroxide solution (6). The composition and condition of the solution used for the deposition are shown in Table I. This solution is similar in composition to that used by Ransom and Zentner for the deposition of low coercivity uniaxial films, except that it is operated at a significantly higher pH. The agitation during deposition was kept at a minimum, merely sufficient to assure temperature and concentration uniformity.

The weight of cobalt and phosphorus deposited was determined by x-ray fluorescence analysis. The amount of phosphorus codeposited was found to be independent of deposit weight, as shown in Fig. 1. However,

[1] E. I. du Pont de Nemours & Co., (Inc.) registered trademark.

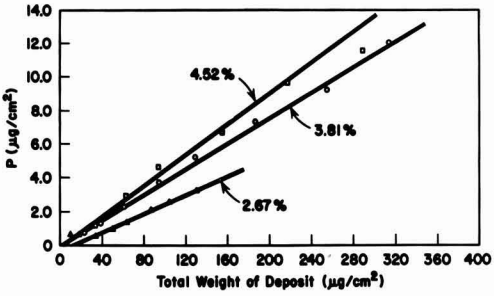

Fig. 1. Weight of phosphorus deposited vs. total deposit weight

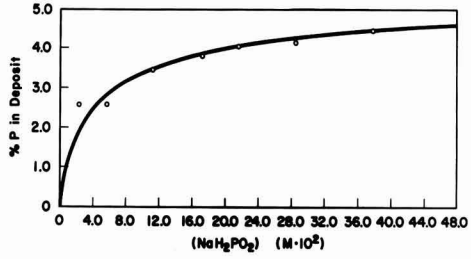

Fig. 2. Dependence of per cent P in deposit on the concentration of NaH_2PO_2.

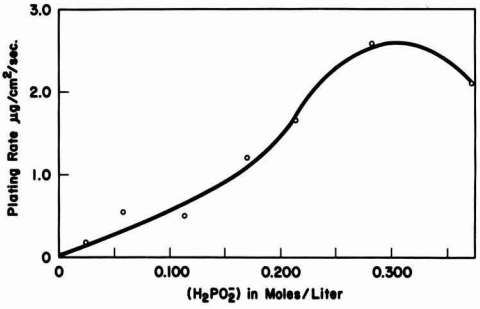

Fig. 3. Plating rate vs. $(H_2PO_2^-)$

above deposit weights of ~ 200 μg/cm², or approximately 2500Å in thickness, there was a tendency for the phosphorus content to decrease with increasing thickness. Since such deposits would tend to exhibit a trend in composition with thickness, these were not included in this study. Consequently only deposits of less than ~ 2500Å were considered. Fortunately it is in this thickness region that the most interesting magnetic behavior is exhibited.

The average phosphorus content for the deposits at each concentration of hypophosphite ion was determined from the slope of such plots as shown in Fig. 1. The dependence of the per cent phosphorus on the hypophosphite content of the solution is shown in Fig. 2. It is apparent that the phosphorus content of the deposits increases as the hypophosphite content of the solution increases. Moreover, there is apparently an approximately logarithmic relationship between the two. Figure 3 shows the dependence of the plating rate on the hypophosphite content of the solution. The rate increases monotonically to ~ 0.3M in hypophosphite and then exhibits a slight decrease as the hypophosphite concentration is further increased. This effect is similar to electroless nickel deposition where an optimum ratio of metal ion to hypophosphite ion exists for maximum deposition rate.

Crystallographic Properties

X-ray diffraction indicated that all deposits were predominantly hexagonal cobalt. The crystallite size of the deposits was estimated from x-ray line broadening. Such estimates gave values in the range 200-1000Å. However, the crystallite sizes so obtained showed no correlation with thickness, phosphorus content, or magnetic properties. In order to obtain significant peaks for x-ray diffraction, it was necessary to use several samples stacked together. This would be expected to produce additional line broadening. In addition, deposit stresses and stacking faults will contribute to the line broadening. Consequently these estimates of crystallite size are in reality the lower limit of the crystallite size in these deposits. All deposits exhibited a preferred orientation of the C-axis in the

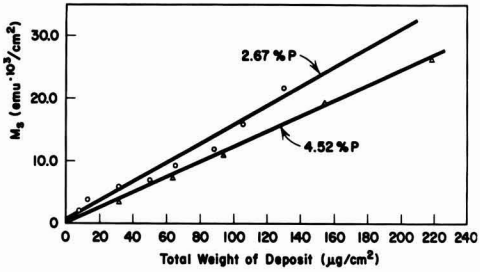

Fig. 4. Dependence of the saturation magnetic moment on deposit weight.

Table II. Values for various phosphorous contents

% P	σ_s emu/gram
2.67	156.0
2.62	147.5
3.45	114.0
3.81	118.0
4.06	120.5
4.22	127.5
4.52	122.5

plane of the substrate. However, a higher degree of orientation was exhibited by the higher phosphorus deposits. Unfortunately it was impossible to obtain an estimate of orientation on deposits of less than ~ 500Å in thickness.

Magnetic Properties

The saturation magnetic moment of the deposits was measured by a Faraday type magnetic balance in a field of 6000 oe. The moments so obtained were found to be independent of deposit thickness. This fact is illustrated by Fig. 4 which is a plot of the magnetic moment *vs.* deposit weight for the two extremes of phosphorus content. The saturation magnetic moment per gram (σ_s) of the material was calculated from the slopes of such plots. Table II illustrates the values so obtained for the various phosphorus contents. At the lowest per cent P the highest values of σ_s are observed. A decrease as the per cent P is increased would be expected whether the phosphorus merely acted at a dilutant or entered in chemical combination with some of the cobalt. However, the observed decrease is not monotonic with increasing per cent P, but exhibits a minimum at ~ 3.5% P.

Measurement of the hysteretic properties of the deposits were made in a vibrating sample magnetometer with a maximum field of approximately 10,000 oe. The squareness (*i.e.*, the ratio of the remanent magnetic moment to the saturation magnetic moment) showed no clear trends with thickness, but the average value decreased from 0.83 to 0.70 as the phosphorus was increased from 2.6 to 4.5%.

For the two lowest phosphorus contents the dependence of the coercivity of the deposits on deposit weight or thickness is shown in Fig. 5. Both of these series had very near the same per cent P, 2.62 and 2.67%. In both cases the coercivity drops as the weight increases from ~ 1100 oe at a deposit weight of ~ 15 $\mu g/cm^2$ approaching a constant value of ~ 300 oe for large deposit weight. Figure 6 is a similar plot for the remaining series of higher per cent P. At 3.45% P a slight maximum begins to appear in the coercivity at ~30 $\mu g/cm^2$. As the per cent P is increased beyond this, the maximum begins to shift out in thickness until at 4.5% P the coercivity appears to increase with increasing weight over the entire weight range. The heights of these maxima, however, are decreasing with increasing per cent P. These points are clarified in Fig. 7 where the value of H_c at the peak and the weight of deposit at which the peak in H_c occurs has been plotted against the per cent P. The value of (H_c) peak drops from ~ 1200 oe at 3.5% P to 650 oe at 4.5% P. Meanwhile, the deposit weight at which the maximum occurs increases from < 20 $\mu g/cm^2$ for the low P deposits to > 200 $\mu g/cm^2$ for the 4.5% P deposits. Since the deposits with the least phosphorus did not exhibit a maximum in H_c for even the thinnest deposits measured, the actual (H_c) peak and weight at the peak would probably be higher and lower respectively than those points entered which merely represent the highest H_c observed.

Figure 8 summarizes the effect of phosphorus content on H_c for constant deposit thickness. The thicknesses have been calculated assuming a density of 8.9 g/cm^3. For a given thickness the coercivity increases to a maximum and then falls as the % P increases. At a deposit thickness of 560Å a maximum coercivity of 1200 oe is reached at ~3.5% P whereas at 2250Å a maximum H_c of ~ 800 oe is reached at 4.2% P. The

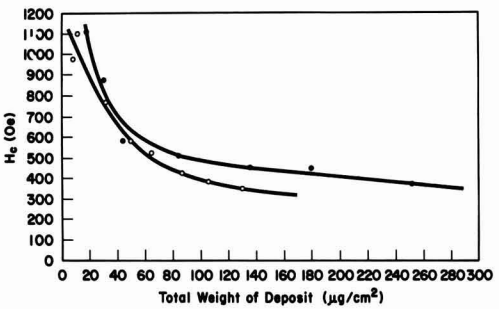

Fig. 5. H_c *vs.* deposit weight. ○ = 2.67% P; circle with x = 2.62% P.

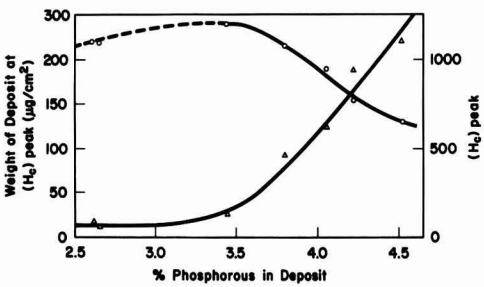

Fig. 7. Dependence of the maximum in H_c on per cent P. ○ = (H_c)p; △ = (wt)p.

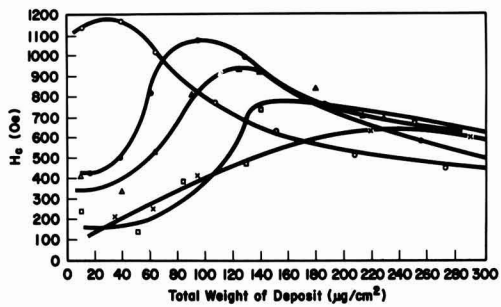

Fig. 6. H_c *vs.* deposit weight. ○ = 3.45% P; • = 3.81% P; △ = 4.06% P; □ = 4.22% P; X = 4.52% P.

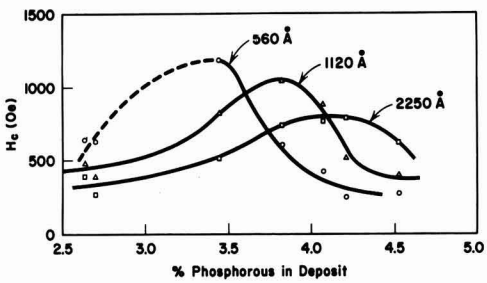

Fig. 8. Dependence of H_c on per cent P for three different thicknesses.

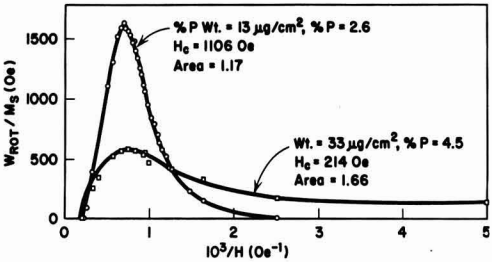

Fig. 9. Dependence of rotational hysteresis on field for two thinner samples of different per cent P.

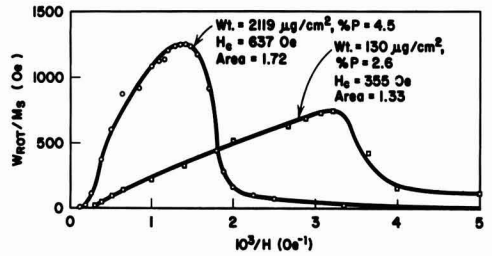

Fig. 10. Dependence of rotational hysteresis on field for two thicker samples of different per cent P.

intermediate thickness deposits of 1120Å reach an intermediate maximum of 1050 oe at an intermediate phosphorus content of 3.8%.

Discussion

The high coercivities observed for many of the samples of chemically deposited cobalt-phosphorus necessitate a single domain model to explain their magnetic properties. Assuming the phosphorus exists as the weakly magnetic Co_2P, 4% by weight of P would correspond to ~25% by volume of Co_2P. At any rate a significant proportion of the volume of these films consists of a nonmagnetic dilutant. A semi-particulate model is therefore reasonable for these films. The high magnetocrystalline anisotropy of cobalt, moreover, demands that these particles exhibit a strong uniaxial character. Consequently these films can be characterized qualitatively as a random (in the plane) assembly of interacting uniaxial particles. It has been shown by Reimer (7) that such a model leads to squarenesses higher than 0.64 (which would be expected for no interactions).

The energy loss in rotational hysteresis as a function of applied field was measured on a number of samples by means of a torque balance. Figure 9 is a plot of this energy, W_{Rot}, normalized for differences in magnetic moment *vs.* the reciprocal of the applied field. The values on the Y axis can be interpreted as the energy per magnetization jump times the number of particles involved. It is apparent that the low thickness low phosphorus sample shows a very narrow distribution of high field rotational processes consistent with its high coercivity. However, the low thickness, high phosphorus sample exhibits a large proportion of low field processes, again consistent with its low coercivity. Figure 10 shows the same results for much thicker films of low and high per cent P. With reference to the high phosphorus film, the distribution is now much sharper and apparently as the film has grown those particles exhibiting low field switching characteristics have disappeared. The low phosphorus film, on the other hand, now has its distribution shifted to much lower fields, indicating the appearance of low field processes as the film has grown.

Table III. Values for sample of three different per cent P

% P	Deposit wt (μg/cm²)	H_c (oe)	R	H_{pk} (oe)
2.67	13	1106	1.17	1390
	50	591	1.89	480
	87	432	2.21	365
	130	355	1.33	310
3.81	16	423	1.32	1670
	61	819	1.67	1350
	95	1069	1.68	1250
	187	774	2.19	750
4.52	33	214	1.66	1330
	63	246	1.89	1000
	94	405	1.23	960
	219	637	1.72	690

The value of the area under these curves has been shown to be characteristic of the mode of magnetization reversal. The theoretical values for the area (8) are (*a*) single-domain model, coherent rotation, 0.4; (*b*) single-domain model, incoherent rotation, 0.4 to 4.0; (*c*) domain wall, 4.0. In Table III the values of R, the area under the curve, are tabulated for samples of three different per cent P values. All values lie in the range 1.2-2.2 and exhibit no trends with thickness or per cent P. These values are consistent with a single domain model involving incoherent reversal, probably a magnetization buckling in the plane of the film. The value of the applied field at which the peak of the rotational hysteresis was observed is also tabulated in Table III. It can be seen that the value of this peak field decreases with increasing thickness in all cases. Figure 11 is a plot of the peak field *vs.* thickness for these samples. The peak field drops much more sharply as the thickness is increased for the low per cent P film than for those of higher phosphorus. Thus in the low per cent P films both the rapid decrease in peak field and especially the significant build up of low field processes as the thickness increases indicate a growth of particles out of the single domain size to particles large enough to support domain walls.

For the high per cent P films the peak field decreases and approaches the value of the coercivity as the thickness builds up and the low field processes disappear. This suggests that the thinner films have a significant portion of very small particles which exhibit a semi-superparamagnetic behavior. The particles grow as the film becomes thicker and enter the single domain size region. The greater the per cent P of the film, the greater is the thickness which must be reached before the contribution of these very small particles disappears. However, at the same time, because of the initial wide distribution of particle size in the higher per cent P films, some particles grow and enter the multidomain region causing a lowering of the maximum coercivity observed as the % P increases.

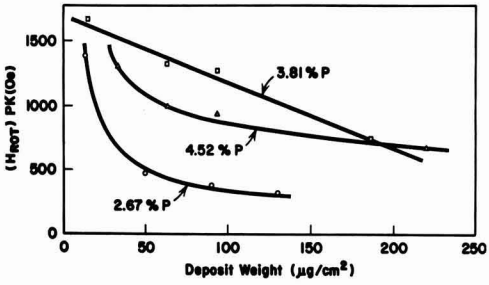

Fig. 11. Rotational hysteresis peak field *vs.* deposit weight

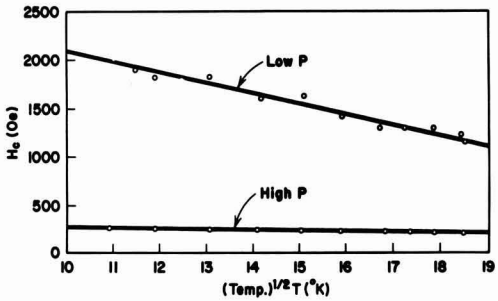

Fig. 12. Dependence of H_c on temperature for two thin deposits of different per cent P.

The temperature dependence of the coercivity of a selected number of these films was measured and the results for two of them are shown in Fig. 12. These particular samples are the thinnest samples of the low and high phosphorus films. The presence of near superparamagnetic particles should contribute a temperature dependence to the coercivity, such that H_c would be proportional to $-T^{1/2}$ if the anisotropy constants for the particles involved were independent of temperature (9). As shown in Fig. 12 the coercivity of these films is approximately proportional to $-T^{1/2}$. However, the low per cent P film shows by far the greatest temperature dependence.

Summary

Table IV summarizes the previous results for a selected number of samples. The temperature dependence of H_c is seen to be greatest for the low per cent P films. This appears to be in conflict with the postulate of less superparamagnetic behavior in these films. However, the uniaxial anisotropy constant for cobalt does increase ~50% in going to 77°K and this alone may be sufficient to account for the observed temperature dependence. All of the samples exhibit an orientation of the C-axis of cobalt in the plane of the film. The degree of orientation, however, is apparently greater for the higher per cent P films. In thin films in which the magnetization may be constrained, due to shape effects, to stay in the plane of the film, this orientation would lead to higher coercivity. However, the difference in orientations indicated here do not seem to play a large role.

Table IV. Summary of results for a selected number of samples

	Low P (2.6%)	Med P (3.8%)	High P (4.5%)
~t(Å)	150Å	180Å	350Å
$\frac{I(002)}{I(100)} \cdot N$	—	—	—
H_c	1000 oe	450 oe	200 oe
% increase of H_c at 77°K	70%	18%	22%
t(Å)	980Å	1070Å	1060Å
$\frac{I(002)}{I(100)} \cdot N$	0.54	0.23	~0
H_c	400 oe	1100 oe	400 oe
% increase of H_c at 77°K	53%	4%	14%
t(Å)	1460Å	2100Å	2460Å
$\frac{I(002)}{I(100)} \cdot N$	0.46	0.09	0.08
H_c	300 oe	700 oe	600 oe
% increase of H_c at 77°K	54%	24%	31%

In conclusion, we have shown that variation of the hypophosphite concentration of this plating solution causes concomitant variations in the plating rate and the per cent P of the resulting films. Below a thickness of ~2500Å the composition and magnetic moment density are independent of thickness. The hysteretic properties are a function of both thickness and per cent P. The study of the magnetic properties indicate that the high per cent P films have smaller particles at higher thicknesses than do the low per cent P films.

Manuscript received Dec. 17, 1965. This paper was presented at the Buffalo Meeting, Oct. 11-14, 1965.

Any discussion of this paper will appear in a Discussion Section to be published in the December 1966 JOURNAL.

REFERENCES

1. R. D. Fisher and W. H. Chilton, *This Journal*, **109**, 485 (1962).
2. J. S. Judge, J. R. Morrison, D. E. Speliotis, and G. Bate, *ibid.*, **112**, 681 (1965).
3. D. E. Speliotis, J. R. Morrison, and J. S. Judge, Proc. of the Intermag. Conf., p. 12.5 (1965).
4. L. D. Ransom and V. Zentner, *This Journal*, **111**, 1423 (1964).
5. E. A. Bergstrom, U. S. Patent #2,702,253.
6. H. Koretzky and B. Leland, U. S. Patent #3,142,582.
7. L. Reimer, *Z. Angew. Phys.*, **17**, 196 (1964).
8. W. D. Doyle, J. E. Rudisill, and S. Shtrikman, *J. Appl. Phys.*, **32**, 1785 (1961).
9. I. S. Jacobs and C. P. Bean, "Magnetism," Vol. 111, Chap. 6, p. 277, G. T. Rado and H. Suhl, Editors, Academic Press, New York (1963).

Gold Plating Directly on Molybdenum

R. M. Finne and W. R. Bracht

Bell Telephone Laboratories, Incorporated, Murray Hill, New Jersey

ABSTRACT

A technique has been developed to electrodeposit gold directly on a molybdenum substrate without prior deposition of other metals. The electrodeposited gold films are adherent and protective against highly corrosive ambients. The process involves the formation of a porous oxide on the molybdenum substrate, deposition of gold into this oxide, and hydrogen reduction of the oxide. During the reduction of the oxide, the gold is mechanically trapped and the substrate in the vicinity of the molybdenum surface is converted to a two-component gold-molybdenum layer. This layer provides a suitable surface for further deposition.

Prior to the development of the technique described in this paper, it had not been possible to electrodeposit gold on molybdenum or molybdenum-manganese substrates to produce an adherent and highly protective coating. Previous techniques have generally depended on the deposition of a more active metal such as copper, nickel, or chromium prior to deposition of gold (1). For many applications, particularly in the semiconductor field, such predepositions are undesirable since they may subsequently diffuse into the gold and degrade its alloying characteristics, or may diffuse into a semiconductor and perturb its electronic

properties. Alternatively, techniques have been proposed which involve the deposition of thin layers of gold followed by heat-treatment in non oxidizing ambients to form alloyed surface regions (2). Attempts to deposit gold directly on molybdenum by employing such standard electroplating techniques together with heat treating have not, in general, yielded acceptable results. This is because of the critical nature of certain preparatory steps in the process. By insuring the formation of a porous oxide on the molybdenum surface, depositing gold into this oxide and reducing the oxide to trap the gold, it has been possible to gold plate directly onto the molybdenum sample.

Apparatus and Materials

The electrodeposition apparatus and materials used were essentially standard in nature, and both still and barrel plating proved suitable. A typical bath construction was as follows: polypropylene tank, quartz immersion heaters, and gold anodes in an anode to cathode area ratio in excess of four to one. The acid citrate gold bath was prepared by mixing 20 ± 1g of sodium gold cyanide (71% gold) and 100 ± 1g of diammonium citrate and water to make one liter of solution. This was then boiled in a hood for 30 min to convert the cyanide gold complex to the citrate complex with the accompanying evolution of HCN. The bath was operated at a current density of 49 ma/in.^{2} at 60°C, and deposited 0.93 mg/cm^2/min. Both acid citrate and alkali cyanide solutions were used successfully.

Substrates used in the initial work were both machined molybdenum studs and molybdenum-manganese films which were silk-screened onto ceramic surfaces. Subsequent work has been done with a great variety of sample shapes and sizes.

Method

Figure 1 shows a schematic flow diagram for the plating method. The following is a description of the optimum procedure developed for our samples.

1. Initial degreasing of the substrates in trichloroethylene.
2. Fire in dry hydrogen (< 2 ppm H_2O) at 1000°C for approximately 10 min. (In no case were the samples passed through the flame curtain on the oven.)
3. Immerse in a solution of four parts NH_4OH (28%) to one part H_2O_2 (30%) for approximately 8 sec at room temperature.
4. Wash in deionized water.
5. Gold strike to deposit 0.15-0.62 mg/cm^2.
6. Wash in deionized water.
7. Fire in dry hydrogen (< 2 ppm H_2O) at 900°C for approximately 10 min.
8. Electrodeposit gold to the final desired thickness (~ 15 mg/cm^2).

Evaluation

The electrodeposited gold was tested for substrate protection against gaseous and liquid ambients, and for adherence to the substrate.

Protection against gaseous ambients was evaluated by exposure of the sample to wet hydrogen at 600°C for 1 hr. Protection against liquid ambients was evaluated by immersion of the sample in a 5 part HNO_3 (70%) —1 part HF (48%) solution at room temperature. The presence of blistering, peeling, or cracking on the sample when viewed under ten power magnification was considered evidence of unsatisfactory plating.

Nonadherence of an electrodeposited gold film would, in all probability, be made evident by a blistering of the coating during the testing described above. However, to test adherence further, a silicon wafer 30 mils in diameter was alloyed to the plated sample and the alloyed wafer was subjected to a shearing force of 9500 psi. If the wafer pulled gold from the substrate, the plate was considered unsatisfactory.

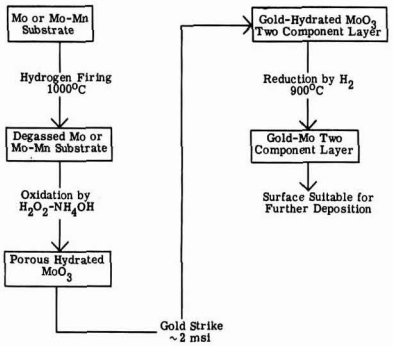

Fig. 1. Flow chart of the optimum processing steps

Discussion

Initial attempts to gold plate directly on molybdenum surfaces resulted in either nonadherent plates or plates which would not survive exposure to corrosive ambients. The substrates were carefully cleaned so that it was not a case of failure caused by surface contamination. These molybdenum samples (20 mils thick) were degassed at 1200°C for 1 hr in a vacuum of 10^{-6} Torr, but were unsatisfactory after plating. We therefore concluded that gassing was not the main problem. Since it is well known that molybdenum forms oxides such as MoO_3 which are stable at low temperatures, we postulated that such oxides were forming a barrier between the gold plate and the molybdenum surface.

Since gold and molybdenum form no alloys, and the solubility of each in the other is negligible (3), it is not possible to form a two-component phase by heating a gold plated molybdenum sample below its melting point. Since gold does not react with molybdenum oxide, chemical bonding cannot occur at the gold plate-substrate interface. Such mechanisms may be instrumental in the formation of satisfactory electrodepositions with metals such as copper, nickel, and chromium.

Instead of attempting to remove the nonporous oxide immediately prior to plating, the technique which was evolved makes use of a porous oxide which is generated on the molybdenum surface by aqueous oxidation. Plating solutions can permeate this type of molybdenum oxide and are deposited in the oxide during the strike. Reduction by hydrogen follows, which converts the molybdenum oxides to molybdenum, physically trapping the gold in a molybdenum matrix. This two-component layer is then suitable for further plating.

The postulated roles played by the significant processing steps are as follows:

1. The firing of dry hydrogen prior to plating serves two purposes: first, it reduces surface oxides; second, it degasses the surface. The temperature of this firing exceeds that of any subsequent processing step.

2. The treatment with ammoniacal peroxide solution forms a porous oxide on the substrate. The major reaction proceeds as in Eq. [1].

$$Mo + 3H_2O_2 \rightarrow MoO_3 \cdot xH_2O + (3\text{-}x)\ H_2O \qquad x = 1, 2 \qquad [1]$$

This oxide dissolves in the ammonium hydroxide forming ammonium molybdate as in Eq. [2].

$$MoO_3 \cdot xH_2O + 2NH_4OH \rightarrow (NH_4)_2MoO_4 + (x+1)H_2O \qquad x = 1, 2 \qquad [2]$$

This etching action forms a fresh surface which reacts to form a porous, hydrated oxide.

3. The gold strike solution permeates the oxide structure.

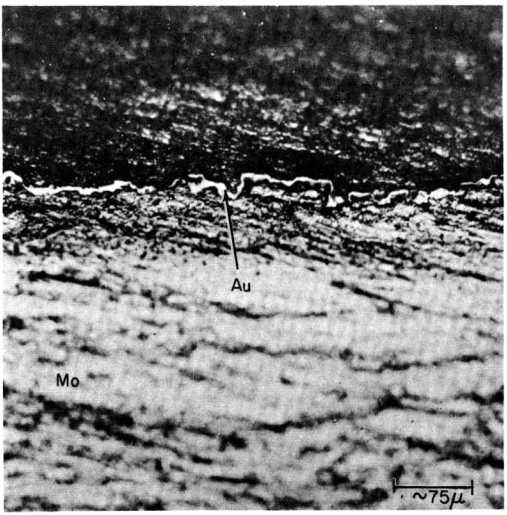

Fig. 2A. Thermally oxidized sample, angle lapped. Magnification *ca.* 170X.

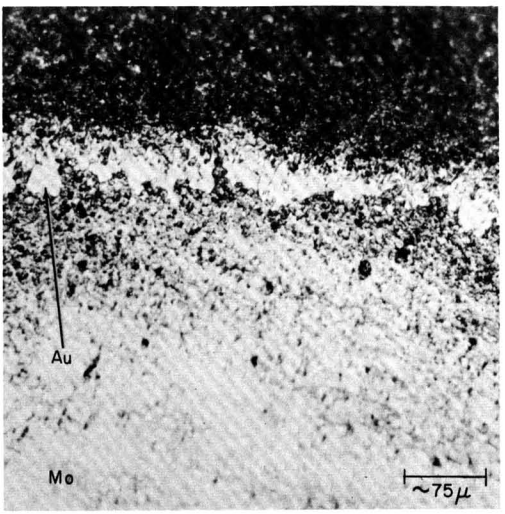

Fig. 3A. Chemically oxidized sample, angle lapped. Magnification *ca.* 170X.

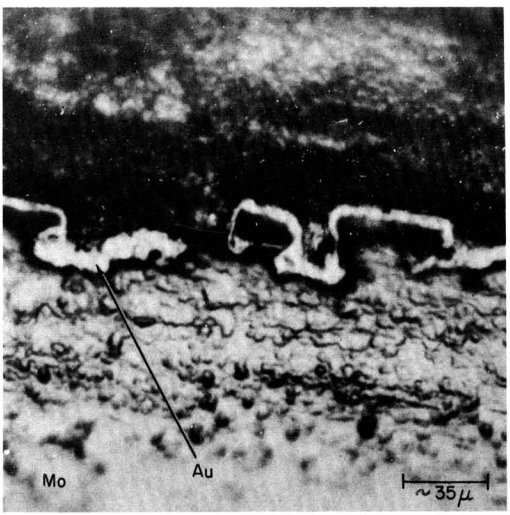

Fig. 2B. Thermally oxidized sample, angle lapped. Magnification *ca.* 670X.

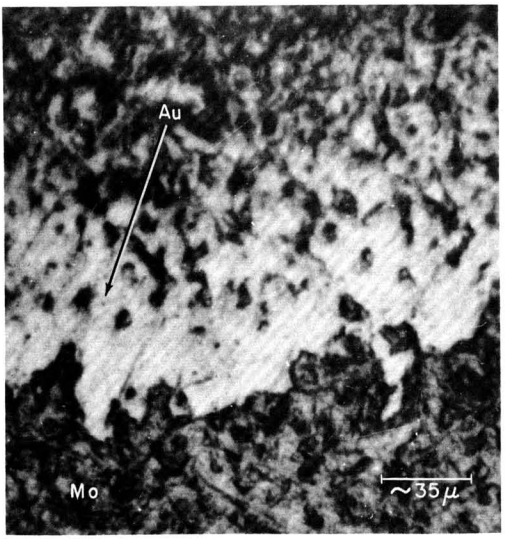

Fig. 3B. Chemically oxidized sample, angle lapped. Magnification *ca.* 670X.

4. The firing in dry hydrogen subsequent to the gold strike reduces the molybdenum oxide to molybdenum as in Eq. [3].

$$MoO_3 \cdot xH_2O + 3H_2 \rightarrow Mo + (3 + x)H_2O \qquad [3]$$
$$x = 1, 2$$

This creates a two-component region at the surface of the substrate which is suitable for further plating by routine techniques.

In order to verify the critical postulated roles, several experiments were performed.

Firing.—The initial hydrogen firing of step two was eliminated from the processing. The resulting samples blistered on heating, predominantly at the corners and edges. This is often characteristic of gassing. From this we may infer that step two is instrumental in degassing the substrate.

In addition, argon was substituted for hydrogen and the final results were satisfactory. This implies that the process is a thermal one and does not depend on the chemical nature of the heating ambient.

Oxidation.—A thermal oxidation was substituted for the ammoniacal peroxide treatment. All plated parts failed the tests. The results of metallographic sectioning and angle lapping are shown in Fig. 2 and 3. In the case of the thermal oxide, the electrodeposited gold appears to rest on the surface of a thin oxide layer. In the case of the chemically produced oxide, the electrodeposited gold appears to have penetrated into the oxide.

In addition, electron micrographs were taken of the oxide surfaces. Figures 4 and 5 show the results for the two types of oxide described. The chemical oxide appears to have a cellular, porous structure while the thermally grown oxide appears to be smooth and continuous.

Strike.—The gold strike was increased in thickness which resulted in an increased porosity of the electrodeposited film. This may be due to the formation of a relatively continuous layer of gold over the gold-permeated oxide. Such a continuous layer might inhibit the reduction of the oxide which takes place in

the following step. It appears desirable, therefore, not to provide complete surface coverage by the strike.

Reduction.—The hydrogen reduction after the strike was eliminated from the process. This resulted in non-adherent electrodepositions. Also, a lowering of the firing temperature produced an increase in the porosity of the gold plate. This step is essential to the process.

Variations in the processing are possible. For example, molybdenum samples which had a large surface to volume ratio and which appeared to be without surface oxide on delivery were processed successfully without the use of the hydrogen firing prior to the gold strike.

Fig. 4. Chemical oxide, electron micrograph, replica. Magnification *ca.* 23,330X.

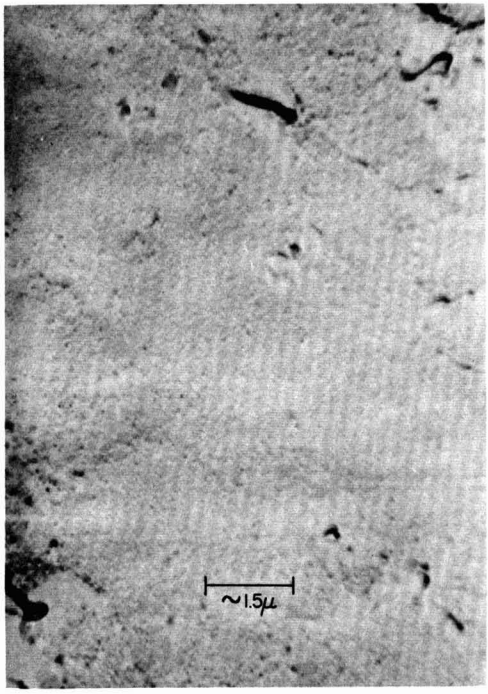

Fig. 5. Thermal oxide, electron micrograph replica. Magnification *ca.* 23,330X.

Fig. 6. Oxide formed with NH_4OH, electron micrograph. Magnification *ca.* 6700X.

Fig. 7. Oxide formed with H_2O_2, electron micrograph. Magnification *ca.* 6700X.

Fig. 8. Oxide formed with H_2O, electron micrograph. Magnification *ca.* 6700X.

This same type of sample was also successfully processed with the substitution of water for the ammoniacal peroxide solution in step three. However, this can only be done with samples which do not require the removal of surface layers for cleaning. Attempts to use only NH_4OH (28%) were successful, but attempts to use H_2O_2 (30%) only were not. Figures 6, 7, and 8 show electron micrographs of the oxide surfaces of samples processed in NH_4OH (28%), H_2O_2 (28%), and water. It can be seen that the cellular structures formed by water, ammonium hydroxide, and the ammoniacal peroxide solution are similar whereas the hydrogen peroxide solution appears to attack the surface more vigorously and produces an extremely rough oxide. This rough surface is apparently not satisfactory for further plating.

This process has also been used on molybdenum-manganese films deposited on ceramics. In this case, the time of the oxide formation step is critical since excessive removal of the thin metal film is undesirable.

Conclusion

The process described can be used to electrodeposit gold on molybdenum and molybdenum-manganese substrates without the use of preplates of other metals. Essential steps in the process are:

1. Formation of a porous molybdenum oxide.
2. Permeation of the oxide with gold, without forming a continuous gold layer over the oxide surface.
3. Reduction of the oxide, which traps the gold in the molybdenum lattice and forms a two-component layer on the surface.

The electrodeposited gold films produced by this process are adherent and protective, and have been plated to thicknesses of over one mil using both still and barrel plating.

Acknowledgments

The authors thank Mrs. A. M. Hunt who performed the electron micrography, and Mr. A. A. Tartaglia who performed the metallurgical sectioning.

Manuscript received Jan. 13, 1966; revised manuscript received March 9, 1966. This paper was presented at the San Francisco Meeting, May 9-13, 1966.

Any discussion of this paper will appear in a Discussion Section to be published in the December 1966 JOURNAL.

REFERENCES

1. Schaer and Beach, U. S. Pat. 2,886,499, May 12, 1959.
2. A. G. Russel, U. S. Pat. 2,816,066, Dec. 10, 1957.
3. M. Hansen, "Constitution of Binary Alloys," p. 217, McGraw-Hill Book Co., Inc., New York (1958).

Protection of Steel from Hydrogen Cracking by Thin Metallic Coatings

I. Matsushima and H. H. Uhlig

Corrosion Laboratory, Massachusetts Institute of Technology, Cambridge, Massachusetts

ABSTRACT

Cold rolled and stress relieved 0.5% carbon steel specimens electroplated with Ni, 0.50-2.5μ thick and bent to the test span after plating are especially resistant to hydrogen cracking when polarized cathodically in dilute sulfuric acid saturated with As_2O_3. Arsenic or an As compound deposits cathodically on the Ni coating which supplements protection by Ni alone. The dual coating is also effective in the presence of additives to H_2SO_4, such as thiourea, which normally accelerate occlusion of hydrogen by steel. The critical hardness value of steel below which some degree of protection is achieved by Ni + As coatings is about Rockwell C 35. Ni coatings alone are protective against sulfide cracking when cathodically protected in 6% NaCl-0.5% acetic acid, saturated with H_2S. The mechanism of protection is apparently one of altering the kinetics of H^+ discharge, resulting in less occlusion of hydrogen by steel. Accordingly, such coatings to be protective need not be continuous.

Limited data have been reported previously on the protective quality of metallic coatings on steel exposed to environments which generate hydrogen by a corrosion reaction, thereby leading to hydrogen cracking (1,2). Still less information is available on the relative effect of such coatings under conditions of continuous polarization which provides cathodic protection to the coating and avoids damage to it by corrosive attack. This situation deserves study both because it leads to a better understanding of the mechanism of protection by coatings and also because it suggests practical means of protecting susceptible steels against damage. This is the subject of the present paper. The problem has become much more important in recent times be-

cause of increased use of high-strength steels which are exposed to many different environments, some of which induce hydrogen cracking.

Probably the most significant data bearing on this problem were presented by Freiman and Titov (3). They measured diffusion rates of hydrogen through Armco iron sheets 0.17 mm thick, cathodically polarized in H_2SO_4 to which $NaAsO_2$ was added. A thin coating of Cu, Sn, Pb, or Ni applied to one side of the sheet effectively slowed down entrance of hydrogen into the iron when H^+ discharged on the coating. Nickel coatings only 0.1-2.5μ (0.004-0.1 mil) thick were especially effective whereas Pb coatings to be similarly effective had to be 10μ (0.4 mil) thick. There was little or no difference in diffusion rates for any of the coatings when H^+ discharged on the iron surface and occluded hydrogen diffused subsequently through the metallic coating.

Tardif and Marquis (4) cathodically charged 0.06% C steel sheet 0.38 mm thick in 2% NaOH at 40°C. They measured diffusion rates of hydrogen through the coated steel and also measured the fracture tendency of the steel after it had been polarized, employing a special deformation test. All coatings, *e.g.*, Cr, Au, Au-Ni, Ni, Cu, Pb, Cd, and Al, except for Zn and Mg, were beneficial to some extent in retarding entry of hydrogen into the steel.

Experimental

The base steel on which coatings were applied was a commercial 1055 steel (0.52% C, 0.81% Mn, 0.01% P, 0.01% S) cold reduced 50% and stress relieved in a salt bath at 400°C for 3 hr. The rolling direction was parallel to the longest dimension. Stress relief heat-treatment was chosen to prolong normal cracking time and thereby improve reproducibility of the present tests from an average of 6 min for the cold-rolled steel to 42 min for the stress-relieved steel. For some experiments, the steel specimens were quenched from 925°C and tempered at various temperatures up to 500°C in a salt bath for 1 hr. Above 500°C specimens were sealed in evacuated Vycor capsules and heated in a furnace for 1 hr. Specimens, as sheared to size, measured 1¾ x 3/16 x 0.041 in. (4.5 x 0.48 x 0.10 cm). After shearing they were abraded to a final No. 0 emery paper which removed approximately 1 mil of all 6 surfaces. They were then degreased in boiling benzene, pickled in 5 v/o HNO_3, 95°C for 1 min, washed, immersed in acetone, and dried in a warm air blast. Specimens were subsequently plated and then bent to the proper span for testing.

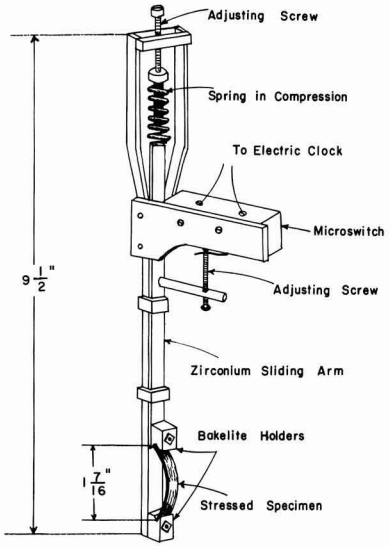

Fig. 1. Apparatus for hydrogen cracking tests

The test apparatus depicted in Fig. 1 was arranged so that specimens under constant spring load were polarized cathodically at 24 ma/cm^2 in 5% H_2SO_4 saturated in most cases with As_2O_3 at room temperature. Failure by cracking tripped a switch connected to an electric clock. That portion of the test apparatus in contact with the electrolyte was constructed of commercial Zr[1] to avoid corrosion. The insulated specimen itself was cathodically protected by the prevailing cathodic current. Specimens were bent beyond the elastic limit to an initial span of 1⅝ in. (4.1 cm), then transferred by means of a metal holder to the notched Bakelite insulators of the test apparatus. A compression spring was adjusted until the final span of the specimen was 1-7/16 in. (3.65 cm), carefully avoiding springback. A nickel wire, previously spot welded to one end of the test specimen, was attached to the negative terminal of a rectifier; the positive terminal was connected to an auxiliary Pt electrode immersed in the electrolyte contained in a 250-ml beaker. Tests were carried out a maximum of 200 hr, lack of failure within this time representing appreciable resistance to hydrogen cracking. Susceptible specimens commonly cracked within a fraction of an hour. For long runs, distilled water and As_2O_3 were added to the electrolyte every 24 hr.

Some tests were carried out in 6% NaCl-0.5% acetic acid saturated with H_2S at room temperature. For those tests, specimens were bent to the usual span and mounted in simple holders of Bakelite. They were placed in a 5-liter glass desiccator vessel and totally immersed in the test solution. Specimens were examined visually for cracks without removing them from the container.

Coatings, when applied, were electrodeposited to a thickness of 0.01-0.5 mil (0.25-12.7μ) as determined by weight gain. Nickel electrodeposits employed a $NiSO_4$-NH_4Cl-boric acid bath, lead coatings a fluoride-boric acid bath, copper coatings a cyanide bath, iron coatings a ferrous sulfate bath, cobalt coatings a cobalt sulfate-boric acid bath, and arsenic coatings a sodium cyanide-As_2O_3 bath. A few specimens were coated with electroless Ni (5).

Results

Cracking times of coated steel specimens are summarized in Table I. Lead coatings were relatively effective if the thickness was at least 0.1 mil, and copper coatings were similarly effective at 0.5 mil. Nickel coatings of 0.5 mil thickness, on the other hand, cracked when the specimen was bent preparatory to testing; such specimens subsequently failed in the H_2-cracking tests. Surprisingly, however, thinner Ni coatings which did not visibly crack afforded protection for a thickness of only 0.02 mil. This thickness seems also to coincide with marked reduction in porosity of the coating as shown by data of Fig. 2. A measure of

[1] Supplied by courtesy of Carborundum Metals Climax, Inc.

Table I. Effect of electrodeposited coatings on H_2 cracking of 1055 steel, cold rolled 50%, annealed 400°C, 3 hr, cathodically polarized in 5% H_2SO_4 + As_2O_3, 24 ma/cm^2 (minimum of 2 specimens for each run)

Coating	Thickness of coating, mils					
	0.00	0.01	0.02	0.05	0.1	0.5
	Avg cracking time, hr					
None	0.7					
Ni		2.4	NC	NC	NC	1.0
Pb		3.3	—	23	NC	NC
Cu		2.5	—	—	1.7	NC
Co		—	—	51	72	10
Fe		—	—	2.3	0.6	—

NC = no cracking in >200 hr.

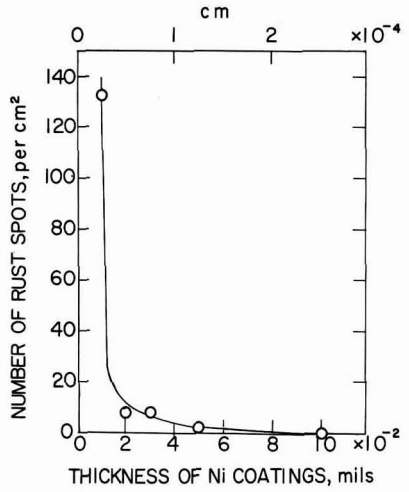

Fig. 2. Porosity of nickel coatings as a function of thickness

porosity was obtained by counting under the microscope the number of rust spots per unit area after immersing specimens horizontally for 10 min in 3% NaCl + 1.5% by volume of 30% H_2O_2. It is unlikely that any of the Ni coatings were truly pore free, so that the protective mechanism of thin Ni coatings probably depends on a critical area ratio of Ni to exposed Fe at pores. This unusual protective quality of Ni coatings prompted a more detailed study of their properties.

The next attempt was to protect a quenched martensitic 1055 steel (Rockwell hardness = C 64), which, compared to the stress relieved cold-rolled material (C 31), is much more sensitive to hydrogen cracking. Uncoated quenched specimens cracked prematurely on bending; tempered at 300°C for 1 hr (C 51) they could be bent but, subsequent to bending, they suffered H_2 cracking within 1/3 min. Data for various tempering temperatures are summarized in Fig. 3. Here it is noted that the quenched steel, tempered subsequently at 300° or 400°C, cracked in very short time whether or not a thin coating of nickel covered the surface. However, at higher tempering temperatures, beginning at 450°C (Rockwell hardness = C 35), the nickel-coated specimens were appreciably more resistant than the uncoated specimens. Since hardness of the steel decreases with increasing tempering temperatures accompanied by decrease in susceptibility to hydrogen

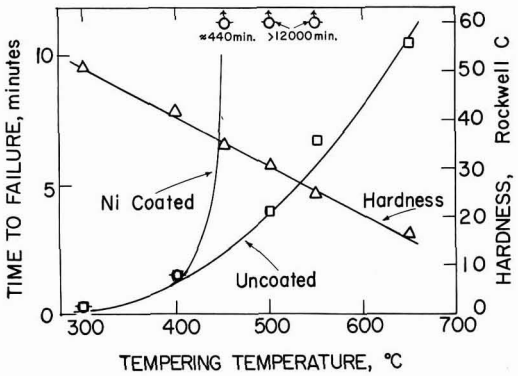

Fig. 3. Times to failure of nickel coated (0.05 mil) and uncoated quenched AISI 1055 steel tempered at various temperatures for 1 hr, 5% H_2SO_4 + As_2O_3 (saturated), 24 ma/cm², room temperature.

Table II. Effect of various catalyst poisons in 5% H_2SO_4 on H_2 cracking of 1055 steel, cold rolled 50%, annealed 400°C, 3 hr, coated with Ni, cathodically polarized 24 ma/cm²

Poison	Avg cracking time
0.05 mil Electrodeposited Ni	
As_2O_3 (sat'd)	>200 hr (3 spec.)
Sb_2O_3 (1.6 g/l)	163 hr (3 spec.)
Thiourea (0.2 g/l)	26 hr (7 spec.)
H_2SeO_3 (0.3 g/l)	14 hr (4 spec.)
0.1 mil Electroless Ni	
As_2O_3 (sat'd)	>200 hr (2 spec.)
Thiourea (0.2 g/l)	2 hr, 169 hr

cracking, it is presumably only below a critical susceptibility (Rockwell hardness <C 35) that the thin Ni coating provides an advantage. It is possible, of course, that Ni coatings would extend their range of effectiveness for more susceptible specimens under less severe conditions of H_2 charging.

Of interest to the mechanism were experiments carried out on Ni-coated specimens using catalyst poisons in H_2SO_4 solution other than As_2O_3. Data are summarized in Table II. Results are also included for 2.5μ (0.1 mil) electroless Ni coatings which were found to behave in much the same manner as electrodeposited coatings. Electroless Ni coatings 3.8μ (0.15 mil) thick were similar in behavior to the thinner coatings. It is obvious that thin Ni coatings are effective in presence of As_2O_3, but less so in presence of other poisons.

Experiments were next carried out to determine whether Ni-coated specimens prepolarized in 5% H_2SO_4 + As_2O_3 afford subsequent protection when cathodically polarized in 5% H_2SO_4 containing other type poisons, *e.g.*, thiourea. The thought behind this experiment was to learn whether protection was supplemented by arsenic deposited on a Ni surface. Also, if arsenic is effective, would it be similarly effective if predeposited from a cyanide bath, or if codeposited along with nickel by adding As_2O_3 to a nickel plating bath. Results are summarized in Table III. Prepolarization in H_2SO_4 + As_2O_3 for 15 hr is effective, the time for which can be shortened by prepolarizing at the boiling temperature of the H_2SO_4 electrolyte. None of the other pretreatments comparatively was as effective. This is a preliminary conclusion which should be substantiated by further tests accompanied by analyses of the electrodeposits. Probably the main reason for lack of protection is that specimens were bent for testing after deposition of As or As + Ni coatings, thereby producing cracks in the coating which allowed hydrogen penetration to the base steel. Ni-plated specimens

Table III. Effect of arsenic plus Ni coatings on H_2 cracking of 1055 steel, cold rolled 50%, annealed 400°C, 3 hr, cathodically polarized in 5% H_2SO_4 + 0.2 g/l thiourea, 24 ma/cm², room temperature

Treatment	Avg cracking time
1. Deposition of As on 0.05 mil Ni from cyanide bath, 5 ma/cm², 0.5 hr.	
Room temperature	55 hr (2 spec.)
Arsenic-coated specimen heated in H_2O, 100°C ½ hr	53 hr (2 spec.)
2. Codeposition of Ni and As, 10 ma/cm², 4 min	
Room temperature	34 hr (6 spec.)
Coated spec. heated 400°C, 3 hr	9 hr (3 spec.)
3. Prepolarization of 0.05 mil Ni in 5% H_2SO_4 + As_2O_3, 24 ma/cm²	
Room temp, 2.5 hr	2.7 hr (2 spec.)
5.0 hr	56 hr (2 spec.)
15.0 hr	NC (2 spec.)
Boiling point, 2.5 hr	77 hr (2 spec.)
5.0 hr	NC (2 spec.)*

NC = no cracking in >200 hr.
* A third spec. failed in 112 hr.

Table IV. Hydrogen cracking of stressed cold rolled 1055 steel, previously cold rolled 50%, annealed 400°C, 3 hr, immersed in 6% NaCl, 0.5% acetic acid saturated with H_2S; with and without cathodic polarization, room temperature

Specimen	Cracking time, days		
Cath. current density →	0	0.05	0.5 ma/cm²
Uncoated	<2	<2	<2
Coated with 0.05 mil Ni	<2	<1	7, NC
The same prepolarized 15 hr in 5% H_2SO_4 + As_2O_3	<2	4-5	NC
Coated with 0.1 mil Ni	<2	<2	NC
The same prepolarized 15 hr in 5% H_2SO_4 + As_2O_3	<2	2-3	NC

NC = no cracking in >8 days.

of Table III prepolarized in H_2SO_4 + As_2O_3 were already stressed to the test span during pretreatment and were then transferred to the H_2SO_4 + thiourea electrolyte without changing the span.

The next series of experiments was conducted to determine to what extent Ni plus As coatings are effective in total immersion tests in 6% NaCl-0.5% acetic acid periodically saturated with H_2S. This test is commonly employed to determine susceptibility of stressed steels to hydrogen cracking or sensitivity to so-called sulfide cracking. The base steel was again 1055 steel, cold rolled and annealed at 400°C, with the thickness of nickel coating being either 0.05 or 0.1 mil. Data are summarized in Table IV. Since all specimens failed within 2 days whether coated with Ni or with Ni plus As, additional tests were carried out with continuous cathodic polarization of the specimens in the same test medium. At 0.05 ma/cm², failure times for some specimens coated with Ni + As were extended, but all specimens failed nevertheless. At a higher current density of 0.5 ma/cm², Ni-coated specimens, except one, survived the maximum test period of 8 days. Protection was obtained whether or not the specimens were prepolarized in the H_2SO_4-As_2O_3 electrolyte. In other words, thin Ni coatings are effective in diminishing H_2 cracking of steel for H_2S-type exposures, but only if the coated steel is cathodically protected. Unlike the polarization experiments in H_2SO_4 previously reported, presence of As on the nickel surface does not seem to be essential, although results at 0.05 ma/cm² suggest that some small advantage results.

Discussion

Although metal coatings conceivably protect against hydrogen penetration into steel by acting as a diffusion barrier, it is not likely that this particular mechanism operates for the thin films now under study. Instead, the coatings apparently act mainly to alter kinetics of hydrogen ion discharge, resulting in less occlusion of hydrogen by the metal electrode. The specific surface properties of the metal are more important, in other words, than its diffusivity for hydrogen. This was demonstrated by results of Freiman and Titov (3) who also proposed that the surface electrochemical factor in their experiments accounted largely for the protective effect of thin metal coatings on diffusion of hydrogen into steel.

The important effect of the electrode surface is also apparent from the large effect on cracking produced by small additions of catalyst poisons, *e.g.*, arsenic compounds, thiourea, sulfur ions, etc., to the electrolyte. In absence of $NaAsO_2$ in their sulfuric acid electrolyte, Freiman and Titov (3) found no hydrogen to diffuse through uncoated steel after cathodic polarization for 2 hr, whereas in the presence of $NaAsO_2$ hydrogen appeared after 1 or 1½ min. Schuetz and Robertson (6) found that CS_2 additions to H_2SO_4 electrolyte increased hydrogen absorption of a cathodically polarized 10% Ni-Fe alloy by a factor of 15. It is known, moreover, that often a highly stressed steel exposed to an acid environment will not hydrogen crack except in presence of compounds like H_2S or As_2O_3.

The present results are the more surprising in view of the beneficial effect of thin Ni coatings associated with As where the latter element instead of increasing hydrogen occlusion by the underlying steel, decreases it. The arsenic retains its beneficial influence even in presence of other poisons such as thiourea (Table III). One exception is in the acetic acid-H_2S test (Table IV) where Ni coatings alone are effective, and As is not required to supplement protection against failure. Addition of As_2O_3 to H_2SO_4 leads to visible cathodic deposition of elemental As or an As compound on the cathode surface, and, as Freiman and Titov (3) showed, if the film is not too thick, occlusion of hydrogen by uncoated steel is increased by its presence. Elemental As has a high value of hydrogen overvoltage apparently leading to increased thermodynamic activity of adsorbed atomic hydrogen on the steel surface and hence to a greater tendency for hydrogen to enter the metal lattice.

Accordingly, the beneficial effect of As associated with a Ni coating can be ascribed to the possibly low hydrogen overvoltage of a chemical compound formed between As and Ni. This hypothesis is supported by the reduced time necessary to achieve protection by the duplex coating when the electrolyte is heated during As deposition which probably favors compound formation (Table III). Raub *et al.* (7) found that when As is codeposited with Ni on an electrode at which H^+ discharges simultaneously, the potential becomes more noble, corresponding to a decrease in hydrogen overvoltage. This shift of potential is in the right direction to explain the effect of the present Ni-As coatings. The Ni coatings containing As by codeposition, on the other hand, were not found to be especially effective, but, as described earlier, this is probably because of the brittle nature of coatings containing arsenic, allowing formation of cracks during bending through which hydrogen can enter the steel. Preliminary potential measurements on the present protective Ni-As coatings confirmed that a lower hydrogen overvoltage results when As is deposited on Ni. The observed difference of 40 mv at 24 ma/cm² (changing with time), was not large, however; hence there is the possibility that factors enter in addition to overvoltage effects. Even for metals like Pb with high H_2 overvoltage, there is apparently little tendency for cathodic hydrogen either to enter the Pb lattice or to transfer occluded H to the underlying steel.

Assuming that a compound is formed between Ni and As, the next step was to identify it by x-ray. The thin black surface layers of several Ni-As coated electrodes were carefully removed and examined in a Debye-Scherrer camera, but only lines of Ni appeared. Patterns were repeated several times with the same results. A black residue which collected on the bottom of the H_2SO_4-As_2O_3 electrolyte after a long period of electrolysis, and which is presumably elemental arsenic, gave an amorphous pattern. Hence it is concluded that if a surface compound of Ni and As forms, it is either amorphous or the layer is too thin for x-ray diffraction. The inability of the Ni-As coatings to protect quenched 1055 steel suggests that the amount of hydrogen necessary to cause failure of the martensitic steel is so small that the present thicknesses of coatings are not sufficiently protective. For tempered martensite, or for cold rolled steel, on the other hand, the apparent required amount of hydrogen is greater, and for this situation the coatings adequately reduce occlusion of hydrogen by steel to a value below that required for failure. The present investigation demonstrates that metal coatings need not be continuous in order to protect steel against hydrogen cracking and that their porosity need only fall below a critical value.

Acknowledgment

This research was supported by the U.S. Army Research Office-Durham, on Contract DA-31-124-

ARO(D)-47 to whom the authors express their appreciation.

Manuscript received Dec. 13, 1965; revised manuscript received March 7, 1966.

Any discussion of this paper will appear in a Discussion Section to be published in the December 1966 JOURNAL.

REFERENCES

1. M. Bartz and C. Rawlins, *Corrosion*, **4**, 205 (1948).
2. D. Warren and G. Beckman, *ibid.*, **13**, 631t (1957).
3. L. Freiman and V. Titov, *Zhur. Fiz. Khim.*, **30**, 882 (1956).
4. H. Tardif and H. Marquis, *Can. Met. Quart.*, **1**, 153 (1962).
5. In accord with No. 1 bath, "Modern Electroplating," Fred Lowenheim, Editor, 2nd ed., p. 700, John Wiley & Sons, Inc., New York (1963).
6. A. Schuetz and W. Robertson, *Corrosion*, **13**, 437t (1957).
7. E. Raub, M. Wittum and S. Gmünd, *Korros. u. Metallschutz*, **15**, 127 (1939).

Impurity Segregation in Binary Compounds

M. R. Lorenz and S. E. Blum

Watson Research Center, International Business Machines Corporation, Yorktown Heights, New York

ABSTRACT

The effect of the pressure of the constituents of a binary compound on the segregation coefficient (k_o) of a substitutional impurity is considered. The theory concerning the incorporation of an impurity is briefly reviewed, and the dependence of k_o on P_M is given for various combinations of electrical character of an impurity and the site the impurity occupies. The impurities In and Sb were studied in CdTe. k_o(In) is inversely proportional to P_{Cd} and k_o(Sb) directly proportional to P_{Cd}. The results are in quantitative agreement with the theoretical prediction if it is assumed that native defects play a negligible role as a source of free carriers or charge compensation. The donor Te, the acceptor Zn, and the amphoteric impurity Sn were studied in InAs by pulling crystals by the Czochralski method at various arsenic pressures. The k_o's follow the predicted behavior. The practical significance of the dependence of k_o on the pressure of compound constituents in relation to materials preparation is discussed briefly.

Research on semiconductor systems has brought about a good understanding of segregation processes and of the factors governing distribution coefficients in binary systems (1). The knowledge acquired in such two-component systems has also been applied to the more complex ternary systems. There have been a number of investigations concerned with various aspects of the segregation of an impurity in a binary compound. Most of this work was done on III-V compounds and much of it has been recently reviewed (2). In many of these studies the segregation coefficients were determined by assuming a pseudobinary system, *i.e.*, an impurity (one component) and a binary compound (the second component). In general the investigations were concerned with segregation in liquid-solid phase equilibria. More recently Chang and Pearson (3) studied solubilities and distribution coefficients of Zn in GaAs and GaP from vapor-solid equilibria while McCaldin (4) studied the Zn-GaAs system as a true three-component system. The behavior of Ge in GaAs was investigated in liquid-solid phase equilibria (5). Segregation of Zn between solid InSb and In-Sb melts of various compositions has also been investigated (6). The solubility of group II, IV, and VI elements in GaP was studied by Trumbore *et al.* (7, 8).

The major aim of this study was to examine the dependence of the distribution coefficient on the site the impurity occupies, the effects of the electrical characteristics of the impurity, and the role of the chemical potential of the component that normally occupies the site. For our experimental investigation we chose the In-As system as a representative of the III-V compounds and the Cd-Te system as a representative of the II-VI compound family. Both compounds are low melting and therefore presented the least difficulty experimentally. Three impurities were studied in InAs, and two impurities were investigated in CdTe.

Theory

We wish to review briefly the theory concerning the incorporation of an impurity atom X in the compound MN. We will use the mass action approach of Kroeger and Vink (9) and follow approaches similar to those used by Thomas (10), McCaldin (4), and Kroeger (11). We confine our attention to impurities which sit on normally occupied lattice sites. Let us assume first that X is a donor which resides on an M site (X_M^D). The equilibrium of X in the solid MN and some external phase (X_l) can be illustrated by the reaction.

$$V_M + X_l = X_{M^D}{}^+ + e^- \qquad (I)$$

where V_M is a neutral M vacancy, $X_{M^D}{}^+$ is the ionized donor, and e^- is a free electron. Making the usual assumption of ideal solution behavior, we write the equation which governs reaction (I) as follows

$$\frac{[X_{M^D}{}^+]\, n}{[V_M][X_l]} = K_1(T) \qquad [1]$$

where $K_1(T)$ is the temperature dependent equilibrium constant. Since all K's are temperature dependent, the bracketed T will hereafter be dropped for simplicity. In general, we are concerned with impurity states which lie close to their respective bands. For such states we can assume that at or near the melting temperature of the compound they are sufficiently ionized that the concentration of the ionized impurity is equal to the total concentration of that impurity, *i.e.*, $[X_M{}^D] = [X_{M^D}{}^+] + [X_{M^D}{}^0] \cong [X_{M^D}{}^+]$. With this assumption we may write the equilibrium segregation coefficient for a donor impurity substituted on an M site, $k_o(X_M{}^D)$

$$k_o(X_M{}^D) \simeq k_o(X_{M^D}{}^+) = \frac{[X_{M^D}{}^+]}{[X_l]} = \frac{V_M K_1}{n} \qquad [2]$$

where k_o describes the solid-liquid equilibrium. Since $[V_M]$ is inversely proportional to the pressure of M. as $P_{M_y}{}^{1/y}$ where y is the number of atoms in the given vapor specie, we can write Eq. [2] as

$$k_o(X_M{}^D) = \frac{K_3}{n\, P_{M_y}{}^{1/y}} \qquad [3]$$

Table I. Dependence of the impurity segregation coefficient, k_o, on lattice sites, P_M, and carrier type and concentration
The K's are temperature dependent constants with subscripts omitted for simplicity. For the definition of k_o see Eq. [2]

Impurity	Character site	X_M^D	X_N^D	X_M^A	X_N^A	$X_{M,N}^{A,D}$
Segregation coefficient		$\frac{K}{n P_{M_y}^{1/y}}$	$\frac{K P_{M_y}^{1/y}}{n}$	$\frac{K}{p P_{M_y}^{1/y}}$	$\frac{K P_{M_y}^{1/y}}{p}$	$\frac{K}{n P_{M_y}^{1/y}} + \frac{K' P_{M_y}^{1/y}}{p}$

Inherent in the above and subsequent treatment are the assumptions that solid MN has a narrow homogeneity range, the impurity concentration is small, the system is nondegenerate, and that Schottky disorder prevails.

If we now consider the same case but let X occupy N sites, we find that

$$k_o(X_N^D) = \frac{K_4}{n P_{N_y}^{1/y}} = \frac{P_{M_y}^{1/y} K_5}{n} \quad [4]$$

From Eq. [3] and [4] we note that the segregation coefficient for an impurity is either directly or inversely proportional to the pressure of M in the system. Similar equations govern the segregation coefficients of acceptors at substitutional sites. There are also a limited number of impurities which can occupy either site readily. If a mass action law is valid for the impurity on each type of site, then

$$k_o(X_{M,N}^{A,D}) = \frac{[X_M^A] + [X_N^D]}{[X_I]} = \frac{K_6}{p P_{M_y}^{1/y}} + \frac{P_{M_y}^{1/y} K_5}{n} \quad [5]$$

where p is the hole concentration. A summary of the dependencies of segregation coefficients on the site the impurities occupy and on the electrical characteristics they have is given in Table I.

Experimental

Cadmium telluride.—The CdTe ingots used in these studies were prepared from high-purity, 6-9's, elements in vacuum-sealed quartz tubes by the Bridgman Drop procedure. Ingots weighed typically about 80g and occupied about 60% of the tube volume. The dopant, In or Sb, was added directly to the Bridgman tube. The cadmium pressure in the system was initially controlled by the excess Cd used. However, it is apparent that the P_{Cd} in the system is changing throughout the freezing period because the composition of the melt is changing. We analyzed only the first 15% of the ingot to freeze and assumed a P_{Cd} corresponding to the initial condition (12-14). This leads to an uncertainty of about 10% in P_{Cd}. The distribution coefficients of indium and antimony were determined at cadmium pressures of 5.3 and 0.08 atm.

Indium arsenide.—The indium arsenide crystals used in these studies were prepared from high purity, 6-9's, elements. The sealed magnetic Czochralski crystal puller used was previously described (15). InAs was synthesized *in situ* and grown in the <111> direction. The solid-liquid interface was always flat and perpendicular to the pull direction. The rotation rate was in all cases 8 rpm. Hall measurements taken on wafers cut perpendicular to the growth axis showed no appreciable variation in carrier concentration within a wafer. Therefore inhomogeneous segregation of the impurities due to faceting effects (26, 27) was assumed to be negligible. The dopants were added directly to the indium charge. The arsenic pressure in the system was maintained at the desired value by the temperature control of condensed arsenic at the coldest portion of the puller tube. Crystal growth was obtained in the usual way. To study the influence of arsenic pressure, the pulling was interrupted and the arsenic reservoir temperature was increased. After arsenic pressure equilibrium was established, the pull was resumed.

Tellurium and tin in InAs were treated as nonvolatile dopants. The initial dopant composition of the melt was therefore known. The dopant concentration in the melt after the pressure change was calculated from the InAs phase diagram (16). The quantity of Te already incorporated in the pulled crystal was taken into account. Our justification for treating Te as a nonvolatile dopant is based on the fact that for our experimental temperature conditions Te is a noncondensable impurity and the gas volume is sufficiently small to make the quantity of Te in the gas phase negligible compared to the total Te in the system.

As in the above case, the dopant zinc was added directly to the melt. However, the zinc concentration in the melt must be calculated differently from the Te or Sn case. When the InAs-zinc melt is in equilibrium with arsenic at a vapor pressure of 0.17 atm, the zinc concentration in the melt is dependent on the vapor pressure of condensed Zn_3As_2 at the arsenic reservoir temperature where solid Zn_3As_2 coexists with solid As. Using Silvestri's data (17), the zinc pressure in the system was calculated. The corresponding concentration of Zn in the melt was calculated from Raoult's law and the vapor pressure of pure Zn at the melt temperature (18). When the minimum temperature in the system was increased to 623°C (P_{As4}= 1.45 atm), condensed Zn_3As_2 still controlled the Zn vapor pressure and condensed arsenic controlled the arsenic pressure. The Zn concentration in the melt was recalculated as above.

Measurements.—The cadmium telluride crystals were analyzed for the dopants by emission spectrochemical analysis. The indium arsenide crystals used were similarly analyzed for the dopants Te and Sn. In addition, the InAs crystals were investigated by measurements of their Hall coefficients. When possible we used Hall bridges; otherwise Van der Pauw samples had to suffice.

Results and Analysis

CdTe.—The results of segregation of In and Sb in CdTe under high and low P_{Cd} are shown in Table II. The first column gives the initial composition and the second column the cadmium pressure associated with the initial composition (12-14). The third column gives the corresponding liquidus temperatures (T_l) (12, 14). C_l is the initial solute concentration in the liquid and C_s is the measured impurity concentration in the solid. The segregation coefficients are shown in the last column. We note that the k_o's for In differ for the two P_{Cd}'s by about a factor of 6. Similarly for Sb the k_o's show a variation by a factor of about 17. The dependence of k_o on P_{Cd} is significant.

Because the k_o's above were not determined at the same temperature, we must rule out the possibility that the variation in k_o is due to the temperature difference. It has been shown empirically for a number of impurities in Si and Ge with k_o's much less than unity that the temperature dependence of the distribution coefficient can be approximated by the expression (19)

$$k = (k_m)^{T_m/T} \quad [6]$$

Here k_m is the segregation coefficient of the solute at infinite dilution; this occurs at the maximum melting point (T_m) of the solvent; k is the segregation coefficient at any temperature, T. Trumbore *et al.* (20)

Table II. Segregation coefficient of In and Sb in CdTe
The k_o for each impurity is given for each of two initial melt compositions. The calculated P_{Cd}, melting point, impurity concentration in the melt C_l, and in the solid C_s are listed.

Atom fraction Cd	Cd pressure atm	T, °K	Solute	C_l *	C_s *‡	C_s** at./cm³	$k_o = \frac{C_s}{C_l}$
0.555	5.3	1308	In	4.45×10^{-4}	3.8×10^{-5}	1.18×10^{18}	8.5×10^{-2}
0.445	0.081	1328	In	4.45×10^{-4}	2.2×10^{-4}	6.84×10^{18}	49×10^{-2}
0.555	5.3	1308	Sb	4.45×10^{-4}	87×10^{-6}	2.7×10^{18}	20×10^{-2}
0.445	0.081	1328	Sb	4.45×10^{-4}	5.2×10^{-6}	1.62×10^{17}	1.2×10^{-2}

* In units of gram atoms solute per gram atoms of solvent (Cd plus Te).
‡ Three separate determinations were made in the first 15% of the solid that froze. The average is shown.
** The intrinsic electron concentration at the above temperatures are, respectively, $n_i(1308°K) = 3.9 \times 10^{17}/cm^3$; $n_i(1328°K) = 4.3 \times 10^{17}/cm^3$.

have shown that Eq. [6] is not applicable over large temperature ranges. For the relatively small temperature differences near the maximum melting point in question here Eq. [6] may serve as a useful estimate. Applying this equation to CdTe (treating the system as a pseudobinary for determining the "pure" temperature dependence), we calculate a change in k_o of about 5% for the 20°K difference shown in Table II. This is a negligible change compared to the experimental observation.

Let us now consider the influence of P_{Cd} and n on the segregation coefficient for the shallow donor In in CdTe (14, 21). We assume substitutional occupation of Cd sites. According to Eq. [3]

$$k_o(In_{Cd}) = \frac{K}{n P_{Cd}}$$

We need to determine the carrier concentration n at the high temperature equilibrium condition. If we assume that the deviation from stoichiometry contributes a negligible number of carriers and that self compensation itself is negligible, then the charge neutrality equation becomes $n - p = [In_{Cd}{}^{D+}]$. Furthermore, the carrier concentration due to the intrinsic process is governed by the relation

$$np = K_i = N_c N_v \exp(E_v - E_c)/kT \qquad [7]$$

where N_c and N_v are the density of states in the conduction and valence band, respectively, E_v and E_c the relative energies of the valence and conduction band edges, k is the Boltzman constant, and T the absolute temperature. Combining Eq. [7] with the charge neutrality equation leads to

$$n^2 - n[In_{Cd}{}^{D+}] = K_i \qquad [8]$$

We evaluate K_i as follows. For the density of states, we have used an effective electron mass (21) of 0.1 m_o and a hole mass of 0.6 m_o (22, 23). The term $E_v - E_c$ is equal to the negative of the band gap energy E_g, which has also been reported as a function of temperature (14). The calculated K_i for 1308°K is 1.52×10^{35} ($E_g = 0.96$ ev) and 1.85×10^{35} ($E_g = 0.95$ ev) at 1328°K. The intrinsic carrier concentrations corresponding to these values are shown at the bottom of Table II. The value of n at 1328°K deduced from Eq. [8] is equal to $[In_{Cd}{}^{D+}] = C_s$. The same holds for n at 1308°K. Therefore

$$k_o(In_{Cd}{}^{D}) = \frac{K}{C_s P_{Cd}}$$

Using the experimental results for $P_{Cd} = 0.081$ atm, we find the temperature dependent constant K_{In} (1328°K) $= 2.7 \times 10^{17}$ atoms atm cm^{-3}. We can now compute the segregation coefficient for $P_{Cd} = 5.3$ atm utilizing the experimentally determined $C_s = 1.2 \times 10^{18}$. The calculated value for k_o is 4.3×10^{-2} which is to be compared with the experimental value of 8.5×10^{-2}. The agreement is good for measurements and analyses of this type. This also gives some justification for our assumption of negligible self-compensation. If appreciable self-compensation occurred, then our results would be in variance with the predicted behavior.

A similar analysis can be made for the impurity Sb which acts as an acceptor and is assumed to be a substitutional impurity residing on the Te site. Again we compute the temperature dependent constant using the data, $P_{Cd} = 5.3$ atm, $p = C_s = 2.7 \times 10^{18}$ and $k_o(Sb_{Te}{}^{A}) = 20 \times 10^{-2}$, and obtain for $K_{Sb}(1308°K)$ a value of 1.02×10^{17}. In calculating the segregation coefficient for $P_{Cd} = 0.081$ atm, we determine p from the neutrality condition and note that $p = 5.2 \times 10^{17} \neq C_s$. The calculated value for $k_o(Sb_{Te}{}^{A}) = 1.6 \times 10^{-2}$ which compares very well with the experimental value of 1.2×10^{-2}. We note that segregation coefficients can change significantly with a change of component pressure. Moreover the analysis shows that there is a near quantitative agreement between experiment and theoretical prediction.

InAs-Te.—The impurity segregation in the InAs system was investigated at constant chemical potentials of the constituents, *i.e.*, crystals of InAs were pulled from the melt at constant As pressure. The ingot was characterized along the growth axis by measuring the carrier concentration (Hall measurements) and by spectrochemical analysis. For Hall measurements, the constant r in the relation $n = r(R_H ec)^{-1}$ was taken as unity. We found that n from electrical measurements was consistently higher than the corresponding [Te] deduced from chemical analysis. This was observed only for Te. We have arbitrarily made the two sets of data coincident by applying a constant multiplying factor of 1.45 to the chemical data (the accuracy of the chemical analysis for Te was ±20% and therefore does not explain the observed difference). The results are shown in Fig. 1.

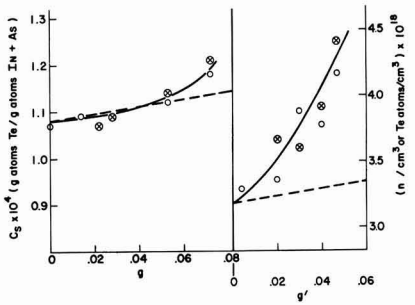

Fig. 1. Tellurium concentration in InAs as a function of the fraction of the melt grown. The data for $P_{As4} = 0.53$ atm and for 1.1 atm are shown. The dotted lines represent the theoretical curves for normal freeze of the off-stoichiometric melts for $k_o = 0.311$ and $C_o = 3.48 \times 10^{-4}$ for the g curve ($T_M = 942°C$) and for $k_o = 0.290$ and $C_o = 3.11 \times 10^{-4}$ for the g' curve ($T_M = 931°C$). ○ represents electrical data and circle with x chemical data. The chemical data was multiplied by a constant factor of 1.45 to bring it into coincidence with the electrical data.

The concentration profile of Te in the solid phase is given by the solid lines. The curve is extrapolated to obtain C_s at $g = 0$ where g is the fraction of melt solidified. Since the initial Te concentration (C_o) in the liquid is known, we can compute the segregation coefficient for the initial P_{As}. After the As pressure change, C_o' was recalculated as described previously, C_s' at $g' = 0$ is obtained as before and k_o' is calculated. All the pertinent data are given in Fig. 1. It is to be noted that the dotted lines correspond to the theoretically predicted modified normal freeze curves which take into account the off-stoichiometry in the liquid phase (24). A strong positive deviation of the experimental data at the higher P_{As} is noted. This is believed to be caused by a too rapid rate of growth. We used the same pulling speed of 12 mm/hr for both arsenic pressures. Although the rate was sufficiently slow for the lower P_{As} which corresponded to a near stoichiometric melt, it was too rapid for the higher P_{As}. For the latter case slower rates are necessary to allow for the diffusion of the excess component As away from the growing interface. It is also suspected that the extrapolation of C_s' to $g' = 0$ leads to a value which is higher than the equilibrium value.

The effect of changing the As pressure during crystal growth is well demonstrated in Fig. 1. The discontinuity at the point of ΔP_{As} is clear. The change in the amount of Te incorporated in the solid is due to two effects. First there is a dilution effect which occurs when additional As is transferred from the reservoir to the melt as a result of increasing P_{As} (24). The second effect, of course, is the one we are mainly concerned with in this investigation. We have sufficient knowledge of the InAs phase equilibria (16) to take into account the dilution effect. Therefore, using $k_o = 0.311$ for $P_{As4} = 0.53$ atm as a standard we can calculate k_o' for $P_{As4}' = 1.1$ atm from the relation

$$k_o' = k_o \frac{n}{n'} \left[\frac{P_{As4}}{P_{As4}'} \right]^{1/4}$$

We assume that the temperature dependence of k is negligible for the small difference in liquidus temperatures, *i.e.*, 942°C *vs.* 931°C. Again, as in the case of CdTe, we assume the simple charge neutrality condition: $n - p = Te_{As}^{D+}$. We have calculated K_i for InAs at 930°C using the following data: $E_G = 0.415$ ev at 2°K (25), $dE_G/dT \simeq 3 \times 10^{-4}$ ev/deg., $m_h = 0.3\ m_o$ (25), and $m_e = 0.03\ m_o$ (25). The assumptions include a constant temperature dependence of E_G and that only the conduction and valence band near $k = 0$ are involved in the intrinsic ionization process. The intrinsic electron concentration was found to be 4.5×10^{18} cm^{-3} which makes $K_i = 2.0 \times 10^{37}$. We calculate the appropriate n's from an equation similar to Eq. [8] and determine $k_o' = 0.28$. This compares favorably with the observed value of 0.29.

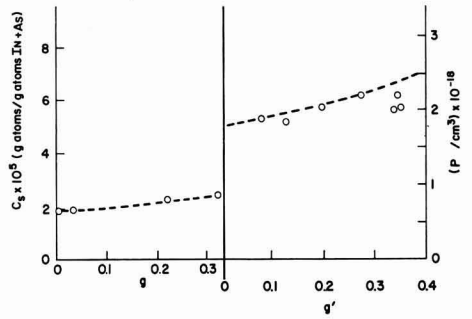

Fig. 2. Zinc concentration in InAs as a function of the fraction of the melt grown. The data are for $P_{As4} = 0.165$ atm and 1.45 atm. The data were obtained from electrical measurements. The dotted lines represent theoretical curves for normal freeze of the off-stoichiometric melts for $k_o = 0.324$ and $C_o = 5.65 \times 10^{-5}$ and for $k_o = 0.421$ and $C_o = 1.2 \times 10^{-4}$ for g ($T_M = 937°$) and g' ($T_M = 920°C$), respectively.

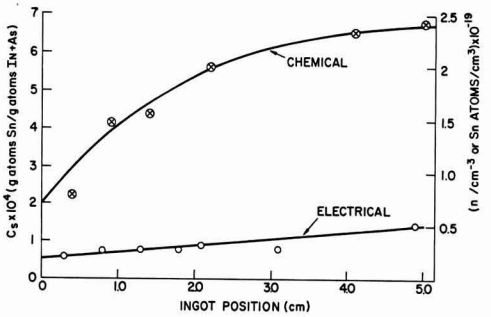

Fig. 3. Concentration of tin and free charge carriers in InAs as a function of length and ingot grown for $P_{As4} = 0.17$ atm; $C_o = 1.226 \times 10^{-3}$; $T_M = 937°C$; $k_o = 1.63 \times 10^{-1}$.

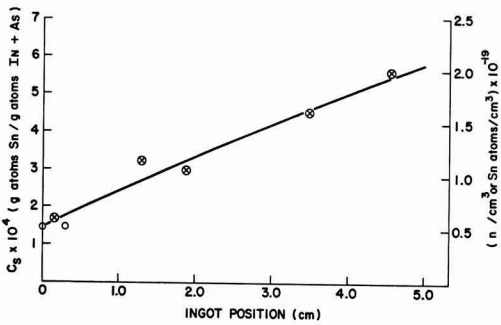

Fig. 4. Concentration of tin and free charge carriers in InAs as a function of length of ingot grown for $C_o = 2.75 \times 10^{-3}$; $T_M = 885°C$; $k_o = 5.34 \times 10^{-2}$; $P_{As4} = 3.5$ atm; ○ electrical data; circle with x chemical data.

For InAs-Zn.—The impurity Zn in InAs occupies In sites and is an acceptor. Essentially the InAs-Zn system was treated like the InAs-Te one. The zinc concentration in the melt, however, was calculated as described in the experimental section.

In characterizing the pulled ingot only electrical measurements were used. The results of this study are shown in Fig. 2. Again, one notes the discontinuity at the point where P_{As} was increased. The theoretical normal freeze curves (24) are much more closely approximated by the data. This is undoubtedly due to the reduction of the pulling rate to 6 mm/hr.

We have analyzed our results along the same line as before. We assume that [Zn] = p, where the latter is the measured hole concentration. We again calculate p at the high-temperature equilibrium from our neutrality condition and K_i. If we use $k_o = 0.32$ for $P_{As4} = 0.165$ atm as a standard, then we would predict k_o for $P_{As4} = 1.45$ atm to be 0.49. This compares favorably with the measured value of 0.42.

InAs-Sn.—Impurities of group IV A of the periodic table have been observed to act both as donors and acceptors in III-V compounds depending on the site they occupy. Tin is this type of amphoteric impurity in InAs. We have grown two ingots of InAs doped with Sn at two different As pressures. The impurity and carrier concentration profiles of the ingots were obtained from chemical analysis, and electrical measurements and are shown in Fig. 3 and 4. The chemical analyses (emission spectroscopy) are precise to ± 20% at the 90% confidence level. The crystal pulled

at 0.17 atm As pressure was mainly single, and electrical measurements were made along most of the ingot. It should be noted in Fig. 3 that the chemical analyses indicate considerably larger concentrations of Sn than found by electrical measurements. We interpret these results as follows. Sn is basically a donor in InAs and therefore at low Sn concentration it prefers the In sites. However, at low P_{As4} as the total Sn concentration increases, the probability of occupation tends to the same value for both sites. Therefore. the free electron concentration stays essentially constant for high concentrations of Sn as is shown in Fig. 3.

At P_{As4} of 3.5 atm it was quite difficult to pull single crystals. Even at the slowest pull speeds attainable with our equipment (3 mm/hr) the ingot was polycrystalline except for the first few mm near the seed, which was single and free of gross defects. After the first centimeter of ingot, void inclusions were observed. These were characteristic of trapped arsenic gas bubbles. It was therefore possible to make electrical measurements only in the first few millimeters of the ingot. The rest of the ingot was characterized by chemical analysis. Results are shown in Fig. 4. We note that for this case the carrier concentration is equal to the concentration of Sn in the initial part of the ingot. We cannot say whether this holds true for the higher concentration of Sn, *i.e.*, for every part of the ingot. Nevertheless, the results indicate that under the higher As pressure the Sn atoms favor the In sites. The results follow the prediction that as the As pressure increases the occupation of As sites by Sn decreases relative to similar occupation of In sites. Along with the decrease of Sn solubility on As sites, there is a decrease in the total distribution coefficient. This is not unexpected. A more quantitative analysis and comparison of the Sn segregation coefficient is unfortunately not possible.

Discussion

We have reviewed the theoretical aspects of impurity incorporation in binary compounds. The primary variables affecting k_o are the temperature, the pressure of the compound constituents, the concentration of the impurity, and the free carrier concentration. Of these variables we have been concerned mainly with the pressure of the compound constituents and how the variation of P_M or P_N affects the segregation coefficient of various impurities. Of primary importance are the sites the impurities occupy. The theoretical predictions were tested experimentally for several impurities in CdTe and InAs. In no cases were the experimental observations in conflict with the theory; moreover, in most cases there was good quantitative agreement. One assumption inherent throughout is that the impurity activity in the liquid phase is not strongly dependent on the composition of the liquid phase. The agreement between theory and experiment indicates that our assumption was justified. It should be noted, however, that the impurity concentration was always dilute. When the liquid phase is appreciably off stoichiometry, *i.e.*, when $M >> N$ or $M << N$ then the assumption of composition independence may no longer be valid.

The dependence of k_o on the chemical potential of the constituents is of practical importance. k_o is a parameter that is useful in either minimizing or maximizing the incorporation of impurities into the host crystal. In addition there is another aspect that is of particular importance with high vapor pressure compounds, *e.g.*, GaAs, InP, etc., where one must maintain good control of P_M usually by temperature control of a reservoir. A fluctuation of P_M may induce temperature fluctuations in the melt, due to the solution or evaporation of the reservoir component. These fluctuations result in variations of k_o, and this may yield inhomogeneities in the growing crystal.

Special consideration must be given to the phase diagram of the binary compound under investigation. In the II-VI systems, either constituent can be used to control the composition of the vapor phase and hence the other phases. Large variations in the component pressure lead to only small variations in the liquid composition as seen in Table II. The III-V compounds on the other hand are generally controlled by the pressure of the group V elements only. In the III-V system the liquidus curves near the binary compound composition are quite flat, and therefore a variation in the component pressure is reflected more strongly in a variation of the liquid composition. The determination of the most suitable conditions must thus take into account the phase diagram of the system.

Acknowledgments

The authors wish to express their appreciation to R. C. Chicotka for growing the InAs crystals, to J. A. Kucza for growing the CdTe crystals, and to W. Reuter for performing the chemical analyses.

Manuscript received Dec. 3, 1965; revised manuscript received March 10, 1966. This paper was presented at the San Francisco Meeting, May 9-13, 1965.

Any discussion of this paper will appear in a Discussion Section to be published in the December 1966 JOURNAL.

REFERENCES

1. See for instance C. D. Thurmond and J. D. Struthers, *J. Phys. Chem.*, **57**, 831 (1953); K. Lehovec, *J. Phys. Chem. Solids*, **23**, 695 (1962).
2. "Compound Semiconductors," Vol. 1, "Preparation of III-V Compounds," R. K. Willardson and H. L. Goering, Editors, Reinhold Publishing Corp., New York (1962); O. Madelung, "Physics of III-V Compounds," Chap. 5, John Wiley & Sons, Inc., New York (1964).
3. L. L. Chang and G. L. Pearson, *J. Phys. Chem. Solids*, **25**, 23 (1964).
4. J. O. McCaldin, *J. Appl. Phys.*, **34**, 1748 (1963).
5. L. J. Vieland and T. Seidel, *ibid.*, **33**, 2414 (1962).
6. U. Merten and A. P. Hatcher, *J. Phys. Chem. Solids*, **23**, 533 (1962).
7. F. A. Trumbore, H. G. White, M. Kowalchik, R. A. Logan, and C. L. Luke, *This Journal*, **112**, 782 (1965).
8. F. A. Trumbore, H. G. White, M. Kowalchik, C. L. Luke, and D. L. Nash, *ibid.*, **112**, 1208 (1965).
9. F. A. Kroeger and H. J. Vink, "Solid State Physics," **3**, pp. 307-435, F. Seitz and D. Turnbull, Editors, Academic Press, New York (1956).
10. D. G. Thomas, "Semiconductors," Chap. 7, N. B. Hannary, Editor, Rheinhold Publishing Corp., New York (1959).
11. F. A. Kroeger, "The Chemistry of Imperfect Crystals, North-Holland Publishing Co., Amsterdam (1964).
12. M. R. Lorenz, *J. Phys. Chem. Solids*, **23**, 939 (1962).
13. M. R. Lorenz, *ibid.*, **23**, 1449 (1962).
14. D. de Nobel, *Philips Research Repts.*, **14**, 361-399 and 430-492 (1959).
15. K. Weiser and S. E. Blum, *This Journal*, **107**, 189C (1960).
16. J. van den Boomgaard and K. Schol, *Philips Research Repts.*, **12**, 127 (1957).
17. V. J. Silvestri, Unpublished results.
18. R. E. Honig, *RCA Rev.*, **23**, 567 (1962).
19. R. N. Hall, *J. Phys. Chem. Solids*, **3**, 63 (1957).
20. F. A. Trumbore, C. R. Isenberg, and E. M. Porbansky, *ibid.*, **9**, 60 (1958).
21. B. Segall, M. R. Lorenz, and R. E. Halsted, *Phys. Rev.*, **129**, 2471 (1963); D. T. F. Marple, **129**, 2466 (1963).
22. S. Yamada, *J. Phys. Soc. Japan*, **15**, 1940 (1960).
23. M. R. Lorenz and B. Segall, *Phys. Lett.*, **7**, 18 (1963).
24. M. R. Lorenz, *J. Appl. Phys.*, **36**, 2908 (1965).
25. A Mooradian and H. Y. Fan, Seventh International Conference on the Physics of Semiconductors, 4 Radiative Recombination in Semiconductors, Paris, p. 39-45 (1964).
26. J. B. Mullin and K. F. Hulme, *Phys. Chem. Solids*, **17**, 1 (1960).
27. J. A. M. Dikhoff, *Solid State Electronics*, **1**, 202 (1960).

Anomalous Behavior of Copper during Acceptor Diffusions into Gallium Arsenide

G. B. Larrabee and J. F. Osborne

Texas Instruments Incorporated, Dallas, Texas

ABSTRACT

A radioactive tracer study of the behavior of copper during acceptor diffusions into gallium arsenide has clearly shown anomalous copper concentration profiles. A pronounced minimum in the copper diffusion profile was found in the vicinity of the electrical p-n junction. The shape and position of this minimum was dependent only on those diffusion conditions (time and temperature) which affected the indiffusing acceptor. Crystal origin, crystal orientation, and annealing had no effect on the copper diffusion profile. It is felt that the minimum or dip in the profile is caused by the large built-in field of the p-n junction which sweeps out the singly charged copper interstitials in the vicinity of the junction.

The diffusion, solubility, and electrical activity of copper in gallium arsenide have been carefully studied (1-3) and with the excellent work of Hall and Racette (4) is now better understood. The behavior of copper in all semiconductors is considerably complicated by the existence of the two copper species, interstitial Cu_i, and substitutional Cu_s. These two species exist together in gallium arsenide and their ratio (Cu_s to Cu_i) is controlled by several factors including the doping of the gallium arsenide. In intrinsic gallium arsenide, this ratio was found to be around 30 (4). This ratio is upset if the material is doped greater than the intrinsic carrier content of the copper content. If the semiconductor is n-type, the ratio is shifted in favor of the substitutional species. Similarly, p-type material shifts the ratio to favor interstitial species. The properties of these two copper species are radically different both during and after diffusion.

Interstitial copper (Cu_i) diffuses very rapidly into gallium arsenide (effective $D \sim 10^{-6}$ cm^2-sec^{-1} at 800°C). Electrically, interstitial copper is a singly charged donor. However, in the crystal the interstitial species reacts with vacancies to produce copper in substitutional sites

$$Cu_i + V = Cu_s$$

Substitutional copper is relatively immobile and appears to be a double acceptor in gallium arsenide (4). Furukawa *et al.* (6, 7) observed only the 0.145 ev copper level but their work did not preclude the presence of the deep level at 0.47 ev. Fuller *et al.* (5) and Allison *et al.* (13) carefully investigated the behavior of copper diffused into n-type gallium arsenide and demonstrated the double acceptor behavior of copper.

The effective diffusion coefficient for copper is a function of the relative abundance of the two copper species which in turn is determined by the dopant. In the formation of a p-n junction, by diffusing an acceptor into n-type material, it is not at all clear how copper will behave. Hall (4) showed that the diffusion coefficient for interstitial copper was independent of the acceptor concentration. However, diffusion into extrinsic n-type gallium arsenide material is complicated by the fact that the copper interstitial solubility is greatly reduced.

This work was initiated to determine the behavior of copper during acceptor diffusions into n-type gallium arsenide.

Experimental Procedure

Each gallium arsenide sample was sawed to a thickness of 30 mils and then lapped and polished until optically flat. The sample was etched in 8:1:1 etch (8 parts H_2SO_4, 1 part 30% H_2O_2, and 1 part H_2O), and rinsed in running deionized water. The radiocopper-64[1] was introduced onto the crystal wafer by equilibrating the crystal in a 1*N* nitric acid solution containing 4 to 5 ppm copper ion (labeled with copper-64) for 30 min. The copper was thereby electrochemically deposited on the gallium arsenide (8). The wafer was then carefully rinsed in deionized water and allowed to dry. The slice was sealed into a 10 cm^3 volume quartz tube[2] with other acceptor diffusants at a pressure of less than 1μ. Unless otherwise stated, all diffusions were carried out at 815°C for 6 hr in a furnace with a 10-in. zone that was flat to ± 1°C. After diffusion, the quartz diffusion ampoules were air quenched, and the diffused gallium arsenide slice was removed. The edges were lapped with a coarse grit on a lapping plate to a depth of at least 500μ. The face of the diffused slice was then incrementally lapped and each lapping was gamma counted using a sodium iodide scintillation detector. Both gamma-ray spectroscopy and half-life studies showed only the presence of copper-64 activity.

Experimental Results

The initial acceptor diffusion studied was manganese into a copper-64 labeled wafer as described in the Experimental Procedure. Figure 1 shows the copper concentration profile as a function of depth into the crystal. As can be seen, a pronounced dip or minimum was obtained that looked much like that reported by Cun-

[2] All quartz used was G.E. 204.

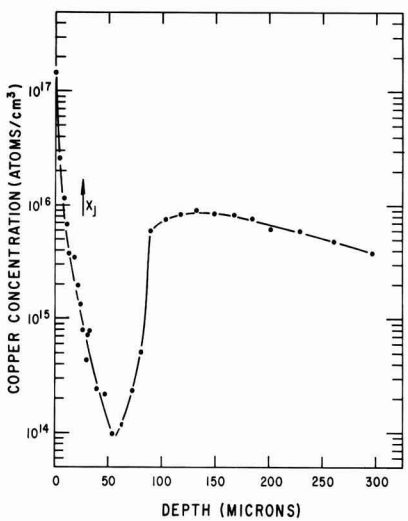

Fig. 1. Typical distribution of copper in n-type gallium arsenide when diffused with manganese at 815°C for 6 hr.

[1] Copper-64 was obtained and assayed from Oak Ridge National Laboratories, Oak Ridge, Tennessee. An average specific activity of 60,000 to 80,000 mc/g was used.

nell and Gooch (9). The surface concentrations of manganese, observed using radiomanganese-54, were of the order of 10^{19} atoms/cc. The diffusion conditions were repeated several times and shown to reproducibly yield this anomaly. It was decided to vary carefully only one experimental parameter at a time in an effort to understand this phenomenon.

Material origin and crystallography.—Several different Texas Instruments n-type pulled gallium arsenide crystals (lightly doped tin and tellurium and undoped, but not intrinsic) as well as some undoped, but not intrinsic Bell and Howell horizontal Bridgeman material were shown to behave in the same manner. This dip in the copper diffusion profile was not peculiar to any one melt grown n-type gallium arsenide crystal. The gallium arsenide material used in the acceptor diffusion reported in this work was tin doped to 4 to 6 x 10^{16} at./cm^3. Heavily doped material as discussed by Schockley and Moll (14) was not investigated as n-type substrates in this study.

Similarly, efforts to show a dependence on crystallographic orientations was not successful. Manganese diffusions into <311>, <111>, and <115> material all yielded copper profiles with a pronounced dip or minimum.

Since most of the diffusion work in this study was carried out on <111> oriented crystals, the effect of the gallium rich (A) face *vs.* the arsenic rich (B) face was investigated. No differences in the copper diffusion profiles were observed. This was not unexpected since <311> and <115> oriented wafers have only very slight A and B face characteristics.

The one material or slice parameter that had the most pronounced effect on the over-all shape of the dip in the copper profile was positioning in the diffusion tube. That is, the face laying up in the diffusion tube consistently showed more pronounced or sharper dips in the profiles than the down face. This observation has added significance when it is coupled with some radiomanganese-54 and -56 work (10) which clearly shows the upper diffusion face to have higher manganese surface concentrations and deeper p-n junction depths. This would imply that the anomalous dip in the copper profile was intimately connected with the indiffusing acceptor and is not dependent on the host crystal.

Diffusion conditions.—On the premise that the dip in the copper profile was caused by the manganese; several diffusion conditions were studied.

Diffusion time.—A manganese diffusion into a copper-64 labeled wafer was carried out as described in the Experimental Procedure except the diffusion time was reduced from 6 to 0.6 hr. The copper diffusion profile is shown in Fig. 2. The depth of the minimum (12μ) is significantly less than in comparable 6 hr diffusions

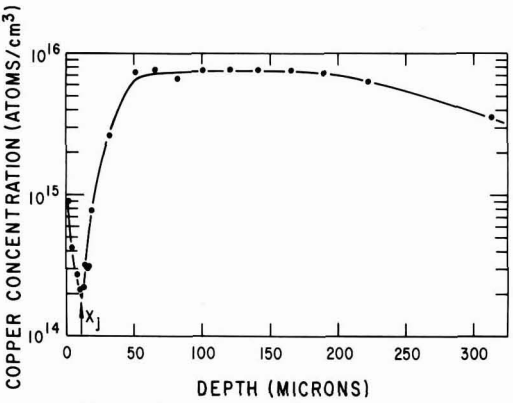

Fig. 2. Effect of diffusion time on the copper distribution during manganese diffusion into n-type gallium arsenide. Diffusion carried out at 815°C for 0.6 hr.

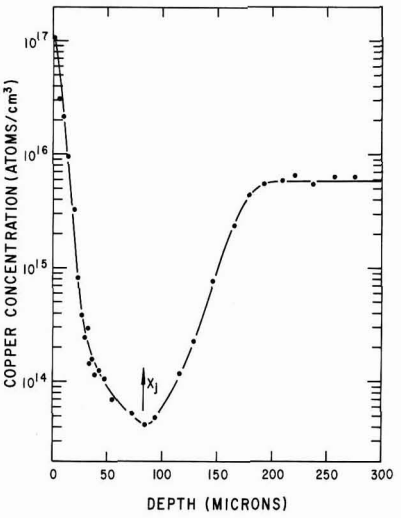

Fig. 3. Effect of increased temperature on the copper concentration profile during the diffusion of manganese into n-type gallium arsenide. Diffusion carried out at 915°C for 6 hr.

which average around 55μ. Since the acceptor diffusion depth would vary with the square root of the diffusion time, one would expect the minimum to be about 1/3 the depth of a comparable 6-hr diffusion. An average of two 0.6-hr diffusions was 15μ which is in good agreement with the time dependent diffusion laws.

Temperature.—A manganese diffusion was carried out as described in the Experimental Procedure but increasing the diffusion temperature to 915°C. As can be seen in Fig. 3, the dip in the copper profile was much wider and the minimum was deeper into the crystal (87μ) than the 815°C diffusions. A diffusion at 1000°C produced a much broader dip with a minimum around 150μ. This change in the shape of dip in the copper profile along with the change in the position of the minimum again strongly suggest a dependence on acceptor behavior and movement.

Annealing.—Two diffusions were carried out under the standard diffusion conditions described earlier. At the end of the 6-hr diffusion one tube was removed and water quenched while the other tube was removed inside a larger Inconel block which took approximately 3 hr to reach room temperature. There was no difference in the shape of the copper diffusion profiles. The anomalous dips occurred at the same depth in the crystal. It appears that the effects of annealing after diffusion are very small.

Other Acceptor diffusants—zinc.—All of the copper-acceptor diffusions reported in this work were carried out using manganese with the exception of two zinc diffusions. In these zinc diffusions all diffusion conditions were as described earlier except that the amount of zinc was chosen to yield a p-n junction at a depth of 20 to 30μ. The copper profile is shown in Fig. 4, and it is apparent that an extremely sharp dip is obtained using zinc.

Here again, the anomalous distribution of copper appears to be closely related to the indiffusing acceptor. It should be noted that the width of the minimum is considerably more narrow than in comparable manganese diffusions.

Absence of acceptor.—To gain some insight into the mechanism of the interaction between the copper and the indiffusing acceptor, a series of diffusions was carried out with copper-64 labeled wafers in the absence of an acceptor. The gallium arsenide used was horizontal Bridgeman grown, undoped, but not intrinsic, with a carrier concentration of 1.2 x 10^{16} electrons/cm^3. The first series of diffusions was run with

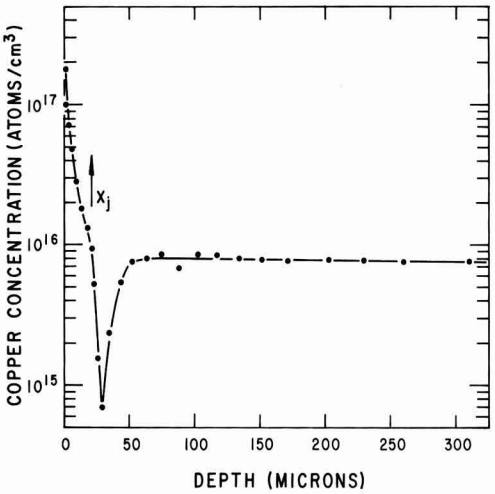

Fig. 4. Copper distribution oberved during zinc diffusion into n-type gallium arsenide at 815°C for 6 hr.

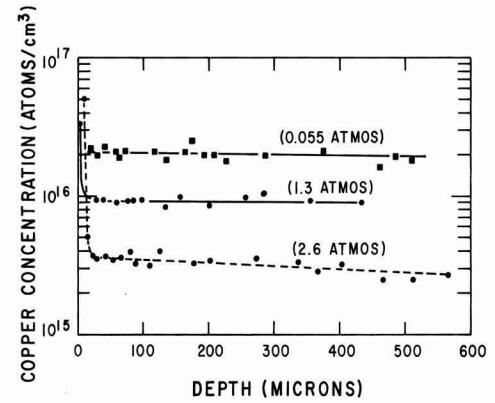

Fig. 5. Effect of excess arsenic pressure (As_4) and the absence of an acceptor on the copper distribution during a 6-hr diffusion into n-type gallium arsenide at 815°C.

varying amounts of excess arsenic in the diffusion ampoule. The excess arsenic would prevent dissociation of the gallium arsenide and would generate gallium vacancies in the crystal near the surface.

The results of three diffusions with varying amounts of excess arsenic in the diffusion tube are shown in Fig. 5. The apparent inhibition of the copper diffusion by the excess arsenic suggests interaction of the copper with gallium vacancies to form immobile substitutional copper. Hall and Racette (4) report reduced solubility of copper in n-type (5×10^{15} electrons/cm^3) gallium arsenide and suggest that this reduced solubility is due to the presence of an arsenic-rich phase at the surface. This suggestion of precipitation of copper arsenide at the surface does not seem to fit the experimental data since in all three cases the amount of arsenic added to the diffusion tube was far in excess of that necessary to react with the small amount of copper on the surface.

Furukawa and Thurmond (6) report a similar decrease in copper solubility with increasing arsenic pressure and explain the dependence by assuming that copper on arsenic sites is singly ionized Cu_{As}^-. It should be noted that the larger dips or minima observed in the copper diffusion profiles during acceptor diffusions were not obtained here.

Discussion

A simple straight forward explanation of the behavior of copper during acceptor diffusions does not appear possible. From the experimental data it is apparent that the minimum or dip in the copper diffusion profile is closely associated with the acceptor and, by implication, the formation of a p-n junction. Any changes made in the diffusion parameters which affect the acceptor impurity are reflected in the copper diffusion concentration profile by changes in the position and shape of the dip.

Kendall (11) has reported a similar phenomenon when indium was diffused into gallium arsenide in the presence of cadmium. Kendall attributes the "uphill" branch to an interaction between interstitial indium (In^{3+}) and gallium vacancies with the vacancies diffusing out of the interior toward the acceptor diffusion zone. The "downhill" side of the dip in the indium profile was attributed to a retardation of the incoming interstitials by the built in field of the acceptors.

Cunnell and Gooch (9) reported a similar anomaly in their investigation of the diffusion of cadmium into gallium arsenide using cadmium-115. Kendall (11) feels that the anomaly observed was due to the rapidly diffusing interstitial indium-115 daughter. Kendall was able to duplicate their results using indium-114 diffusing simultaneously with nonradioactive cadmium.

The electrical p-n junction in all the manganese and zinc-copper diffusions in this work were found to occur just at the minimum or slightly to the left of the minimum. In no case was the junction found to the right or deeper than the minimum of the dip in the copper diffusion profile.

In any explanation or interpretation of the behavior of copper during acceptor diffusions, the solubility data of Hall and Racette (4) must be carefully examined. Hall and Racette clearly showed that copper had high solubility in extrinsic p-type gallium arsenide because of enhanced interstitial solubility. This enhanced solubility of an impurity as a function of doping in a semiconductor is the same as that explained by Riess, Fuller, and Morin (15) using chemical interactions in silicon and germanium. Shockley and Moll (14) explained this same enhanced solubility of a charged impurity in a semiconductor using band theory by using the Fermi level as a measure of the dopant concentration. None of these workers predict the depressed solubility for copper in the vicinity of the pn junction that was observed in this work. At the temperatures used in these diffusions (815°C) and the low copper concentrations used, there is no question of solubility limitations. At 815°C the n-type substrates used in this work are intrinsic (E_F near mid gap) and Hall (4) observed no distinguishable difference between the copper solubility in semi-insulating (E_F mid gap) and extrinsic n-type material. On the basis of these solubility considerations, one would expect enhanced copper solubility in the p-region and a flat distribution in the n-region. But there should be no pronounced minimum or anomaly in the copper diffusion profile. For the Shockley-Moll model (14) to explain the concentration difference observed in Fig. 3, for example, it would be necessary for $e^{\Delta E_F/kT} = 3 \times 10^2$ on the n side of the p-n junction. That is the Fermi level would have to move about 0.57 ev which is not reasonable because at 815°C the band gap has decreased to around 1.0 ev ($\beta_G = -4.9 \times 10^{-4}$ ev/°K). The Fermi level for 1×10^{19} Mn/cm^3 in 1×10^{16} electrons/cm^3 material is 0.24 ev above the valence band edge and the n-type substrate Fermi level is mid gap ($E_F \sim 0.5$ ev) at 815°C.

Copper is known to diffuse by the dissociative mechanism (1) and has an effective D of approximately 5×10^{-6} cm^2/sec (1) at 815°C. The time required for the interstitial copper to saturate the 30 mil wafers used in this work would be in the order of 10 min which is small compared to the total 6-hr diffusion time used. We feel that the copper rapidly diffuses

throughout the wafer during the first 10 min of the 360-min diffusion cycle and then redistributes as the slower acceptor diffusion proceeds. This is supported by our experimental data on the 0.6-hr diffusion where the copper was profiled for 350μ (half-way through 30 mil wafer) (Fig. 2) into the crystal and found to be more or less uniformly distributed past the usual minimum.

Hall and Racette (4) showed that the mobile copper interstitial species was a singly charged donor by using drift measurements in an electric field. The drift field used was small (2 v/cm) compared to the built in field caused by acceptor gradients and p-n junctions ($\sim$ 600 v/cm) (12). It would be reasonable to expect this large built-in field to sweep the singly charged copper interstitials out of the region of the p-n junction. The enhanced interstitial solubility in the p-type region would not adversely affect this movement and would lead to the formation of a sharp minimum in the copper diffusion profile because of the solubility minimum observed by Hall (4) in slightly extrinsic p-type material. The copper concentration after the junction would then rise to an equilibrium level and be flat in the n-type bulk region of the crystal.

Acknowledgment

The authors wish to thank R. W. Haisty and P. Hoyt for their helpful discussions and for supplying some of the gallium arsenide samples used in this work. Their grateful acknowledgment is due to R. A. Reynolds for his discussions.

Manuscript received Jan. 31, 1966.

Any discussion of this paper will appear in a Discussion Section to be published in the December 1966 JOURNAL.

REFERENCES

1. C. S. Fuller and J. M. Whelan, *J. Phys. Chem. Solids*, **6**, 173 (1958).
2. J. Blanc and L. R. Weisburg, *ibid.*, **25**, 221 (1964).
3. D. F. Rose, D. Meyerhofer, and R. V. Jensen, *J. Appl. Phys.*, **31**, 1105 (1960).
4. R. N. Hall and J. H. Racette, *ibid.*, **35**, 379 (1964).
5. C. S. Fuller, H. W. Allison, and K. B. Walfstirn, *J. Phys. Chem. Solids*, **25**, 1329 (1964).
6. Y. Furukawa and C. D. Thurmond, *ibid.*, **26**, 1535 (1965).
7. Y. Furukawa, *ibid.*, **26**, 1869 (1965).
8. G. B. Larrabee, *This Journal*, **108**, 1130 (1961).
9. F. A. Cunnell and C. H. Gooch, *Nature*, **188**, 1096 (1960).
10. G. B. Larrabee, Unpublished work.
11. D. L. Kendall, *Appl. Phys. Letters*, **4**, 67 (1964).
12. F. M. Smits, *Ergeb. Exak. Naturwiss.*, **31**, 167 (1959).
13. H. W. Allison and C. S. Fuller, *J. Appl. Phys.*, **36**, 2519 (1965).
14. W. Shockley and J. L. Moll, *Phys. Rev.*, **119**, 1480 (1960).
15. H. Riess, C. S. Fuller, and F. J. Morin, *Bell Sys. Tech. J.*, **35**, 535 (1956).

Compositional X-Ray Topography

J. K. Howard[1] and R. D. Dobrott

Texas Instruments Incorporated, Dallas, Texas

ABSTRACT

The advent of new semiconductor materials frequently demands new methods of investigating and defining those growth flaws which can degrade device performance. A new x-ray topographic method and concept were developed to study the defect structures in the heteroepitaxial systems. Compositional x-ray topography is an extension of the scanning-reflection method, which permits a nondestructive evaluation of the perfection in the substrate, deposit, and heterojunction. The theory and limitations of this method are discussed. Compositional x-ray topography was applied to the study of homogeneity and perfection in various heteroepitaxial systems, *i.e.*, GaAs-GaP, GaAs-InAs.

Heteroepitaxial systems have become the focus of many new device concepts (1, 2). Epitaxial deposition of pseudobinary alloys such as Ga(As, P) onto GaAs substrates has received considerable attention in the semiconductor industry (3-9). Layers of (Ga, In)As have also been deposited on single crystal GaAs substrates yielding material from which light-emitting diodes, mixer diodes, and varactor diodes can be fabricated (2). The crystalline perfection and homogeneity of these deposits is of importance in fabricating devices from this material. Since imperfections reflect the growth process, a knowledge of their concentration and type will permit a better understanding of the deposition parameters and clarify their effect on the deposit quality. Previous investigators have utilized back-reflection Laue methods and powder diffraction techniques to ascertain information on the structural quality and homogeneity of their deposits (4, 6). These methods are time consuming and yield results which may not be characteristic of the bulk deposit.

X-ray topography is a nondestructive method of evaluating the defect structure of many monocrystalline materials (10-18). The extinction contrast transmission method was developed by Lang (10) and modified by Schwuttke (13-15) for the study of semiconductor grade silicon. Defects in GaAs have been investigated by the anomalous transmission topographic method (16). The scanning-reflection x-ray topographic method (17) was developed to map imperfections over large area crystal surfaces (18). Compositional x-ray topography introduces a new concept to the field of x-ray topography. This method is capable of nondestructively examining the defects created at the heterojunction and "tracking" them through the deposit.

[1] Present address: IBM Systems Development Division, Fishkill, New York.

Scanning-Reflection X-Ray Topography (SRT)

Using the transmission arrangement, Schwuttke (15) was able to study dislocation arrays in silicon epitaxial deposits. The dislocation density of the silicon substrates was nearly zero in most cases; the superposition of the substrate flaws on the topographic image did not prevent the imperfections in the deposit from being discerned. The dislocation density of GaAs is usually $> 5 \times 10^3$ cm^{-2} which prevents exact identification of deposit flaws in the transmission topographs. Since the total thickness of the GaAs deposit and substrate produced a value of $\mu t >> 1$, anomalous transmission must be used if a nondestructive analysis is required (16).

The scanning-reflection method was designed to inspect the active growth surface of the GaAs substrate for mechanically induced damage and grown-in de-

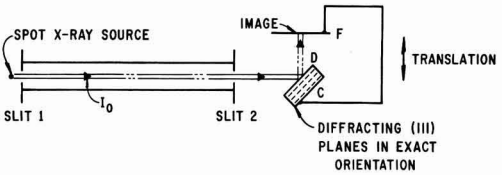

Fig. 1. Experimental arrangement for scanning-reflection x-ray topography.

fects. After deposition, another topograph revealed only the defect array in the GaAs deposit (17, 18); an attempt was made to relate the deposit flaws to either the substrate preparation and/or perfection, or the deposition parameter.

The experimental arrangement is depicted in Fig. 1. The substrate crystal (C) in diffracting position is coupled to a film holder (F) mounted perpendicular to the diffracted beam (D). The incident beam (I_0) is restricted by slits (S_1) and (S_2); slit (S_2) is adjusted until only the $K\alpha_1$ component of the characteristic radiation can diffract. The ribbon-shaped incident beam (25 x 0.05 mm) impinges on the crystal at the proper angle, and a projected image of the flaws in the irradiated material is formed on the photographic plate. An image of the entire slice is obtained by translating the coupled film-sample unit perpendicular to the incident beam or parallel to the slice surface. The sequence of examination (substrate topograph-deposition-deposit topograph) is tedious and can introduce a contamination and/or strain problem because of handling. A more desirable method of inspection would permit *in situ* examination of the substrate and epitaxial film perfection after deposition.

Principle of Compositional X-ray Topography

Compositional x-ray topography is an application of the scanning-reflection x-ray topographic method. The perfection, homogeneity, and single crystallinity of many heteroepitaxial systems can be investigated with this method. The diffraction angle depends on the lattice parameter (which can be calculated or experimentally determined); the substrate and film can be examined separately by the employment of the proper diffraction angle. Only that volume element in the irradiated material which has the desired lattice parameter will diffract to form the topographic image. This method of examination is effective to the depth of penetration of the incident x-ray beam. The maximum penetration depth, D (microns), can be expressed by the relation

$$D = -\ln A \cdot 10^4 / \left(\frac{\mu}{\rho} \cdot \rho \left[\csc(\theta - \psi) + \csc(\theta + \psi) \right] \right) \quad [1]$$

μ/ρ (cm^2/g) is the mass absorption coefficient, ρ (g/cm^3) is the density, θ the diffraction angle, ψ the angle between the slice surface and the diffracting planes, and A is the fractional attenuation of the incident beam.

A plot of the penetration depth as a function of $\theta - \psi$ (angle between the incident beam and the slice surface) is shown in Fig. 2. For a given radiation, crystal growth axis, and reflecting plane, the $\theta - \psi$ value can be calculated and the penetration depth determined. The graph depicts D in GaAs for various wavelengths of radiation ($A = 0.1$); this plot is a good approximation for Ga(As, P).[2]

[2] Experimental verification of $\theta - \psi = 45°$ (copper radiation) consists of determining the Ga(As, P) thickness which completely attenuates the (333) reflection of the substrate. The composition measurement developed by Miller (19) and employed by Dobrott (20) indicated that a 25μ Ga(As, P) deposit eliminated the (333) GaAs reflection ($\theta - \psi = 45°$) as compared to 21.8μ calculated from Eq. [1].

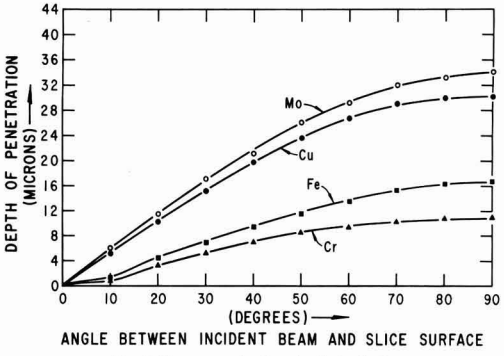

Fig. 2. X-ray penetration depth in GaAs

The principles of compositional x-ray topography are only satisfied under certain conditions: (*a*) the total film thickness is less than the penetration depth of the incident x-ray beam; (*b*) the diffraction angles of the film and substrate are sufficiently separated to insure exact angular selection; (*c*) the absorption coefficient is constant for each compositional layer. These restrictions, however, can be utilized to gauge the quality of the deposit.

Compositional x-ray topography applied to the GaAs-GaP *and* GaAs-InAs *heteroepitaxial systems.*— The variation of lattice parameter and composition has been shown to be linear in the GaAs-GaP and GaAs-InAs alloy systems (5, 21). Since the difference between the diffraction angles for GaAs and GaP (or GaAs and InAs) is small compared to θ, then θ_x (where x is the mole fraction of GaP) has been shown to vary directly with composition (20). A plot of these variables is depicted in Fig. 3 for the case of a Ga(As, P) film deposited on a (111) GaAs substrate. The Δ 2θ value changes from the (333) reflection of GaAs to the (333) reflection of GaP (copper Kα radiation). Because of this linearity, the mole fraction of GaP, x, can be related to the diffraction angle by the expression

$$2\theta\,[GaAs_{1-x}P_x] = x \cdot 2\theta\,[GaP] + (1-x) \cdot 2\theta\,[GaAs] \quad [2]$$

Similar relationships exist for other reflections, *i.e.*, the {440} reflections of GaAs and GaP. The composi-

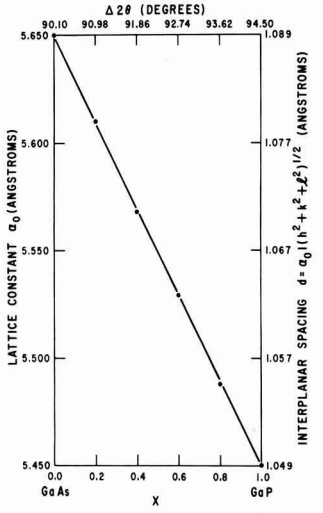

Fig. 3. Plot showing the linear relationship between the mole fraction of GaP and the diffraction angle; •, Rubenstein.

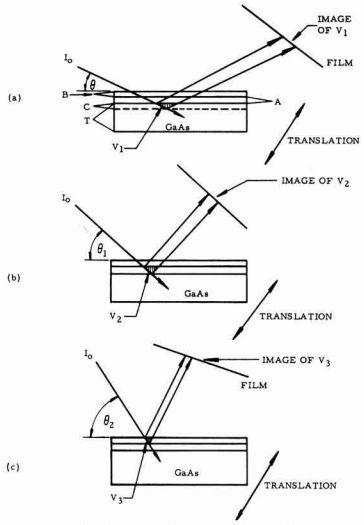

Fig. 4. Conceptual diagram for compositional x-ray topography. Each layer can be diffracted separately by utilizing the diffraction angle which corresponds to the lattice parameter (composition) of that layer.

tion of the alloy deposit determines the diffraction angle.

Figure 4 depicts an idealized case of the GaAs-GaP heteroepitaxial system. Epitaxial layers A and B have been sequentially deposited on a GaAs substrate. Assume that the A layer has a composition $GaAs_{1-x_1}P_{x_1}$ and diffraction occurs when the incident beam impinges at an angle θ_1 with respect to the diffracting planes which are parallel to the slice plane. The B layer has a GaP concentration x_2, $GaAs_{1-x_2}P_{x_2}$, where $x_1 << x_2$. This layer is in diffraction position when the incident beam impinges at an angle θ_2 where θ (GaAs) $< \theta_1 < \theta_2$. In Fig. 4(*a*) the incident beam I_0 strikes the crystal at the angle θ, and only the GaAs substrate is properly oriented. The beam penetrates to a depth C below the substrate surface; a volume element, V_1, diffracts coherently to form the topographic image. The image of the defects in V_1 is registered on the film plate placed perpendicular to the diffracted beam. As the crystal-film unit is translated perpendicular to the incident beam, the diffracting volume V_1 is "swept" parallel to the diffracting planes. This total image displays the perfection of the substrate in the C layer. If the crystal is rotated about an axis perpendicular to the plane of Fig. 4, the incident beam now impinges at an angle θ_1. The A layer is now in diffracting position [Fig. 4(b)]. The volume element V_2 bounded by the incident and diffracted beams diffracts to form an image of the flaws in V_2. Subsequent translation permits the A layer to be examined independent of the B layer and the substrate. The perfection of the B layer can be determined in a similar manner [Fig. 4(c)]. If Fig. 4 represents a cleaved {110} surface perpendicular to the plane of the slice, then (SRT) topographs of this surface would reveal compositional changes in the growth direction.

Experimental

Materials.—Single crystals of GaAs were grown using the Czochralski method; the growth axis was parallel to either the [111] or [100]. In the case of the crystals grown on the (111) plane, slices were cut 5° off (111) toward <100>. The slice thickness after sawing with an ID saw was approximately 0.030 in. The slices were then chemically polished on the (111)-B [or the (100)] face with a solution of NaOCl: H_2O (22). These slices were employed as substrate material following a brief etch ($8H_2SO_4:H_2O:H_2O_2$).

An open-tube vapor transport system was used to deposit epitaxially the Ga(As, P) or (Ga, In)As alloy on the GaAs substrate (1-3).

Composition measurement and x-ray procedure.—The sample (film/substrate) was clip-mounted on a goniometer head which was at the end of a shaft. The shaft was inserted into a standard Norelco diffractometer. Characteristic copper radiation was employed in the measurement; the diffracted radiation was rendered monochromatic with a focusing monochromator. The substrate was then aligned to diffract the (333) reflection in the case of a (111) sample. The (400) reflection was utilized if the substrate was (100). However, asymmetric reflections have been employed for specific applications. The sample was scanned between the angular limits of the alloy, *i.e.*, 2θ [GaAs] to 2θ [GaP]. The Ga(As, P) reflection occurs between these angles. Since the diffraction angle of the GaAs substrate was known, the substrate reflection acts as an internal standard. Since Vegard's laws hold in the GaAs-GaP alloy system and the interplanar spacing, d, can be determined from the alloy peak position, then the mole fraction of GaP can be calculated from the expression

$$x = (d\,\mathrm{Ga(As,P)} - d\,\mathrm{GaAs}) / (d\,\mathrm{GaP} - d\,\mathrm{GaAs}) \quad [3]$$

x can also be calculated from Eq. [2] as θ_x is linear with d in the alloy range.

The composition measurement uniquely determined the diffraction angles of the compositional layers in the deposit. These angles are used to align each layer for (SRT) topographs. An open-tube detector was used to establish the diffraction peaks; receiving slits were employed to culminate the alignment. Previous investigators have employed the standard powder diffraction methods to determine composition; this method is destructive and time consuming (4, 6).

The sample was mounted on a standard goniometer head in the (SRT) camera. The GaAs substrate was oriented with a scintillation detector-ratemeter circuit. The diffraction angles of the deposit are found by rotating the sample about the ω axis. The topographs were obtained with copper radiation. The effective size of the focus was 100μ (Jarrell-Ash microfocus generator). Nickel foil (0.002 in.) was placed over the film holder to filter the radiation diffracted from the sample. Kodak type A plates were utilized; the average exposure time was 1½ hr.

Results and Discussion

Inhomogeneity.—A composition measurement performed on a (100) deposit of (Ga,In)As yielded the (400) diffraction angle of 64.2°; the GaAs reflection was registered at 66.2° (Fig. 5). This angular separa-

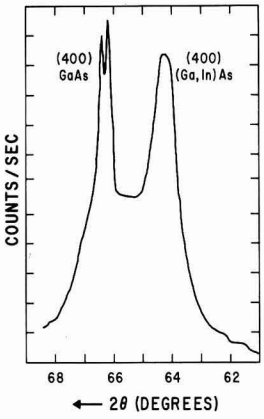

Fig. 5. Diffraction scan to determine the composition of an inhomogeneous deposit of (Ga,In)As.

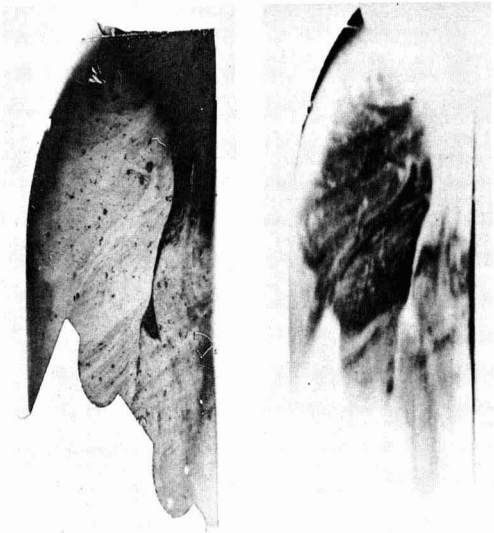

Fig. 6(a). (left). (400) topograph reveals inhomogeneous regions in the (100) deposit of (Ga,In)As; the alloy reflection was used to form the topographic image: (b) (right) the relative contrast was reversed when the GaAs diffraction angle was employed to obtain the (400) topograph.

tion corresponds to a 50% InAs alloy. The (400) topograph of the alloy layer reveals an image which exhibits nonuniform darkening (Fig. 6a). The central region of the image is of lower contrast than the periphery. The relative contrast was reversed by the employment of the GaAs diffraction angle to form the topographic image (Fig. 6b). The GaAs layer is coherently incorporated into the alloy matrix. This layer acts as an absorber, which attenuates the intensity diffracted from this region. These topographs map the spatial position of the compositional variations in the deposit.

A (111)-B (Ga, In)As deposit was also evaluated for composition (Fig. 7). The (333) alloy peak was displaced 2.5° from the (333) GaAs reflection. The (333) topograph of the 35% InAs layer revealed large areas of null contrast in the matrix (Fig. 8). The inhomogeneous region was shown to be GaAs rich in the same manner as Fig. 6a and Fig. 6b.

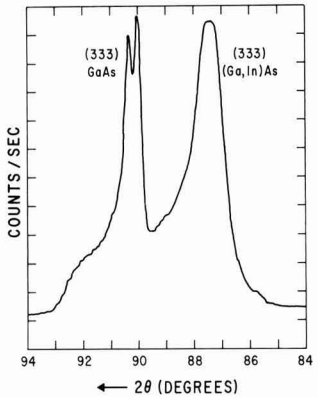

Fig. 7. Diffraction scan of an inhomogeneous (111) deposit of (Ga,In)As. The alloy composition was 35% InAs.

The scanning-reflection x-ray topographic method was employed to investigate planar variations in composition over large area deposits of (Ga, In)As. This type of analysis has certain advantages in the detection of gross inhomogeneity in the alloy deposits: (*a*) the scanning and /or counting time which would be involved in an electron microprobe analysis of these large area deposits would be impractical; (*b*) the shape of the alloy peak (composition measurement) has been shown to be sensitive to inhomogeneity, but no inference can be made to the spatial distribution of the inhomogeneous regions; (*c*) the reflectivity method (20) could not detect small variations in composition across the surface. X-ray topography clearly differentiated two regions in a Ga(As,P) deposit which differed by only 3% GaP (18). The topographic method is a fast, semiquantitative, and nondestructive technique to evaluate homogeneity.

Reflectivity measurements have been employed to determine axial changes in composition of Ga(As,P) epitaxial deposits (20). Homogeneity can be evaluated by incrementally etching the deposit, in conjunction with compositional determinations by reflectivity; the reflectivity measurements determine the composition at the surface only. This measurement can be quantitative (x-ray standards), but is a destructive process which involves a long evaluation time.

Compositional x-ray topography can also be applied to the evaluation of axial changes in composition. The method is simple, nondestructive, and yields a very sensitive qualitative display of the compositional changes encountered during epitaxial growth. A (111)-B Ga(As,P) deposit (0.002 in. thickness) was

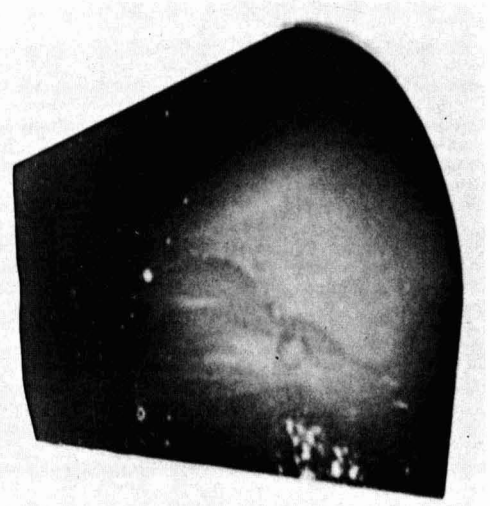

Fig. 8. The (333) topograph of the (111)-B deposit of (Ga,In)As which reveals a compositional gradient across the slice.

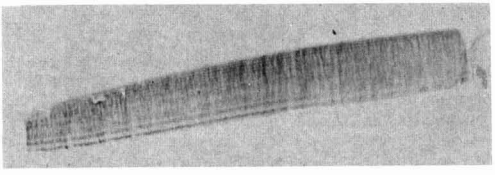

Fig. 9. The (220) topograph of a cleaved surface perpendicular to the (111) slice plane. The deposit image reveals lamella of different composition.

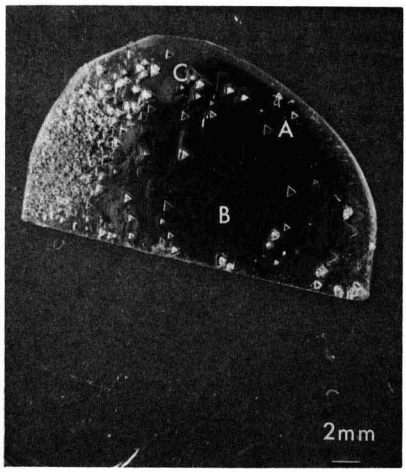

Fig. 10. Numerous hillocks on a (111)-B Ga(As,P) epitaxial film

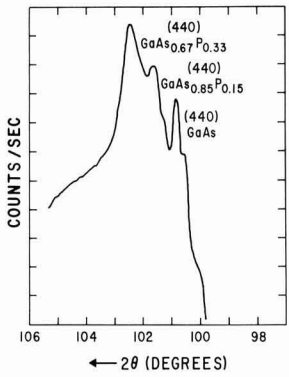

Fig. 11. Composition scan of Ga(As,P) deposit with hillocks

cleaved to expose a {110} cleavage plane normal to the plane of the slice. This is a standard technique to determine film thickness by interferiometric methods. A $(2\bar{2}0)$ topograph of the cleaved surface is shown in Fig. 9. The image consists of a series of alternating light and dark lines.

Since the sample was aligned to diffract Ga(As,P), the substrate image was not observed. The deposit image revealed dark lines traversing the width of the film. These lines correspond to regions of fixed composition, whereas the light lines (no contrast) represent lamella of different composition. The spacing between the lines decreases during growth which indicates that the deposit was approaching a constant composition. This effect has been observed in many alloy deposits and could degrade the efficiency of light-emitters fabricated from this material (23).

Hillocks.—Hillocks (localized surface protrusions) have been observed on epitaxial deposits of silicon (24-26), germanium (27-28), and GaAs (29). More recently, these (or similar) defects were detected in epitaxial deposits of Ga(As,P) and (Ga,In)As. Compositional x-ray topography was used to study the morphology of these flaws in Ga(As,P).

Numerous hillocks were obtained in a (111)-B deposit of Ga(As,P) (Fig. 10). The thickness of the film was determined to be 14μ. A composition measurement was obtained by the employment of the asymmetric (440) reflection. The diffraction scan is shown in Fig. 11. The (440) GaAs reflection was registered at 100.8°; the (440) $GaAs_{0.85}P_{0.15}$ layer and the (440) $GaAs_{0.67}P_{0.33}$ layer yielded diffraction angles of 101.6° and 102.5°, respectively. The relative peak heights indicate that the 15% GaP layer was the initial deposit, *i.e.*, this reflection was attenuated by absorption more than the 33% GaP layer. The diffraction angles were then used to align each layer for (SRT) topographs.

The (440) topograph of the GaAs substrate (Fig. 12a) reveals the hillocks as triangular regions of null contrast. The image shapes are either sharp (arrow A), diffuse (arrow B), or diffuse with a definite triangular center (C). The lack of contrast observed in the hillock images indicated that they are misoriented with respect to the substrate which corresponds, in this case, to a difference in composition. The (440) topograph of the $GaAs_{0.67}P_{0.33}$ layer also displayed the hillocks as regions of reduced contrast (Fig. 12b). The intense darkening in this image was the result of local cracks in the deposit which indicates the effect that hillock formation can have on the deposit quality. The sample was then oriented to diffract the $GaAs_{0.85}P_{0.15}$ layer; the (440) topograph exhibits only the hillock images (Fig. 12c). The matrix was misoriented for diffraction.

The hillocks are probably generated at the substrate interface since their composition corresponds to the 15% GaP layer. The final compositional layer (33% GaP) forms around the hillocks and frequently overgrows these defects. A diffuse image was observed in Fig. 12a (arrow B), and no image was registered in

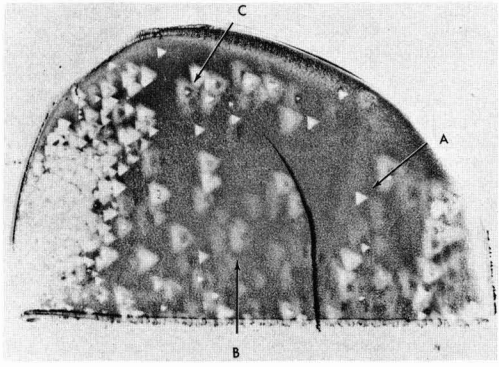

Fig. 12(a). The (440) topograph of the GaAs substrate which reveals the hillocks as triangular regions of null contrast. The dark line traversing the image is a spurious reflection.

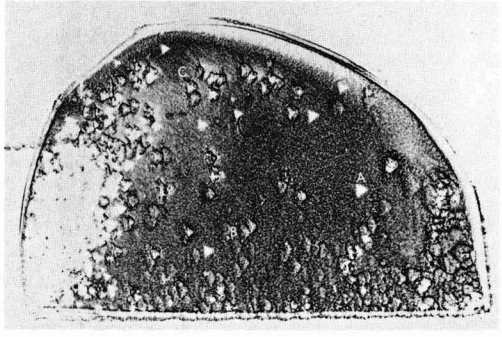

Fig. 12(b). The (440) topograph of the $GaAs_{0.67}P_{0.33}$ layer; the dark contrast results from local cracks in the deposit.

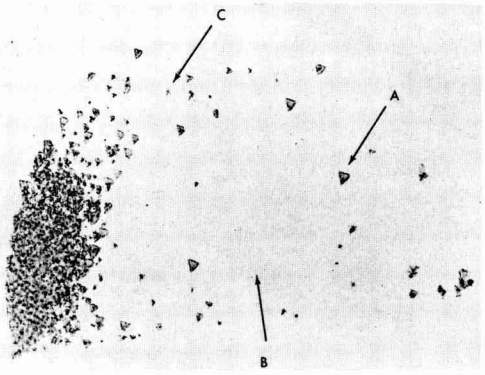

Fig. 12(c). The (440) topograph of the $GaAs_{0.85}P_{0.15}$ layer, only the hillocks are in diffracting position.

Fig. 12c. However, other hillocks protrude through the top layer (arrow A). The hillocks which protruded through the surface layer are revealed as triangles in Fig. 12c (arrow A). The partially overgrown hillocks (C) produce the diffuse images with null contrast centers (Fig. 12a, arrow C); only the triangular center can be seen in Fig. 12c.

The sample was angle-lapped and stained (Fe-HNO_3) on a 5° bevel to reveal the cross section of a hillock (Fig. 13). The dark irregular line, A, is the substrate and $GaAs_{0.85}P_{0.15}$ layer interface. The line at B is the junction between the $GaAs_{0.85}P_{0.15}$ and $GaAs_{0.67}P_{0.33}$ layers. The hillock, C, has the same stain as the $GaAs_{0.85}P_{0.15}$ layer which confirms the x-ray results. This hillock was determined to be 7μ above the $GaAs_{0.85}P_{0.15}$ layer.

Summary and Conclusions

The joint application of x-ray topography (SRT) and a diffractometer method to determine composition (compositional x-ray topography) has been shown to be an effective method to study the structural perfection and homogeneity of epitaxial Ga(As,P) and (Ga, In)As. Some results of this investigation are: (*a*) a planar compositional gradient was observed in (Ga,In)As deposits; the inhomogeneous regions were spatially located, and their composition was shown to be GaAs rich; (*b*) axial changes in composition were detected in a Ga(As,P) deposit (presumed to be constant composition); (*c*) the composition of hillocks generated at the substrate-$GaAs_{0.85}P_{0.15}$ layer interface was determined to be 15% GaP; (*d*) the hillocks (15% GaP) were frequently overgrown by a 33% GaP layer, and local cracking of this layer appeared to be related to the existence of hillocks.

Although this investigation was restricted to the GaAs-GaP and GaAs-InAs heteroepitaxial systems, this method has been successfully used to study stress relief mechanisms in deposits of germanium on silicon substrates (30). Another application concerns the perfection of (Ga, In)As which was deposited in holes that were cut (etched) into heavily dislocated monocrystals of GaAs (31). The dislocation density at the GaAs-(Ga,In)As heterojunction has also been compared to the dislocation density characteristic of the deposit (32). This type of examination is of interest in the determination of structural flaws created by lattice mismatch.

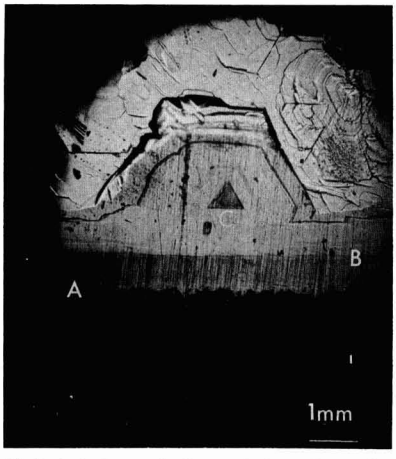

Fig. 13. Optical micrograph of an angle-lap and stain (Fe-HNO_3) junction; a hillock and two different compositional layers are displayed. Magnification, approximately 100X.

Acknowledgments

The authors gratefully acknowledge the interest and cooperation of the Materials Science Research Laboratory. In particular, Dr. R. W. Conrad supplied the (Ga,In)As samples; the Ga(As,P) sample was grown by Dr. R. H. Cox. Dr. D. W. Shaw is to be thanked for helpful discussions on hillocks. Mr. James A. Arnold performed the x-ray composition measurements.

Manuscript received Dec. 9, 1965; revised manuscript received Feb. 17, 1966. This paper was presented at the Buffalo Meeting, Oct. 10-14, 1965.

Any discussion of this paper will appear in a Discussion Section to be published in the December 1966 JOURNAL.

REFERENCES

1. "Development of Gallium Arsenide-Phosphide Graded Band-GaP Base Transistor Structures," Contract No. NObsr 91238, Final Report 1964.
2. "Research and Investigation of Gallium Arsenide-Indium Arsenide Alloy System," Contract No. AF 33(615)-1272, Final Report 1965.
3. W. F. Finch and E. W. Mehal, *This Journal*, **111**, 815 (1964).
4. G. E. Gottlieb, *ibid.*, **112**, 192 (1965).
5. M. Rubenstein, *ibid.*, **112**, 426 (1965).
6. San-Mei Ku, *ibid.*, **110**, 991 (1963).
7. E. M. Hull, *ibid.*, **111**, 1295 (1964).
8. G. R. Antell, *J. Appl. Phys.*, **31**, 1686 (1960).
9. Papers Presented on Technical Conference on Solid/Solid Interfaces, Electronic Properties, Boston, Mass., Aug. 31-Sept. 2, 1964, Trans. AIME, March 1965.
10. A. R. Lang, *J. Appl. Phys.*, **30**, 1748 (1958).
11. U. Bonse, *Z. Physik*, **153**, 278 (1958).
12. J. B. Newkirk, *Trans. AIME*, **215**, 483 (1959).
13. G. H. Schwuttke, *J. Appl. Phys.*, **33**, 2760 (1962).
14. G. H. Schwuttke, *ibid.*, **36**, 2712 (1965).
15. G. H. Schwuttke and V. Sils, *Bull. Amer. Phys. Soc.*, **2**, 48 (1964).
16. E. D. Jungbluth, *This Journal*, **112**, 580 (1965).
17. J. K. Howard and R. D. Dobrott, *Appl. Phys. Letters*, **7**, 101 (1965).
18. J. K. Howard and R. H. Cox, In press.
19. D. P. Miller, Unpublished results.
20. E. W. Williams, R. H. Cox, and R. D. Dobrott, To be published.
21. J. C. Woolley and K. W. Blazey, *J. Phys. Chem. Solids*, **25**, 713 (1964).

22. A. Reisman and R. Rohr, *This Journal*, **111**, 1425 (1964).
23. D. Kendall, Private communication.
24. S. Mendelson in *Single Crystal Films* (Conference at Blue Bell, Pa., May 1963), p. 251, M. H. Francombe and H. Sato, Editors, Pergamon Press Inc., New York (1964).
25. D. P. Miller, S. B. Watelski, and C. R. Moore, *J. Appl. Phys.*, **34**, 2813 (1963).
26. S. Mendelson, *ibid.*, **36**, 2525 (1965).
27. M. Takabayashi, *J. Appl. Phys. Japan*, **1**, 22 (1962).
28. T. Arizumi and T. Akasaki, *ibid.*, **2**, 143 (1963).
29. J. A. Amick in "Single Crystal Films" (Conference at Blue Bell, Pa., May 1963), p. 283, M. H. Francombe and H. Sato, Editors, Pergamon Press Inc., New York (1964).
30. J. K. Howard, Unpublished results.
31. J. K. Howard, R. W. Conrad, and D. W. Shaw, To be published.
32. J. K. Howard, To be published.

Potential of a Platinum Electrode at Low Partial Pressures of Hydrogen and Oxygen

II. An Improved Gas-Tight System with a Negligible Oxygen Leak

Sigmund Schuldiner, Bernard J. Piersma,[1] and Theodore B. Warner

United States Naval Research Laboratory, Washington, D. C.

ABSTRACT

A tight electrochemical system was constructed in which the P_{O_2} above the cell solution was $<10^{-9}$ atm. Comparing potentials with data from a previous paper (1) showed that very small amounts of O_2 leaking into a closed system can have marked effects on potential behavior at low P_{H_2}. Reduction of the oxygen leak to negligible proportions showed that: (*a*) the Nernst equilibrium relation for the H^+/H_2 couple holds only for P_{H_2} in excess of 10^{-6} atm; (*b*) at low P_{H_2}, trace amounts of O_2, even in the presence of several orders of magnitude more hydrogen, acted as an electrode poison causing a positive deviation from the theoretical Nernst behavior; (*c*) in O_2-free solution, at P_{H_2} below 10^{-6} atm, the potential remained at 0.18v positive to NHE and was independent of P_{H_2}. The potential-determining reaction in this region may be an exchange of H^+ in solution with H atoms dermasorbed in the Pt. The potential *vs.* oxygen partial pressure relation was essentially the same as found in previous work from this laboratory. Residual hydrogen associated with Pt at potentials from 0.18 to 0.2v did not react with oxygen.

In the first paper of this series, Warner and Schuldiner (1) determined open-circuit rest potentials on bright platinum as a function of oxygen or hydrogen partial pressures from 10^{-2} to 10^{-7} atm. The oxygen leakage (from air) into the cell was estimated to give a partial pressure of about 10^{-7} atm. The Nernst equilibrium relation for the H^+/H_2 couple held only at hydrogen partial pressures in excess of 1×10^{-4} atm. At hydrogen pressures smaller than this value the measured potentials were positive to the theoretical Nernst values. No satisfactory explanation could be given for this deviation, but it was felt that the trace of oxygen leaking into the system might be the cause. Even though a correction for the oxygen leak, assuming complete reaction with hydrogen at the Pt surface, was made, trace amounts of oxygen could possibly have remained on the surface when the hydrogen partial pressure was below 10^{-4} atm. This oxygen might then act as a poison for the H^+/H_2 exchange (even though the hydrogen partial pressure was several orders of magnitude higher) and give potentials positive to the theoretical equilibrium values. To determine if such traces of oxygen could affect the potential at low hydrogen pressures it was necessary to improve our gas-tight system to reduce further the leakage of oxygen into the cell. This was done in three ways: (*a*) improved purification of the helium carrier gas (Fig. 1) using two Meyer-Ronge (2) columns instead of one; (*b*) construction of a more compact gas purification and cell system; (*c*) installation of the critical part of the gas purification system, the gas generator, and the cell in a controlled environment box under an atmosphere of nitrogen (Fig. 2). Thus the outside of the system was exposed to nitrogen rather than air. The partial pressure of O_2 in the environment box was maintained at $5 \pm 2 \times 10^{-4}$ atm. This meant that at the outside of the system the O_2 pressure was reduced by 1/400 of the value in air.

[1] National Academy of Sciences, National Research Council Postdoctoral Research Associate.

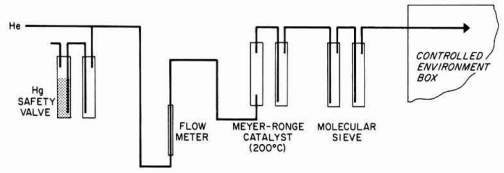

Fig. 1. Helium purification train outside of controlled environment box.

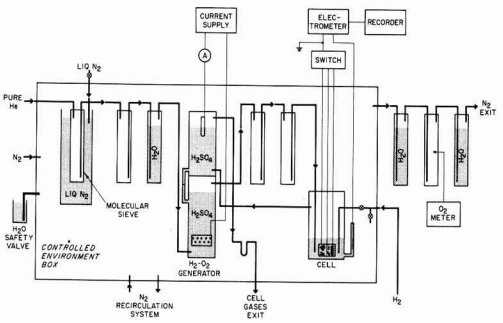

Fig. 2. Electrochemical system inside of controlled environment box and associated equipment.

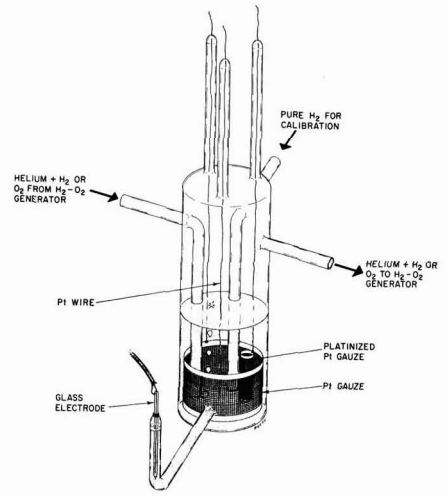

Fig. 3. Schematic of electrolytic cell. Glass pipe connections were actually used for electrode and gas connections and to connect upper and lower section of cell compartment. [See Fig. 1, p. 1143 of ref. (3) for illustration showing construction of cell.]

This improved gas-tight system reduced the oxygen leak into the cell to immeasurable proportions and, as the data will show, strongly affected the hydrogen pressure *vs.* potential relation.

Experimental

Apparatus.—The electrochemical cell (3) (Fig. 3) contained a miniature glass electrode, a Pt wire electrode 5 cm long with a 0.064 cm diameter, a large Pt gauze electrode (~100 cm^2), and a large tightly rolled cylinder of Pt gauze platinized in lead-free platinic acid (total geometric area about 30 cm^2). The electrolyte was 1M H_2SO_4 maintained at 25° ± 2°C. The helium purification train, electrolytic H_2 or O_2 generator (1), cell, and controlled environment system are shown in Fig. 1 and 2. The two stopcocks leading to the cell (Fig. 2) were Kern high-vacuum greaseless stopcocks with Viton A diaphragms. The controlled environment box was manufactured by Vacuum/Atmospheres Corporation and was 45 in. long by 30 in. deep by 33 in. high. The liquid nitrogen cold trap consisted of a molecular sieve (Linde 5A) column in a Linde LD 10 liter Dewar. This Dewar flask was filled *via* an insulated copper pipe which led outside the box where it was shut off with a valve. Copper tubing connected the helium tank to the flow meter. From this point the system was glass with one Viton A O-ring connection between the two Meyer-Ronge catalyst columns. At the end of the second molecular sieve column a gold-plated (to prevent diffusion of hydrogen in from the room atmosphere) copper tube was connected with a second Viton A O-ring. This gold-plated copper tube conducted the purified helium into the environment box to the cold trap. Therefore, even though two Viton A seals were used outside the box, one seal was between the two Meyer-Ronge columns so any trace of O_2 which diffused through it was removed by the second Meyer-Ronge column. The second seal outside the box was in front of the molecular sieve-liquid N_2 cold trap so that any O_2 which diffused through this O-ring would be frozen out. Since the liquid N_2 cold trap was inside the environment box, diffusion of O_2 through any of the other seals was minimized. The manufacturer of the Viton-A O-rings claims a seal good to 10^{-6} Torr, and previous work (1) indicated an oxygen leak in the entire system equivalent to about 10^{-7} atm, so with the new system used we feel that the oxygen leak within the cell should not exceed 10^{-9} atm. In any case, attempts to determine the amount of oxygen leaking into the cell from the atmosphere were fruitless because of its extremely low concentration.

An N_2 atmosphere inside the environment box was obtained by passing tank N_2 into the box for several days until O_2 partial pressure inside the box dropped to about 10^{-3} atm. The flow of N_2 was then reduced, and the gas inside the box was recirculated through a bed of copper turnings at 450°C to remove oxygen. Recirculation was *via* a high-speed gas pump with a flow of about 1.5 l/min. It was soon discovered that the evaporation of liquid N_2 maintained a sufficient gas flow through the environment box and the tank N_2 was eliminated. Once the O_2 pressure dropped to 5 x 10^{-4} atm, as determined on the outlet side with a Beckman, Model E2 oxygen analyzer, recirculating N_2 was no longer helpful in reducing the O_2 partial pressure. From that point on the only sources of N_2 needed were from the evaporation of liquid N_2 and from the tank N_2 used to pump liquid N_2 into the Dewar. It was necessary to fill the Dewar every two weeks. This operation resulted in a large influx of N_2 into the box so that a large outlet valve from the box had to be kept open to keep the internal pressure below 5 in. of water in excess of atmospheric pressure. In addition a water-filled safety valve was attached to the box. This valve would release N_2 when the pressure inside of the box exceeded 5 in. of water above normal atmospheric pressure.

Electrical connections were made as shown in Fig. 2. A system of rotary switches was used to alternate every 5 min from one Pt electrode in the cell to another. The potential between each Pt electrode and the glass reference electrode was measured with a Keithley 610A electrometer and displayed alternately on a Varian recorder.

Procedure.—Glassware was cleaned with boiling nitric acid and rinsed 12 to 15 times with triply distilled water (one stage of distillation from alkaline permanganate solution, another from water containing fumed phosphoric acid, the final two stages being from a quartz still). The sulfuric acid solution was preelectrolyzed for three days at 50 ma. This was followed by calibration of the glass electrode against the platinum electrodes in H_2 saturated solution at 1 atm pressure. Hydrogen flow was then replaced with a flow of pure helium always maintained at 40 std ml/min. Pressure within the cell was about 10 Torr above atmospheric. The hydrogen line was disconnected, flushed, and filled with helium. The environment box was then sealed and air was replaced with N_2 by the procedure described above. Either hydrogen or oxygen was introduced into the helium carrier gas by the special electrolytic H_2 or O_2 generator (1) designed at this laboratory. Gas generation rates were calculated from constant electrolysis currents. The partial pressures were calculated from the rate of flow of helium (known to 5%) and the rates of H_2 or O_2 generation (known to 1%).

The rate of attainment of steady-state potentials was very dependent on electrode area, especially at partial pressures below 10^{-6} atm. The platinized Pt electrode area was so large that at low partial pressures this electrode lagged far behind the other two Pt electrodes. All three electrodes would come to the same potential given sufficient time, but the platinized Pt electrode required such a long time (months) at very low partial pressures that in most measurements only enough time was allowed for the Pt wire and gauze to come to the same steady-state values. The experiments which gave the data recorded in this paper took about 11 months. Several runs up and down the pressure scale were taken.

When pure helium or helium mixtures with low hydrogen partial pressures flowed through the cell, the addition of liquid N_2 to the cold trap caused the Pt

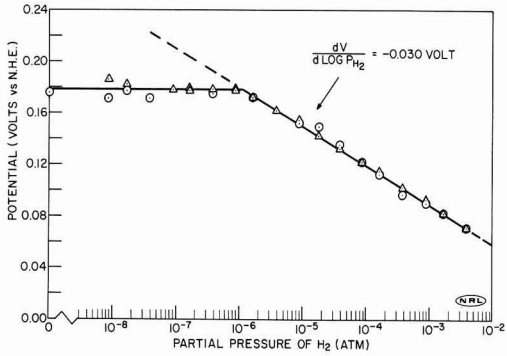

Fig. 4. Relation between hydrogen partial pressure and rest potentials. Dashed line shows normal Nernst potential relation for H^+/H_2 exchange; ○ decreasing H_2 pressure; △ increasing H_2 pressure.

wire and gauze electrode potentials to deviate in a positive direction. Several hours were required for these electrodes to recover their original potentials. We attribute this effect to a trace of O_2 which was introduced during the cooling of the environment box (its temperature usually decreased to about 17°C during the filling of the Dewar). This cooling caused a decrease in pressure in two arms of the cell, and the space above the solution in these compartments decreased as the cell solution rose slightly in them. This may have caused a trace of oxygen trapped in these side arms or in the counter electrode side of the gas generator to go into solution and/or caused a further removal of traces of oxygen associated with the interior walls of the glass system. The rise of solution in these side arms showed that leaks did not exist. In any case liquid N_2 was added only once every 14 days so that this effect was minimized.

Results and Discussion

Experimental results.—The experimental results are shown in Fig. 4 for the hydrogen electrode and in Fig. 5 for the oxygen electrode. Values were obtained with both increasing and decreasing gas partial pressures and were taken only after steady-state potentials were reached. For hydrogen partial pressures below 10^{-5} atm, steady-state meant no significant change in potential (values constant within ± 3 mv, and no monotonic trend within this uncertainty) on the Pt wire and gauze for at least several days. Their potentials generally agreed to 2 mv, with occasional differences of 5-7 mv. For the platinized platinum gauze at the lowest partial pressures, the electrode continually changed in the expected direction, but at such a slow rate that we did not normally wait for this electrode to reach the steady-state value of the other two electrodes.

For oxygen partial pressures, the rate of attainment of steady-state potentials for decreasing oxygen pressures was very slow, even for the Pt wire. Here also the potentials shown in Fig. 5 represent values that were unchanged for at least several days, but because of extreme system sluggishness, agreement between electrodes was poorer (5-30 mv) and random variations with time larger. Experiments were conducted also in which the gas flow was changed from helium containing first hydrogen and then oxygen and *vice versa*. This made no difference in the final rest potential providing one waited long enough for the rest potential to be attained.

In one experiment, after the electrodes were exposed to oxygen-containing helium for over two months, the oxygen flow was cut off. The rest potential on the Pt wire was reached in about one week (0.2v). Then, to test the purity of the solution, the cleanliness of the electrodes, and the tightness of the entire system, a single constant current pulse was applied to the Pt wire in the helium-saturated solution. This test took place six months after cleaning and closing the system. An anodic charging curve of the first applied current pulse gave an oscilloscopic trace which showed a small hydrogen region from 0.2 to 0.4v followed by double layer and linear oxygen regions. The shape of the charging curve met our published (4) requirements for a clean Pt surface free of detectable amounts of either oxidizable or unoxidizable organic contaminants or of electrode poisons. The fact that hydrogen was still associated with the Pt surface after such a long exposure to oxygen was unexpected, but it does account for the relatively low positive potentials of Pt observed in helium-saturated solution.

Effect of oxygen leak.—In order to estimate the maximum possible amount of oxygen which leaked into the cell, the following experiment was carried out. After passing pure helium through the cell for five days, the average potential of the three Pt electrodes was 0.175v. The sequence of changing the partial pressure of either oxygen or hydrogen in the cell to the values shown in Fig. 6 was then carried out. At the end of each time noted for the given partial pressure shown in Fig. 6 the potential of the Pt wire, the electrode with the fastest response, is shown. It should be noted that these are not the final rest potentials at these partial pressures. These results are for the purpose of demonstrating the effects of small alternate additions of oxygen and hydrogen on the potential. As the data show, potentials are sensitive to oxygen partial pressures as low as 4.4×10^{-9} atm and hydrogen partial pressures as low as 8.7×10^{-9} atm. From this we can conclude that the oxygen leak into the system cannot be, at most, more than enough to give a partial pressure of 10^{-9} atm. In fact, from the relatively fast response times shown in Fig. 6, one can conclude

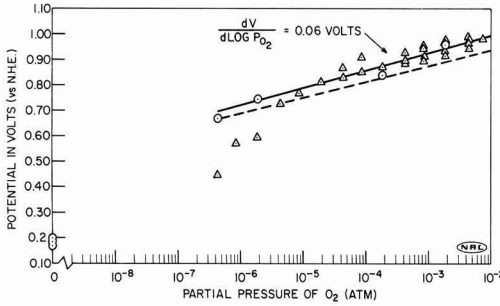

Fig. 5. Relation between oxygen partial pressure and rest potentials. Dashed line indicates average values previously obtained at this laboratory (1, 3); ○ decreasing O_2 pressure; △, increasing O_2 pressure.

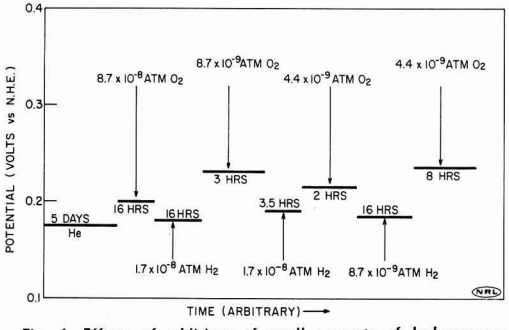

Fig. 6. Effects of additions of small amounts of hydrogen or oxygen on potential of Pt wire.

that the oxygen leak, expressed in terms of resulting partial pressure, was likely under 10^{-10} atm.

Platinum rest potentials vs. P_{H_2} or P_{O_2}.—The data in Fig. 4 demonstrate that a normal Nernst equilibrium relation between potential and log P_{H_2} exists down to 1 x 10^{-6} atm of hydrogen. At lower hydrogen pressures the potential is independent of P_{H_2}, this implies that the exchange current density of the H^+/H_2 exchange at P_{H_2} below 10^{-6} atm is so low [$\approx$1.4 x 10^{-9} amp/cm^2 (5)] that another potential-determining reaction takes over. Such a reaction could be

$$Pt\text{-}H \rightleftarrows Pt + H^+ + e$$

where Pt-H either represents hydrogen atoms dermasorbed in the Pt skin or an alloy of Pt and H atoms. Schuldiner, Castellan, and Hoare (6) concluded that a similar potential-determining reaction took place on α Pd-H alloys.

Luk'yanycheva and Bagotskii (7) determined the initial open-circuit potentials of carefully degassed platinum in 1*N* H_2SO_4 degassed under vacuum. These potentials were 0.210 and 0.215v. They observed that these rest potentials are close to the point of zero charge of platinum.

Our measurements in helium-saturated solution gave rest potentials 15-50 mv more negative than those of Luk'yanycheva and Bagotskii. In addition, the fact that we were able to find a small amount of hydrogen associated with the electrode after prolonged exposure to oxygen showed that the rest potentials we found in helium-saturated solutions and the plateau at 0.178v shown in Fig. 4 are influenced by hydrogen.

Since the potential plateau in Fig. 4 is below the theoretical Nernst line, oxygen is not a factor as it was in the first paper of this series (1). The stability of Pt-H in this region is demonstrated by the rest potential in pure helium-saturated solution. The experiments which showed that after an electrode has been in oxygen-rich helium the rest potential in pure helium is about the same indicate that this residual hydrogen does not react with oxygen. In addition, it shows that sorbed oxygen is in equilibrium with O_2 gas because when the O_2 pressure drops to zero the oxygen coverage of the surface appears to drop to zero. The stability of this residual hydrogen indicates that it is irreversibly sorbed with respect to H_2 and supports the repeatedly stated view from this laboratory that this hydrogen is dermasorbed in the Pt skin and may be alloyed with Pt. The hydrogen content of the Pt electrode apparently did not change with H_2 partial pressures below 10^{-6} atm, as indicated by the unchanging electrode potential in this region. This may be contrasted with the dependence of hydrogen content of α Pd-H on H_2 partial pressure as shown by Moon (8). However, much smaller amounts of H are involved than in the case of α Pd-H alloys.

One may argue that the plateau shown in Fig. 4 is due to an organic or other trace material in solution. However, the cleanliness test made after the system was used for six months shows that this possibility is unlikely. In addition, finding hydrogen associated with the platinum after long exposure to oxygen indicates that hydrogen determines the potential. Another experiment to show the effects of hydrogen on potential was made by determining the rest potential in pure helium followed by addition of oxygen to give a more positive rest potential followed by the addition of less than 10^{-6} atm H_2 which then gave the same rest potentials shown in Fig. 4. Furthermore, the total area of Pt in solution was so large that impurity levels, which were below the detectable limit of our cleanliness test (4), would be so minute that even the traces of oxygen or hydrogen used would overcome their effects (as was demonstrated by the reported tests).

The possibility must also be considered that the 0.2v open-circuit potentials under pure helium could be due to leakage of hydrogen into the gas stream from the Pd-tube counter electrode in the electrolytic gas generator. The design of the gas generator made this improbable. Additional evidence that this did not occur came from the following experiment: after the electrodes were exposed to a He + O_2 mixture, pure helium was substituted. While the potentials were changing to less positive values the electrolyte contact with the Pd counter electrode in the gas generator was broken. The rate of potential change on the Pt electrodes in the cell did not change significantly, and final rest potentials were the same as previously found.

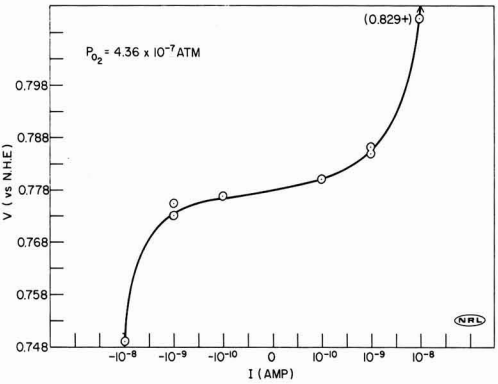

Fig. 7. Anodic and cathodic polarization of Pt wire electrode

The rest potentials shown in Fig. 5 give essentially the same dependence of potential on oxygen partial pressure as was previously determined (1, 3). There was, however, a significant difference. The broken line in Fig. 5 represents the average data previously found (1, 3) and as can be seen the data from this investigation indicated the same slope but an upward displacement of the average curve by about 40 mv. The reason for this difference is unknown. Stirring effects, effect of platinized Pt, effects of light, etc., were all checked and none seemed to be important. It also should be noted that the low potential values found at increasing very low oxygen partial pressures is most likely due to the very long times required to attain steady state. Decreasing values of oxygen partial pressures fell on the straight line shown in Fig. 5. A current-voltage relation was determined at P_{O_2} = 4.36 x 10^{-7} atm and is shown in Fig. 7. The open-circuit potential was a little above the rest potential later found. The data in this curve indicate that the potential is determined by a reversible reaction involving oxygen.

In previous work (1, 3) it was suggested that the potential was determined by an O_2/HO_2 exchange. The results found in this work confirm this.

Conclusions

1. True steady-state open-circuit potentials can be obtained and maintained when sufficient steps are taken to insure solution and gas purity and electrode cleanliness.

2. Considerable periods of time (up to a month or more) are required to establish steady-state potentials with low partial pressures (below 10^{-4} atm) of H_2 or O_2. Response times are faster with hydrogen.

3. At low partial pressures, the surface area becomes dominating in the time for establishment of steady-state potentials. At higher partial pressures, the surface/volume ratio of the electrode is the determining factor.

4. The oxygen background in this improved system is less than 10^{-9} atm.

5. The deviation from Nernst behavior previously reported (1) for the hydrogen electrode was due to the effects of small amounts of oxygen poisoning the hydrogen equilibrium.

6. Below hydrogen partial pressures of 10^{-6} atm, the steady-state potential is independent of P_{H_2}, *i.e.*, the Nernst potential relation for the H^+/H_2 equilibrium is not valid below 10^{-6} atm.

7. The potential plateau observed at 0.18v for hydrogen partial pressures below 10^{-6} atm is not due to an organic impurity.

8. The 0.18v potential is believed to be established by an equilibrium involving hydrogen ions in solution and hydrogen atoms dermasorbed in the electrode (or alloyed with the Pt). This reaction has an exchange current density on the order of 10^{-9} amp/cm^2.

9. The residual hydrogen associated with Pt at potentials from 0.18 to 0.2v did not react with oxygen.

10. The potential-oxygen partial pressure relation found had the same slope as previously reported (1, 3) although potentials at the same partial pressures ran about 40 mv higher.

Manuscript received Feb. 16, 1966.

Any discussion of this paper will appear in a Discussion Section to be published in the December 1966 JOURNAL.

REFERENCES

1. T. B. Warner and S. Schuldiner, *This Journal*, **112**, 853 (1965).
2. F. R. Meyer and G. Ronge, *Angew. Chem.*, **52**, 637 (1939).
3. S. Schuldiner and R. M. Roe, *This Journal*, **110**, 332, 1142, (1963).
4. S. Schuldiner and T. B. Warner, *J. Phys. Chem.*, **68**, 1223 (1964).
5. S. Schuldiner, *This Journal*, **106**, 891 (1959).
6. S. Schuldiner, G. W. Castellan, and J. P. Hoare. *J. Chem. Phys.*, **28**, 16 (1958).
7. V. I. Luk'yanycheva and V. S. Bagotskii, *Dokl. Akad. Nauk, SSSR*, **155**, 160 (1964).
8. K. A. Moon, *J. Phys. Chem.*, **60**, 502 (1956).

Electrochemical Measurement of the Available Surface Area of Carbon-Supported Platinum

J. F. Connolly, R. J. Flannery, and G. Aronowitz

Research and Development Department, American Oil Company, Whiting, Indiana

ABSTRACT

The measurement of charge consumed in the galvanostatic stripping of adsorbed oxygen or hydrogen from carbon-supported platinum surfaces gave a measure of the area of platinum in contact with solution. A combination of the two methods proved superior to either used alone. The combination compensated for the charge consumed on the carbon with sufficient accuracy to permit measurements down to the region where the platinum area is 1/100 of the support area. Comparison with x-ray diffraction measurements suggests that, with high platinum concentrations on low area carbons, standard platinum deposition techniques yield electrodes in which much of the platinum surface is not in contact with solution.

When platinized porous-carbon electrodes are used in fuel cells, some of the platinum may be unavailable because it is physically inaccessible to the solution or because of adsorbed material on its surface. Knowledge of the available area of the platinum is useful for optimizing cell performance. X-ray diffraction does not exclude unavailable platinum area and may miss very small crystallites. However, electrochemical methods can be expected to measure only platinum which is in contact with solution, and there should be no lower limit on the size of platinum crystallites which can be detected.

The areas of unsupported metals can, in principle, be measured by four electrochemical techniques: measurements of capacitance (1), measurement of exchange currents (2), stripping or deposition of oxygen (3), and stripping or deposition of hydrogen (4). The first technique has been applied to a number of unsupported metals (1), while the other three would be useful only in special cases.

For platinum supported by a porous-carbon electrode, capacitance measurement may be ruled out because the capacitance of the platinum will not differ enough from that of the support, and because pore resistance makes capacitance difficult to measure. Likewise, measurements of exchange currents will in general be thwarted by mass transfer limitations in a porous electrode and where this is not the case, as in hydrogen evolution, by excessive pore resistance.

However, the oxygen and hydrogen stripping methods are probably unaffected by mass transfer in a porous electrode although nonuniform current distribution due to pore resistance has some effect on the form of the "arrest" (a region of minimal slope in the potential *vs.* charge curve). Therefore, these two methods were investigated, singly and in combination, with a series of platinized porous-carbon electrodes having a broad range of surface areas and platinum loadings. The major difficulty encountered was in correcting for the charge consumed on the carbon support, the area of which was many times the platinum area. This problem was solved to the extent that cases in which the platinum area is as small as 1/100 of the support area can be handled.

Experimental

The measurements were carried out in an H-cell, connected to a mercurous sulfate-mercury reference electrode through a Luggin capillary. Carbon-supported platinum electrodes were held between tantalum screens mounted in a tantalum holder. Potential was controlled by a Wenking potentiostat, and mercury wetted relays were used for switching to a galvanostat which consisted of resistors and a 90v battery. Voltage variations were followed on a Tektronix oscilloscope and recorded with a Polaroid camera.

The arms of the H-cell were separated by a medium glass frit and could be flushed with helium to remove oxygen. Preelectrolyzed 1M H_2SO_4, prepared from permanganate-distilled conductivity water, was the electrolyte in the cell, in the bridge to the reference electrode, and in the reference electrode compartment. For comparison with the mercurous sulfate-mercury reference electrode, the working compartment was frequently converted to a hydrogen reference electrode. This was done by inserting a platinized platinum electrode into the compartment and changing the flushing gas from helium to hydrogen. All voltages are given with reference to this "hydrogen electrode in the same solution." Ohmic voltage drops not

Table I. Electrode properties

Carbon	Area of block carbon, m^2/g	w/o Pt	Carbon[a] charge ratio, $Q_{C,O}/Q_{C,H}$	Carbon charge, % of O arrest, $100Q_{C,O}/Q_{T,O}$	Carbon charge, % of H arrest, $100Q_{C,H}/Q_{T,H}$
NC60	0.4[b]	4.2	6.9	0	0
NC60	0.4[b]	0.9	6.9	55	30
NC60	0.4[b]	1.0	6.9	55	30
FC11	3.0	4.4	6.4	5	0
FC21	1.0	1.0	6.5	30	15
PC59H	5.4	4.9	7.0	15	5
PC139	1.6	1.0	6.3	40	20
PC57H	1.3	0.8	6.6	50	35
FC14	10	5.2	6.4	10	5
FC11	3.0	1.1	6.4	15	5
PC59H	5.4	1.1	7.0	45	25
AC[c]	11[c]	4.8	5.6	45	25
FC14	10	1.1	6.4	35	15
PC62	200	20.4	6.8	55	30
PC62	200	7.2	6.8	60	30
PC64	700	27.7	5.1	70	50
PC62	200	4.8	6.8	75	50

[a] Charge consumed by blank powdered carbon from 1.1 to 0.35v divided by charge consumed from 0.05 to 0.30v.
[b] Estimated from apparent integral capacitance and gas chromatography.
[c] Powder. Courtesy sample from R. G. Haldeman (8).
Weight per cent = w/o.

eliminated by the Luggin capillary were corrected for by noting the gap in the oscilloscope trace at the beginning of a galvanostatic pulse.

The carbons, in block form, were platinized by impregnating with a solution containing chloroplatinic and oxalic acids, and then heating to 160°-180°C in an inert atmosphere for 8 hr. The reduction was completed by adding hydrazine and excess reagents were leached out in distilled water. In a few cases hydrogen of hydrazine alone was used as the reducing agent. Because these procedures did not give uniform platinum loadings, the platinized carbons were powdered before samples were taken for platinum analysis, x-ray diffraction, and electrochemical area measurements.

Carbon supports were obtained from National Carbon (NC), Pure Carbon (FC), Stackpole (PC), and American Cyanamid (AC). The manufacturer's designations and areas of the block form are listed in Table I. When powdered, the carbons having low surface areas all increased in area, as indicated by apparent integral capacitance in the 0.05-0.30v range. This is reflected in the large carbon charge consumptions listed in the last two columns of Table I. The surface areas of the high-area carbons were relatively little affected by powdering.

To form the electrodes, platinized-carbon powders were mixed with Teflon suspension, dried at room temperature, and pressed at 50,000 psi. The finished electrodes contained 3% Teflon and were strong enough to hold together in solution as long as they were supported between tantalum screens. Because the Teflon bonding procedure often made platinized carbons electrochemically inactive the electrodes were anodized at 1.2-1.4v for 10 to 30 min. However, care had to be used to obtain the mildest possible activating conditions in each case because anodizing roughens the carbons.

The affect of grinding and Teflon bonding on the platinum area measurements was ascertained as follows: Electrochemical measurements were made on several chips of solid platinized carbon. The chips were then processed into Teflon-bonded electrodes and the electrochemical measurements were repeated. The results showed that apparent losses in platinum area caused by the electrode-forming procedure were less than 10% as long as the Teflon-bonded electrodes were sufficiently anodized.

Immediately prior to oxygen stripping, the electrodes were pretreated by holding at 1.4v for 1 min. Before hydrogen stripping they were held at 1.2-1.4v for 1 min and then at 0.05v for 1 min. After

[1] This behavior and the comparison with x-rays to be made later indicate that the surface migration of hydrogen from platinum to carbon observed for gas-solid systems at high temperatures (5) is not a problem in the present case.

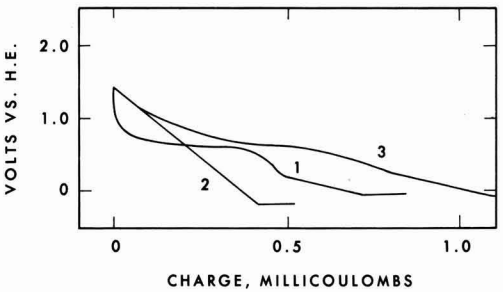

Fig. 1. Oxygen reduction: curve 1, 1 cm^2 Pt; curve 2, 15 cm^2 carbon; curve 3, Pt on carbon.

the first 30 sec there was very little change of arrest length with time at 0.05v,[1] unless the solution contained oxidizable impurities. These treatments were in addition to any necessary to cure poisoning of the Teflon-bonded electrodes.

The current densities during the galvanostatic strippings were adjusted to give an over-all voltage change rate of about 0.05v/sec. This required current densities of 0.5 to 1.0 $\mu a/cm^2$ of true area for the blank carbon electrodes, and higher values for the platinum loaded electrodes. Under these conditions 5-10 mg electrodes required total currents ranging from 0.1 to 25 ma. For any particular blank carbon sample the charge consumption in the 1.1 to 0.35 or 0.05 to 0.30 voltage intervals usually decreased or increased by about 10% for a fivefold increase or decrease in current density. The platinum loaded carbons were less affected by changes in current density. The current necessary for holding a sample at a particular voltage before switching to the galvanostat was less than 5% of the stripping current.

Oxygen Arrest

The arrest formed when adsorbed oxygen is stripped galvanostatically from a pure platinum electrode is illustrated by curve 1 in Fig. 1. The arrest starts near 1.1v and is complete at 0.35v. A potential *vs.* charge curve for a blank carbon electrode of moderate area is nearly linear as shown by curve 2. The effects of using carbon-supported platinum, rather than solid platinum, are to lengthen the oxygen arrest and to make its end points less distinct. These effects are illustrated in Fig. 1 by curve 3, in which 40% of the charge is being consumed on the carbon support. Because of the lack of distinctness in the arrest end points, measurements were made by using the end points which were consistently observed for those cases where the end points were distinct, *i.e.*, 1.1 and 0.35v.

For electrodes which have all been anodized in the same way, the charge consumed on platinum in the oxygen arrest is proportional to the platinum area, *i.e.*

$$A_{Pt} = Q_{Pt,O}/k_O = (Q_{T,O} - Q_{C,O})/k_O \qquad [1]$$

where A_{Pt} is the available platinum area, $Q_{Pt,O}$ is the charge consumed on the platinum in the oxygen arrest, k_O is a proportionality constant, $Q_{T,O}$ is the total charge consumed in the electrode in the oxygen arrest, and $Q_{C,O}$ is the charge consumed on the carbon support.

Because we did not have a platinum sample of known roughness, the results of Laitinen and Enke (3), corrected for the difference between H_2SO_4 and $HClO_4$ electrolytes (6), were used to estimate the proportionality constant k_O. This procedure gave 0.45 mc/cm^2 of true platinum area, for the charge consumed between 1.1 and 0.35v after pretreatment at 1.4v for 1 min.

$Q_{C,O}$, the charge consumed on the support, can be assigned in part to double layer capacitance and probably even in greater measure to oxygen adsorbed on

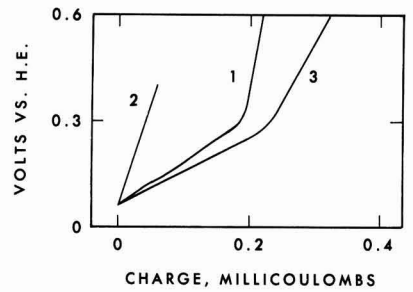

Fig. 2. Hydrogen oxidation: curve 1, 1 cm² Pt; curve 2, 15 cm² carbon; curve 3, Pt on carbon.

the carbon. This effect was small per unit area (an apparent integral capacitance of about 20 μf/cm² over the interval 1.1 to 0.35v) but, because the carbon area ranged up to 100 times that of the platinum, a major correction was necessary in most cases. It was evaluated by making a separate stripping measurement on an electrode formed from a nonplatinized sample of the same support. This procedure involved considerable uncertainty because of possible differences between the carbon supports of the platinized and nonplatinized electrodes. These differences could be expected to occur because of: nonuniform carbons, differences in grinding during the electrode preparation procedure, effect on the carbon of the chemicals used for platinizing, blockage of pores by platinum, and small differences in the stripping measurements.

Hydrogen Arrest

The arrest formed when adsorbed hydrogen is stripped galvanostatically from a pure platinum electrode is illustrated by curve 1 of Fig. 2. In the illustration the arrest commences at 0.05v and is complete near 0.30v. The hydrogen arrest for carbon-supported platinum differs from that of solid platinum in three aspects. It is longer, the faint fine structure is lost, and the change in slope near 0.30v is less sharp. These effects are illustrated by curve 3 in Fig. 3 in which 20% of the charge is being consumed on the carbon support.

The hydrogen arrest is analogous to the oxygen arrest in that the platinum areas of electrodes which have had like pretreatment will be proportional to the charge consumed on the platinum, *i.e.*

$$A_{Pt} = Q_{Pt,H}/k_H = (Q_{T,H} - Q_{C,H})/k_H \qquad [2]$$

where $Q_{Pt,H}$ is the charge consumed on the platinum in the hydrogen arrest, k_H is a proportionality constant, $Q_{T,H}$ is the total charge consumed in the electrode in the hydrogen arrest, and $Q_{C,H}$ is the charge consumed on the carbon support.

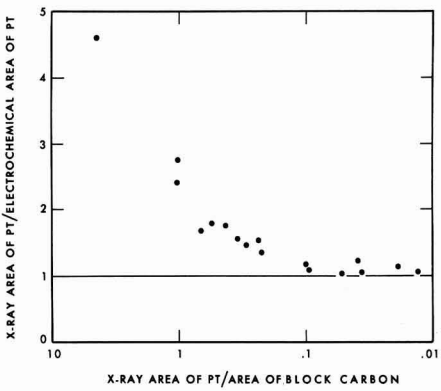

Fig. 3. Comparison of x-ray and electrochemical platinum areas

The proportionality constant k_H was determined by using pure platinum electrodes whose areas had been determined from the length of the oxygen arrest. This gave 0.19 mc/cm² of platinum for the charge consumed between 0.05 and 0.30v on bright platinum and platinized platinum electrodes which had been exposed to the atmosphere for several days. Freshly prepared electrodes gave a value 20% higher. The lower value was adopted because the aged electrodes should be a better approximation to the situation encountered with carbon-supported platinum. The carbon charge consumptions $Q_{C,H}$ were measured on nonplatinized carbon electrodes and are subject to the uncertainties listed in the oxygen arrest section.

Because $Q_{C,H} < Q_{C,O}$, the accuracies of the hydrogen arrest and oxygen arrest methods differ. To evaluate the relative uncertainty we will assume that the main error in an area measurement is due to the uncertainty in determining the charge consumed on the support. If this charge consumption is uncertain by some value e in per cent, then the percentage errors in the area determination by the oxygen and hydrogen arrest methods are

$$\Delta_O = eQ_{C,O}/Q_{Pt,O} \qquad [3]$$

and

$$\Delta_H = eQ_{C,H}/Q_{Pt,H} \qquad [4]$$

Now $Q_{Pt,H}/Q_{Pt,O} = k_H/k_O = 0.19/0.45$ and, as shown in Table I, $Q_{C,O}/Q_{C,H}$ is about 6.5. Thus, measurements of carbon-supported platinum areas, made using the oxygen arrest, should contain an error 2.7 times larger than those made using the hydrogen arrest.

Therefore, where the ratio of platinum area to support area is low, the hydrogen arrest method should give the better result. However, when this ratio is large, greater ease of activation (leading to earlier achievement of a reproducible state) and insensitivity to solution impurities (which do not adsorb as readily in the surface oxide formation region) favor using the oxygen arrest.

Oxygen and Hydrogen Arrests Used in Combination

As the platinum to carbon area ratio approaches 0.01 the fraction of the charge consumed in the carbon in the oxygen arrest reaches 75% and the fraction consumed in the hydrogen arrest reaches 50%. Thus, unless the carbon charge consumption is accurately known these methods become useless.

For reasons discussed in the oxygen arrest section, a separate measurement on the nonplatinized carbon does not give an accurate value for the charge consumption of the carbon in a platinized carbon. To get reasonable accuracy a method which uses direct measurements on the platinized carbon, with minimal dependence on blank carbon measurements, is desirable. Such a method is obtained by combining the oxygen-arrest and hydrogen-arrest charge consumptions as measured on the platinized-carbon electrode, with the ratio of the charges consumed by the support in the same regions as measured on a blank-carbon electrode, *i.e.*, from Eq. [1], [2], and

$$r = Q_{C,O}/Q_{C,H} \qquad [5]$$

we obtain

$$A_{Pt} = (rQ_{T,H} - Q_{T,O})/(rk_H - k_O) \qquad [6]$$

Thus the measured area of platinum becomes dependent on a ratio of carbon charge consumptions rather than on their absolute values.

The superiority of this combination method lies in its minimizing of dependence on blank carbon electrode measurements. Thus r should, as measured on the blank carbon electrode, apply to the platinized electrode with much greater accuracy than similarly measured absolute values of carbon charge consumption; *e.g.*, the plugging of carbon pores by platinum

Table II. Comparison of measurements of the area of carbon-supported platinum

Carbon area, m^2/g	w/o Pt	Area[a] ratio, Pt to carbon	Pt area, m^2/g Pt: O Arrest[b]	H Arrest	Combination	X-ray[c]
0.4	4.2	4.5	4	7	9	38,44
0.4	0.9	1.0		16	16	41,48
0.4	1.0	1.0		18	18	38,45
3.0	4.4	0.60	23	24	25	39,46
1.0	1.0	0.55	26	29	31	52,59
5.4	4.9	0.45	24	25	25	40,48
1.6	1.0	0.35	31	34	36	52,59
1.3	0.8	0.30	44	36	32	43,51
10	5.2	0.20	27	28	28	39,46
3.0	1.1	0.20	38	41	44	55,62
5.4	1.1	0.10	44	41	40	43,51
11	4.8	0.10	26	22	19	17,25
10	1.1	0.05	44	46	46	43,51
200	20.4	0.04		25	25	27,34
200	7.2	0.04		109	95	89,96
700	27.7	0.02		43	30	30,38
200	4.8	0.01		44	47	47,53

[a] X-ray area of Pt divided by area of block carbon.
[b] Values are omitted where charge consumption of the carbon support (Table I) is greater than 50% of the total.
[c] The two areas listed are from the calculation methods of Jones (7) and Warren (7), respectively.

of the platinized-carbon electrodes causes major reductions in the absolute values of the carbon charge consumptions in the oxygen and hydrogen arrests. However, their ratio, r, should not be appreciably affected.

Results

The platinum areas of carbon-supported platinum electrodes were measured for a variety of carbon supports and platinum loadings. Table II compares the results for carbons having areas from 0.4 to 700 m^2/g and for platinum loadings from 1 to 28%. The reproducibility of these measurements was about 10% for the oxygen-arrest method and the hydrogen-arrest method, as long as the charge consumption on the carbon supports did not exceed 25% of the total charge consumed in the arrest. The combination method (Eq. [6]) gave a reproducibility of 10% or better for all of the electrodes.

If numerator and denominator of Eq. [3] are each divided by $Q_{T,O}$, the total charge in the oxygen arrest, we see that the uncertainty in the platinum area increases in proportion to $P/(100-P)$, where $P = 100Q_{C,O}/Q_{T,O}$ is taken from Table I. Thus when the percentage of the charge consumed on the support is 75%, the error is three times as large as when this consumption is 50%.

Expressions for the charge consumed on the supports in carbon-supported platinum electrodes can be derived from Eq. [1], [2], and [5], *i.e.*

$$\frac{Q_{C,O}}{Q_{T,O}} = r\left(1 - \frac{k_O}{k_H}\frac{Q_{T,H}}{Q_{T,O}}\; r - \frac{k_O}{k_H}\right)$$

$$\frac{Q_{C,H}}{Q_{T,H}} = \left(\frac{Q_{T,O}}{Q_{T,H}} - \frac{k_O}{k_H}\; r - \frac{k_O}{k_H}\right)$$

Calculated fractions of total charge consumption due to carbon are listed in Table I.

The platinum areas in the last column of Table II were obtained from crystallite sizes measured by x-ray diffraction. The average crystallite sizes derived from x-ray spectra depend on the calculation method because assumptions about particle size distribution differ. The two areas listed are from crystallite sizes calculated by the method of Jones (7) and Warren's method (7), respectively. The model for calculating platinum areas from crystallite sizes was that of cubes with one face obscured by contact with the support surface.

Figure 3 compares the electrochemical platinum area values, obtained by combining the oxygen and hydrogen arrests (Eq. [6]), with the averaged x-ray results. The agreement between the electrochemical and x-ray surface areas gets progressively better, as evidenced by the x-ray to electrochemical area ratio approaching 1, as the platinum to carbon area ratio decreases. After the latter ratio reaches 0.10 the agreement stays within experimental error.[2] This behavior suggests that the crystallites are crowded at high platinum to carbon area ratios (at least in the case of the preparation methods used here) and hence much of the platinum surface does not contact the solution. Thus, while the x-ray method sometimes gives areas which are "truer" they are not always "available."

Conclusion

Carbon-supported platinum surface area measurements, using a combination of the arrests due to adsorbed oxygen reduction and adsorbed hydrogen oxidation, are feasible at least down to a platinum to carbon area ratio of 0.01, and are much more accurate than values obtained from either method alone. When the charge consumption on the carbon support is very small, one method is sufficient, adsorbed oxygen reduction probably being more reliable.

Comparison of the electrochemical method with x-rays shows good agreement for high area carbons, but when platinum is crowded onto a low area support agreement with x-rays is poor; probably because much of the platinum area is inaccessible to wetting. In the latter case, the electrochemical area measurement is to be preferred for predicting the performance of fuel cell electrodes.

Acknowledgments

The authors thank B. L. Meyers for making the x-ray measurements and R. F. Waters for platinizing the electrodes.

Manuscript received Feb. 7, 1966.

Any discussion of this paper will appear in a Discussion Section to be published in the December 1966 JOURNAL.

REFERENCES

1. R. J. Brodd and N. Hackerman, *This Journal*, **104**, 704 (1957).
2. B. E. Conway, "Electrode Processes," p. 105, Ronald Press, New York (1965).
3. H. A. Laitinen and C. G. Enke, *This Journal*, **107**, 773 (1960).
4. F. G. Will, *ibid.*, **112**, 451 (1965).
5. A. J. Robell, E. V. Ballou, and M. Boudart, *J. Phys. Chem.*, **68**, 2748 (1964).
6. J. S. Mayell and S. H. Langer, *This Journal*, **111**, 438 (1964).
7. H. P. Klug and L. E. Alexander, "X-ray Diffraction Procedures," p. 506, John Wiley & Sons, Inc., New York (1954).
8. R. G. Haldeman, W. P. Colman, S. H. Langer, and W. A. Barber, "Fuel Cell Systems," p. 106, American Chemical Society, Washington, D. C. (1965).

[2] In view of the arbitrary assumptions made in obtaining crystallite sizes and then in choosing a model to calculate areas, the consistency deserves more note than the absolute agreement.

The Electrochemical Reduction of Oxygen on Electrodes Partially Immersed in Phosphoric Acid

R. J. Roethlein and H. J. R. Maget

Direct Energy Conversion Operation, General Electric Company, Lynn, Massachusetts

ABSTRACT

Diffusion-controlled currents for the reduction of oxygen in phosphoric acid for partially immersed electrode structures which have an intrinsic meniscus and thin film extending over their surface can be predicted from a general rate equation. For platinum black electrodes, and temperatures ranging from 25° to 170°C, the limiting current varies linearly with the square root of electrolyte conductivity, electrode polarization, and oxygen partial pressure. The increased current obtained on partially immersed electrodes has been shown to be associated with a very narrow region starting approximately 0.28 cm (the height of the meniscus) above the bulk of the electrolyte solution. Approximate calculations of the activation energy of diffusion using parameters from the rate equation give values which are close to those expected for a diffusional process. Good agreement is obtained between theoretical and experimentally determined values of the limiting current at 25°C. Equations have been derived to describe the interfacial liquid-gas geometry of the intrinsic meniscus and film formed by contact of the electrolyte with the electrode.

The purpose of this work was the development of an analytical model needed to interpret the behavior of oxygen (air) electrodes operating at high temperatures (less than about 170°C), in concentrated phosphoric acid [greater than 85 w/o (weight per cent)]. Since practical electrode structures frequently display rather complex interfacial geometries and geometric characteristics, investigations of transport phenomena were carried out on a simplified model of an oxygen cathode, *i.e.*, a single pore.

The reported experimental work was conducted to determine the rate-controlling reactions associated with the electrochemical reduction of oxygen. Earlier work conducted in presence of sulfuric acid (1) had shown the importance of the liquid electrolyte film and electrode surface roughness on local and total currents observed on simulated single macropores. This paper presents some results obtained at higher temperatures.

Experimental

Apparatus.—The experiments were carried out in a Pyrex cell consisting of a large central compartment and two smaller sections separated from the main section by fine pore fritted glass disks. The middle compartment which served as the test electrode section also contained a thermometer well and a gas bubbler which was capable of keeping a steady gaseous flow over the electrolyte solution. One of the side compartments contained a platinum black mesh electrode which served as the counter electrode. The other section served as a reference cell and had a Luggin capillary extending into the main compartment. The reference consisted of two platinum black electrodes with a constant current of 1.0 ma flowing between them. The electrode which evolved hydrogen gas came to a steady overpotential within a few minutes; this then served as the reference potential.

The test electrode consisted of a cylindrical piece of platinum tubing (99.99%) pure, 1.0 cm long, 1.5 cm in diameter, and 0.2 cm in wall thickness. The electrode assembly was essentially the same as that described in a previous paper (1) except that only one cylindrical section was employed as the test electrode. A modified 10/30 Teflon gland provided a closed system and still enabled the electrode structure to be raised or lowered into solution without allowing the system to be open to the atmosphere. Measurements of electrode height above the solution were made by means of a specially modified L. S. Starret Vernier height gauge with an accuracy of $\pm$ 1.2 x 10^{-3} cm.

The height and shape of meniscus and film were determined by electrical methods. The resistance measurements were obtained by means of a semicircular platinum foil 1.0 cm in diameter and 1.27 x 10^{-2} cm thick, sealed between two cylindrical glass tubes and finely polished to form a continuous smooth surface. Electrical contact was made by spot-welding a platinum wire to the foil inside the glass cylinder. The Starret Vernier height gauge could raise or lower the glass tube into the electrolyte. Resistance measurements were obtained by means of an a-c resistance bridge operating at 1000 cps.

The electrode surface was pretreated by electrodeposition of platinum from a 3 w/o chloroplatinic acid solution (with traces of lead acetate) at 10 ma/cm^2 for 12, 60, and 240 sec.

Procedure.—Polarization measurements were made with a "fast rise" Wenking potentiostat (Model 61 TR) which has an operating potential source of $\pm$ 2v, a current measurement accuracy of 1.5% full scale, and a zero point stability of 5 mv/day. All gases used in these experiments were of a high grade prepurified quality. A silicone oil constant temperature bath maintained the desired study temperature within $\pm$ 1°C.

All reactant gases were preheated and humidified by passing through a gas bubbler which contained electrolyte at the same temperatures and concentration as that in the test cell.

The various phosphoric acid concentrations used in these experiments were prepared from C.P. Reagent Grade stock solution using doubly distilled water containing less than 0.4 ppm impurities.

Experimental Results and Discussion

Interfacial liquid-gas geometry.—Resistance measurements can be used to determine the liquid-gas interfacial geometry at the meniscus-film boundary. Figure 1 presents a plot of ohmic resistance divided by the electrolyte resistivity *vs.* x/h, the relative position in the meniscus (h = total intrinsic meniscus height, x = variable distance above the electrolyte level). Only a gradual resistance increase with height is observed in the meniscus region. However, on entering the thin film region, the resistance increases rapidly. The slope of this linear increase can be used to calculate the electrolyte film thickness.

The interfacial liquid-gas geometry of the intrinsic meniscus and film can be approximated by the expression

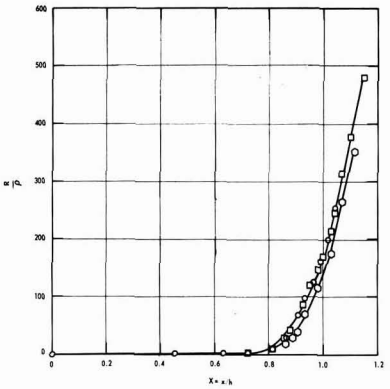

Fig. 1. Normalized ohmic resistance *vs.* relative position in the meniscus. *R*, measured resistance; *ρ*, electrolyte resistance; *x*, height above electrolyte level; *h*, height of meniscus, 0.28 cm; □, ○, 95.8 w/o H_3PO_4, 130°C; ○, 96.5 w/o H_3PO_4, 140°C.

$$\delta = \delta_h + A(1-X)^2 \text{ for } X \leq 1 \qquad [1]$$

where δ = meniscus thickness, cm; δ_h = film thickness, cm; $X = x/h$ represents the relative position in the meniscus; A can be theoretically evaluated from properties of the electrolyte, as presented by Landau and Lifshitz (2). However, since the surface tension of phosphoric acid at these temperatures is not known, it is better to evaluate A from resistance measurements.

It can be shown (1) that, near the meniscus-film interface, the ionic resistance is expressed by

$$R(x) = \frac{\rho h}{2b\pi} \frac{1}{(A\,\delta_h)^{1/2}} \left\{ \frac{\pi}{2} - \tan^{-1}\left(\frac{A}{\delta_h}\right)^{1/2}(1-X) \right\} \qquad [2]$$

where ρ = electrolyte resistivity, ohm-cm and b = electrode radius, cm. The film thickness δ_h can be determined from the slope of the linear section of the resistance plot

$$\left(\frac{dR}{dX}\right)_f = \frac{\rho h}{2\pi b\,\delta_h} \qquad [3]$$

The constant (A) can be evaluated from the total meniscus resistance, R_m at $X = 1$, for which

$$R_m = \frac{\rho h}{4b(A\,\delta_h)^{1/2}} \qquad [4]$$

For the experimental results presented in Fig. 1, the film thickness is calculated to be 0.5μ. The resistance can be represented by

$$R = 253\left\{ \frac{\pi}{2} - \tan^{-1} 16\,(1-X) \right\} \qquad [5]$$

and the meniscus-film geometry by

$$\delta = [0.5 + 130\,(1-X)^2]\,10^{-4} \qquad [6]$$

for values of $X \geq 0.9$, *i.e.*, at a level in the meniscus and film where the largest contribution to the total current is observed.

Current-potential behavior.—Current voltage curves taken on platinum black electrodes at elevated temperatures for the reduction of oxygen in phosphoric acid are similar to those obtained at lower temperatures in sulfuric acid (1). Raising the electrode out of solution causes an increase in current up to a maximum value obtained when the full meniscus and film are formed on the electrode surface. This behavior is represented in Fig. 2. For overvoltages greater than

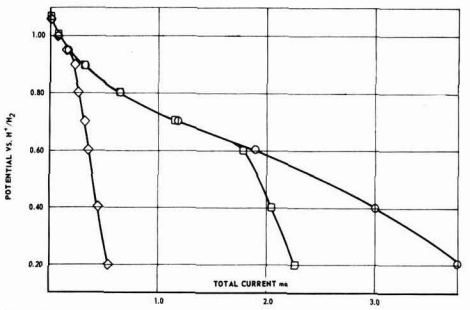

Fig. 2. Current-potential behavior as a function of electrode position. 97.8 w/o H_3PO_4, 150°C, pure O_2. Electrode position: ○, full meniscus and film; □, partial meniscus; ◇, submerged.

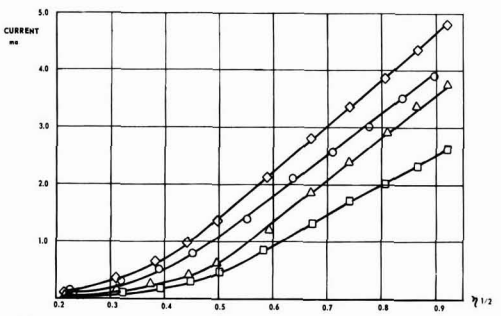

Fig. 3. Total current *vs.* square root of electrode polarization

	w/o H_3PO_4	Temp, °C	Deposition time, sec.
○	93.7	144	12
□	93.7	115	12
◇	92.6	144	240
△	97.8	144	60

about 0.25v (*vs.* electrode rest potential) *i.e.*, at potentials outside the region of activation overvoltage, the current follows a square-root relationship with overvoltage. This experimental result is presented in Fig. 3 for various electrolyte concentrations, temperatures, and surface roughnesses.

The variation of the current with position, above the electrolyte level, obtained at constant potential is also similar to that observed in sulfuric acid. The electrode current rises sharply in a narrow region which coincides with the boundary between upper meniscus and thin film which are formed on the electrode surface above the level of the bulk electrolyte. Figure 4 represents a typical variation of the current

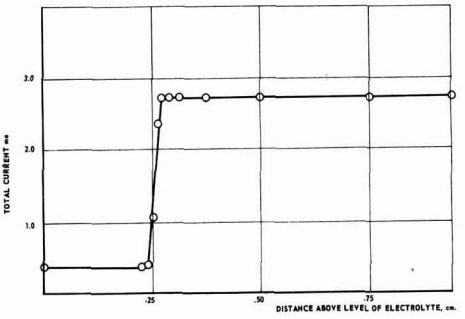

Fig. 4. Current *vs.* height behavior of a platinum black electrode at a constant potential of +0.400v *vs.* H^+/H_2. 93.7 w/o H_3PO_4, 150°C, pure O_2.

Table I. Dependence of electrode current on oxygen partial pressure (total pressure: 1 atm)

Partial pressure of oxygen, P_{O_2}, atm	Total current, i_L ma	$i_L/P_{O_2}^{1/2}$	Electrolyte concentration, w/o	Temp, °C
1.00	2.95	2.95	97.8	144
0.50*	2.05	2.90	97.8	144
0.21*	1.30	2.84	97.8	144
1.00	1.85	1.85	100	120
0.50	1.20	1.70	100	120
0.21	0.84	1.88	100	120
1.00	3.20	3.20	51.1	25
0.50	2.30	3.25	51.1	25
0.21	1.50	3.28	51.1	25
1.00	0.35	0.35	92.5	25
0.50	0.25	0.36	92.5	25
0.21	0.16	0.35	92.5	25

* All data obtained for binary mixtures O_2-N_2.

with electrode position; the height of the meniscus is approximately 0.28 cm (identical to the value observed in 1*N* and 10*N* H_2SO_4). Further withdrawal of the electrode from the electrolyte does not produce additional variations in current once the full meniscus and film have been formed.

On a partially immersed platinum black electrode the limiting current shows a linear variation with the square-root of the oxygen partial pressure. This relationship is valid for varying concentrations of H_3PO_4 (5-100 w/o) and over the complete temperature range of this study, *i.e.*, 25°-170°C. Characteristic values are reported in Table I.

Relationship between limiting current and conductivity.—Extensive studies were conducted to determine the current on partially immersed platinum black electrodes in the high phosphoric acid concentration range, from 80 to 100 w/o. It was found that the currents obtained at a constant potential of 0.400v *vs.* H^+/H_2 varied in a monotonic manner with the square root of the conductivity, Fig. 5. Two slopes were obtained: one in the low conductivity region which extrapolates to zero, as expected, and another in the higher conductivity range where the linear dependence is mantained over a large conductivity range from 0.36 to 0.64 $(\text{ohm-cm})^{-1}$. Since the conductivity varies nearly linearly with temperature (3), it is not possible to explain the monotonic variation of the current, as presented in Fig. 5, on the basis of abrupt variations in conductivity in the temperature range between 110° and 170°C. (The measured currents were divided by the square root of the oxygen partial pressure to correct for water vapor pressure above the electrolyte since under experimental conditions the vapor pressure of water could be as high as 410 mm Hg.) Experimental results are presented in Fig. 5 as a function of the square root of electrolyte conductivity, since the correlation of the result was based on the assumption that currents on partially immersed electrodes can be predicted from the following general equation (4, 5) derived for hydrogen oxidation

$$i_L = \pi D\,(n\mathbf{F}C\mathcal{D}\mathcal{H}\eta)^{1/2} \qquad [7]$$

where D = diameter of the cylinder, 1.5 cm; n = number of electrons; $\mathbf{F}$ = Faraday's constant; $\mathcal{H}$ = electrolyte conductivity $(\text{ohm-cm})^{-1}$; C = concentration of oxygen in phosphoric acid, mole/cm^3; $\mathcal{D}$ = diffusion coefficient, cm^2/sec.; η = polarization from open circuit, volts. Verification of the above equation will be shown for a region where limited values for solubilities and diffusion coefficients are either available or can be reasonably estimated.

A possible explanation for the increased slope at higher electrolyte conductivities and temperatures may be based on the change of oxygen solubility and diffusion coefficient in phosphoric acid at elevated temperatures. The combination of these parameters plays an important role in determining the limiting current.

The dependence of current on conductivity was further verified by adding $NaH_2PO_4 \cdot H_2O$ to a H_3PO_4 solution in order to decrease the electrolyte conductivity. [400g of $NaH_2PO_4 \cdot H_2O$ added to a liter of 85% H_3PO_4 yielded a conductivity of 0.33 $(\text{ohm-cm})^{-1}$ at 130°C as compared to 0.49 $(\text{ohm-cm})^{-1}$ for a salt-free identical acid concentration.] The current obtained from the lowered conductivity fell within the predicted value for the current at this conductivity (see Fig. 5).

Variation of electrode surface roughness did show some effect on current behavior. Platinum black was electrodeposited on the cylindrical electrode for 12, 60, and 240 sec at 10 ma/cm^2. Several concentrations were investigated for each roughness, and the currents were observed to increase with increasing surface roughness. Variations, however, were not large, *i.e.*, a current increase of 30% was observed for the highest as compared to the lowest surface roughness.

Current-temperature relationship.—Temperature effects on the currents, measured at 0.4v *vs.* H^+/H_2, are appreciable, as can be observed from Fig. 6 for various electrolyte concentrations, once corrected for oxygen partial pressure and electrolyte conductivity.

Since the conductivity does not vary appreciably with temperature for concentrated solutions (3), the slopes of $i_L/(\mathcal{H}P_{O_2})^{1/2}$ *vs.* 1/T, at constant potential, represent the contribution of solubility and diffusivity to an activation energy. Solubility measurements reported in the literature (6, 8) for high concentrations

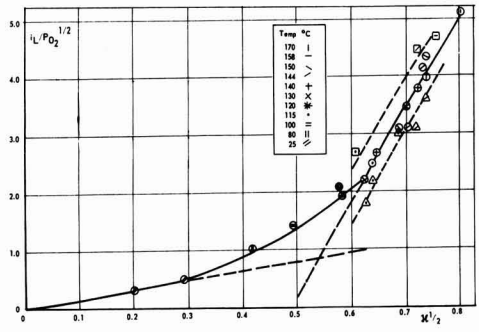

Fig. 5. $i_L/P_{O_2}^{1/2}$ *vs.* $\mathcal{H}^{1/2}$ for the reduction of O_2 in concentrated H_3PO_4 solutions from 25° to 170°C. Deposition time at 10 ma/cm^2: □, 240 sec; ○, 60 sec; △, 12 sec; •, addition of $NaH_2PO_4 \cdot H_2O$.

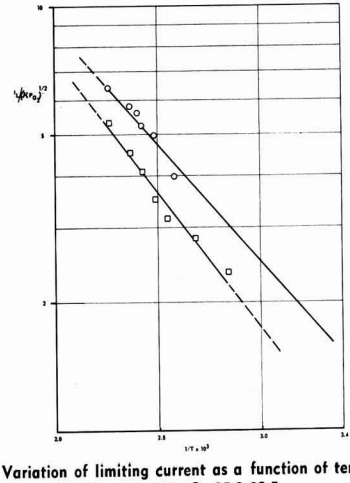

Fig. 6. Variation of limiting current as a function of temperature. Weight per cent H_3PO_4: □, 100; ○, 85.8-92.5.

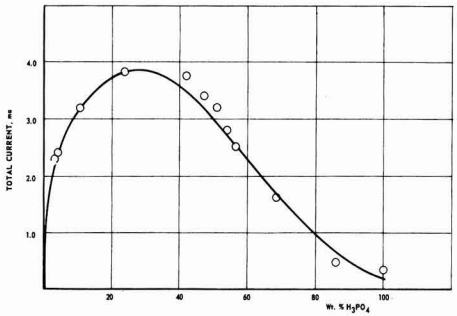

Fig. 7. Values of the limiting current on a partially immersed platinum black electrode for O_2 reduction in various concentrations of H_3PO_4 at 25°C; ———, calculated from equation $i_L = \pi D \{nFC\mathcal{D}\ \mathcal{H}\eta\}^{1/2}$; ○, experimental points.

of H_3PO_4 between 25° and 170°C allow one to estimate a heat of dissolution of 1 kcal/mole. The slopes of Fig. 6, once corrected for this heat of dissolution, yield activation energies of 4.1 and 4.3 kcal/mole, which are within the range of values expected for diffusion-controlled processes.

Variation of limiting current with phosphoric acid concentration.—Currents for the reduction of oxygen on a partially immersed platinum black electrode were obtained potentiostatically at an applied potential of 0.400v *vs.* H^+/H_2 as a function of phosphoric acid concentration at 25°C. Results plotted in Fig. 7 show good agreement with the theoretical values calculated from the general equation assuming a mass transport-controlled process on a partially immersed electrode displaying a full meniscus and thin film on its extended surface, Eq. [7]. Data for the electrolyte conductivity and oxygen solubility is available in the literature (3, 6, 8). Since no data are available for the diffusion coefficient of oxygen in phosphoric acid at 25°C values were estimated from the equation of Wilke and Chang (7). Table II presents the values for the conductivity, oxygen solubility, and diffusivity in phosphoric acid at 25°C as a function of acid concentration, used to calculate the current reported in Fig. 7.

Lack of data concerning the diffusivity of oxygen in concentrated phosphoric acid does not allow to prove the application of Eq. [7] to currents measured at higher temperatures. However, on the assumption that Eq. [7] is applicable, it is possible from available data on oxygen solubility, electrolyte conductivity, and measured limiting currents to estimate diffusion coefficients. From the computed values presented in Fig. 8 for the temperature range from 25° to 170°C good agreement is obtained between the calculated values and two experimental results measured in 85.5 w/o H_3PO_4 (8). These results suggest that this method may be used to determine rapidly the product of solubility and diffusivity.

Conclusions

The electrochemical reduction of oxygen on partially immersed platinum black electrodes in phosphoric acid, from room temperature to 170°C, occurs mainly

Table II. Variation of electrolyte conductivity, oxygen solubility, and diffusivity for various phosphoric acid concentrations at 25°C

H_3PO_4 w/o	Conductivity (ohm-cm)$^{-1}$	Solubility moles/cm^3 × 10^6	Diffusion coefficient cm^2/sec × 10^5
0	—	1.26	2.60
5	0.040	1.18	2.42
10	0.070	1.10	2.20
20	0.123	0.96	2.00
40	0.222	0.73	1.40
60	0.213	0.52	0.87
80	0.117	0.32	0.42
100	0.030	0.13	0.10

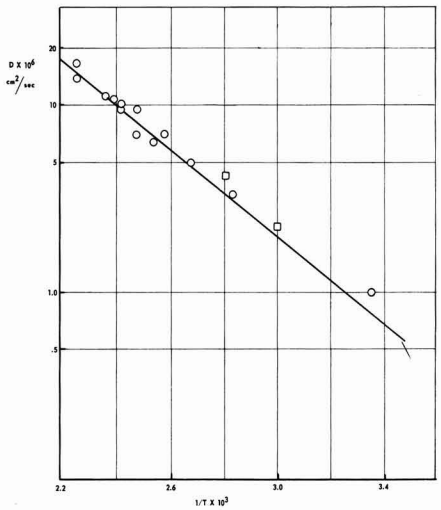

Fig. 8. Variation of O_2 diffusion coefficient in concentrated phosphoric acid as a function of temperature: ○, calculated; □, measured.

in the upper meniscus and thin film region of the electrode surface. This was shown by the increased current associated with the gradual withdrawal of a submerged electrode, potentiostatically polarized, into a condition of partial immersion. The height of the meniscus in phosphoric acid even at elevated temperatures is the same as that found for sulfuric acid at room temperature, *i.e.*, approximately 0.28 cm.

Using a general equation which describes diffusion-controlled limiting currents for an electrode having a meniscus and film, good agreement has been obtained between the observed currents and those predicted from the equation over the entire concentration range of phosphoric acid at 25°C. For higher temperatures, results obtained show that the limiting currents also depend on the square root of electrolyte conductivity, polarization, and oxygen partial pressure. In addition, diffusion coefficients obtained by the use of this equation show good agreement with experimentally measured values of this parameter. This suggests that this general equation is also applicable to temperatures up to 170°C.

Further proof of the validity of this equation is exemplified by the approximate values obtained for the activation energy of diffusion for two different acid concentrations. The values obtained are in the approximate range of energies associated with diffusional processes. This same equation may be able to predict currents at other temperatures once sufficient data are obtained for oxygen solubility and diffusivity in phosphoric acid.

From the resistance measurements, equations have been derived to describe the interfacial liquid-gas geometry of the intrinsic meniscus and film formed by contact of the electrolyte with the electrode. These measurements have also provided an approximate value of the film thickness immediately above the intrinsic meniscus, 0.5μ.

Manuscript received Aug. 2, 1965; revised manuscript received Feb. 21, 1966. This paper was presented at the San Francisco Meeting, May 9-13, 1965.

Any discussion of this paper will appear in a Discussion Section to be published in the December 1966 JOURNAL.

REFERENCES

1. H. J. R. Maget and R. J. Roethlein, *This Journal*, **112**, 1034 (1965).

2. L. D. Landau and E. M. Lifshitz, "Fluid Mechanics," p. 235, Pergamon Press, New York (1959).
3. Monsanto, Phosphoric Acid, Technical Bulletin 1-239. Also D. Macdonald, Technical Summary Report No. 4, Dec. 1963; Contract Da-44-00-ENG-4909, USERDL, Ft. Belvoir, Va.
4. F. Will, *This Journal*, **110**, 145 (1963).
5. Carl Wagner, Unpublished results.
6. D. Macdonald, Technical Summary Report No. 6, 1 July '64-31 Dec. '64, Contract DA-44-009-ENG-4909, USERDL, Ft. Belvoir, Va.
7. Reid and Sherwood, "The Properties of Gases and Liquids," McGraw Publishing Co., New York.
8. K. E. Gubbins and R. D. Walker, Solubility and Diffusivity of Hydrocarbons and Oxygen in Fuel Cell Electrolytes, Contract No. DA-49-186-AMC-45(X), Harry Diamond Laboratories, Final Report, June 30, 1965.

The Electrochemical Oxidation of Ethylene

Comparison of Results by the Potential Sweep and Steady-State Methods

E. Gileadi,[1] G. Stoner, and J. O'M. Bockris

Electrochemistry Laboratory, John Harrison Laboratory of Chemistry,

University of Pennsylvania, Philadelphia, Pennsylvania

ABSTRACT

The electrochemical oxidation of ethylene on platinum electrodes in 1*N* sulfuric acid at 80°C was studied by the potential sweep method over a wide range of sweep rates (10^{-5} — 2 v/sec). The results were compared with those obtained previously under steady-state conditions. Over three decades of sweep rate (2×10^{-3} — 2 v/sec) an apparent Tafel slope of approximately $2.3 \times 3\ RT/\mathbf{F}$ was observed. This was shown to be consistent with the behavior for a totally irreversible diffusion-controlled reaction. In the same region the peak potential V_M was found to shift 65 mv/decade increase in sweep rate and the peak current i_M was proportional to the square root of the sweep rate with a proportionality constant in agreement with the calculated value.

It is shown that the application of the potential sweep may change the mechanism of the process taking place (in the present case the change is from activation control in steady state to diffusion control during potential sweep). During potential sweep a totally irreversible, diffusion-controlled reaction will give rise to a linear Tafel plot with a slope about 35% higher than the mechanistically significant slope of $2.3\ RT/\alpha\mathbf{F}$. Further, an apparent passivation region can be observed, due to depletion of the solution near the electrolyte from reactant molecules and quite independent of the nature of the electrode surface. During potential sweep measurements the partial coverages θ by various species on the surface cannot reach their steady-state value. The kinetic parameters derived from such measurement, therefore, cannot be used to represent the results under steady-state conditions, unless the sweep rate is made sufficiently slow to correspond in practice to steady state.

The anodic oxidation of ethylene on platinum electrodes in 1*N* H_2SO_4 at 80°C has been studied recently (1). From the kinetic parameters obtained under steady-state condition a mechanism has been suggested, with water discharge as the rate-determining step, preceded by equilibrium adsorption of ethylene (1). This mechanism was further confirmed by a comparative study of the electrochemical oxidation of a number of unsaturated hydrocarbons under identical conditions (2) and by recent tracer studies (3). Independent electrosorption measurements for ethylene (4) and benzene (5) in the same system by a radiotracer technique yielded further support for the above mechanism. Thus, for the rate-determining step

$$H_2O \rightarrow OH_{ads} + H^+ + e \qquad [1]$$

the rate equation was given as

$$i = i_o\,(1 - \theta)\,\exp\,(\beta V\mathbf{F}/RT) \qquad [2]$$

where θ represent the total surface coverage which in the linear Tafel region (0.4 — 0.8v RHE) is essentially equal to the coverage by unreacted adsorbed organic molecules. Under the conditions studied [*i.e.*, with ethylene bubbled through the solution or with liquid benzene at equilibrium with the solution (1, 2)] the surface coverage by organic is in the saturation region (4, 5), and hence θ may be considered independent of potential, giving rise to

$$b = \left(\frac{\partial V}{\partial \log i}\right)_{T,C_i} = \frac{2.3\ RT}{\beta\mathbf{F}} \sim 2.3 \times (2RT/\mathbf{F}) \qquad [3]$$

[1] Present address: Chemistry Department, Tel-Aviv University, Tel-Aviv, Israel.

The negative reaction order observed is also consistent with the adsorption data for this mechanism since, while θ remains essentially constant in the saturation region, the term $(1 - \theta)$ can vary substantially and give rise to a decreased reaction rate with increasing bulk concentration of the organic.

Most recent studies of electrochemical oxidation of potential fuels have relied on nonsteady-state techniques, in particular the potential sweep method (6, 7) and cyclic voltametry (8). The results of such measurements have not usually been interpreted in terms of a molecular mechanism.

In the present work the electrochemical oxidation of ethylene on bright and platinized platinum electrodes in 1*N* H_2SO_4 at 80°C was studied as a function of sweep rate over a wide range (1×10^{-5} — 2v/sec). The results obtained in this manner are compared with previous results of steady-state measurements in the same system, and the limitations of the application of potential sweep techniques for the study of the kinetics of complex electrode reactions are brought out. The potential sweep technique has been applied previously to the oxidation of ethylene on rotating disk platinum electrodes (9), but the effect of sweep rate has not been considered.

Experimental

Cell, electrodes, and solution.—A standard three-compartment all-glass cell was employed with glass frits separating the compartments. A bright platinum wire of 1 cm^2 served as working electrode and was treated anodically and cathodically as described pre-

viously (1). For lower sweep rates a 50 cm^2 planar bright platinum electrode was used, and for comparison a small 1 cm^2 planar platinized Pt electrode was employed. A Hg/Hg_2SO_4 reference electrode in the same solution was used and a large platinized platinum gauze served as the counter electrode.

Solutions were made up from Baker Analyzed sulfuric acid in distilled water. C. P. grade ethylene (99.5% purity) and prepurified nitrogen (99.996% purity) were employed.

Electrical circuit.—The potential between the working and reference electrode was controlled by a Wenking potentiostat, and the current between the working and counter electrode was recorded on a Moseley "Autograph" recorder model 680 in parallel with a variable shunt resistance. For slow potental sweeps the reference potential fed into the potentiostat was varied with motor drive potentiometers connected to a battery. For faster sweep rates a transistorized triangular sweep generator constructed in this laboratory was employed (10), which could supply a symmetrical triangular wave form with sweep rates in the range of 10^{-3} — 10^3 v/sec. During measurements at higher sweep rates the current was recorded as a function of potential on a Tektronix model 564 memory oscilloscope used as an X — Y recorder (with the time base replaced by a differential amplifier type 2A63 plug-in unit). The oscillographic traces were photographed with a model C-12 oscilloscope poloroid camera.

Procedure.—Electrodes prepared in the manner described elsewhere (1) were introduced into the sulfuric acid solution, and prepurified nitrogen was bubbled through until the rest potential of approximately 0.25v NHE was reached. Ethylene was then introduced into the cell, and sufficient time was allowed for adsorption equilibrium at this potential to be reached (15-30 min). All data reported here refer to a single anodic sweep. Good reproducibility between different runs in the same solution and runs on different days in different solutions was obtained.

Results

Current-potential relationship.—The current-potential relationships obtained at three sweep rates are represented in Fig. 1 as a plot of current density *vs.* potential. The same results are shown in semilogarithmic form in Fig. 2 as V *vs.* log i. The variation of b, the apparent Tafel slope observed experimentally with sweep rate, is shown in Fig. 3. A constant value of $b = 2.3 \times (3\ RT/\mathbf{F})$ is observed for sweep rates of 2×10^{-3} up to 2 v/sec. The steady-state value of $b = 2.3 \times (2\ RT/\mathbf{F})$ is approached only at very slow sweep rates of the order of 10^{-5} v/sec.

Peak current and potential.—Figure 4 shows a plot of the peak current i_M as a function of the sweep rate v on a log-log scale. A linear plot results for sweep rates above a few mv/sec, with a slope of approximately 0.5. At lower sweep rates the peak currents are much smaller and depend only to a very small extent on sweep rate. Results obtained for a platinized Pt electrode are shown for comparison.

The potential V_M at which the current reaches a maximum is plotted in Fig. 5 as a function of log v. A

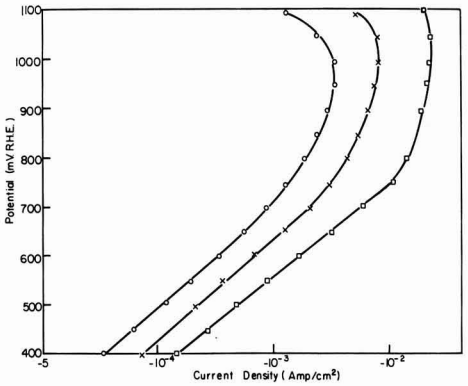

Fig. 2. Results of Fig. 1 plotted on a semilogarithmic scale

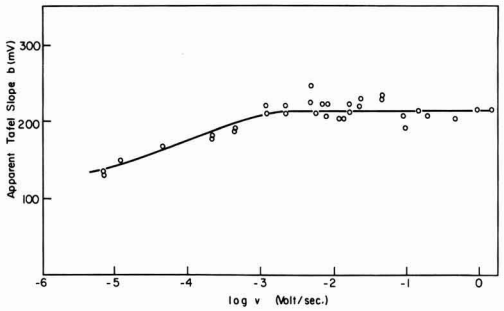

Fig. 3. Apparent Tafel slope $b = dV/d \log i$ as a function of log v

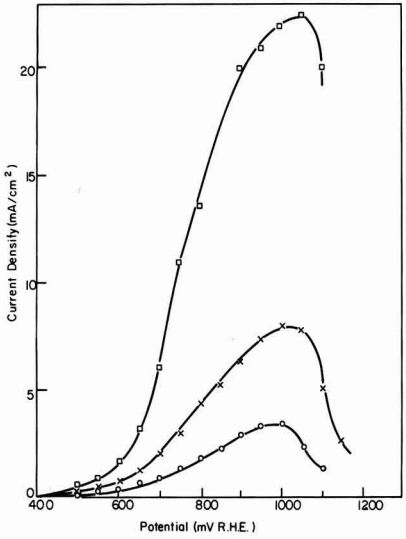

Fig. 1. Current density-potential plots at three sweep rates: □, 0.1 v/sec; X, 0.013 v/sec; ○, 0.0022 v/sec.

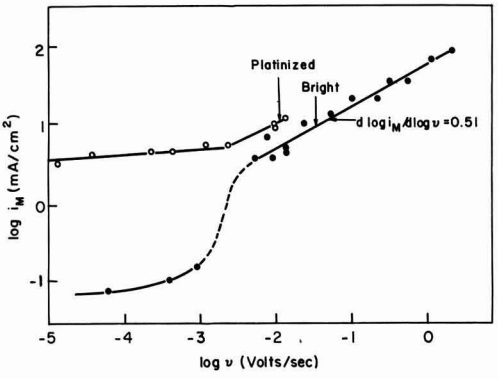

Fig. 4. Peak current density i_M as a function of sweep rate on a log-log scale; ○, platinized Pt; ●, bright Pt.

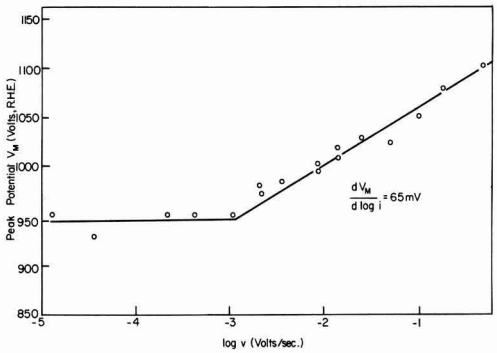

Fig. 5. Peak potential V_M as a function of log v

slope of $dV_M/d \log v \sim 2.3 \times (RT/\mathbf{F})$ is obtained for sweep rates higher than a few mv/sec. At lower sweep rates V_M is essentially independent of sweep rate and the same for bright and platinized electrodes. It should be noted that the break in the lines in Fig. 3, 4, and 5 occur at the same sweep rate, within experimental error.

Discussion

The peak current.—For a totally irreversible, diffusion-controlled reaction the current density during potential sweep has been shown (11, 12) to be given by an equation of the following form

$$i = \pi^{1/2} n\mathbf{F}\beta^{1/2} D^{1/2} C^o \chi(\beta t) \quad [4]$$

where (utilizing for this equation Delahay's symbol)

$$\beta = \frac{\alpha n_a \mathbf{F}}{RT} v \quad [5]$$

n and n_a are the number of electrons transferred in the over-all reaction and in the rate-determining step, respectively; α is the transfer coefficient, D the diffusion constant, C^o the bulk concentration of reactant, and $\chi(\beta t)$ is a complex function of (βt) which has been given numerically as a function of (βt). It is noted that during a linear potential sweep

$$V = V_i + vt \quad [6]$$

where V_i is the initial value of the potential at the $t = 0$. Hence from Eq. [5] and [6]

$$\beta t = \frac{\alpha n_a \mathbf{F}}{RT} (V - V_i) \quad [7]$$

and the function $\chi(\beta t)$ may be regarded as dependent on potential. The variation of $\chi(\beta t)$ with (βt) has been calculated by Delahay (11). In view of relationships [4] and [7] this also reflects the variation of the current density with potential.

At the peak potential $\chi(\beta t)$ has a value of 0.282. With $D = 1.7 \times 10^{-5}$ cm²/sec (9), $C^o = 2.2 \times 10^{-6}$ mole/cm³ (9), $n_a\alpha = 0.5$ and $n = 12$, Eq. [4] yields

$$i_M = 23v^{1/2} \text{ ma/cm}^2 \text{ (real area)} \quad [8]$$

The experimental relationship obtained from Fig. 4 is

$$i_M = 60\, v^{1/2} \text{ ma/cm}^2 \text{ (apparent area)} \quad [8a]$$

The discrepancy between calculated and observed results may be due in part to the uncertainty in the values of D and C^o used, and in part to departure from semi-infinite linear diffusion in the experimental set-up. Below a sweep rate of a few millivolts per second the peak current on bright platinum drops drastically to lower values corresponding to the activation-controlled process taking place at steady state with a much smaller dependence on sweep rate, which can probably be associated with the slow "time effects" observed in steady-state measurements. A comparison of results on bright and platinized Pt lends further support for the diffusion-controlled behavior postulated here for the higher sweep rate region. At low sweep rates the current density on platinized Pt is found to be about 40-50 times higher than on bright Pt. Taking a roughness factor of 2 for the bright surface this gives rise to a reasonable value of 80-100 for the roughness factor on the platinized surface. At higher sweep rates the line for platinized Pt parallels that for bright Pt, but the ratio of current densities is only approximately 2.0. For a diffusion-controlled process the current is determined largely by the apparent surface area. The slightly larger current densities observed on platinized Pt are probably due to surface irregularities of dimensions similar to or larger than the diffusion layer thickness.

Variation of peak potential with sweep rate.—The relationship between peak potential and sweep rate has been given by Delahay (11, 12) as

$$V_M = V_i + \frac{RT}{\alpha n_a \mathbf{F}}\left[0.77 - \ln(k/D^{1/2}) + \tfrac{1}{2}\ln\left(\frac{\alpha n_a \mathbf{F}}{RT} v\right)\right] \quad [9]$$

where k is the (potential dependent) specific rate constant at the potential V_i. Thus

$$\frac{\partial V_M}{\partial \log v} = \frac{2.3\ RT}{2\alpha n_a \mathbf{F}} = 2.3 \times (RT/\mathbf{F}) \text{ for } \alpha n_a = 0.5 \quad [10]$$

In Fig. 5 a slope of $\partial V_M/\partial \log v = 65$ mv is obtained, in agreement with Eq. [10] ($2.3 \times RT/\mathbf{F} = 70$ mv at 80°C).

It is important to note the fact that a peak in the $i - V$ relationship is obtained here for a diffusion-controlled reaction, independent of the state of the electrode surface. This may account for some of the apparent passivation regions which have been reported in studies of the anodic oxidation of organic fuels by the potential sweep method. The position of the peak depends, among other things, on the specific rate constant of the reaction studied, but not on the bulk concentration of reactant (cf. Eq. [9]). When stable intermediates are formed in the reaction sequence in concentrations not negligible with respect to the concentration of the reactants several "diffusion peaks" of this kind could be observed on the polarogram. This has already been pointed out by Delahay (12), but has apparently been disregarded in subsequent work.

Observed Tafel slope.—Figure 3 shows the variation of Tafel slope with sweep rate. The steady-state value of $2.3 \times 2\ RT/\mathbf{F}$ is only approached at very low sweep rates $V < 10^{-5}$ v/sec in this system. As the sweep rate is increased above 10^{-5} v/sec, the observed Tafel slope increases steadily toward a value of $2.3 \times 3\ RT/\mathbf{F}$. Above approximately 2×10^{-3} v/sec the Tafel slope remains constant independent of sweep rate over three decades of sweep rate up to $v = 2$ v/sec. The region of constant Tafel slope of $2.3 \times 3\ RT/\mathbf{F}$ coincides with the upper regions of Fig. 4 and 5 where $d \log i_M/d \log v = 0.5$ and $dV_M/d \log v = 2.3\ RT/\mathbf{F}$, respectively, corresponding to diffusion-controlled kinetics.

The existence of a linear Tafel region for a diffusion-controlled reaction is only due to the particular method of measurement (*i.e.*, the potential sweep method), and the observed slope of $2.3 \times 3\ RT/\mathbf{F}$ (which is not normally encountered in kinetic studies of activation controlled reactions) can be shown to be consistent with the water discharge mechanism postulated earlier as the rate-determining step under steady-state conditions.

Figure 6 gives a plot of (βt) *vs.* $\log \chi(\beta t)$ which was constructed from the plot of $\chi(\beta t)$ *vs.* (βt) given by Delahay (11, 12). From this plot one finds numerically

$$\partial(\beta t)/\partial \log \chi(\beta t) = 3.1 \quad [11]$$

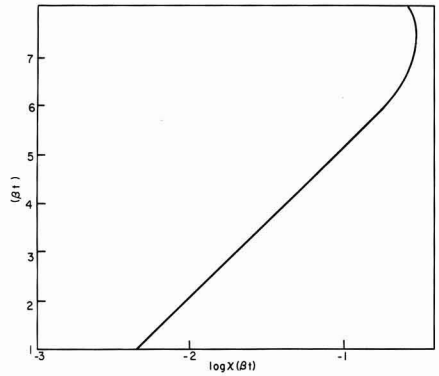

Fig. 6. (βt) plotted vs. the function log $\chi(\beta t)$

and

$$\frac{\partial V}{\partial \log i} = \frac{\partial V}{\partial \log \chi(\beta t)} \times \frac{\partial \log \chi(\beta t)}{\partial \log i} \quad [12]$$

From Eq. [4]

$$\partial \log \chi(\beta t)/\partial \log i = 1 \quad [13]$$

and from Eq. [7]

$$\partial V = \frac{RT}{\alpha n_a \mathbf{F}} \partial(\beta t) \quad [14]$$

Combining Eq. [12]-[14] one has

$$\frac{\partial V}{\partial \log i} = \frac{RT}{\alpha n_a \mathbf{F}} \frac{\partial(\beta t)}{\partial \log \chi(\beta t)} = \frac{3.1\,RT}{\alpha n_a \mathbf{F}}$$

$$= \left(\frac{3.1}{2.3}\right) \times \frac{2.3\,RT}{\alpha n_a \mathbf{F}} \quad [15]$$

Thus a linear Tafel relation with a slope 35% higher than the mechanistically significant slope of 2.3 $RT/\alpha n_a \mathbf{F}$ can result due to diffusion control during the potential sweep. In the case studied here, the observed Tafel slope of b = 210 mv is consistent (at 80°C) with the above interpretation if αn_a = 0.45. This is in agreement with the steady-state value of α = 0.46-0.50 reported for this system.

Limitations of the potential sweep method.—The mechanism of the anodic oxidation of ethylene on Pt electrodes has been established previously on the basis of kinetic parameters obtained under steady-state conditions (1), as discussed in the introduction. The critical question to be answered here is what type of mechanistic information could have been derived from the potential sweep data presented in this paper alone. The answer to this question will then bear relevance to the limited applicability of the slow potential sweep technique for the study of mechanisms of anodic oxidation of organic fuels. Typical sweep rates used by various authors for mechanistic studies are in the range of 10-100 mv/sec (*e.g.*, Griffith and Rhodes (9) used v = 26 mv/sec, Breiter (6) used v = 35 mv/sec), and thus the behavior observed here in the upper sweep rate region (2 x 10^{-3} — 2 v/sec) will be discussed below.

As has been shown above, the relationship between peak current, peak potential, and sweep rate satisfies Eq. [4] and [9] which have been derived (11, 12) for a totally irreversible diffusion-controlled reaction. This should be contrasted with the activation-controlled kinetics established at steady state. Further, a positive pressure effect is observed during the sweep measurement while at steady-state negative reaction orders were observed for ethylene (1) and several other unsaturated hydrocarbons (2). Thus, the results of potential sweep measurements would indicate that the reaction is diffusion controlled. This, however, will have little effect on the operation of a fuel cell, the characteristics of which will be determined by the steady-state activation-controlled kinetics.

The transition from activation control at steady state to diffusion control during the transient is unusual and arises due to the time dependence of the partial coverage θ during the transient. It will be remembered that the steady-state current is proportional to the term $(1 - \theta)$ (Eq. [2]). Also direct adsorption measurements show (4) that θ must be very high and $(1 - \theta)$ is probably of the order of 10^{-2} or less. During the potential sweep transient the reactant at and near the electrode is used up and θ decreases. Under these conditions the water discharge step can occur a hundred times or more faster and, it is no longer rate limiting for the over-all process.

The observed Tafel slope can be discussed next. If measurements at a single sweep rate were performed, any slope between 2.3 x 2 $RT/\mathbf{F}$ and 2.3 x 3 $RT/\mathbf{F}$ could be obtained, depending on the sweep rate chosen. The observation that the Tafel slope is independent of sweep rate over a wide range is no indication that it is also equal to the value which would be obtained at steady state, as shown above. If it is established that the system is a totally irreversible, diffusion-controlled reaction (as is the case in the present study), the mechanistically significant Tafel line can be calculated from the observed value (Eq. [15]). This again will only be relevant, however, to the kinetic behavior during the transient which may be entirely different from that observed at steady state.

In conclusion, the potential sweep technique is not generally applicable to kinetic studies because the system is altered by the measurement. In a proper study, when correction for sweep rate and diffusion effects are made, the kinetic behavior of the system during the sweep may be evaluated. This, however, may be quite different from the steady-state behavior which is the only one relevant for the continuous operation of electrochemical energy converters.

Conclusions

The kinetic parameters calculated from measurements employing the potential sweep or cyclic voltametry technique cannot be used directly as diagnostic criteria for mechanistic determinations. In general three regions of potential sweep rate may be expected to occur. At sufficiently low sweep rates (region A) the steady state of the system is not significantly disturbed by the sweep, and the kinetic parameters observed are independent of sweep rate. At intermediate sweep rates (region B) the reaction can be diffusion controlled. This region is characterized by a linear dependence of peak current i_M on the square root of the sweep rate and (for totally irreversible reactions) a linear dependence of the peak potential V_M or log v, with a slope of $\partial V_M/\partial \log v$ = 2.3 $RT/2\alpha n_a \mathbf{F}$ (11, 12). In this region a linear Tafel behavior can also be observed with a slope which is about 35% higher than the mechanistically significant slope of 2.3 $RT/\alpha n_a \mathbf{F}$. Finally, at very high sweep rates (region C) most of the Faradaic current is associated with oxidation of reactants which have been adsorbed on the surface before application of the sweep; or with adsorption or desorption of intermediates formed in the reaction sequence. Region C is characterized by a linear dependence of the current on sweep rate [the current may be regarded as pseudocapacitative in this region in that it obeys the simple relationship $i = Cv$ where C is the effective pseudocapacity of the system under a given set of conditions (13)]. A linear plot of V_M *vs.* log v will result in this region. The slope, however, will be 2.3 $RT/\alpha \mathbf{F}$, *i.e.*, twice that observed in the diffusion controlled region (14).

The sweep rate corresponding to the three regions discussed above will depend on the specific rate con-

stants of the reactions studied, the concentration of reactants in the bulk of the solution and other factors. In the case of ethylene oxidation on platinum electrodes at 80°C studied here, region A corresponds to $v < 10^{-5}$ v/sec. Region B spreads from $v = 2 \times 10^{-3}$ up to 2 v/sec, and region C probably starts at $v > 100$ v/sec. In certain cases these regions may tend to overlap, and in particular diffusion controlled conditions may not be observed experimentally at high reactant concentration and for systems where steady state can be reached rapidly.

The peak current and subsequent decrease in current with increasing potential (quasi-passivation region) observed in steady-state and slow sweep measurements (region A) have been associated with formation of oxide layers on the surface. In contrast, the apparent passivation in regions B and C are due to a depletion of the electrolyte near the electrode from reactant molecules and to a decrease of the combustible adsorbed reactant on the surface, respectively, and are independent of the state of the electrode surface. Several such peaks may occur in region B if stable intermediates are formed in substantial amounts in the reaction sequence, or due to impurities in the fuel or in the electrolyte.

Acknowledgment

Financial support for this work by U.S. Engineers Research and Development Laboratory, Fort Belvoir, Va., under Contract No. DA44-009-AMC-469(7) is gratefully acknowledged.

Manuscript received Oct. 8, 1965.

Any discussion of this paper will appear in a Discussion Section to be published in the December 1966 JOURNAL.

REFERENCES

1. H. Wroblowa, B. J. Piersma, and J. O'M. Bockris, *J. Electroanal. Chem.*, **6**, 401 (1963).
2. J. O'M. Bockris, H. Wroblowa, E. Gileadi, and B. J. Piersma, *Trans. Faraday Soc.*, **61**, 2531 (1965).
3. H. Wroblowa, A. T. Kuhn, and J. O'M. Bockris, In preparation.
4. E. Gileadi, B. T. Rubin, and J. O'M. Bockris, *J. Phys. Chem.*, **69**, 3335 (1965).
5. W. Heiland, E. Gileadi, and J. O'M. Bockris, *J. Phys. Chem.*, **70** (1966).
6. M. W. Breiter, *Electrochim. Acta*, **8**, 973 (1963).
7. S. Gilman and M. W. Breiter, *This Journal*, **109**, 1099 (1962).
8. A. L. Juliard and H. Shalit, *ibid.*, **110**, 1002 (1963).
9. L. R. Griffith and D. R. Rhodes, Fuel Cells and CEP Technical Manual 32 (1963).
10. B. D. Cahan, To be published.
11. P. Delahay, *J. Am. Chem. Soc.*, **75**, 1190 (1953).
12. P. Delahay, "New Instrumental Methods in Electrochemistry," Interscience Publishers, Inc., New York (1954).
13. B. E. Conway, E. Gileadi, and H. Kozlowska-Angerstein, *This Journal*, **112**, 341 (1965).
14. S. Srinivasan and E. Gileadi, *Electrochim. Acta*, **11**, 321 (1966).

Current Distribution at a Gas-Electrode-Electrolyte Interface

I. Experimental Observations

Douglas N. Bennion[1] and Charles W. Tobias

Department of Chemical Engineering, University of California, Berkeley, California

ABSTRACT

The variation of current density along a cylindrical, partially immersed electrode relative to the position of the apparent or intrinsic meniscus has been measured as a function of total applied current. Measurements of current distribution are reported for the cathodic reduction of O_2 gas in aqueous KOH electrolyte on sectioned Ni and Ag electrodes. A thin film of electrolyte was observed to exist above the intrinsic meniscus. It was found that the charge transfer which takes place at the electrode-electrolyte surface occurs almost totally above the bottom of the intrinsic meniscus, and that a large portion of this charge transfer occurs in the thin film as high as 1-5 mm above the top of the intrinsic meniscus. However, as the total current is increased, the charge transfer reaction is gradually crowded closer to the top of the intrinsic meniscus, and a smaller fraction of current passes up into the film. On nickel the current is more uniformly distributed in the upper areas of the thin film than on silver.

Many of the possible fuels and oxidants proposed for use in fuel cells are gases. To gain an understanding of the dynamic behavior of electrodes involving gaseous reactants, analysis of transport phenomena at gas electrode-electrolyte interfaces is necessary. Various studies of porous media involving only electrode-electrolyte interfaces have been presented recently (1-4). The presence of a gas phase provides additional problems which are to be considered here.

Porous electrodes are used to increase the reaction area per unit volume and, in the case of gaseous reactants, to provide separation between gas and electrolyte. In such electrodes, many simultaneous and consecutive processes occur, and the nature and extent of the actual reaction area within the pores is not well defined or understood. A plane electrode partially immersed in an electrolytic solution offers a simpler system for studying the behavior of gas electrode-electrolyte interfaces.

[1] Present address: Department of Engineering, University of California, Los Angeles, California.

In 1957 Wagner (5) postulated that a thin film of electrolyte exists above the visible meniscus on the surface of a partially immersed electrode and that the electrode surface in contact with this thin film should contribute appreciably to the charge transfer reaction.

In their study of current density distribution of oxygen reduction on copper, Weber, Meissner, and Sama (6) did not consider the possibility of the existence of a thin electrolyte film above the intrinsic or readily visible meniscus. Will (7, 8), in experiments involving oxidation of hydrogen in sulfuric acid on platinum, observed the variation of the total current with the length of platinum extending above the liquid level of the electrolytic solution at a constant applied overpotential. Will concluded that a thin film did exist above the intrinsic meniscus and that most of the charge transfer reaction occurred in a narrow region adjacent to the upper edge of the meniscus. He also showed that surface migration of hydrogen along the platinum was not a significant mode of mass transfer.

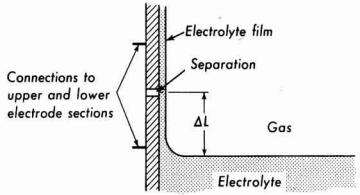

Fig. 1. Schematic representation of gas electrolyte interface showing the insulating separator. ΔL could be changed by raising or lowering the electrolyte level.

Diffusion of hydrogen through the film was determined to be the rate-controlling step. This was the first really definitive experiment to show the role of thin electrolyte films. However, as the platinum electrode was extended further and further out of the electrolyte, new area on which an electrolyte film could exist was produced. Thus, the film geometry and resulting current distribution changed during the course of an experiment.

The present work was undertaken to investigate the role of the thin film during oxygen reduction, and to obtain a quantitative description of the transport processes involved. For experimental work, oxygen gas, aqueous 3.5M KOH, and either nickel or silver electrodes were chosen.

Experimental Equipment and Procedures

The objective was to measure the variation of current density along a partially immersed electrode relative to the position of the bulk electrolyte surface. In order to accomplish this, sectioned electrodes (9) were employed. The sections must be insulated electrically from one another, and the insulating separators should not significantly disturb the geometry of the thin liquid film on the surface of the electrode. Also, the sections of the metal electrode must be at the same potential.

In order to satisfy these requirements as closely as possible, only two sections and a single separation were used (see Fig. 1). With this approach, the variation in the current from each section could be measured as a function of the distance, ΔL, of the bulk electrolyte level below the separation (see Fig. 1). The sum of the two currents equals the total; therefore, only one of the currents is independent. In order to compare the results of different total currents more easily, the per cent current out of the top section, defined as %C.O.T. = (Current out top section) (100)/(Total Current), was used as the independent variable.

The experimental procedure involved determination of the %C.O.T. as a function of ΔL at various total currents on nickel and silver electrodes. To determine the actual current density variation, one plots the %C.O.T. *vs.* ΔL and takes the slope of this curve. The slope at a given value of ΔL, in cm^{-1}, times the applied current, I, in microamperes per centimeter of electrode circumference, gives the transfer current density at a height ΔL above the electrolyte level. The readings were consistent to within 3% for a single run except at the lowest current levels when variations up to 10% of the measured current were inherent in the circuit design.

To avoid edge effects cylindrical electrodes were used. Electrodes of both 0.8045 and 1.465 in. in diameter were used. The current, I, in microamperes per centimeter times the electrode diameter, gives the total current. The working length of the electrode was approximately 12 cm; this was found to be long enough to avoid appreciable end effects at the top and bottom. The electrode was constructed using a cylindrical plexiglass spindle over which two cylinders of nickel[2] (or silver[3]) were slipped (see Fig. 2.). These were separated by a thin "gasket" made from a sheet of oriented polystyrene 25μ thick. This thickness was necessary to insure that no metallic electrical connection occurred between the two sections.

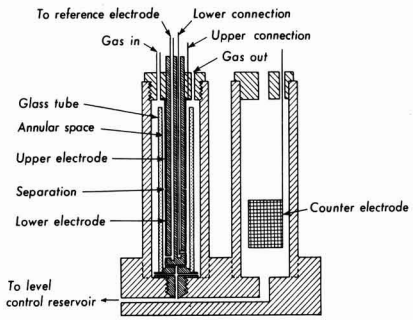

Fig. 2. Cross-sectional view of cell used for measurement of distribution of current relative to position of meniscus.

In order to avoid the possibility of systematic errors and to confirm the reproducibility of the data, 2 different silver cells and 5 separate nickel cells were built. The procedures in constructing the separations in the working electrodes (such as rounding the corners of the electrode where it contacts the insulating jacket) were modified slightly to see if the results were affected. No effects on the results were noted from these changes. For one of the silver electrodes, runs were also made with the 25μ thick polystyrene gasket replaced by a separator made from filter paper approximately 70 microns thick. This was done to check the results for any dependence on the nature of the material used as the separator.

The cell consisted of two cylindrical compartments as shown in Fig. 2. The cylindrical electrode spindle described above was screwed into the left-hand compartment. In the right-hand compartment, nickel screens served as the counter electrode. The over-all reaction at the working electrode was

$$O_2 + 2H_2O + 4e^- = 4\,OH^-$$

The reaction at the counter electrode was the reverse of the above reaction. The reactions were driven externally by a constant current power supply.[4]

The two compartments mentioned above were connected to a storage reservoir, not shown in Fig. 2. By carefully adjusting the height of the reservoir, the liquid level in the cell compartments could be accurately adjusted. The value of ΔL was determined by measuring the height of the bulk liquid and the height of the separation, to ± 0.05 mm, using a cathetometer.

The electrolyte entered the working electrode compartment through radial holes drilled in the lower part of the plexiglass spindle. This provided for an axially symmetric electric field. To align the electric field more nearly parallel to the electrode and to reduce convection effects, a precision-bore glass tube was placed over the electrode as shown in Fig. 2. The bulk electrolyte was confined in an annular space about 1 mm wide. The bottom of the meniscus was used as the reference level for measuring ΔL. The distance from the bottom of the meniscus to the top of the apparent or "intrinsic" meniscus was in the range of 0.6-1.1 mm. The electrolyte in the cell outside the jacket did not participate in the reaction and need not be considered.

Convection currents in the electrolyte below the meniscus would tend to give abnormally high currents from the bottom section. The precision-bore glass jacket which confined the electrolyte next to the electrode in an annular region reduced this effect. Smaller

[2] The nickel was 99.5% pure. The principal impurities were Mn and Fe.

[3] The silver was 99.95% pure.

[4] Electronics Measurements, Inc., Constant Current Power Supply, Model C612.

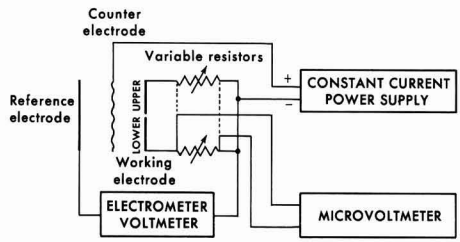

Fig. 3. Power and measurement circuit for sectioned electrode cell.

spacing would have reduced the probability of convection further (10), but this would have caused more severe relative variations in the annular space. The value chosen was considered to be a suitable compromise.

The readings were sensitive to the surface conditions of the electrodes. If any oxide formed on either the nickel or silver electrodes, the results were not reproducible. Care was always taken that, following polishing,[5] the electrode was immediately placed in the cell and cathodically polarized to prevent oxide formation. The current was increased to approximately 200 ma yielding vigorous hydrogen evolution. During the 24-48 hr cleaning period, the electrolyte was changed each 2-5 hr The cleanliness of the surface was considered satisfactory when, on lowering the electrolytic level, the surface remained uniformly wetted.

Electrolytic contact was made to a Hg, HgO reference electrode through a hole drilled lengthwise down the spindle and out through a small hole at the bottom of the metal electrode (11). Electrical connection to the bottom section of the electrode was made with a nickel rod down a hole in the spindle. A stainless steel screw went through the electrode and was threaded into the nickel rod. The electrical connection to the top section was made by a nickel plate in the bottom of the cap. When the cap was screwed down, the nickel plate pressed down on the upper electrode section and completed the contact. The resistances due to these connections were less than 0.1 ohm.

Figure 3 shows a schematic drawing of the electrical circuit. Before the measurements were started, the variable resistors[6] were set at zero; the two electrode sections were then shorted together and thus were at the same potential. When measurements were to be made, the resistances were increased until a measurable voltage drop[7] was obtained. When properly adjusted, the potential drop across each resistor was equal. As small a voltage drop as practical was used so that errors in balancing would be negligible. These potential differences varied between 10 and 1000 μv for the lowest and highest total applied currents. From the voltage drop and the known resistance, the current from each section could be calculated. The potential of the working electrode with respect to the Hg, HgO reference cell was measured with an electrometer.[8]

The start-up procedure was to refill the cell with 3.5M KOH, begin bleeding in O_2 saturated with water with respect to 3.5M KOH, and to set the total current at a fixed level. The liquid level was then lowered to near the bottom of the electrode, corresponding to a large value of ΔL. The cell was left for about 15 hr to allow the liquid film to drain and reach an equilibrium thickness. The level was next raised a small distance and a set of readings were taken. After each set of readings, the level was raised again and in this manner a series of readings for different values of ΔL were obtained. Observations were made at 30-min intervals to allow steady-state conditions to prevail during readings. At each electrolyte level the value of %C.O.T. could easily be calculated.

[5] Of the various polishing compounds, "Flow-five" aluminum oxide proved to be the most satisfactory. Although the roughness of surfaces was different depending on the polishing compounds used, no significant differences in the pattern of current distribution resulted.

[6] General Radio type 1432-U or 1432-K decade resistance boxes were used.

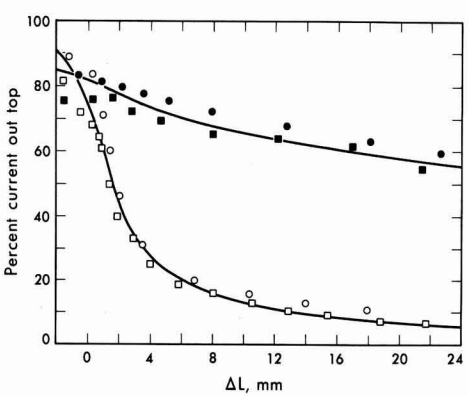

Fig. 4. Penetration of current in the electrolyte film. $I = 4.84$ μa/cm. Upper curve: nickel cathode, cells No. 2 and 3, runs 6 and 6'; lower curve: silver cathode, cell No. 4, runs No. 6 and 15.

Experimental Results

Exploratory experiments showed (12) that after the electrolyte level was lowered, a thin electrolyte film was left behind on the exposed electrode. The fraction of current from the upper section was very high but it dropped off with time. This decrease with time continued for up to 90 hours, after which a steady-state value remained as long as the run was continued, for several more days in some cases. This behavior was attributed to the draining of the electrolytic film which was initially thick but became thinner as draining progressed. Thicker films have a small resistance and thus tend to allow penetration of the current higher into the film.

Simple optical observations were made in an attempt to observe the film and determine its thickness by light interference techniques. The existence of the film was confirmed by the observation of weak interference colors when white incident light was used and by the observation of a "wake" when a small corner of tissue paper was drawn over the surface. Quantitative measurements of the film thickness were beyond the scope of this work. Müller (13) has made a detailed investigation of the optical properties of thin electrolytic films on nickel electrodes and found that in the range of 2-5 mm above the meniscus the film thickness is in the order of 1μ for 3.5M KOH.

Plots showing %C.O.T. as a function of ΔL are shown in Fig. 4, 5, and 6 for 4.84, 15.4, and 48.4 μa/cm applied current, respectively. Figure 7 shows the observed dependence of the electrode potential on the applied current.

A feature to be noted is that at higher currents the reaction tends to be concentrated nearer the top of the intrinsic meniscus. A comparison of the results for equal applied currents shows that the reaction on nickel spreads significantly more into the film than on silver.

One of the requirements of the sectioned electrode was that the separation should not disrupt the film. This becomes especially important when it is realized that the electrolyte film is about 1μ thick and the separation is 25μ wide. Such a wide gasket obviously causes some distortion. The possible distortion effects can be broken down into three categories as follows:

[7] This voltage drop was measured using a Keithly model 149 millimicrovoltmeter.

[8] Keithly Model 610R electrometer was used here. Its internal resistance is rated at 10^{14} ohms or greater.

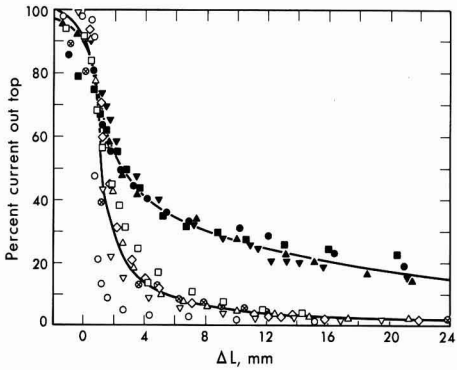

Fig. 5. Penetration of current in the electrolyte film. $I = 15.4$ μa/cm. Upper curve: solid symbols, experimental points, nickel cathode, cells No. 2 and 3, runs 5 and 5'; lower curve: open symbols, experimental points, silver cathode, cell No. 4, runs 5, 11, and 14.

1. Assume that the insulating gasket is perfectly flush with the metal surface and that the film thickness does not vary. The only error from such an ideal situation results from no electrode reaction occurring along the insulating section. This inactive length of the film will act as an "unnatural" resistance. If this occurs near the bottom of the film where the current might reach 100 μa/cm as a maximum and if the film is 1μ thick, the "unnatural" resistance will cause a potential drop of 4.2 mv. This compares to a total potential drop in the film of about 140 mv.

2. Referring to case 1, the net effect of the separation might be such that the film appears to be thicker as it passes the separation. For this situation, the "unnatural" resistance will be lowered, and the error will be less than for case 1.

3. The situation might also be an effective thinning of the film as it passes the separation. At worst, this thinning will occur along the full length of the separation. A thinning of this type, for example, to one-fourth of the normal thickness, will increase the "unnatural" resistance so that, using the example of case 1, the added potential drop would be 19 mv. Such an added potential drop would cause a shift in the results, such that less current would pass to the upper section than on an uninterrupted surface.

The reproducibility of the data was confirmed by using different cells of slightly modified design. Similarly, no change in the results was detected by replacing the 25μ thick polystyrene separator with a 70μ thick separator made from filter paper (see Fig. 5 and 6).

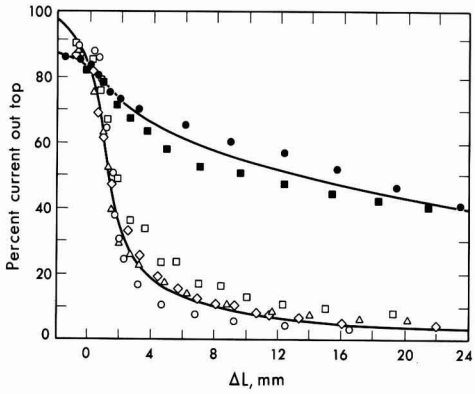

Fig. 6. Penetration of current in the electrolyte film. $I = 48.4$ μa/cm. Upper curve: solid symbols, experimental points, nickel cathode, cells No. 2, 3, and 7; runs 4, 4', 19, 20; lower curve: open symbols, experimental points, silver cathode, cells No. 4 and 6, runs 4, 10, 13, 19, 20.

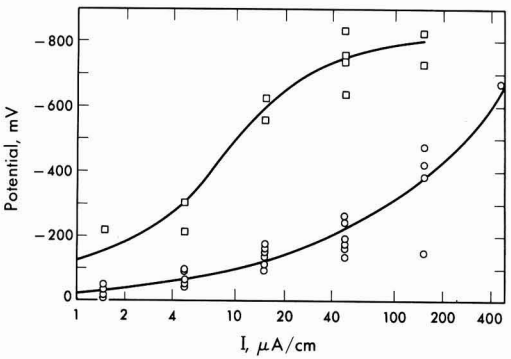

Fig. 7. Potential of the oxygen cathode (not corrected for ohmic drop) relative to the Hg/HgO reference electrode. Upper curve, nickel cathode; lower curve, silver cathode.

From these observations it is concluded that the film on the separator was not significantly thinner than on the adjacent metal surfaces. The maximum error in the current out the top, due to the presence of the separator, is estimated to be 3%.

Discussion

These experiments have confirmed that a stable, thin film of electrolyte adheres to the electrode surface above the top of the intrinsic meniscus. A large part of the reaction takes place on the surface of the electrode exposed to this film. The reaction rate drops off very rapidly within the visible meniscus and is very small along the electrode area exposed to the bulk electrolyte. The obvious reason for the abrupt decrease in reaction rate on the electrode surface below the intrinsic meniscus is mass transport limitation of the molecular oxygen. However, the controlling factors in the film region can arise from other sources.

Will (7, 8) concluded that the rate-limiting step was the mass transfer of gaseous reactant, hydrogen in this case, through the film to the electrode surface. He also found that the reaction rate dropped off very rapidly above the "top of the intrinsic meniscus." The observations with the oxygen-KOH system show that the reaction rate remains appreciable for several millimeters above the "top of the intrinsic meniscus." In addition, it is observed that the reaction extends further up the film for nickel than for silver.

It is also possible that the limiting step can be charge transfer at the electrode surface. It is known that silver is a better catalyst for the reduction of oxygen than is nickel (14). Thus one would expect that if the dependence of charge transfer "overpotential" on current density were higher for nickel than for silver, the reaction would tend to "spread out" or be distributed over a wider area, thus further up into the film.

Both the charge transfer and mass transfer overpotential tend to cause the reaction to spread out farther. It is the potential drop in the film which limits the extension of the reaction up into the film. From either standpoint, if the film were thicker, the reaction would tend to extend further into the film. Observations made during the initial stages when the film was draining confirm this argument.[9]

[9] A greater penetration of current up into the film on nickel relative to silver could be explained qualitatively by a significantly larger film thickness on nickel. Although precise observations regarding the film thickness on nickel were not available at the time this work was concluded, preliminary data by Müller (13) indicated that the film thickness on silver is actually somewhat greater than on nickel.

Conclusions[10]

1. The existence of a thin film of electrolyte above the intrinsic meniscus on clean nickel and silver has been confirmed. The thickness of this film is established as being in the order of magnitude of wave length of visible light.

2. For the cathodic oxygen electrode, current density distribution measurements on cylindrical nickel and silver electrodes established that a large portion of the current arises in the thin electrolytic film above the intrinsic meniscus. The fraction of current transferred as much as 10-20 mm above the bottom of the intrinsic meniscus is not negligible.

3. The thicker the film and the smaller the applied current, the further the current spreads over the electrode surface covered by the film. At a given value of applied current, the reaction is concentrated nearer the intrinsic meniscus on silver than on nickel surfaces.

Acknowledgment

This work was supported by the Advanced Research Project Agency through the U.S. Army Electronic Laboratory.

Manuscript received June 2, 1965. Revised manuscript received Jan. 10, 1966.

[10] After the completion of this manuscript, an account of the work of Yu A. Mazitov *et al.* (15) has come to the authors' attention. Current distribution along a silver wire in the reduction of oxygen in 10.6*N* KOH was measured by the method originally used by Will (7, 8). Although their experimental observations are in qualitative agreement with the results presented above, the reader's attention is called to the use of an uninterrupted cathode and the much shorter draining times (3-4 min) reported by Mazitov *et al.*

Any discussion of this paper will appear in a Discussion Section to be published in the December 1966 JOURNAL.

REFERENCES

1. J. S. Newman and C. W. Tobias, *This Journal*, **109**, 1183 (1962).
2. E. A. Grens, II, and C. W. Tobias, *Ber. Bunsen Ges. Physik. Chem.*, **3**, 236 (1964).
3. J. L. Bomben, Master's Thesis, University of California, Department of Chemical Engineering, September 1963.
4. J. Euler and W. Nonnenmacher, *Electrochim. Acta*, **2**, 268 (1960).
5. Carl Wagner, Private communication.
6. H. C. Weber, H. P. Meissner, and D. A. Sama, *This Journal*, **109**, 884 (1962).
7. F. G. Will, *ibid.*, **110**, 145 (1963).
8. F. G. Will, *ibid.*, **110**, 152 (1963).
9. E. Mantzell, *Z. Elektrochem.*, **42**, 303 (1936).
10. U. Böhm, N. Ibl, and A. M. Frei, Paper presented at the 13th CITCE Meeting in Rome, Sept. 24-29, 1962; in press *Electrochim. Acta*.
11. M. Eisenberg, C. W. Tobias, and C. R. Wilke, *This Journal*, **102**, 415 (1955).
12. D. N. Bennion, Dissertation, University of California, Berkeley, June 1964.
13. R. H. Müller, Extended Abstracts of Theoretical Division, **2**, 19, The Electrochemical Society, New York.
14. H. M. Dittman, E. W. Justi, and A. W. Winsel, "DSK Electrodes for the Cathodic Reduction of Oxygen," in "Fuel Cells," Vol. II, G. J. Young, Editor, Reinhold Publishing Corp., New York (1963).
15. Yu A. Mazitov, K. I. Rosenthal, and V. I. Vesilowskii, *Zhur. Fis. Khim.*, **38**, 449 (1964).

Current Distribution at a Gas-Electrode-Electrolyte Interface

II. Theoretical Treatment

Douglas N. Bennion[1] and Charles W. Tobias

Department of Chemical Engineering, University of California, Berkeley, California

ABSTRACT

The dynamic behavior of a cathodic oxygen electrode is critically dependent on charge and mass transport preceding and following the charge transfer recation at the electrolyte-electrode interface. A mathematical model is presented which takes into account diffusion and migration of relevant substances and the solubility of oxygen in the electrolyte. The model accounts for the concentration dependence of transport properties. A comparison of the theoretical and experimental results indicates that the current density distribution is controlled by a balance between charge transfer overpotential and ohmic resistance drop in the electrolyte film. Because of the much greater length of diffusion paths, and consequent slowness of oxygen transport, a relatively small fraction of the charge transfer reaction occurs on the electrode area below the top of the intrinsic meniscus.

An experimental study (1) in this laboratory has shown that on partially immersed gas electrodes a thin film of electrolyte may exist on the electrode above the bulk electrolyte, and when this film exists the electrochemical reaction takes place primarily on the surface of the electrode which contacts the thin film.

By considering several possible physical models Wagner (2), in 1957, demonstrated the likelihood of the importance of thin electrolyte films in actual gas electrodes. Since then, various models have been proposed which attempt to duplicate more closely actual physical conditions. Will (3, 4) was able to explain his experimental results obtained on partially immersed, plane electrodes in terms of a theoretical model. His model did not include consideration of charge transfer overpotential, and the only transport property of the electrolyte employed was the conductivity which he assumed to be invariant. Grens *et al.* (5) in a model geometrically similar to the one by Will included an Erdey-Gruz-Volmer-type charge transfer overpotential expression. Transport of ions by both diffusion and migration is accounted for, and the movement of water is assumed to occur only in the electrolyte phase. Grens *et al.* were able to show how systems can become charge transfer or mass transfer limited depending on the magnitude of the physical parameters involved. Although variations of transport properties were not considered, their model predicts large concentration gradients in the thin film. It should be noted that, of these models, only that of Will has been compared directly to experiments, and that his model incorporated features characteristic of the hydrogen, sulfuric acid, platinum system.

The above theories provide primarily a guide to understanding the detailed behavior of the electrode reaction within and near a thin electrolyte film which

[1] Present address: Department of Engineering, University of California, Los Angeles, California.

may exist on plane, metal electrodes. Other models have been proposed which attempt to explain the behavior of porous electrodes in terms of certain assumed microstructures of the porous matrix. Some recent models by Gurevich (6), Rockett (7), Iczkowski (8), and Burshtein *et al.* (9), have incorporated the possibility of a thin film existing on the walls of the gas filled pores or cavities within the electrode. Of these, the one by Burshtein *et al.* is of particular interest, since it includes a transformation of a rather sophisticated model into one where equations developed for two-phase porous electrodes can be applied (10-12). In Burshtein *et al.'s* model, a detailed description of what is taking place within the thin film is not undertaken, and a simple, linear relation between the local overpotential and the current being transferred is assumed.

The theoretical model to be presented here is one in which the details of the film behavior are described. Our model is to be for the oxygen, KOH, silver system and is to include a realistic charge transfer overpotential relation. It also allows for variation of electrolyte composition and consequent changes in the solubility of oxygen and in the transport properties of oxygen and KOH. Consideration is given to whether water transport occurs in the gas phase or the liquid phase. Direct comparison of the theoretical model and experimental results is designed to further our understanding of the system and its controlling features.

The Mathematical Model

Geometric considerations.—The model describes an oxygen half-cell operating cathodically in aqueous KOH electrolyte. From the analysis of experimental results (1) it has been concluded that a large portion of the reaction takes place in a thin film which extends above the bulk electrolyte on the surface of the electrode. Measurements of the film thickness by Müller (13) show that the thickness of this film decreases with height above the bulk liquid. However, the per cent change in thickness is small compared to the observed per cent changes in the reaction rate over comparable distances (15). In our model, to avoid unnecessary mathematical difficulties, the thin film is assumed to have a constant thickness, δ.

Since the current density was observed to spread out over a comparatively large area, the charge transferred in the vicinity of the curved meniscus is small compared to the total current. This suggests that the precise geometry of the meniscus is not important (1, 3, 4). Consequently, in our model (see Fig. 1) the thin film is assumed to change its thickness abruptly.

Mass transport considerations.—Mathematically, the model is one dimensional. No variations in concentration, c, or current density, i, across the width of the film are considered. Oxygen is assumed to reach the electrode by diffusion in the x direction through the upper film (see Fig. 1). In the lower (bulk) electrolyte region oxygen is assumed to move only in the negative y direction. The consumption of oxygen through reaction at the electrode is treated as a homogeneous sink term (see Eq. [10]).

The system is assumed to be at steady state. The over-all electrode reaction is

$$O_2 + 2H_2O + 4e^- = 4\,OH^-$$

The rate of reaction at the electrode is proportional to the transfer current density, J. J is taken as positive when the reaction proceeds from left to right as written. In the thin film, O_2 migrates toward the electrode in the x direction, OH^- ions move down the film, and the K^+ ions remain stationary at steady state. The water can reach a reaction site by two mechanisms or combinations thereof. It can diffuse up into the film countercurrently to the OH^- ions or condense from the gas phase onto the film surface and diffuse cocurrently with the oxygen. Convection is assumed to be negligible.

Equations for electrolytic transport.—Algebraically, the ionic fluxes and the water flux can be written as

$$N_+ = 0$$

$$N_- = -i/F$$

$$N_o = -\tfrac{1}{2}\,Q\,N_-$$

$$v^\star = \frac{1}{c_T}(N_+ + N_- + N_o) = \frac{-i}{c_T F}\left(1 - \frac{Q}{2}\right) \qquad [1]$$

By electroneutrality

$$c_+ = c_- = c \qquad [2]$$

Q is equal to unity if the water is supplied wholly by diffusion up the film, and it is equal to zero if supplied totally by condensation from the gas phase. It seems reasonable that one mechanism or the other will be controlling so that Q will be assumed to equal either one or zero. The model is not suitable for fractional values of Q.

The equations representing the flow of current and movement of the K^+ and OH^- ions have been discussed elsewhere (14, 15). Incorporating the concentration dependence of the transport properties, and assuming use of a Hg/HgO reference electrode, we obtain

$$i = \kappa\nabla\Phi - \frac{\kappa}{F}RT\,\nabla \ln a\left[\frac{2B}{A+B} + \frac{c}{c_o}\right] \qquad [3]$$

$$N_+ = \frac{-\mathcal{D}}{RT}\frac{\nu_+}{\nu}c\nabla\mu_e + \frac{t_+^\star i}{Fz_+} + c_+ v^\star \qquad [4]$$

$$N_- = \frac{-\mathcal{D}\nu_-}{RT\,\nu}c\nabla\mu_e + \frac{t_-^\star i}{Fz_-} + c_- v^\star \qquad [5]$$

$$\frac{-z_+z_-\,eF\sqrt{\nu c c_T}}{\kappa\mu} = G + \frac{AB}{\nu_+A+\nu_-B}\frac{\sqrt{\nu c_o}}{\sqrt{cc_T}} \qquad [6]$$

$$\mathcal{D} = \frac{\nu kT/\mu}{\nu_+A+\nu_-B} \qquad [7]$$

$$t_+^\star = 1 - t_-^\star = \frac{c_-}{c_T} + \frac{c_o}{c_T}\frac{B}{A+B} \qquad [8]$$

Values of A, B, and G for KOH are (14, 15): $A = 28.89 \times 10^{-8}$ cm; $B = 8.63 \times 10^{-8}$ cm; $G = 9.63 \times 10^{-8}$ cm.

Equations for oxygen transport.—In the thin film, oxygen diffusion can be represented by

$$J = \frac{FD_1[(p/p^o)c_1^o - c_1]}{\delta}, \quad (y \geqq 0) \qquad [9]$$

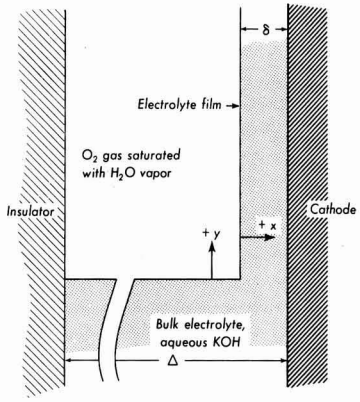

Fig. 1. Mathematical model of the gas-electrolyte-electrode interface.

The transfer current density, J, is equal to the oxygen flux times $4F$. It is assumed that Henry's law holds and that p is the partial pressure of oxygen in atmospheres. D_1 is the diffusion coefficient of oxygen at the concentration of KOH existing at the point under consideration in the film. The numerical calculations were easily adapted to allow for the variation of D_1 as a function of the KOH concentration (16) at different positions in the film.

In the lower or bulk electrolyte region the following equation applies to steady-state oxygen transport.

$$D_1 \frac{d^2c_1}{dy^2} = \frac{J}{4F\Delta}, \quad (y \leqq 0) \qquad [10]$$

Equations relating current and overpotential[2].—A relationship between local overpotential and local transfer current density, J, is still needed. A review of the literature on the kinetics of the oxygen electrode (15, 36) indicates that a generally accepted kinetic description for the oxygen electrode is not yet available (17-19). Based on work by Krasilshchikov, Nefodova, Belina, and Andreeva (20-25) and by Bagotskii and Yablokova (26), a sequence of elementary steps emerges which seems to be satisfactory for use with Ag, Au, and Hg electrodes. From this reaction sequence, summarized by Vetter (36), the following kinetic expression can be developed (15)

$$J = k[O_2]^{\alpha}[OH^-]^{\lambda}[H_2O]^{\gamma} \left\{ e^{\frac{4(\alpha-1)F\eta}{RT}} - e^{\frac{4\alpha F\eta}{RT}} \right\} \qquad [11]$$

where k is a constant, square brackets indicate the activity of the enclosed species, and η is the overpotential defined as the potential of the working electrode compared to a reversible oxygen electrode located just outside the double layer. For a silver electrode in alkaline solution

$$\alpha = 0.625, \lambda = 0.5, \gamma = 0.5 \qquad [12]$$

Work on carbon electrodes (27-30) also seems to support the above mentioned reaction sequence. As mentioned in the Appendix, the kinetics of oxygen reduction on nickel seems more complex. For the case of silver it is assumed that Eq. [11] is applicable at any point on the electrode, *i.e.*, k and α are true constants without any dependence on η or position on the surface. For nickel electrodes Eq. [11] would have to be replaced by an expression of a probably more complex nature, accounting for the dependence of the rate-controlling step (or steps) with η. A generally applicable reaction sequence or kinetic rate expression for the reduction of oxygen on nickel does not appear available (17, 18, 31, 32). For this reason no attempt is made to apply the present mathematical model to the nickel electrode.

Equations relating charge transfer current density and current density in the solution.—Two relations are needed in addition to the equations already mentioned. Since charge must be conserved, the transfer current density, J, and the current density in the solution, i, which is assumed to vary only in the y direction, are related by

$$J = -\delta \frac{di}{dy}, \ (y \geqq 0); \quad J = -\Delta \frac{di}{dy}, \ (y \leqq 0) \qquad [13]$$

It is convenient to replace the potential of the reversible oxygen electrode by that of a Hg/HgO reference electrode

$$\eta = -\Phi - \frac{RT}{4F} \ln \{[O_2]/p\} \qquad [14]$$

Here Φ is the potential of the Hg/HgO reference electrode with respect to the working electrode.

[2] A more detailed discussion is given in the Appendix.

Activities used in kinetic equation.—The activities of the reacting species are assumed to be represented by the following:

$[O_2]$ is assumed to be the concentration of oxygen with unit activity being the concentration of oxygen in equilibrium with gaseous oxygen at a partial pressure of one atmosphere. In the numerical work it was possible to allow the solubility of the oxygen to depend on the concentration of KOH.[3]

$[OH^-]$ is assumed to be the same as the mean ionic activity, a, of the KOH. The activity coefficients were taken from Robinson and Stokes (33). The activity at a KOH concentration of 3.866M is taken to be unity.

$[c_o]$ is assumed to be the concentration of free water. This is determined by subtracting from the total water concentration the concentration of water that is associated with the KOH ions (14, 15). Unit activity is assumed to be the activity of water in 3.866M KOH solution.

Numerical solution.—There are 5 dependent variables, c, c_1, J, η, and i. These are related by Eq. [3], [4], [9] or [10], [11], and [13]. Equation [9] is used in the upper film and Eq. [10] in the lower region. Equation [14] allows one to convert from η to Φ when desirable. The equations are slightly different for the upper and lower sections. The two sections are solved for separately and their boundary conditions matched, since the potential and current are continuous in the electrolyte.

The boundary conditions at the top of the upper film are $y \to +\infty$, $\eta \to 0$, and $i \to 0$.

The boundary conditions at the bottom of electrode are: at $y =$ bottom of electrode, $\eta = \eta_o$ or $i = i_o$.

The equations are nonlinear, 1st, and 2nd order differential equations. They were transformed into finite difference form and solved numerically using an IBM 7090 digital computer. In a numerical sense, it was possible to solve the equations for the thin film region exactly. That is, no iterations were necessary. This was accomplished through an appropriate change of variables. In the lower section, it was necessary to linearize the equations, put them in matrix form, and solve the matrix (15). The nonlinearities were mild, and only three or four iterations were necessary. The method appeared to be stable and to converge rapidly to the correct answer.

Theoretical Results and Comparison with Experimental Observations

Explanation of figures.—Experimental results are summarized in Fig. 2 through 6. A comparison between the calculated variation of current above a

[3] The solubility of oxygen at 25°C in aqueous KOH and for a total pressure of 1 atm as determined in this laboratory (16) may be represented by

$$c_1 = (1.18 \times 10^{-3} \text{ mole/liter}) \exp(-0.405c)$$

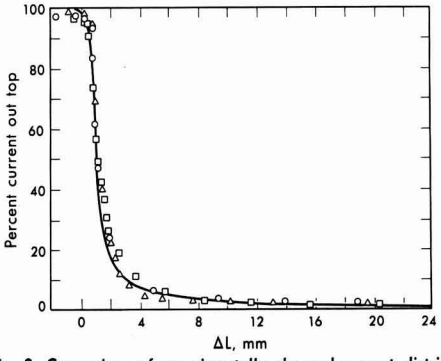

Fig. 2. Comparison of experimentally observed current distribution with the distribution calculated using the theoretical model. Nickel cathode, I = 154 μa/cm. Cell No. 4, runs 7, 9, and 12. Numerical solution with $\delta = 2.25\mu$, $i_o = 1.76 \times 10^{-9}$ amp/cm^2. Open symbols, experimental points, silver.

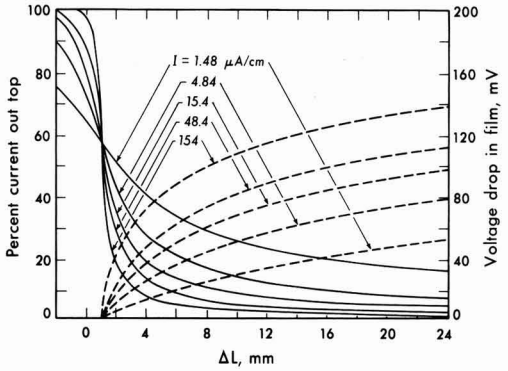

Fig. 3. Theoretical variation of potential and per cent current relative to the meniscus level as a function of applied current.

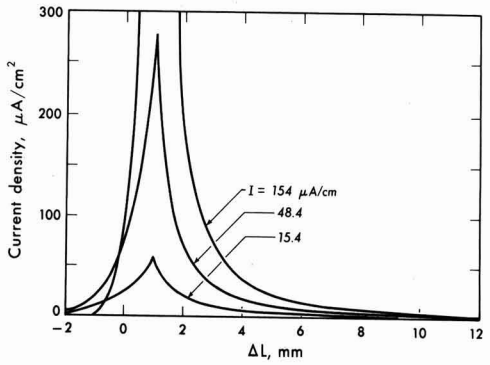

Fig. 5. Theoretical current density distribution relative to the position of the meniscus. High current range.

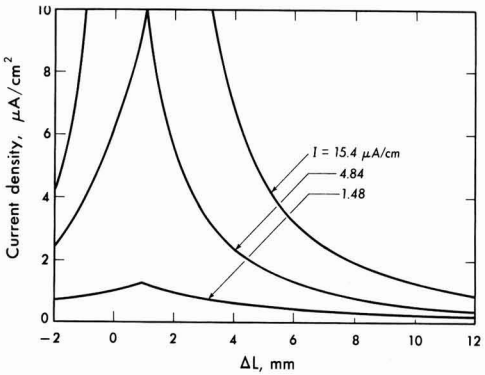

Fig. 4. Theoretical current density distribution relative to the position of the meniscus. Low current range.

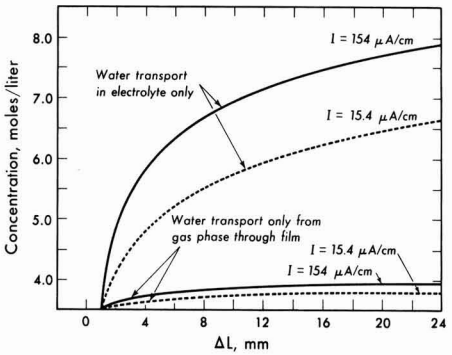

Fig. 6. Calculated variation of KOH concentration in the electrolyte film.

fixed point on the electrode, ΔL, and the experimental observations corresponding to similar conditions is given in Fig. 2. Experimental observations at 48.4, 15.4, and 1.48 μa/cm were presented in Part I, Fig. 4-6. In these figures the curves referring to the silver electrode are those calculated by using parameters as described below, while those for nickel represent a qualitative fitting of the data. No experimental data are available for the voltage variation in the film.

Figure 3 shows the theoretical variation of potential and the per cent current above a fixed point on the electrode as a function of applied current. Figures 4 and 5 present the calculated current density variation along the electrode. The curves in Fig. 3 are the integrals of the curves in Fig. 4 and 5 for corresponding total applied currents. Figure 6 shows computed examples of variation in the concentration of KOH in the film as a function of electrode height. A comparison is made between the concentration variations for both modes of water transport to the reaction sites.

Current distribution and the square meniscus assumption.—ΔL is the independent variable used in the experimental work which indicates position on the electrode relative to the bottom of the intrinsic or visible meniscus. The variable y is used in the theoretical work to indicate position along the electrode relative to the sudden, right-angle widening of the thin film. In order to make direct comparison between the two approaches, y and ΔL must be properly related.

The distance from the top of the intrinsic meniscus over which the current density remains appreciable is to be noted. Even at the lowest currents observed (1.45 μa/cm), the area lying under the level of the bottom of the intrinsic meniscus contributes less than a third to the total current. At the highest currents observed (154 μa/cm) this fraction falls to below a hundredth. The discontinuity of the current density distribution curves at ΔL of 1 mm (see Fig. 4 and 5) results from the square shaped meniscus used in the model. In reality, the transition from the charge transfer and conductance controlled region in the film to the oxygen mass transport controlled area below the top of the intrinsic meniscus occurs over a finite length near the top of the intrinsic meniscus. However, the current density drops off rapidly as the film begins to thicken from approximately 1μ to a thickness in the order of 1 mm at the bottom of the intrinsic meniscus, over a vertical distance of approximately 1 mm. The region of high current density at the bottom of the thin film contributes a large portion of the total current. However, the reaction remains appreciable for several millimeters above the intrinsic meniscus. Due to the large area available in the upper film, the contribution to the total current from that region is appreciable.

In matching the theoretical and experimental current distribution curves, it was found that $y = 0$ corresponded to a ΔL of 1 mm. This implies that below the level of 1 mm above the bottom of the intrinsic meniscus the film thickness is sufficient to cause oxygen transport to become controlling.

A theoretical treatment using a curved meniscus and a tapered film is possible. However, it appears this would greatly increase the numerical complexity due to a second geometric dimension. Such a modification is not expected to yield significant further information or insight. It is established by experimental evi-

dence (1) and a reasonably realistic, theoretical model that an overwhelming proportion of the current originates well above the bottom of the intrinsic meniscus. The changes in the pattern of the current density distribution that can be expected if one substitutes a smoothly curving meniscus for the square meniscus are not expected to be appreciable.

Effect of i_o.—Of the parameters which appear in the numerical calculations, several can be calculated from independent experimental data. Where values are not available, reasonable estimates have to be made.

The shape and position of the theoretical current distribution curves depends on the reaction orders, α, λ, and γ. These appear as the exponents of the OH^-, H_2O, and O_2 activities, respectively, in Eq. [11].[4] The values of α, λ, γ given in Eq. [12] were based on the reaction sequence, rate-controlling step, ($HO_2 + e^- = HO_2^-$), and the value of the transfer coefficient recommended by Krasilshchikov (18). There are, of course, a very large number of reaction sequences and rate-controlling steps which might be chosen. Calculations involving another rate-controlling step ($O_2 + e^- = O_2^-$) yielded a good fit of the experimental data only when unrealistic values of δ were employed.

The parameter known with the least certainty is k in Eq. [11]. When multiplied by the concentration terms raised to the appropriate power in Eq. [11], k can be identified with an exchange current density, i_o. A value for i_o in the order of 10^{-9} amp/cm^2 was found to "fit" the data best. However, this could be varied by plus or minus three orders of magnitude with little effect on the position or shape of the theoretical curve. Although literature reports on measurements of i_o for the oxygen electrode vary widely, a comparison to the Tafel lines shown by Belina and Krasilshchikov (25) indicate that the value used is not unreasonable. The relatively insignificant changes in distribution calculated for i_o's ranging from 10^{-6} to 10^{-12} amp/cm^2 are to be expected, since in the current density ranges used in the computations, except for large values of ΔL, the electrode operated in the Tafel region. Thus a change in i_o results in shifting the potential of the electrode by a constant value, not affecting the distribution of current at a fixed value of total current.

Effect of the film thickness parameter, δ.—The theoretical results were very sensitive to changes in the film thickness parameter, δ. It should be remembered that in reality the film tapers while the model assumed δ to be constant. Since the current extends further up the film at low currents, it is to be expected that the effective average film thickness will decrease with decreasing total current. For the indicated total applied currents, the following values of δ yielded good agreement between the experimental data and our model

I	1.48 μa/cm	4.84 μa/cm	15.4 μa/cm	48.4 μa/cm	154 μa/cm
δ	0.33μ	0.43μ	0.75μ	1.50μ	2.25μ

The values of δ used in the numerical solutions are in reasonable agreement with the average film thicknesses obtained by Müller (13, 15), who noted that the average film thickness increases significantly with increasing cathodic current.

As confirmed by our model, experimental observations have shown that the current density distribution varies a great deal while the film is draining, *i.e.*, while the film thickness is diminishing with time. In thinning films, the over-all overpotential increases and the reaction spreads less and less into the film.

Consideration of the tapering of the film may be justified after sufficient data on film thickness variations with position and current density become available. Otherwise, the introduction of a second geometric variable would require another adjustable parameter (the slope or curvature of the film) without appreciably contributing to the physical understanding of the phenomena observed.

Influence of variable transport parameters and water transport.—In the present work, current distributions were calculated both with constant and variable transport properties. Although the assumption of constant (average) properties did not yield significantly different distributions, this finding should be regarded as valid only under the specific experimental conditions employed. By providing water to the reaction sites through the film from the vapor phase, the steady-state concentration gradient in the film is quite mild compared to the case when water transport occurs by diffusion from the bulk electrolyte in the liquid phase (see Fig. 6).

The high concentration gradients which are predicted when water is assumed to be transported only within the film cause the KOH concentration to exceed the saturation limit. It is suggested that in actual porous gas electrodes water is supplied to the reaction site, at least in part, by condensation from the vapor phase.

Oxygen transport.—Except for the region below the meniscus, oxygen transport should not be a limiting factor. The numerical results show that throughout and across the entire length of the film, the activity of oxygen is very close to unity,[5] *i.e.*, nearly identical to the activity at the electrolyte-gas interface. However, once one moves below the meniscus where the diffusion path for the oxygen becomes large, the oxygen activity drops quickly resulting in the rapid decrease in current density below the top of the intrinsic meniscus.

Rate-controlling process.—Since our model shows that the oxygen activity does not vary noticeably in the thin film, it follows that the penetration of the reaction into the film depends on a balance between the charge transfer overpotential and resistance drop in the electrolyte. As stated in Part I, the significant differences between behavior of the nickel and silver electrodes suggest this to be the case.

Will (3) in his work with the hydrogen electrode on platinum found that the transport of hydrogen gas to the electrode surface through the thin film was controlling, along with ohmic resistance drop, except at very low currents. This is not in contradiction with the results found for the oxygen electrode. The hydrogen electrode on platinum is much more reversible than is oxygen on silver. Consequently, the concentration of current in the immediate vicinity of the intrinsic meniscus is rendered less possible in the case of oxygen, and charge transfer overpotential along with the ohmic drop in the film can be expected to control the current distribution.

Conclusion

In the foregoing treatment it is shown that the current distribution under an electrolyte film above the intrinsic meniscus of an oxygen cathode on silver may be quite successfully described by a rational theoretical model. Realistic geometric and kinetic parameters yield a good agreement between the calculated distributions and those observed experimentally.

Oxygen transport is not limiting in the thin upper film. The current density distribution in this region arises from a balance between charge transfer overpotential and resistance drop in the film. Below the intrinsic meniscus, the bulk electrolyte region, the oxygen activity decreases rapidly due to the mass transport limitations of dissolved oxygen. Thus, the current density is small in this region. The high con-

[4] Note that the parameter α is related to (but not the same as) the transfer coefficient.

[5] It should be remembered that, although the activity remains constant, the concentration of oxygen varies along the length of the film due to the decreasing solubility with increasing KOH concentration.

centration gradients which result when water is not supplied from the gas phase point to the desirability of supplying water as vapor in the oxygen gas.

Acknowledgment

This work was supported by the Advanced Research Project Agency through the U.S. Army Electronic Laboratory.

Manuscript received June 2, 1965; revised manuscript received Jan. 10, 1966.

Any discussion of this paper will appear in a Discussion Section to be published in the December 1966 JOURNAL.

NOMENCLATURE

A, B, C	subsidiary transport properties defined so as to reduce the concentration dependence, Å
a	mean molar activity of KOH $= f_{\pm}c$
c	$c_+/\nu_+ = c_-/\nu_-$ — concentration of KOH, mole/cm^3
c_1	concentration of oxygen, mole/cm^3
c_1^o	saturation concentration of oxygen under a partial pressure of 1 atm, mole/cm^3-atm
c_+	concentration of K^+, mole/cm^3
c_-	concentration of OH^-, mole/cm^3
c_o	concentration of water, mole/cm^3
c_T	$= c_+ + c_- + c_o$ — total concentration, including solvent
D_1	diffusion coefficient of oxygen in aqueous KOH, cm^2/sec
$\mathcal{D}$	molecular diffusion coefficient of KOH based on activity gradients, cm^2/sec
e	electronic charge, coulombs
e^-	symbol for an electron
$f_{\pm}$	mean molar activity coefficient. [Values from ref. (33) were used.]
F	Faraday's constant, coulombs/equivalent
i	current density in the solution, amp/cm^2
i_o	exchange current density, amp/cm^2
J	transfer current density, amp/cm^2
k	kinetic parameter related to exchange current density, amp/cm^2
N_+	flux of K^+, mole/cm^2-sec
N_-	flux of OH^-, mole/cm^2-sec
N_o	flux of H_2O, mole/cm^2-sec
p	partial pressure of oxygen, atm
p^o	reference pressure, 1 atm.
Q	one when H_2O is transferred in liquid phase; zero when H_2O transferred in the gas phase
R	universal gas constant, joule/mole-°K
$t\star$	transference number of species i with respect to molar average velocity
T	absolute temperature, °K
$v\star$	molar average velocity, cm/sec
x	coordinate perpendicular to the plane of the electrode, cm
y	coordinate parallel to the electrode in the vertical direction, the independent variable, cm
z_i	valence or charge number of species i, negative for anions
α	kinetic parameter related to reaction order of oxygen and to the transfer coefficient
γ	kinetic parameter indicating reaction order of H_2O
δ	film thickness, μ
Δ	width of annular electrolyte region below meniscus, cm
η	overpotential referred to a reversible oxygen electrode, volts
κ	conductivity, mho/cm
λ	kinetic parameter indicating reaction order of OH^-
μ_e	chemical potential of KOH, joule/mole. (RT ln $f_{\pm}$ c)
μ	viscosity, poise
ν_+	number of cations per molecule of electrolyte
ν_-	number of anions per molecule of electrolyte
ν	$= \nu_+ + \nu_-$
Φ	overpotential referred to a reversible Hg/HgO electrode, volts

APPENDIX

Notes of the Kinetics of the Oxygen Electrode

There has been accumulated a body of information which suggests that hydrogen peroxide is an intermediate in oxygen reduction (19-31, 34-36). Although the evidence is fairly conclusive for such electrodes as Ag, Hg, C, and Au, it appears that there may be competing sequences of steps on such electrodes as Pt and Ni (17, 18, 31, 34). At this point only the former category of electrodes appears amenable to a simple kinetic analysis.

A review of the above mentioned references indicates that the assumption of the following sequence of elementary kinetic steps is reasonable on Ag, Hg, C and Au electrodes.

1. $O_2 + M = MO_2$
2. $MO_2 + e^- = MO_2^-$
3. $MO_2^- + H_2O = MHO_2 + OH^-$
4. $MHO_2 + e^- = MHO_2^-$
5. $MHO_2^- + H_2O = MH_2O_2 + OH^-$
6. $MH_2O_2 + e^- = MOH + OH^-$
7. $MOH + e^- = M + OH^-$

The M represents an adsorption site and, when associated with a molecular symbol, implies that the molecule is adsorbed. It is possible for any adsorbed molecule on the right side of an equation to desorb before reacting in the next step. The O_2^- and HO_2 are so reactive that this is unlikely. The desorption of HO_2^- or H_2O_2 (depending on the pH) could occur. However, there is evidence (20, 25) which indicates that on silver and in alkaline solution the rate of desorption is small compared to reaction by steps 6 and 7. It should be noted that, because the O_2^- and HO_2 radicals are very reactive, they have not been positively identified.

It appears that the adsorption step is not rate controlling and that either step 2 or 4 is rate determining. The choice appears to depend on pH and on the electrode material. For silver in alkaline solution step 4 appears to be rate controlling. With these assumptions, the kinetic expression can be written as

$$J = k[O_2]^{\frac{\alpha_4 + 2}{4}} [H_2O]^{\alpha_4} [OH^-]^{(1-\alpha_4)} \left\{ e^{\frac{(\alpha_4 - 2)F\eta}{RT}} - e^{\frac{(\alpha_4 + 2)F\eta}{RT}} \right\}$$

where J is the local transfer current density, α_4 is the transfer coefficient for step 4, η is the local overpotential, and k is a kinetic rate constant. Brackets signify the activity of the enclosed species.

On electrode surfaces such as nickel and platinum it appears that other sequences of elementary steps may compete with those outlined above (17-19, 31, 34, 37). On such materials, metal oxides may appear in some of the elementary steps. It is likely that the rate-controlling step and indeed the whole rate-controlling sequence of steps may depend on the local potential. Until more precise information is available on the kinetic parameters the distribution of oxygen reduction on such a surface cannot be predicted.

REFERENCES

1. D. N. Bennion and C. W. Tobias, *This Journal*, **113**, 589 (1966).
2. Carl Wagner, Private communication dated June 13, 1957.
3. F. G. Will, *This Journal*, **110**, 145 (1963).
4. F. G. Will, *ibid.*, **110**, 152 (1963).
5. E. A. Grens, II, R. M. Turner, and T. Katan, *Advanced Energy Conversion*, **4**, 109 (1964).
6. I. G. Gurevich, *Inzhener, Fiz. Zhur., Akad. Nauk Belorus, SSR*, **2**, 78 (1959).
7. J. A. Rockett, Extended Abstracts of Battery Division, Vol. 8, New York Meeting of The Electrochemical Society, 1963.
8. R. P. Iczkowski, *This Journal*, **111**, 605 (1964).
9. R. Chs. Burshtein, V. S. Markin, A. G. Pshenichnikov, V. A. Chismadgev, and Y. G. Chirkov, *Electrochim. Acta*, **9**, 773 (1964).
10. J. S. Newman and C. W. Tobias, *This Journal*, **109**, 1183 (1962).
11. E. A. Grens, II, and C. W. Tobias, *Ber. Bunsen Ges., Phys. Chem.*, **68**, 236 (1964).
12. J. Euler and W. Nonnenmacher, *Electrochim. Acta*, **2**, 268 ((1960).
13. R. H. Müller, Extended Abstracts of the Theoretical Electrochemistry Division, Vol. 2, p. 19, Toronto Meeting of The Electrochemical Society (1964).

14. J. S. Newman, D. N. Bennion, and C. W. Tobias, *Ber. Bunsen Ges. Phy. Chem.*, **69**, 608 (1965).
15. D. N. Bennion, "Phenomena at a Gas-Electrode-Electrolyte Interface," Dissertation, University of California, Berkeley, June 1964.
16. R. Davis, G. L. Horvath, and C. W. Tobias, *Electrochim. Acta*, in press.
17. D. T. Sawyer and L. V. Interrante, *J. Electroanal. Chem.*, **2**, 310 (1961).
18. A. I. Krasilshchikov, "Electrochemical Reactions of Oxygen," Soviet Electrochemistry, *Trudy 4-go Soveshchaniya Po Elektrokhimi*, II (1956). (English translation, *Soviet Electrochemistry*, Vol. II, Consultants Bureau, New York (1961).
19. J. O'M. Bockris and A. K. M. Huq, *Proc. Roy. Soc. London*, **A237**, 277 (1956).
20. A. I. Krasilshchikov, *Zhur. Fiz. Khim.*, **26**, 216 (1952).
21. A. I. Krasilshchikov, *ibid.*, **21**, 849 (1947).
22. I. D. Nefedova and A. I. Krasilshchikov, *ibid.*, **21**, 855 (1947).
23. A. I. Krasilshchikov, *ibid.*, **23**, 332 (1949).
24. A. I. Krasilshchikov and V. A. Andreeva, *ibid.*, **27**, 389 (1953).
25. T. N. Belina and A. I. Krasilshchikov, *ibid.*, **28**, 1286 (1954).
26. V. S. Bagotskii and I. E. Yablokova, *ibid.*, **27**, 1663 (1953).
27. W. G. Berl, *J. (and Trans.) Electrochem. Soc.*, **93**, 128 (1948).
28. R. S. Weizz and S. S. Jaffe, *ibid.*, **93**, 128 (1948).
29. M. O. Davis, M. Clark, E. Yeager, and F. Hovorka, *This Journal*, **106**, 56 (1959).
30. Ernest Yeager and Akiya Kozawa, "Kinetic Factors in Fuel Cell Systems: The Oxygen Electrode," paper presented before the Sixth AGARD Combustion and Propulsion Colloqium on "Energy Sources and Energy Conversion," sponsored by NATO, Cannes, France, March 16-20, 1964.
31. J. J. Lingane, *J. Electroanal. Chem.*, **2**, 296 (1961).
32. L. N. Nekrasov and L. Muller, *Akad. Nauk SSSR*, **149**, 5 (Physical Chemistry Section) 1107 (1963).
33. R. A. Robinson and R. H. Stokes, *Ind. Eng. Chem.*, **4**, 461 (1935).
34. W. G. Berl, *This Journal*, **83**, 253 (1943).
35. A. Frumkin, L. Nekrasov, B. Levich, and Ju. Ivanov, *J. Electroanal. Chem.*, **1**, 84 (1959).
36. K. J. Vetter, "Electrochemische Kinetik," Springer-Verlag, Berlin (1961).
37. D. Bianchi and T. Mussini, *Electrochim. Acta*, **10**, 445 (1965).

Tracer Diffusion Measurements in Mixtures of Molten Alkali Carbonates

P. L. Spedding and R. Mills

Diffusion Research Unit, Research School of Physical Sciences,

Australian National University, Canberra, Australia

ABSTRACT

Tracer diffusion[1] coefficients have been measured for Na^+ ion in Li_2CO_3, for Na^+ and $CO_3^=$ ions in the binary eutectic $Li/NaCO_3$, for K^+ and $CO_3^=$ ions in the binary eutectic Li/KCO_3, and for Na^+, K^+, and $CO_3^=$ ions in the binary eutectic Na/KCO_3. The magnitudes of the diffusion coefficients and the derived experimental activation energies are discussed in relation to previous studies. Preliminary work designed to test the Lumsden model for interaction in binary mixtures is also presented.

We have recently reported (1) tracer diffusion measurements for the pure Na_2CO_3 melt and for various ions in the eutectic mixture $Li/Na/KCO_3$. As a result of this study, interesting comparisons became available of the experimental activation energies for the transport processes of conductance, viscous flow, and diffusion. This led us to believe that an extension of these studies to binary mixtures would be profitable. The work has now been extended to include Li_2CO_3 and the binary $Li/NaCO_3$, Li/KCO_3, and Na/KCO_3 eutectics.

A recent publication by Moynihan and Laity (2) uses the Lumsden (3) model to explain the change in mobility of ions in binary mixtures. In addition, we have, therefore, made some preliminary tracer diffusion measurements in certain binary systems with a view to being able to test this model further. As stated in the first paper of the series, we believe also that transport studies in the general area of molten alkali carbonates will be of value in high-temperature fuel cell work.

Experimental

Apparatus and materials.—Full details of the apparatus and materials used were given in a previous paper (1).

Procedure.—The major portion of the procedure used has also been reported previously (1). However, several modifications and refinements of this procedure have now been made. For example, originally the diffusion tubes were held vertically in a small auxiliary furnace and filled by manual placement of a charged filling capillary. Successful location of the capillary was difficult, and so the method was modified. The charged capillary was momentarily removed from the auxiliary furnace and placed in the diffusion tube. The capillary and attached tube were then placed in the furnace in an almost horizontal position for temperature equilibration. The tube was then brought to a vertical position on the top of an inclined plane (leading to a locating hole) and filled by a combination of manual manipulation and capillary air pressure. Occasionally bubbles were formed in the diffusion tube with this method (about 12% of tubes filled), but its rapidity made it more attractive than the more reliable vacuum filling technique.

Difficulty was experienced with the lithium carbonate experiments in removing the solid salt from the diffusion tubes due to binding of the vibratory drill bit. Consequently the salt was drilled out manually. To minimize this tedious procedure the initial activity was, in this case, determined by a weighing-counting method similar to that used by Angell and Tomlinson (4).

Problems arose in the counting analyses due to drift in the counting rates arising from various causes. Procedures have been developed in this laboratory which minimize this source of error, in particular a rotational counting technique due to Albright (5). With this technique the initial (C_o) and final (C_{av}) radio-

[1] In a previous study on the alkali carbonates (1) the term "trace-ion diffusion" has been used. However, it has been inferred from the measurements in that study that the unit involved in tracer diffusion is not necessarily a single ion so that the more general term is now preferred.

active solutions were counted alternatively in two separate counting trains, 1 and 2. The two counting containers, a and b, were then interchanged and the alternate counting procedure repeated. The count rate, in such a case, would be equal to the sum of products of the radioactive solution concentration, the container counting efficiency, α, and the equipment counting efficiency, β. The counts are then grouped so as to eliminate the long term drift

$$\text{Count ratio} = \frac{C_{av}\ (\alpha_a\beta_1 + \alpha_b\beta_2)}{C_o\ (\alpha_b\beta_1 + \alpha_a\beta_2)}$$

Assuming that $\alpha_b = (1 + x)\ \alpha_a$ and $\beta_2 = (1 + y)\beta_1$ where x and y are very small and also constant, then by substitution

$$\text{Count ratio} = \frac{C_{av}}{C_o}\ \frac{\alpha_a\beta_1\ [1 + (1 + x)\ (1 + y)]}{\alpha_a\beta_1\ [(1 + y) + (1 + x)]}$$

$$\simeq \frac{C_{av}}{C_o}$$

With a sufficient number of counts, a counting reproducibility of better than $\pm$ 0.1% has been achieved using this method which is more than sufficient counting accuracy for the open-ended capillary.

Auxiliary Measurements

End Effects.—Errors due to the end effects associated with the open-ended capillary method were discussed in a preliminary way in the previous study (1), and it was concluded that an experimentally derived flow region existed in which the Δl effect was negligible. However, as there has been a certain amount of controversy in the literature concerning the effect, we have now made a more detailed analysis using boundary layer theory (6, 7).

The boundary layer refers to the region of progressive reduction of velocity from the main stream value to zero at the adhering molecular layer on the solid surface. When a liquid flows past an open-ended capillary at stream-lined velocities (Fig. 1), a boundary layer is formed at the leading edge and a point of three-way separation at the trailing edge of the capillary. This latter would cause a trailing turbulent region to be set up in the form of Karman's vortex streets. This latter condition occurs at $Re_0 \gtrsim 1$ for a cylinder in cross flow (7), where Re_0 is the Reynolds number referred to the external capillary diameter. The boundary layer increases in thickness across the capillary tube face until it meets the turbulent front set up by the trailing edge. With increased flow velocity a turbulent profile would occur at a steadily decreasing critical distance from the leading edge. The lower point of this turbulent profile would sweep down through the boundary layer disturbing the liquid in the vicinity of the capillary face and result in high diffusion coefficients being recorded. Calculation shows that this turbulent front begins to remove radioactivity from the bore of the capillary at high velocities (Re_0 = 1,484) *i.e.*, well beyond the range normally considered in relation to the Δl effect.

Further, the measured diffusion coefficients for aqueous solution (Fig. 2) show an initial sharp rise and then a steady increase up to about Re_0 = 190 whereafter the rise is increasingly rapid. It is obvious, therefore, that the Δl effect is not primarily caused by the external boundary layer, but must be due to phenomena within its precincts. This conclusion is reinforced by consideration of plots of measured diffusion coefficients in various media against Re_0 (Fig. 3). These graphs exhibit no similarity among different media such as aqueous solutions and molten metals and salts; an occurrence which would be expected had the Δl effect depended primarily on the external boundary layer. The fact is that the dense molten media consistently show a more pronounced effect.

At first sight, it would seem more realistic to plot the measured diffusion data against Re_1, the Reynolds number determined by using the diameter of the capillary bore, since the phenomena causing the Δl effect are in the vicinity of the capillary bore and encompassed by the external boundary layer. Such plots do materially change the relative order among the different media shown in the lower part of Fig. 3, but reasonable agreement is still lacking. This helps

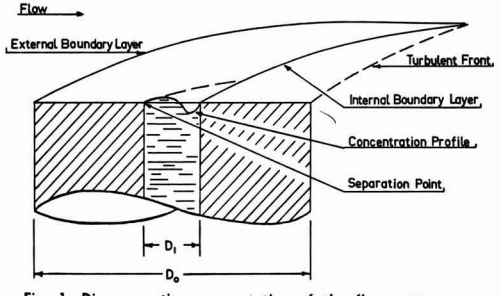

Fig. 1. Diagrammatic representation of the flow patterns over a capillary face.

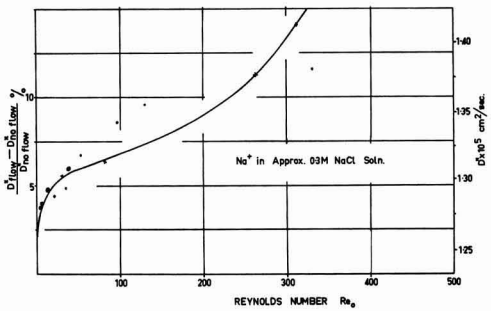

Fig. 2. Variation in measured diffusion coefficient with increasing flow over the capillary face. X, Mills (8); •, Rastas and Kivalo (9).

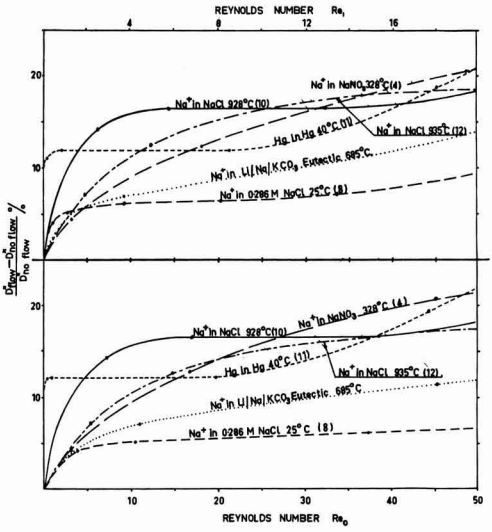

Fig. 3. Effect of flow conditions on the measured diffusion coefficients in various liquid media. In the upper section the flow is referred to the capillary bore and in the lower section to the external capillary diameter.

to confirm our conclusion that the flow phenomena causing the Δl effect are unconnected with the external boundary layer. Reference to Fig. 1 shows how we envisage the flow disturbance. The leading edge of the capillary bore constitutes a point of separation while another internal boundary layer is set up at its trailing edge. This latter formation would be very disturbed because of the concave nature of the surface of the bore wall presented to the flow. The total effect of these inner disturbances is that a wave-shaped profile is established over the mouth of the bore, rising above the datum of the capillary face at the leading edge and sweeping down into the capillary bore just prior to the trailing edge. Within a certain limited flow region these two effects would cancel (within experimental error), and the Δl effect would in essence be eliminated which is in line with the experimental findings of Mills (8). Dye experiments in aqueous solution have visually confirmed that these two opposing effects are, in fact, present.

The lack of similarity of the Re_1 plots of measured diffusion coefficients for the different media illustrated in the upper part of Fig. 3 could well be caused by the differing experimental conditions involved. A temperature gradient is imposed purposely in dense media to prevent the occurrence of thermal mixing. No such provision was made in the aqueous solution measurements where apparently the much narrower capillary diameter employed effectively suppressed thermal mixing. The imposed temperature gradient also would stabilize the no flow condition in the molten salts resulting in the much greater flow influence shown in the lower part of Fig. 3. The intermediate position of the alkali metal carbonate eutectic results substantiates this view as the temperature gradient employed was considerably smaller than that normally used for molten salts. The difference between the no flow and imposed flow conditions is affected also by the temperature of the bath. For example in Fig. 4 the diffusion coefficients determined for the no flow and $Re_0 = 12$ flow conditions are plotted as a function of temperature. It should be noted in passing that, due to the relatively large viscosity change involved, flow rates were altered with temperature to ensure a constant Reynolds number and consequently comparable flow conditions. The difference between the two values is observed to diminish with increased temperature as thermal movement in the main salt bath increasingly affects the conditions at the capillary mouth.

Effect of CO_2.—Certain $CO_3^=$ anion diffusion experiments in the Li/KCO_3 eutectic were conducted under conditions of excessive CO_2 pressure to ascertain if dissolved CO_2 in the melt would materially affect the results. Normally the apparatus was maintained under a CO_2 pressure well in excess of the respective dissociation pressures of the melts in order to ensure constant composition. With double the normal CO_2 pressure, no observable variation was detected in the measured diffusion coefficients so the possibility of a CO_2 effect could be discounted.

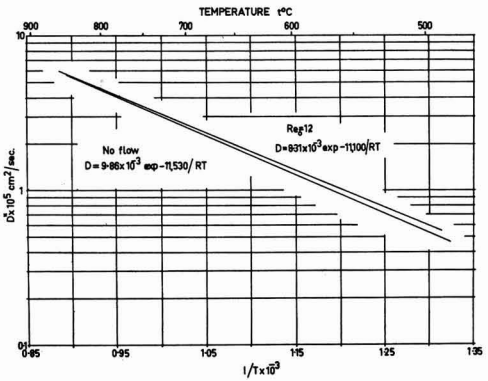

Fig. 4. Measured diffusion coefficients of Na^+ ion in $Li/Na/KCO_3$ ternary eutectic for the no flow and corrected flow conditions.

Results

The data for tracer diffusion of the various ions in the melts investigated are detailed in Tables I to IV.

Table I. Tracer diffusion in $Li/NaCO_3$ eutectic melt (53.3/46.7 mole %)

Temp, °C	$D^*_{Na^+} \times 10^5$, cm²/sec	Temp, °C	$D^*_{CO_3^=} \times 10^5$, cm²/sec
580	1.47	569	0.70
	1.49		0.72
	1.49		0.73
632	2.24	622	1.08
	2.19		1.08
	2.28		1.06
671	2.75	680	1.73
	2.70		1.68
	2.81		1.69
768	4.78	720	2.24
	4.82		2.18
	4.89		2.19
811	5.99	789	3.03
	5.86		3.03
853	7.09		3.03
	7.43	842	3.87
	7.23		3.82
			3.83

$D^*_{Na^+} = (9.81 \pm 0.14) \times 10^{-3} \exp -(10{,}990 \pm 140)/RT$
$D^*_{CO_3^=} = (7.36 \pm 0.32) \times 10^{-3} \exp -(11{,}560 \pm 120)/RT$

Table II. Tracer diffusion in Li/KCO_3 eutectic melt (42.7/57.3 mole %)

Temp, °C	$D^*_{K^+} \times 10^5$, cm²/sec	Temp, °C	$D^*_{CO_3^=} \times 10^5$, cm²/sec
614	1.07	575	0.69
	1.11		0.72
650	1.35		0.71
	1.36		0.69
	1.42	645	1.20
	1.37		1.20
698	1.84		1.19
	1.84	694	1.59
	1.83		1.67
	1.90		1.62
761	2.68	750	2.29
	2.68		2.30
	2.60		2.35
814	3.50	789	2.92
	3.51		2.93
	3.54		2.88
860	4.24		2.88
	4.29	862	4.13
	4.48		4.17
	4.19		4.10

$D^*_{K^+} = (7.26 \pm 0.43) \times 10^{-3} \exp -(11{,}490 \pm 120)/RT$
$D^*_{CO_3^=} = (7.94 \pm 0.41) \times 10^{-3} \exp -(11{,}860 \pm 100)/RT$

Table III. Tracer diffusion in Na/KCO_3 eutectic melt (58.0/42.0 mole %)

Temp, °C	$D^*_{Na^+} \times 10^5$, cm²/sec	Temp, °C	$D^*_{K^+} \times 10^5$, cm²/sec	Temp, °C	$D^*_{CO_3^=} \times 10^5$, cm²/sec
810	3.32	793	2.86	756	1.22
	3.34		2.91		1.18
840	3.97	850	3.60		1.28
	3.80		3.77	797	1.53
	3.87		3.76		1.49
862	4.35	872	4.18		1.52
	4.31		4.20	819	1.79
	4.43	904	4.94		1.65
904	5.36		4.94		1.72
	5.30		4.96	855	1.94
932	6.07		4.82		2.01
	5.96	912	4.89		1.95
965	6.60		4.91		1.88
	6.33		5.01	891	2.22
			5.01		2.21
		963	6.04		2.36
			6.12	919	2.68
			6.26		2.60

$D^*_{Na^+} = (8.18 \pm 0.74) \times 10^{-3} \exp -(11{,}820 \pm 220)/RT$
$D^*_{K^+} = (7.61 \pm 0.52) \times 10^{-3} \exp -(11{,}840 \pm 170)/RT$
$D^*_{CO_3^=} = (2.71 \pm 0.30) \times 10^{-3} \exp -(11{,}030 \pm 120)/RT$

Table IV. Tracer diffusion in Li_2CO_3 melt

Temp, °C	$D^*_{Na^+} \times 10^5$, cm²/sec
809	1.46
	1.51
858	1.70
	1.78
871	1.80
905	2.12
	2.25

$$D^*_{Na^+} = (1.32 \pm 0.44) \times 10^{-3} \quad \exp - (9{,}630 \pm 370)/RT$$

The constants in the equations were calculated by the method of least squares.

Discussion

The diffusion data from this study together with those from our previous paper, are represented in Fig. 5 in the form of Arrhenius graphs (log D *vs.* $1/T$). Comparing first the magnitudes of the various diffusion coefficients it can be seen that for any given medium, the diffusion mobility varies inversely with the ionic radius. For ions isotopic to a species in the medium similar trends have been observed in alkali metal nitrates (13) and in their binary mixtures (14). It should be noted, however, that this type of dependence does not necessarily hold for nonisotopic trace species as has been shown by Ketelaar and Honig (15).

Another feature which is brought out by Fig. 5 is the marked change in diffusion mobility which is shown by both Na^+ and $CO_3^=$ ions in different media. The Na^+ ion, for instance, has a high coefficient in all the eutectics and in pure Na_2CO_3, but a much lower value in pure Li_2CO_3. This is contrary to what might have been expected if certain aspects of the Lumsden model (3) had been considered to apply. These aspects concern the preferential polarization of anions by the smaller cations in a binary melt. On this model, in Li_2CO_3 the $CO_3^=$ anions would presumably be strongly polarized thus leaving the Na^+ ions with more freedom of movement compared to that in the pure Na_2CO_3 melt. An explanation for the low Na^+ ion mobility can, however, be given if we accept a lattice picture for molten carbonates. The pure Li_2CO_3 melt can then be visualized as a fairly close-packed anion-type lattice, with the small Li^+ ions fitting into the interstices. The trace sodium ions introduced would slightly expand the lattice in their neighborhood, but basically it would remain as in the pure salt. Under these conditions a low diffusion mobility would be expected. As a cooperative act is probably involved, the $CO_3^=$ ion might be expected to have a fairly low mobility in this melt also, but further experiments will be made shortly to check this prediction.

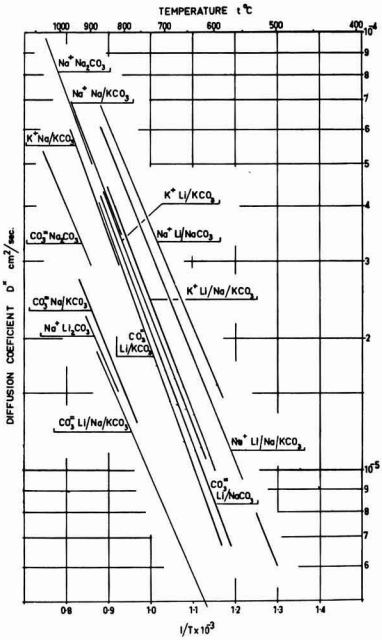

Fig. 5. Arrhenius graphs of the measured diffusion coefficients of various ions in pure alkali metal carbonates and their binary and ternary eutectics.

The $CO_3^=$ ion has a low mobility in the Na/K and Li/Na/K eutectics and pure Na_2CO_3, but it almost exactly doubles in the Li/K and Li/Na eutectics. There is no obvious explanation for the marked change in diffusion mobility between the two groups of melts. One cannot attribute it solely to greater distortion arising from difference in ion size in the binary eutectics containing lithium because this factor would also operate in the ternary eutectic. The measurement of tracer-diffusion coefficients of the Li^+ ion may help to resolve this problem.

The slopes of the curves in Fig. 5 give the "Arrhenius activation energy" for tracer-diffusion. As stated in our previous paper (1) the exact significance of these energies and their relation to theory are not known. However, it is generally agreed that they have qualitative value in the interpretation of the mode of diffusion in molten salts. In Table V we have tabulated these experimental activation energies together with those available for other transport processes.

The differences between the experimental activation energies for conductance, viscous flow, and tracer diffusion, and possible qualitative explanations of these differences have been discussed in our first paper. In brief, the high activation energy for viscous flow in the pure melt was attributed in part to the necessity to shear a lattice which derives its stability from the coulombic forces between the ions. The low value for conductance was explained by the ability of cations to migrate through the lattice without appreciable disturbance whereas the constancy of the diffusion activation energies suggested some kind of cooperative act between anion and cation. The new data which have been added reinforce these conclusions. In particular the similarity between the diffusional activation energies for all ions studied in the six media is again most striking. The inference that diffusional movement in these melts proceeds by some cooperative act, which may be a coupled vacancy mechanism, ion-pair motion, or cluster movement, seems inescapable. At the moment evidence from other fields as summarized by Janz and co-workers (16) favors the ion-pair concept of the form $(M^+CO_3^=)^-$.

The appearance of a recent paper by Moynihan and Laity (2) in which they predicted that tracer diffusion coefficients in binary melts might be expected to show a closer linear dependence with composition than the

Table V. Experimental activation energies of transport in alkali carbonate melts

Medium	E_Δ, kcal/eq.	E_{visc}, kcal/mole	E_D*, kcal/mole
Na_2CO_3	4.23 (16a)	25.7 (16b)	12.2 (Na⁺)
			10.6 ($CO_3^=$)
Li_2CO_3	4.60 (16d)		9.6 (Na⁺)
$Li/NaCO_3$ eutectic	4.53 (16d)		11.0 (Na⁺)
			11.6 ($CO_3^=$)
Li/KCO_3 eutectic	4.49 (16d)		11.5 (K⁺)
			11.9 ($CO_3^=$)
Na/KCO_3 eutectic	3.96 (16d)		11.8 (Na⁺)
			11.8 (K⁺)
			11.0 ($CO_3^=$)
$Li/Na/KCO_3$ eutectic	6.46 (16c)	10.7 (16b)	11.1 (Na⁺)
			11.9 (K⁺)
			10.1 ($CO_3^=$)

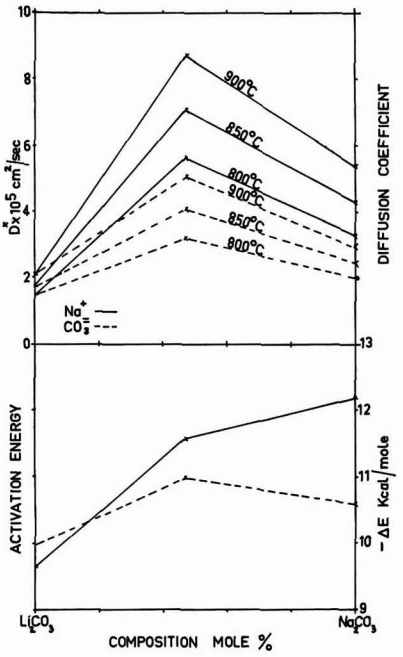

Fig. 6. Activation energies and tracer-diffusion coefficients of Na^+ cation and $CO_3^=$ anion in Li_2CO_3/Na_2CO_3 mixtures.

ionic conductances, prompted us to make preliminary measurements of this kind. These measurements are for Na^+ and $CO_3^=$ ions at the eutectic composition of the $Li/NaCO_3$ binary mixture, Na^+ in Li_2CO_3 and Na_2CO_3 and $CO_3^=$ in Na_2CO_3. The results are shown in graphical form in Fig. 6. For the reasons outlined earlier, we have tentatively assigned a value for $CO_3^=$ ion in Li_2CO_3 equivalent to that for Na^+ ion. It is evident that the tracer diffusion coefficients for Na^+ and $CO_3^=$ at the indicated temperatures are by no means linear with composition, but instead show a marked positive deviation from the additivity line. This is to be compared with the results of Lantelme and Chemla (14) in the alkali nitrates who have reported a positive deviation for K^+ in $KNO_3/LiNO_3$ mixtures. Other cations, however, exhibit a near linear dependence. Further points of interest are that the Na^+ ion diffusion mobility is lower in Li_2CO_3 than in Na_2CO_3 which is in contrast to cation diffusion in the alkali nitrates. Lantelme and Chemla (14) have shown that Li^+, Na^+, and K^+ ions diffuse faster when going over a composition range from KNO_3 to $LiNO_3$. However they have reported more recently (17) that for NO_3^- ion the values diminish as the mixtures are enriched in $LiNO_3$. The high values of the coefficients at the eutectic point are also noteworthy, and these may well represent maxima on the curves. As our measurements were made at a series of temperatures, we have also been able to determine experimental activation energies and these are shown in the lower part of Fig. 6. The values for Na^+ ion rise fairly steadily, and those for $CO_3^=$ ion indicate a maximum. Such trends are not readily explained, and we therefore propose to make measurements to explore this type of behavior further.

We have also made a detailed study of the conductance for this binary system and obtained a negative deviation from the addition line for two of the binary systems. These differences between the two processes serve to reemphasize that the mechanisms of conduction and tracer diffusion in molten salts may differ considerably. (The reservation should be made that the tracer diffusion of Li^+ ion would also need to be measured in order to say definitely that the processes are different in character.) This fact of course has previously been inferred from attempts to apply the Nernst-Einstein equation and from the marked difference between the Arrhenius activation energies for the two processes.

In the context of the fuel cell electrolyte problem, it may be noted that, although $CO_3^=$ ion diffusion is considerably faster in the binary than the ternary eutectics, this seems to have little or no effect in reducing polarization in molten salt cells. Both the binary $Li/NaCO_3$ and the ternary $Li/Na/KCO_3$ eutectics have been used as fuel cell electrolytes and the voltage losses are very comparable in each case (18).

Acknowledgment

Grateful acknowledgment is made to the Reserve Bank of Australia for a grant for fuel cell research, part of which has been used to finance the above study.

Manuscript received Nov. 29, 1965.

Any discussion of this paper will appear in a Discussion Section to be published in the December 1966 JOURNAL.

REFERENCES

1. P. L. Spedding and R. Mills, *This Journal*, **112**, 594 (1965).
2. C. T. Moynihan and R. W. Laity, *J. Phys. Chem.*, **68**, 3312 (1964).
3. J. Lumsden, *Discussions Faraday Soc.*, **32**, 138 (1961).
4. C. A. Angell and J. W. Tomlinson, *ibid.*, **32**, 237 (1961).
5. J. G. Albright, Unpublished work.
6. H. Schlichting, "Boundary Layer Theory," McGraw-Hill Book Co., New York (1955).
7. E. R. G. Eckert and R. M. Drake, "Heat and Mass Transfer," McGraw-Hill Book Co., New York (1959).
8. R. Mills, *J. Am. Chem. Soc.*, **77**, 6116 (1955).
9. J. Rastas and P. Kivalo, *Acta Polytechnica Scandinavica*, **C35** (1964).
10. J. O'M. Bockris and G. W. Hooper, *Discussion Faraday Soc.*, **32**, 218 (1961).
11. J. F. Kasener, R. J. Russel, and R. C. Grace, *Trans. Am. Soc. Metals*, **55**, 858 (1962).
12. A. Z. Borucka, J. O'M. Bockris, and J. A. Kitchener, *Proc. Roy. Soc.*, **A241**, 554 (1957).
13. A. S. Dworkin, R. B. Escue, and E. R. Van Artsdalen, *J. Phys. Chem.*, **64**, 872 (1960).
14. F. Lantelme and M. Chemla, *C. R. Acad. Sci., Paris*, **258**, 1484 (1964).
15. J. A. A. Ketelaar and E. P. Honig, *J. Phys. Chem.*, **68**, 1596 (1964).
16. (a) G. J. Janz and M. R. Lorenz, *This Journal*, **108**, 1052 (1961); (b) G. J. Janz and F. Saegusa, *ibid.*, **110**, 452 (1963); (c) Ward and G. J. Janz, *Electrochim. Acta*, **10**, 849 (1965); (d) Unpublished work.
17. F. Lantelme and M. Chemla, Abstracts, 16th C.I.T.C.E. Meeting, Budapest, 217 (Sept. 1965).
18. G. J. Young, "Fuel Cells," Chap. 6, 8, Reinhold Publishing Co. New York (1960).

The Role of Crystalline Orientation on the Behavior of Copper as Electrode in Chloride Solutions[1]

Ugo Bertocci

Solid State Division, Oak Ridge National Laboratory, Oak Ridge, Tennessee

ABSTRACT

Single crystal copper electrodes having (100), (110), (111), and (321) orientations, as well as polycrystalline specimens, have been used as electrodes in chloride solutions containing cuprous ions, previously equilibrated with copper metal under a hydrogen atmosphere. Anodic and cathodic overvoltages as a function of current density have been recorded in the range from 10^{-7} to 10^{-3} amp/cm^2. Faceting patterns formed by electrolysis at various current densities, as well as those formed by corrosion in nonequilibrated solutions, have been examined, using both the optical microscope and the double-circle reflection goniometer. In all instances, it has been found that the behavior of (100) oriented surfaces was quite different from that of all other orientations investigated. The overvoltages recorded for (100) electrodes were considerably higher, exhibiting an extremely high $(d\eta/di)_{i=0}$ of the order of 10^5 ohm-cm^2. Lower overvoltages were found on the other close-packed orientations, differences between them being only minor, and the lowest values were exhibited by (321) oriented electrodes.

The faceting behavior of (100) surfaces was also different from that of all other orientations: whereas (100) developed only facets vicinal to {100}, the other surfaces formed a completely different set of facets, including {111} and {110}. By correlating the overvoltage data and the faceting structure, some suggestions are made concerning the relative influence of elementary processes, such as nucleation of new steps and their motion across the surfaces on the kinetic behavior. The most likely conclusion at this stage seems to be that the rate-determining step is linked to the removal or addition of atoms to the surface steps.

The study of the electrochemical behavior of copper in halide solutions presents the possibility of examining the electrode reaction between copper metal and cuprous ions, since divalent copper plays only a minor role. In addition, in such solutions the etching pattern can be made very sensitive to the structure of the crystalline phase, as evidenced by the formation of pits at dislocations (1). Overvoltage data for copper in chloride solutions being relatively scarce, it was interesting to collect information on the kinetic behavior in such systems as a function of crystal orientation, particularly in the low current density range, where the properties of the metal surface can be rate determining.

In this paper the results of some experiments showing the influence of crystal orientation on the electrochemical behavior of copper are described and discussed.

Experimental Methods

The copper crystals used for the experiments were disk-shaped slices cut from 99.999% Cu single crystal slugs. The dislocation density was of the order of 10^5/cm^2. The cutting method has already been described (2). In order to obtain orientations as close as possible to the desired ones (usually within one half of a degree or less), before polishing the surfaces on the lapping wheel, the etched crystals were positioned on an adjustable holder, using a microscope fitted with the Nomarski interference contrast attachment to control their orientation. The technique employed to measure the orientation of etching facets, as well as the modifications to the microscope, are described elsewhere (3).

After a final electropolishing in a phosphoric acid bath, the crystals were mounted in the electrolysis cell against glass tubings, having beveled Teflon gaskets at their ends, so that the electrodes exposed only one orientation to the solution. Three crystals were mounted in the same cell. A more detailed description of the cell has been given in a previous paper (4). The cell was evacuated and filled with purified hydrogen several times, and then the solution, which had been equilibrated with copper metal, was transferred in the cell under hydrogen pressure.

Overvoltage measurements were carried out by passing a constant current pulse between the electrode under investigation and an auxiliary electrode by means of a group of dry cells and a large resistance in series. The voltage *vs.* time curves were recorded on a strip chart recorder coupled to a high-impedance amplifier. In most experiments the reference electrode was a saturated calomel electrode. Sometimes the curves were recorded on a cathode-ray oscilloscope, a suitable timing device giving the required synchronization to display the signal on the scope screen.

Because of the small currents employed and the high conductivity of the solution, no device for minimizing the errors due to ohmic drop was used; checks carried out comparing data taken from reference electrodes positioned at different distances from the electrode under study, as well as inspection of the voltage-time curves on the cathode ray oscilloscope, showed that the ohmic drops included in the readings were always negligible.

For qualitative information on the relative rate of attack of different orientations, some etching experiments were also carried out on spherical single crystals; their surfaces were prepared by electropolishing in a phosphoric acid bath.

After the experiments the copper electrodes were examined under the optical microscope, and the orientation of the faceting pattern obtained was studied by means of a double circle reflection goniometer.

Experimental Results

Preliminary investigations were directed to finding whether specimens having different surface orientation exhibited different equilibrium potentials. It was soon realized, however, that the solutions always contained cupric ions in excess of the equilibrium concentration and therefore the electrodes were corroding. The corrosion rate, due to oxygen leakage into the cell, was estimated to be of the order of 20-50 μa/cm^2,

[1] Research sponsored by the U. S. Atomic Energy Commission under contract with Union Carbide Corporation.

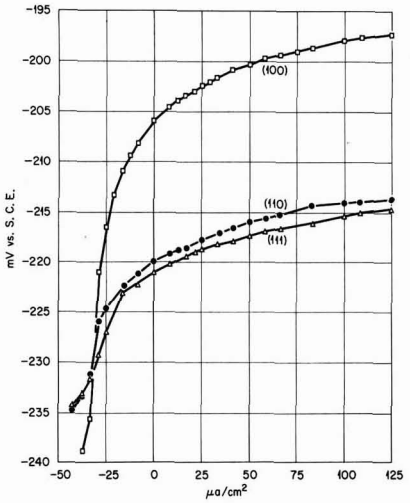

Fig. 1. Overvoltages of Cu single crystals in 0.03M Cu, 2.7M HCl under slow corrosion; temperature 23.5°C.

as calculated from the increase of Cu concentration in solution.

Further improvements in the experimental setup reduced the corrosion rate below any detectable value; accordingly, the former experiments will be referred to as experiments under corrosion, and the latter ones as experiments in absence of detectable corrosion. Even in the latter case, however, it is believed that the solution composition was not that corresponding to equilibrium, and the experimental results are interpreted according to this assumption.

Experiments under corrosion.—The potential differences between different surface orientations under slow corrosion conditions showed that after a very short period of time a steady state was reached in which the (100) orientation was nobler than (110) and (111) by about 15 mv. This potential difference could be maintained within 3 to 5 mv for periods of time as long as 16 days, after which the experiment was stopped. (111) crystals were slightly more negative than (110). Potential *vs.* current density curves recorded on these slowly corroding specimens are shown in Fig. 1. The overvoltage curves for the various orientations intersect at a certain value of cathodic current density. This value is approximately equal to the corrosion rate determined from the increase with time in copper concentration in solution.

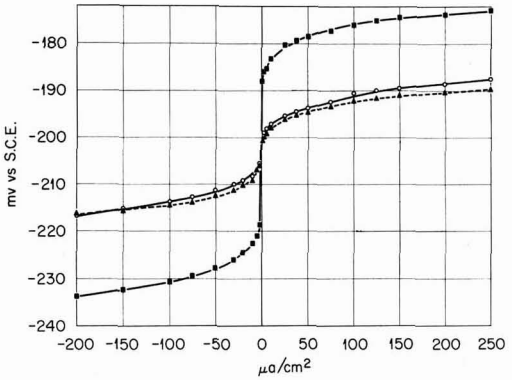

Fig. 2. Overvoltages of Cu in 0.09M Cu, 2M KCl, 1M HCl. ■ (100), ▲ (111), ○ (321); temperature 23.5°C.

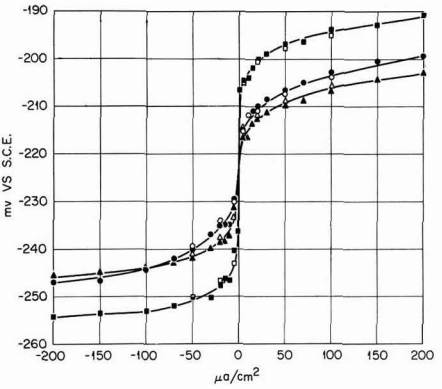

Fig. 3. Overvoltages of Cu in 0.04M Cu, 2.7M HCl. Decreasing CD, □ (100); △ (321); ○ polycrystalline; increasing CD, ■ (100); ▲ (321); ●, polycrystalline; temperature 23.5°C.

Inspection of the surfaces after the test showed extensive faceting on all orientations. On (100) crystals shallow square pits were formed at an early stage, and they subsequently grew to cover the whole surface, leaving it uniformly faceted. The (111) crystals had large plateaus of the original (111) orientation, bounded by steep walls; (110) surfaces were covered by grooves oriented toward <110>. Examination with the reflection goniometer revealed that the original (100) orientation had disappeared completely, and the facets formed lay in a region between 2° and 4° from (100), producing a square reflection pattern with corners toward <100>. The reflection patterns for (110), (111), and (321) orientations were remarkably similar to each other: sharp reflections were found at {111} and {110}, and also there was a diffuse reflection around {100} approximately square-shaped with corners about 15° from {100} toward <100>.

Experiments in absence of detectable corrosion.—The overvoltage *vs.* current density curves obtained in absence of detectable corrosion are given in Fig. 2 and 3. In order to determine the point where the curves relative to different surface orientations intersect and where they exhibit the maximum slope, the extremely low anodic and cathodic current density range was examined in detail (Fig. 4 and 5). The results show that the cathodic and anodic branches of

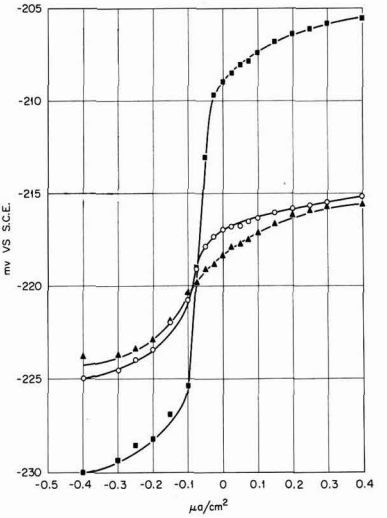

Fig. 4. Overvoltages of Cu in 0.04M Cu, 2.7M HCl. ■ (100), ▲ (321), ○ polycrystalline; temperature 23.5°C.

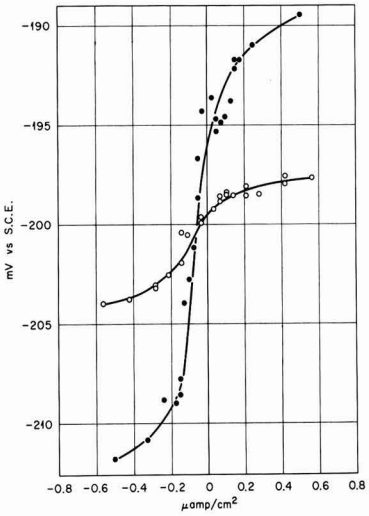

Fig. 5. Overvoltages of Cu in 0.09M Cu, 2M KCl, 1M HCl. ● (100), ○ (111); temperature 23.5°C.

the overvoltage curves are symmetric with respect to a middle point which, within the accuracy of the experimental method, is common to all crystal orientations. The point of intersection corresponds to a cathodic current density, whose value tended to become smaller with time: typically it was about 0.8-0.5 $\mu a/cm^2$ on the first few days after introduction of the solution and then decreased to less than 0.1 $\mu a/cm^2$. During this period the overvoltage curves did not vary except for a translation along the current density axis.

Evaluation of the maximum slope of the overvoltage curves is rather inaccurate: for (100) crystals the value ranges from 10^5 to 4.10^5 ohm-cm^2, whereas the other orientations give values from 10^4 to 7.10^4 ohm-cm^2.

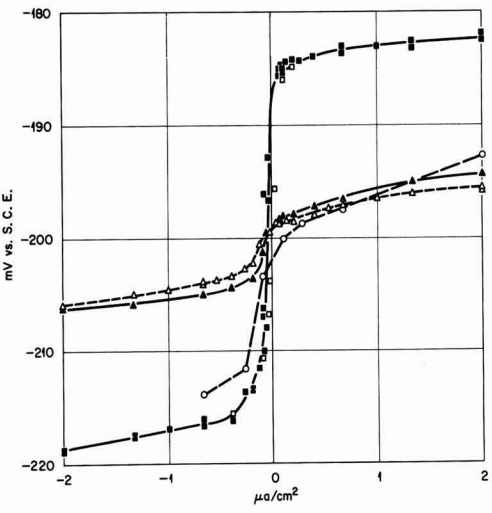

Fig. 6. Effect of anodic attack and cathodic deposition on overvoltages of Cu single crystals. ■ (100); □ (100) after anodic attack at 3.3 $\mu a/cm^2$ (12.8 mcoul/cm^2); ○ (100) after cathodic deposition at 3.3 $\mu a/cm^2$ (13.4 mcoul/cm^2); ▲ (111); △ (111) after anodic attack at 3.3 $\mu a/cm^2$ (0.298 coul/cm^2). Solution: 0.09M Cu, 2M KCl, 1M HCl; temperature 23.5°C.

The effect of extensive electrolysis on the overvoltage curves was investigated, and some of the results are given in Fig. 6. For (111) orientations and also for all orientations other than (100), anodic attack tends to lower slightly the overvoltage curves, whereas (100) surfaces are hardly affected. Extended cathodic deposition on (100) crystals greatly affects the anodic branch of the overvoltage curve, which becomes similar to that found for other orientations, but has a much smaller effect on the cathodic values. An anodic attack approximately equal to one-half of the preceding cathodic pulse is generally sufficient for restoring the usual overvoltage curve.

After a cathodic current pulse the electrode potential decayed to its open-circuit value in two stages, separated by an inflection point of minimum slope; the potential value of the inflection point was found to be very close to that of the middle point about which the overvoltage *vs.* current density curves are symmetric. The decay time was longer the greater the quantity of electricity of the preceding cathodic pulse, the inflection point becoming a plateau of almost constant potential. The phenomenon is similar to that observed on polycrystalline zinc in acidic solutions (5).

After a sufficiently long anodic attack the faceting pattern could be observed. It was found that the surface structure as well as the reflection pattern was the same as that observed under corrosion conditions, provided that the current density chosen was of the same order of magnitude. Some changes were detected in the faceting pattern for dissolution at higher current densities; for instance, a reflection spot corresponding to {47,20,0} was quite clearly observed on (111) and (321) crystals attacked at 1 ma/cm^2, whereas at the same current density (100) surfaces developed, besides the usual pattern, facets very close to the {100} orientations at 90° from the original one. On the whole, however, the etching pattern was found to be rather insensitive to anodic current density in the range studied.

After etching spherical single crystals, small bright areas were found at {111} and {110}, as well as a square-shaped area around {100}, with corners about 15° from [100] toward <100>. The remainder of the sphere was heavily faceted, but no attempt was made to measure the orientations of the facets formed.

Discussion

The high resistance for the electrode reaction in the low current density range as deduced by the slope of the overvoltage curves places such stringent requirements on the magnitude of the rate of spontaneous processes, (for example, corrosion caused by an excess of cupric ions over the equilibrium concentration), which can be allowed without significant departure of the electrodes from the equilibrium potential, that it is impossible to attach thermodynamic significance to the open-circuit potentials. The fact, however, that the curves relative to different orientations as measured in the same solution intersect for the same value of potential and current density, plus the fact that the overvoltage curves are symmetric with respect to the intersection point, which lies on the point of maximum slope, lend support to the conclusion that the potential associated with the intersection point is the equilibrium potential for all copper electrodes investigated. If the validity of this criterion for determining the equilibrium potential is accepted, it can be concluded that single crystals of different orientation, as well as polycrystalline electrodes, have the same equilibrium potential, or at least that the differences are smaller than 1 to 2 mv. Analogous conclusions had been previously reached for copper single crystals in sulfate solutions (4). All the differences recorded between rest potentials can be easily accounted for in terms of differences in their kinetic behavior.

If the point where the various curves intersect can be assumed to correspond to the equilibrium potential,

the cathodic current density necessary to maintain such a potential will correspond to the reduction of cupric ions diffusing from the bulk of the solution to the electrode

$$(i)_{\eta=0} = \frac{FD_{Cu^{++}}}{\delta}\left[Cu^{++}{}_{eq} \exp\left(\frac{\mathbf{F}}{RT}\eta'\right) - Cu^{++}{}_{bulk} \right] \quad [1]$$

where δ is the thickness of the diffusion layer, $Cu^{++}{}_{eq}$ and $Cu^{++}{}_{bulk}$ are total concentrations of Cu^{++} ions, whether free or as chloride complexes, at equilibrium and in the bulk, $D_{Cu^{++}}$ is the diffusion coefficient valid for the solution composition in which the experiment is carried out, and η' is the overvoltage for the reaction

$$Cu^{+} \rightleftarrows Cu^{++} + \theta \quad [2]$$

Here the assumption is made that homogeneous equilibria are fast and that transference numbers for copper ions are negligibly small, because of the large excess of indifferent electrolyte. The results shown in Fig. 1, where even for relatively large values for $(i)_{\eta=0}(\sim 30\ \mu a/cm^2)$ the point of maximum slope in the overvoltage curves corresponds to the same current density for (100), (110), and (111) crystals, indicate either that η' is relatively insensitive to orientation or that it is negligibly small. The second alternative can be reasonably accepted when the current density is of the order of 10^{-7} amp/cm^2. In this case formula [1] can be employed to estimate the excess of Cu^{++} in the bulk over the equilibrium concentration. The evaluation of the product $D_{Cu^{++}}(Cu^{++})$ is unfortunately very difficult, since the values of the stability constants for cupric chloride complexes, as quoted in the literature, vary considerably from author to author (6). The diffusion coefficient is probably abnormally large, as shown by the negative transference number of copper in complex cupric chloride solutions (7). By assuming a value of 100 amp cm/mole for $FD_{Cu^{++}}/\delta$ and considering that $Cu^{++}{}_{eq}$ should be of the order of 10^{-11} mole/cm^3, a current density of 10^{-7} amp/cm^2 would indicate that the concentration in the bulk of the solution was from 20 to 100 times greater than the equilibrium value.

Because of the extreme steepness of the overvoltage curve at very low current densities, particularly in the case of (100) surfaces, the question can be raised as to whether any process involving dissolution or deposition actually takes place in this range, or only the redox reaction [2], which does not involve any alteration of the metal surface, occurs at the electrode. If one assumes that reaction [2] occurs without appreciable overvoltage, around the equilibrium potential the slope of the overvoltage curve as given by reaction [2] alone is (8)

$$\left(\frac{d\eta}{di}\right)_{\eta=0} = \frac{RT\,\delta}{F^2 D_{Cu^{++}}(Cu^{++}{}_{eq})}$$

Again the calculation entails the knowledge of the product $D_{Cu^{++}}(Cu^{++}{}_{eq})$, and it is subject to the uncertainties already mentioned. Using the most reliable data, the reaction resistance due only to reaction [2] should be about 10 megaohms-cm^2, that is, more than a factor of ten higher than the value measured on (100) surfaces. This would support the conclusion that deposition or dissolution occur at a nonzero rate for every overvoltage value.

The homogeneous reaction

$$CuCl'_2 \rightleftarrows Cu^{+} + 2Cl' \quad [3]$$

which in chloride solution is coupled to the electrode reaction, was not found to have any effect on the over-all reaction rate in the range of current densities investigated. Since the equilibrium potential of Cu with respect to SCE is about —0.2v, the Cu^{+} ion activity is of the order of 10^{-8} mole/liter. If reaction [3] were slow, a small limiting current for the cathodic discharge should be found. The experimental results, however, have shown that no limiting current phenomena can be detected.

The shape of the decay curves after short cathodic pulses, as well as the effect of extensive deposition on (100) crystals on the subsequent anodic overvoltages can be explained by assuming that the surface structure of the deposits is different from that formed by anodic attack. Therefore, after a cathodic pulse under conditions of slight corrosion, the freshly deposited copper will exhibit a low anodic overvoltage, giving rise to an inflection in the decay curve. Accordingly, the potential of the inflection was the closer to the point of maximum slope of the overvoltage curve, the smaller was the departure from equilibrium in solution, and it was found to be in general more positive, by a few millivolts, than the equilibrium value as determined in the way outlined in the first part of this discussion. After extensive deposition on a (100) surface, anodic overvoltages similar to those on the other orientations could be measured, until dissolution eliminated the surfaces having low overvoltage. Although no systematic examination of the surface structure of cathodic deposits has been made, some instances of formation of facets never observed after anodic attack on (100) crystals were found.

Conclusions

Examination of the experimental results does not indicate that on any orientation the nucleation of new steps is rate determining, since extensive anodic attack leading to a faceted surface has little influence on the overvoltage values. Comparison of the overvoltage curves of (111) and (321) crystals supports the same conclusion. On (321) surfaces no nucleation is theoretically required for the dissolution or crystallization process; nevertheless, the overvoltages are very close to those measured on a close-packed surface like the (111). The facets formed on (111) and (321) have the same orientation, but on the latter the number of edges is significantly greater, which would account for the slightly lower reaction resistance, but fails to single out the formation of new steps as the kinetically decisive phenomenon.

It is therefore likely that the motion of steps is rate controlling; on (100) crystals such a motion is very slow and difficult, so that the surface is left covered by steps giving the characteristic faceting pattern slightly misoriented from (100); on the other orientations, steps move at a much higher speed, and this accounts for the lower overvoltages as well as for the faceting pattern: smooth (111) facets are formed, and the steps interact easily forming orientations at large angles from the original surfaces. Not all difficulties in interpreting the results are eliminated by such a conclusion; one would expect a greater influence of the number of steps on the surface if their motion were the slowest process. Above a relatively low current density, however, the overvoltage curve flattens out considerably, so that an increase in number of steps will cause a small decrease in overvoltage. Moreover. microscopic observation shows that on (111), (110), and (321) crystals a large part of the new surface area created by faceting is oriented about 15° from (100), an orientation having rather high reaction resistance, as evidenced by the etching pattern on spherical single crystals.

On the cathodic side, the remarkable influence of extended deposition on the subsequent anodic overvoltages of (100) orientations indicated that the deposit does not have the same surface structure as the substrate. Incorporation of the deposited copper into the lattice occurs slowly, as indicated by the inflection points in the decay curve after short cathodic pulses.

The shape of the overvoltage curves, however, suggests the hypothesis that a nucleation process is necessary to initiate the removal of copper from the steps or its addition to them.

Manuscript received Nov. 1, 1965.

Any discussion of this paper will appear in a Discussion Section to be published in the December 1966 JOURNAL.

REFERENCES

1. U. Bertocci, L. D. Hulett, and L. H. Jenkins, *This Journal*, **110**, 1190 (1963).
2. F. W. Young, Jr., and T. R. Wilson, *Rev. Sci. Inst.*, **32**, 559 (1961).
3. U. Bertocci and T. S. Noggle, In press.
4. L. H. Jenkins and U. Bertocci, *This Journal*, **112**, 517 (1965).
5. U. Bertocci, *Rend. Ist. Lombardo Sci. e. Lett.*, **91**, 39 (1957).
6. L. G. Sillén and A. E. Martell, "Stability Constants of Metal Ion Complexes," The Chemical Society, London (1964).
7. J. Bjerrum, *Kem. Maanedsblad*, **26**, 24 (1945); V. Kohlschütter, *Ber. deutsch. chem. Ges.*, **37**, 1153 (1904); S. B. Watkins and H. G. Denham, *J. Chem. Soc.*, **115**, 1269 (1919).
8. U. Bertocci, *Electrochim. Acta*, In press.

Induced Polarization of Porous and Tubular Electrodes[1]

F. A. Posey and S. S. Misra

Chemistry Division, Oak Ridge National Laboratory, Oak Ridge, Tennessee

ABSTRACT

The apparent resistance of solutions contained in porous or tubular electrodes is affected by the presence of oxidizable and reducible substances in solution. Passage of current is accompanied by a gradient of potential in the solution phase so that a gradient of the interfacial potential difference is induced throughout the length of the electrode. As a consequence of the induced polarization, anodic and cathodic reactions occur near opposite ends of the electrode. A number of boundary value problems corresponding to this physical situation have been solved. The relations suggest that induced polarization measurements can be used to determine the concentration of oxidizable and reducible substances in flowing streams, to measure corrosion rates of pipes or porous metals, and to estimate transfer coefficients and exchange current densities of electrochemical reactions.

The conductivity of electrolytes in porous nonconducting materials is not difficult to measure in principle, and measurements of this type have been made for various purposes. As noted by Ksenzhek, Kalinovskii, and Baskin (1), it is more difficult to measure the conductivity of solutions inside porous or tubular metallic electrodes. This is particularly true when oxidation reduction reactions can occur at the metal-solution interface. Passage of current through the solution phase induces a gradient of the interfacial potential difference throughout the length of the electrode. As a consequence of this gradient, anodic reactions occur at the pore walls near one end of the electrode, and cathodic reactions take place near the other end. A fraction of the total current is conducted by ions in the solution phase, and the rest of the current is conducted by electrons in the metallic phase; this fraction depends on the geometrical properties of the electrode, the characteristics of the electrolyte and the electrochemical reactions, and the position inside the electrode. A number of boundary value problems corresponding to this physical situation have been solved by use of methods for the calculation of polarization in porous electrodes (2). The results are presented below together with some experimental measurements which support the theory. The relations obtained suggest that induced polarization of porous and tubular electrodes can be used to determine the concentration of oxidizable and reducible substances in flowing streams, to measure corrosion rates of pipes or porous metals, and to estimate certain parameters of electrochemical reactions.

Experimental Configuration

A schematic diagram of the experimental arrangement for measurement of induced polarization of porous or tubular electrodes is shown in Fig. 1. The total current (i) is passed from the front side ($x = 0$) to the back side ($x = l$) of the electrode by use of auxiliary polarizing electrodes. No current lead is attached to the porous electrode itself; potential changes which occur in this electrode are induced by passage of current between the polarizing electrodes. The potential of the front or back sides and the total potential drop through the electrode may be measured by use of reference electrodes situated at $x = 0$ and $x = l$. Passage of current in the direction shown in Fig. 1 induces a negative change in interfacial potential difference (negative polarization) near $x = 0$ and a positive polarization near $x = l$. When oxidizable and reducible substances are present in solution, cathodic reactions can occur near $x = 0$ as a consequence of the induced negative polarization and, correspondingly, anodic reactions can occur near $x = l$. This electrode configuration is essentially the same as the bipolar electrode studied by Tomassi and co-workers (3-6) as a means of coupling electrochemical processes.

Induced Polarization with Linear Rate Law

The solution resistance in porous or tubular electrodes, measured in the absence of oxidizable and reducible substances by use of the configuration of Fig. 1, is given simply by Eq. [1], where R_o is the resistance of electrolyte

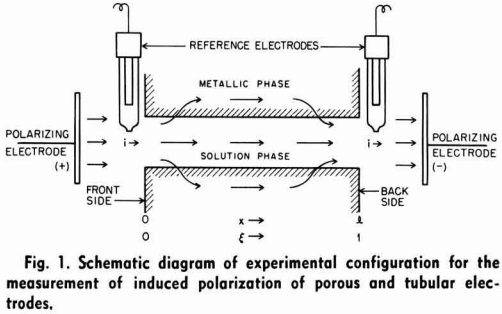

Fig. 1. Schematic diagram of experimental configuration for the measurement of induced polarization of porous and tubular electrodes.

[1] Research sponsored by The Office of Saline Water, U. S. Department of the Interior, under Union Carbide Corporation's contract with the U. S. Atomic Energy Commission.

$$R_o = \frac{\phi_s(0) - \phi_s(l)}{i} = \frac{l}{\sigma A} \qquad [1]$$

in the pores (ohm), $\phi_s(0)$ and $\phi_s(l)$ are potentials in the solution phase at $x = 0$ and $x = l$ (volt), i is total current (amp), l is pore length (cm), σ is specific conductance of the electrolyte ($ohm^{-1}cm^{-1}$), and A is total cross-sectional area of electrolyte (cm^2). In the presence of oxidation reduction reactions the measured or apparent resistance, R_{app}, is less than R_o because of the shunting effect of the current carried by the metallic phase, which is assumed to have negligible resistivity (see below, however). The apparent resistance may be calculated in certain cases by solution of Eq. [2], which is the fundamental differential equation for potential

$$\frac{d^2\eta(x)}{dx^2} = \frac{S}{\sigma A} j(x) \qquad [2]$$

distributions in one-dimensional porous electrodes (2, 7-9). In Eq. [2], $\eta(x)$ is the polarization or change in interfacial potential difference at the point x induced by passage of current (i), S is interfacial surface area per unit length of electrode (cm^2/cm), and $j(x)$ is the current density of the interfacial reaction (amp/cm^2). Boundary conditions corresponding to the configuration of Fig. 1 are given by Eq. [3]. For the case of a simple

$$\left(\frac{d\eta(x)}{dx}\right)_{x=0} = \left(\frac{d\eta(x)}{dx}\right)_{x=l} = \frac{i}{\sigma A} \qquad [3]$$

oxidation reduction reaction, the rate law may be assumed to be of the conventional form given by Eq. [4], where j_o is the exchange current density

$$j(x) = j_o\{\exp[\beta n \mathcal{F}\eta(x)/RT] - \exp[-(1-\beta)n\mathcal{F}\eta(x)/RT]\} \qquad [4]$$

(amp/cm^2), n is the electron number, β is the (anodic) transfer coefficient, and $RT/\mathcal{F}$ is the thermal volt equivalent. We assume that non-Faradaic currents and changes of reactant concentrations because of the electrochemical reaction are negligible as well as effects due to diffusion, migration, and convection of reactants and to the structure of the double layer.[2]

For sufficiently small values of polarization, Eq. [4] may be linearized to give the rate law of Eq. [5]. Substitution of Eq. [5] into Eq. [2]

$$j(x) = \frac{nj_o\mathcal{F}\eta(x)}{RT} \qquad [5]$$

and integration of the resulting expression with use of the conditions of Eq. [3] lead to the potential distribution of Eq. [6] in terms of the

$$\frac{\eta(\xi)}{i\,R_o} = \frac{\cosh[\sqrt{\kappa}\cdot\xi] - \cosh[\sqrt{\kappa}(1-\xi)]}{\sqrt{\kappa}\cdot\sinh(\sqrt{\kappa})} \qquad [6]$$

dimensionless parameters $\xi = x/l$ and $\kappa = Sj_o l^2 n\mathcal{F}/\sigma ART$. The parameter κ is essentially a ratio of solution impedance to interfacial impedance. Relative potential distributions calculated from Eq. [6] are shown in Fig. 2 as a function of the parameter κ. When κ is less than unity, no appreciable interfacial reaction occurs and the measured resistance should be essentially that given by Eq. [1]. For values of κ large with respect to unity, an appreciable fraction of the current is carried by the metallic phase and R_{app} is less than R_o.

Equation [7] gives the ratio of the apparent resistance to the resistance

$$\frac{R_{app}}{R_o} = 2\,\frac{\cosh(\sqrt{\kappa}) - 1}{\sqrt{\kappa}\cdot\sinh(\sqrt{\kappa})} \qquad [7]$$

[2] Concentration effects may be minimized experimentally by use of flowing solutions. Some of the restrictions cited above are relaxed later in considering transient effects.

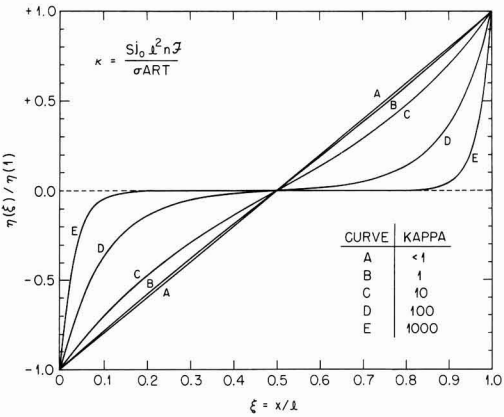

Fig. 2. Relative potential distribution in porous or tubular electrodes as a function of the dimensionless parameter κ.

of the electrolyte (cf. Eq. [1]). The fraction of the total current which is carried by the metallic phase is given by Eq. [8]. For large values of κ,

$$\text{Current fraction} = \frac{\cosh\left(\frac{1}{2}\sqrt{\kappa}\right) - 1}{\cosh\left(\frac{1}{2}\sqrt{\kappa}\right)} \qquad [8]$$

an appreciable region exists inside the electrode where essentially no polarization occurs on passage of current (cf. curve E of Fig. 2). This behavior resembles the phenomenon of the Faraday shield. Variation of the apparent resistance with the parameter κ as predicted by Eq. [7] is shown in Fig. 3. For large values of κ the apparent resistance is inversely proportional to $\sqrt{\kappa}$. The curve in Fig. 3 may be used to estimate κ from measurements of R_{app} if R_o is known. The quotient $1/\sqrt{\kappa}$ is a measure of the degree of penetration of an electrochemical process into a porous electrode (2). Since κ is proportional to j_o, and j_o depends on the concentrations of oxidizable and reducible species (cf. Eq. [10]), Eq. [7] should be applicable to analysis of concentrations of oxidation reduction couples in flowing streams. The relation given by Eq. [7] and shown in Fig. 3 may also be used to estimate corrosion rates of pipes or porous metals from measurements of the apparent resistance. In this case κ is replaced by κ_{corr} of Eq. [9], where j_{corr} is

$$\kappa_{corr} = \frac{S\,j_{corr}\,l^2\,(\beta_a n_a + \beta_c n_c)\mathcal{F}}{\sigma ART} \qquad [9]$$

the current density of the corrosion reaction in the absence of external polarization (amp/cm^2), β_a and β_c are transfer coefficients of the anodic and cathodic

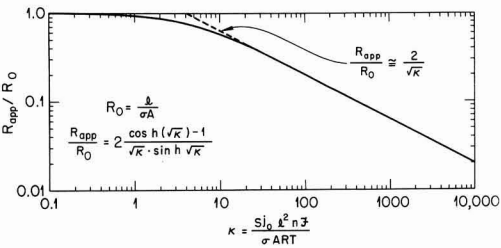

Fig. 3. Variation of the apparent resistance of porous or tubular electrodes with the parameter κ.

processes, and n_a and n_c are the corresponding electron numbers.

Determination of the Transfer Coefficient by Induced Polarization

The transfer coefficient of oxidation reduction reactions may be determined by measurement of induced polarization when the linear rate of law of Eq. [5] is a good approximation. The exchange current density may be expressed by Eq. [10] where j_o^o is the standard exchange current density including

$$j_o = j_o^o C_R^{(1-\beta)} C_o^{\beta} \qquad [10]$$

activity coefficients (amp-cm/mole) and C_R and C_o (mole/cm^3) are concentrations of anodic and cathodic reactants, respectively (10). When C_R and C_o are large enough so that R_{app}/R_o is less than about 0.5 (cf. Fig. 3), Eq. [7] reduces to $R_{app}/R_o = 2/\sqrt{\kappa}$ and substitution of the relation for κ leads to Eq. [11]. In Eq. [11], $\kappa_o = S\, j_o^o\, l^2\, nF/\sigma ART$. Combination of Eq. [10]

$$\frac{j_o}{j_o^o} = \frac{4}{\kappa_o}\left(\frac{R_o}{R_{app}}\right)^2 \qquad [11]$$

and [11] leads to Eq. [12] which shows that a log-log plot of $C_R(R_{app}/R_o)^2$

$$C_R\left(\frac{R_{app}}{R_o}\right)^2 = \frac{4}{\kappa_o}\left(\frac{C_R}{C_o}\right)^{\beta} \qquad [12]$$

against (C_o/C_R) should be linear with a slope of $-\beta$.

Figure 4 shows a plot of the type suggested by Eq. [12] for induced polarization of the ferrocyanide-ferricyanide couple in 0.5M K_2SO_4 at 25°C in a gold tube. The apparent resistance was measured as a function of the ratio of concentrations of oxidized and reduced species (ferricyanide and ferrocyanide concentrations varied in the range 10^{-3} to $10^{-2}M$). The line shown in Fig. 4 corresponds to a transfer coefficient of 1/2. Our data seem to support this value of the transfer coefficient, which was also reported by others (11). The data of Fig. 4 correspond to $R_{app}/R_o \cong 0.15$ so that $\kappa \cong 2 \times 10^2$.

Induced Polarization Curves

Solution of Eq. [2] for the more general rate law of Eq. [4] cannot be accomplished explicitly for arbitrary values of the transfer coefficient. However, numerical methods of solution may be used and Fig. 5

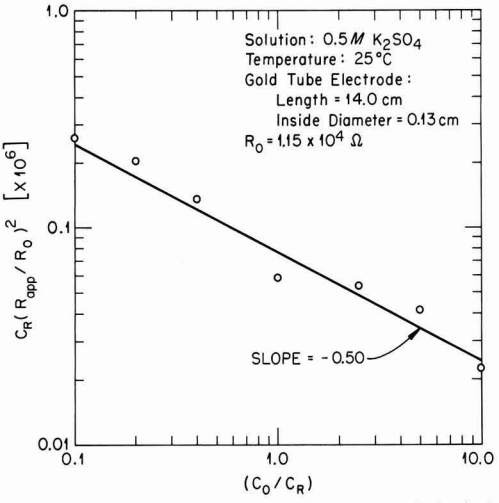

Fig. 4. Determination of the transfer coefficient of the ferricyanide-ferrocyanide couple by induced polarization of a tubular gold electrode.

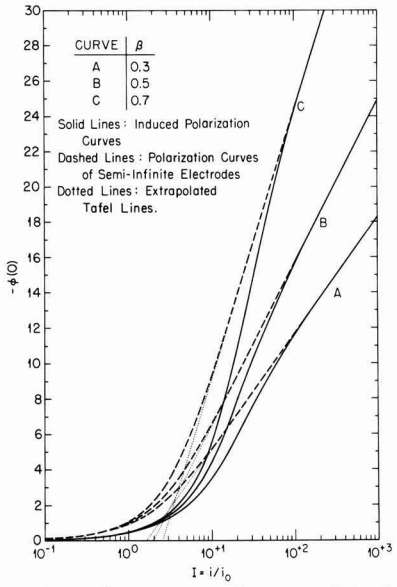

Fig. 5. Induced polarization curves of porous or tubular electrodes as a function of the transfer coefficient, β, for the case $\kappa = 1$.

shows a set of induced polarization curves calculated by use of a high-speed digital computer[3] as a function of the transfer coefficient (β) for the case, $\kappa = 1$. Combination of Eq. [2] and [4] leads to Eq. [13] in which $\phi(\xi) = nF\eta(\xi)/RT$.

$$\frac{d^2\phi(\xi)}{d\xi^2} = \kappa\{\exp[\beta\phi(\xi)] - \exp[-(1-\beta)\phi(\xi)]\} \qquad [13]$$

The sigmoid solid curves in Fig. 5 are solutions of Eq. [13]; $\phi(0)$ is the (reduced) polarization at $\xi = 0$ and $I = i/i_o = i/Slj_o$ is a dimensionless current variable [i_o is the total exchange current (amp)]. At high currents ($i >> i_o$), the induced polarization curve approaches that of a semi-infinite porous or tubular electrode (2). Equation [14] gives the Tafel line

$$I = \left(\frac{2}{\beta\kappa}\right)^{1/2} \exp[-\beta\phi(0)/2] \qquad [14]$$

for this region. At low currents ($i << i_o$), the linear rate law of Eq. [5] is a good approximation and the polarization curve may be calculated from Eq. [6]; this result is given by Eq. [15]. No simple relation can be derived

$$\frac{\phi(0)}{I} = -\sqrt{\kappa}\,\frac{\cosh(\sqrt{\kappa}) - 1}{\sinh(\sqrt{\kappa})} \qquad [15]$$

for the transition region between low and high currents.

Dissymmetry Potentials

One of the unique aspects of induced polarization measurements is the fact that the magnitude of the

[3] Equation [13] was integrated numerically on a computer (Control Data Corporation Model 1604-A) with boundary conditions analogous to those of Eq. [3] by use of a Runge-Kutta method. An initial value of $\phi(0)$ was assumed and the corresponding potential distribution computed from an explicit difference scheme. The interfacial reaction rate distribution was then computed and tested for equality of total anodic and cathodic currents. The sign and magnitude of any difference determined a new value for $\phi(0)$ and the computation cycle was repeated until successive iterations showed little improvement. A similar procedure was used to compute the initial potential distribution in the solution of Eq. [19] and [20]. Concentration changes in successive time intervals were determined by Eq. [20] in difference form; substitution of new concentrations into Eq. [18] then allowed computation of a new potential distribution by solution of Eq. [19] using the iterative procedure noted above.

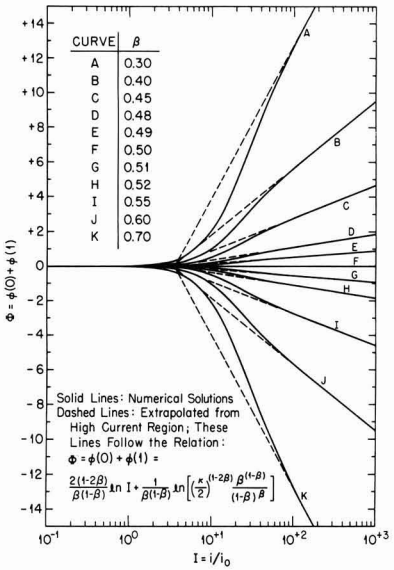

Fig. 6. Dissymmetry potential as a function of applied current and of the transfer coefficient, β, for induced polarization of porous or tubular electrodes ($\kappa = 1$).

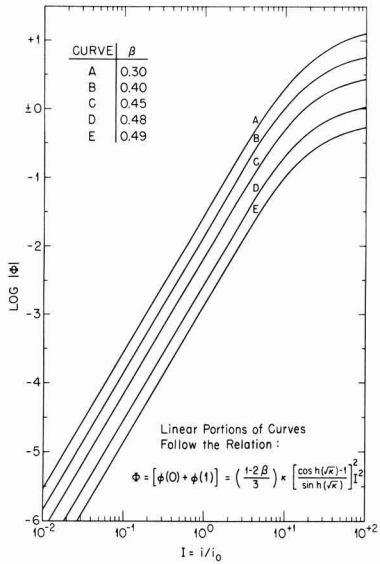

Fig. 7. Dissymmetry potential of porous or tubular electrodes in the region of small currents as a function of the transfer coefficient, β, for the case $\kappa = 1$.

observed polarization of the front side ($x = 0$) may be different from that of the back side ($x = l$). This occurs when $\beta \neq 1/2$ in Eq. [4] so that the rate law is not symmetrical. The sum $\Phi = \phi(0) + \phi(1)$ may be defined as the dissymmetry potential. It is positive or negative depending on whether β is less than or greater than 1/2, respectively. Measurements of the dissymmetry potential (Φ) may be used to determine both β and κ for an oxidation reduction reaction in a porous or tubular electrode.

Figure 6 shows dissymmetry potentials for induced polarization as a function of the reduced current ($I = i/i_o$) and of the (anodic) transfer coefficient (β) for the case, $\kappa = 1$. A Tafel region is observed at sufficiently high currents and the relation for the Tafel line is given by Eq. [16] which was derived by combination of Tafel expressions like Eq. [14]

$$\Phi = \frac{2(1-2\beta)}{\beta(1-\beta)} \ln I + \frac{1}{\beta(1-\beta)} \ln \left[\left(\frac{\kappa}{2}\right)^{(1-2\beta)} \frac{\beta^{(1-\beta)}}{(1-\beta)^{\beta}} \right] \quad [16]$$

for $\phi(0)$ and $\phi(1)$. The slope of the Tafel line depends only on β, and the intercept at $\Phi = 0$ depends on both κ and β. The parameter $\kappa(Sj_o l^2 nF/\sigma ART)$ may be expressed as $\kappa = i_o R_o f$, where $f = n\,\mathcal{F}/RT$ (volt^{-1}), so that the total exchange current of the oxidation reduction reaction (i_o) may be determined easily if R_o is known.

The dissymmetry potential remains finite even at very low currents. Figure 7 shows Φ plotted as a function of current (log-log plot) for a number of values of β when $\kappa = 1$. This type of plot should be useful in detecting small deviations of β from the value 1/2. Expansion of Eq. [4] to quadratic terms and substitution into Eq. [2] yield an expression which can be solved to give Φ in the region of low currents; this relation is given by Eq. [17]

$$\Phi = \left(\frac{1-2\beta}{3}\right)\kappa \left[\frac{\cosh(\sqrt{\kappa}) - 1}{\sinh(\sqrt{\kappa})}\right]^2 I^2 \quad [17]$$

Figure 7 shows that Eq. [17] holds up to $I \cong 5$. The dissymmetry potential varies with the square of the applied current for $I < 5$. If $\kappa = i_o R_o f$ is known, β may be calculated by use of Eq. [17].

Concentration Transients

The solutions for induced polarization effects discussed above apply only when reactant concentrations are essentially constant during a measurement both with respect to time and with respect to position inside the electrode. In the absence of solution flow through the electrode, however, reactant concentrations will change as a result of the Faradaic reactions at the metal-solution interface. The reaction rate at the interface for a simple oxidation-reduction reaction can be expressed as usual (10) by Eq. [18], where $\rho(\xi, t)$ is the reduced reaction rate, $C_R(\xi, t)$ and $C_o(\xi, t)$

$$\rho(\xi,t) = \frac{j(\xi,t)}{j_o} = \frac{C_R(\xi,t)}{C^o} \exp[\beta\phi(\xi,t)] - \frac{C_o(\xi,t)}{C^o} \exp[-(1-\beta)\phi(\xi,t)] \quad [18]$$

are concentrations of reduced and oxidized species, respectively (mole/cm^3), C^o is the initial concentration (we assume for simplicity that $C_R(\xi, 0) = C_o(\xi, 0) = C^o$), and j_o is the initial exchange current density. The potential distribution obeys Eq. [19], which is a form of Eq. [2], providing excess

$$\frac{\partial^2\phi(\xi,t)}{\partial\xi^2} = \kappa \cdot \rho(\xi,t) \quad [19]$$

inert electrolyte is present or reactant and product have the same conductivity contribution. The concentrations may be assumed to change with time approximately according to Eq. [20], where $\theta = nFC^oAl/i_o$ is a time constant

$$\frac{\partial[C_o(\xi,t)/C^o]}{\partial t} = -\frac{\partial[C_R(\xi,t)/C^o]}{\partial t} = \frac{\rho(\xi,t)}{\theta} \quad [20]$$

(sec). We assume that tube or pore sizes are small compared with distances over which appreciable concentration changes occur. The time constant θ is the ratio of the total coulombs available from complete

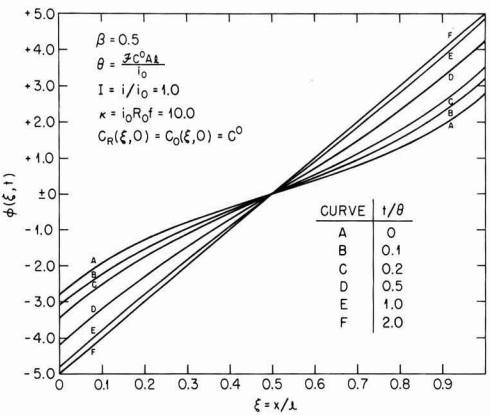

Fig. 8. Variation of induced polarization with time due to oxidation reduction reactions in the interior of a porous or tubular electrode.

reaction of either the oxidized or reduced species to the initial exchange current of the reaction. Potential and concentration transients are obtained by simultaneous solution of Eq. [19] and [20] with use of the boundary conditions of Eq. [21].

$$\left(\frac{\partial\phi(\xi,t)}{\partial\xi}\right)_{\xi=0} = \left(\frac{\partial\phi(\xi,t)}{\partial\xi}\right)_{\xi=1} = \kappa I \qquad [21]$$

Although general solutions of this system of equations are not obtainable in terms of explicit functions, numerical methods may be used to find solutions for particular values of the parameters, β, κ, and I.

Figures 8, 9, and 10 show how the polarization, the reactant concentrations, and the reaction rate change with time and with position in the electrode during the course of a transient. These results were obtained by use of a high-speed digital computer;[3] parameters used were $\beta = 1/2$, $I = 1.0$, and $\kappa = 10.0$. Initially most of the reaction occurs near the ends of the electrode (cf. Fig. 10). With time a reaction "wave" is propagated toward the center of the electrode. Oxidized species react to form reduced species near $\xi = 0$, and the reverse reaction occurs near $\xi = 1$ (cf. Fig. 9). In the new steady state the gradient of the polarization is constant throughout the length of the electrode so that $\phi(1) - \phi(0) = \kappa I$ (cf. curve F of Fig. 8), interfacial reactions no longer occur anywhere in

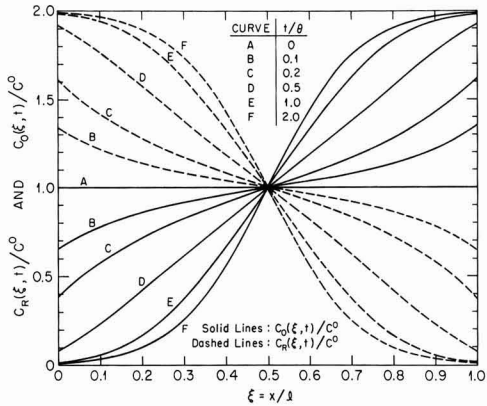

Fig. 9. Variation of reactant concentration profiles with time due to oxidation reduction reactions in the interior of a porous or tubular electrode ($\beta = 0.5$; $\kappa = 10.0$; $I = 1.0$).

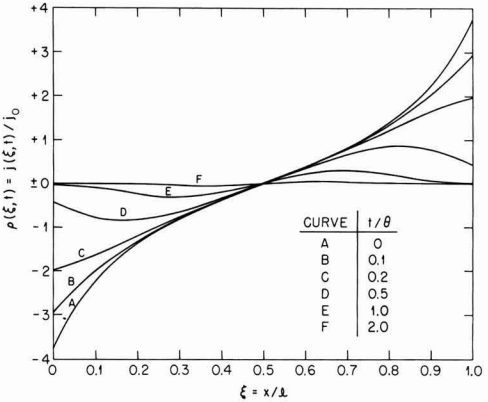

Fig. 10. Variation of current density profile with time due to oxidation reduction reactions in the interior of a porous or tubular electrode ($\beta = 0.5$; $\kappa = 10.0$; $I = 1.0$).

the electrode, and concentrations of oxidized and reduced species are related by the Nernst equation, $C_O(\xi,\infty)/C_R(\xi,\infty) = \exp[\phi(\xi,\infty)]$. During the concentration transient the apparent resistance increases from its initial value up to the limit R_0, the electrolyte resistance which would be observed if no oxidation reduction couple were present in the solution. The time constant θ may be useful as a semi-quantitative measure of the time required for concentration transients in induced polarization measurements. If measurements of apparent resistance are made within about 0.01 θ, no significant concentration changes should occur.

Induced Charging of the Double Layer

Induced charging of the double layer in porous or tubular electrodes in which no Faradaic reactions can occur produces charging transients similar to those obtained by direct galvanostatic charging of porous electrodes. The induced double layer charging transient may be obtained by solution of Eq. [22] (12, 13). The time constant τ is equal to $SCl^2/\sigma A$ where C is the

$$\frac{\partial^2\phi(\xi,t)}{\partial\xi^2} = \tau\frac{\partial\phi(\xi,t)}{\partial\tau} \qquad [22]$$

differential capacity per unit area (farad/cm^2). Alternatively, $\tau = R_oC_T$ where $R_o = l/\sigma A$ is the resistance of the electrolyte as before and $C_T = SCl$ is the total differential capacity (farad). The initial condition is given by $\phi(\xi,0) = 0$ and the boundary conditions are the same as those of Eq. [21]. The induced double layer charging transient is given by Eq. [23] and Fig. 11

$$\frac{\phi(\xi,t)}{\kappa I} = \frac{2}{\pi^2}\sum_{k=1}^{\infty}\frac{(-1)^k}{k^2}\{\cos[\pi k\xi] - \cos[\pi k(1-\xi]\}\{1-\exp[-\pi^2k^2t/\tau]\} \qquad [23]$$

shows a plot of the measurable potential transients against t/τ and against $(t/\tau)^{1/2}$. During the initial moments the potentials $\phi(0,t)$ and $\phi(1,t)$ follow the $\sqrt{t}$ law of Eq. [24]. In a plot of $\phi(0,t)$ or $\phi(1,t)$ against $\sqrt{t}$, the

$$\lim_{t\to 0} -\frac{\phi(0,t)}{\kappa I} = \lim_{t\to 0}\frac{\phi(1,t)}{\kappa I} = 2\left(\frac{t}{\pi\tau}\right)^{1/2} \qquad [24]$$

initial slope of the charging transient is inversely proportional to $(R_oC_T)^{1/2}$. The final steady state is given by $\phi(\xi,\infty)/\kappa I = \xi - (1/2)$ so that $\phi(1,\infty) - \phi(0,\infty) = \kappa I$, which is equivalent to Eq. [1]. Both R_o

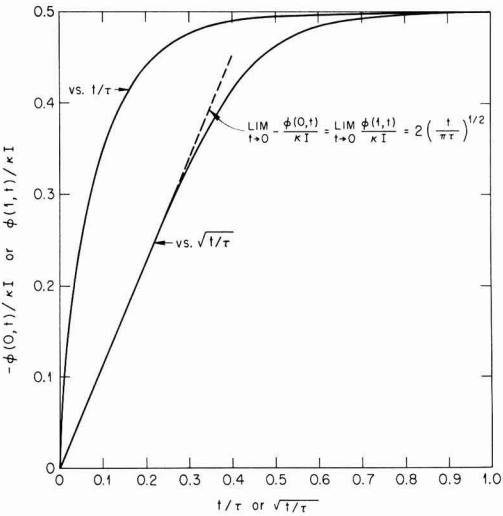

Fig. 11. Induced charging of the double layer in porous or tubular electrodes in the absence of faradaic reactions.

and C_T may be determined from induced charging transients by use of these relations.

Effect of Conductance of Metallic Phase

The relations derived above for induced polarization and charging transients may be corrected for situations where the conductivity of the metallic phase is comparable to that of the liquid phase. When potential gradients can occur in the metallic (electron conducting) phase, Eq. [2] may be replaced by Eq. [25], where σ_s and σ_m are specific conductances of solution and metal

$$\frac{d^2\eta(x)}{dx^2} = S\left(\frac{1}{\sigma_s A_s} + \frac{1}{\sigma_m A_m}\right) j(x) \qquad [25]$$

phases, respectively, and A_s and A_m are the corresponding cross-sectional areas. The net result of this correction is that κ must be replaced by

$$\kappa' = \frac{S j_o \ln F}{RT}\left(\frac{l}{\sigma_s A_s} + \frac{l}{\sigma_m A_m}\right) = i_o\,(R_o + R_m) f$$

where $R_m = l/\sigma_m A_m$ is the resistance of the metallic phase (ohm). In a similar manner the time constant for charging of the double layer (τ) must be replaced by $\tau' = C_T(R_o + R_m)$. The forms of all equations in which κ and τ appear (*e.g.*, Eq. [6] and [22]) are left unchanged by this substitution.

Summary

Solutions are presented above to several one-dimensional boundary value problems which occur in the theory of induced polarization of porous or tubular electrodes. Measurements of induced polarization may find application in analysis of flowing streams because the apparent resistance is sensitive to the presence of oxidation reduction reactions which can occur at the interface. Induced polarization may also prove to be useful as a monitor of corrosion rates of pipes or porous metals. In addition, certain parameters of importance in electrode kinetics (transfer coefficient and exchange current density) may be estimated in a unique manner from measurements of the dissymmetry potential or the apparent resistance. More elaborate models which include factors not treated here (diffusion and convection of reactants, reactions with consecutive charge-transfer steps, etc.) may be devised which might suggest other possibilities for the utilization of induced polarization measurements on porous and tubular electrodes.

Manuscript received Sept. 7, 1965; revised manuscript received Feb. 24, 1966. This paper was presented at the Cleveland Meeting, May 1-6, 1966.

Any discussion of this paper will appear in a Discussion Section to be published in the December 1966 JOURNAL.

REFERENCES

1. O. S. Ksenzhek, E. A. Kalinovskii, and E. L. Baskin, *Zhur. Priklad. Khim.*, **37**, 1045 (1964); *Russian J. Appl. Chem.*, **37**, 1048 (1964).
2. F. A. Posey, *This Journal*, **111**, 1173 (1964).
3. W. Tomassi, *Compt rend.*, **256**, 3093 (1963).
4. W. Tomassi, *Przemysl Chem.*, **42**, 345, 410 (1963).
5. W. Tomassi, H. Jankowska, and R. Milek, *ibid.*, **43**, 6 (1964).
6. W. Tomassi, H. Jankowska, S. Pietrzyk, and J. Brylka, *Electrochim. Acta*, **10**, 605 (1964).
7. V. S. Daniel'-Bek, *Zhur. Fiz Khim.*, **22**, 697 (1948).
8. J. S. Newman and C. W. Tobias, *This Journal*, **109**, 1183 (1962).
9. E. A. Grens, II, and C. W. Tobias, *Ber Bunsenges. physik. Chem.*, **68**, 236 (1964).
10. P. Delahay, "Double Layer and Electrode Kinetics," Interscience, New York (1965).
11. N. Tanaka and R. Tamamushi, *Electrochim. Acta*, **9**, 963 (1964).
12. R. de Levie, *ibid.*, **8**, 751 (1963).
13. F. A. Posey and T. Morozumi, *This Journal*, **113**, 176 (1966).

SYMBOLS

A, A_s	cross-sectional area of electrolyte in porous or tubular electrode, cm^2
A_m	cross-sectional area of metallic phase in porous or tubular electrode, cm^2
C	differential capacity per unit area, farad/cm^2
C_T	total differential capacity, farad.
$C_R, C_R(\xi,t)$	concentration of reduced species in solution, mole/cm^3
$C_o, C_o(\xi,t)$	concentration of oxidized species in solution, mole/cm^3
C^o	$= C_R(\xi,0) = C_o(\xi,0)$; initial concentration of oxidized and reduced species, mole/cm^3
f	$= nF/RT$, reciprocal thermal volt equivalent, volt^{-1}
F	Faraday constant, coulomb/equivalent
i	total current passed through porous or tubular electrode, amp
i_o	$= Sj_o l$; total exchange current, amp
I	$= i/i_o$; dimensionless reduced total current
$j(x), j(\xi,t)$	current density of interfacial reaction, amp/cm^2
j_o	exchange current density, amp/cm^2
j_o^o	standard exchange current density, amp-cm/mole
j_{corr}	corrosion current density, amp/cm^2
k	summation index
l	length of porous or tubular electrode, cm
n	electron number of oxidation reduction reaction
n_a, n_c	electron numbers of anodic and cathodic reactions, respectively
RT/F	thermal volt equivalent, v
R_o	$= l/\sigma A = l/\sigma_s A_s$; resistance of solution phase in absence of oxidation reduction reactions, ohm
R_m	$= l/\sigma_m A_m$; resistance of metallic phase, ohm
R_{app}	$= [\eta(l) - \eta(0)]/i$; apparent resistance of porous or tubular electrode, ohm
S	interfacial area of porous or tubular electrode per unit length, cm^2/cm
t	time, sec
x	distance coordinate, cm
β, β_a	anodic transfer coefficient.
β_c	cathodic transfer coefficient
$\eta(x)$	change of interfacial potential difference by induced polarization, volt
θ	$= nFC^oAl/i_o$; time constant for concentration transients, sec

κ = $Sj_o l^2 n\ \mathcal{F}/\sigma ART = i_o R_o l$; dimensionless resistance parameter, a ratio of solution impedance to interfacial impedance

κ_o = $\kappa j_o^o/j_o$

κ' = $i_o(R_o + R_m)l = \kappa(R_o + R_M)/R_o$

κ_{corr} = $Sj_{corr} l^2(\beta_a n_a + \beta_c n_c)\ \mathcal{F}/\sigma ART$; dimensionless resistance parameter useful for estimating corrosion rates of pipes or porous metals

ξ = x/l; dimensionless distance coordinate

$\rho(\xi,t)$ = $j(\xi,t)/j_o$; dimensionless reduced reaction rate.

σ,σ_s specific conductance of solution phase, $ohm^{-1}cm^{-1}$

σ_m specific conductance of metallic phase, $ohm^{-1}cm^{-1}$

τ = $SCl^2/\sigma A = R_o C_T$; time constant for charging of double layer, sec

τ' = $C_T(R_o + R_M)$

$\phi_s(x)$ potential of solution phase, volt

$\phi(\xi),\phi(\xi,t)$ = $f \cdot \eta(\xi,t)$; dimensionless reduced change in interfacial potential difference induced by passage of current

Φ = $\phi(0) + \phi(1)$; dimensionless dissymmetry potential.

Electrochemical Processes in Thin Films

1. Preliminary Survey of the Roles of Convection and Concentration Polarization

E. N. Lightfoot

Department of Chemical Engineering, University of Wisconsin, Madison, Wisconsin

ABSTRACT

An analysis is made of the roles of convection and concentration polarization during oxidation of hydrogen in acidic supermeniscus films. In this preliminary analysis activation overvoltage is assumed constant throughout the reaction zone. It is concluded that both convection and concentration polarization are important, and that they are in part responsible for formation of films above the normal meniscus. It is postulated that concentration polarization induces water recirculation, up in the surrounding vapor phase, and down as a gravity-driven falling film on the anode surface. Calculated film heights and thicknesses are in agreement with published observations.

Recently there has been considerable interest in electrochemical processes taking place at the wetted surfaces of metallic rods partially immersed in electrolyte solutions. This interest stems in large part from the outstanding work of Will (1) and from the belief that studies in such systems will give improved insight into the behavior of porous electrodes.

Up to the present, however, analysis of the diffusional processes contributing to the electrolytic current have been incomplete, and the postulated presence of very thin films above the equilibrium meniscus has not been adequately explained. It is felt by the author that more thorough study of these factors is in order, and, indeed, that electrode behavior cannot be adequately understood until these uncertainties are resolved.

The present paper reports a preliminary analysis of convection and concentration polarization relative to immobilization of electrochemically inactive solutes. In spite of the approximations introduced, this development indicates that both convection and concentration polarization are important and that their effects should be further studied. Of particular importance is the strong probability that systems of this type can be influenced by gravitational forces and hence both by configuration and orientation of the electrode.

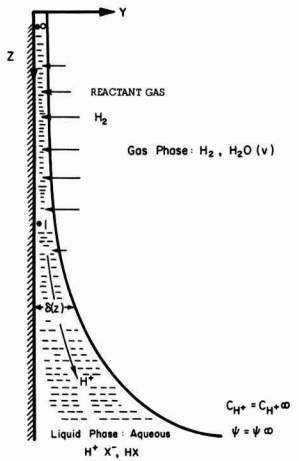

Fig. 1. System considered

The system considered is pictured in Fig. 1. It consists of an electrolyte meniscus adjacent to a vertical electrode surface and quite possibly distorted from normal meniscus shape in its upper regions. This distortion may be due to hydrodynamic effects, as discussed below, or to the presence of a liquid film of as yet undetermined origin. In any event, it is assumed that the gas-diffusion path is short compared to that for the discharging ions, so that migration of the two will be one-dimensional in each case, and mutually perpendicular.

Behavior of the system can be described in terms of conservation relations for the diffusing species, and of electric charge, the Nernst equation, and Kirchoff's voltage law. Where convection is to be considered the equation of fluid motion must also be used, with possible serious complication of the problem at hand. Only simple falling films will be considered in this initial development, but a more thorough analysis is planned in which natural convection and the effects of surface-tension forces will be taken into account.

Continuity Relations

For our present purposes we shall consider the solution to contain only hydrogen ions, one unspecified anion X^-, a very small amount of dissolved hydrogen, and water.[1] It will be further assumed that diffusion coefficients are concentration independent throughout the reaction zone and that diffusional coupling between species is unimportant. Finally, it will be assumed that water is the major constituent so that the

[1] Partially dissociated electrolytes can be handled by an extension of the development presented here, but in this case both the dissociation equilibrium and rate constants must be known.

divergences of both the mass-average and molar-average velocities are zero. We then need explicit continuity equations only for hydrogen and the two ionic species.

The continuity equation for hydrogen is particularly simple and may be written directly in integral form as

$$N_{H_2} = \frac{\mathcal{D}_{H_2 m}}{\delta(z)} [c_{H_2}^{\circ} - c_{H_2}(0, z)] \quad [1]$$

where $c_{H_2}^{\circ}$ is the solubility of hydrogen in the electrolyte. This equation may be rewritten in terms of the rate of increase of electrolytic current in the z-direction, since this current is produced solely by oxidation of hydrogen. We thus obtain

$$\boxed{dI/dz = [2PF\mathcal{D}_{H_2 m}/\delta(z)][c_{H_2}^{\circ} - c_{H_2}(0, z)]} \quad [2]$$

Since the entire electrolytic current is carried by the hydrogen ions, we may write the continuity equations for the ionic species as

$$H^+: \; I_z = -FP\delta(z) \left\{ \mathcal{D}_{H^+ m} \left(\frac{dc_{H^+}}{dz} + c_{H^+} \frac{d\Psi}{dz} \right) - c_{H^+} v_z^* \right\} \text{ (hydrogen ion)} \quad [3]$$

$$X^-: \; 0 = -\mathcal{D}_{X^- m} \left(\frac{dc_{H^+}}{dz} - c_H + \frac{d\Psi}{dz} \right) + c_{H^+} v_z^* \text{ (anion, } X^-) \quad [4]$$

Use of these pseudobinary diffusion expressions has been amply justified for reasonably dilute electrolytes and should be satisfactory for our limited present purposes. The assumptions of uniform electrolytic current density and negligible curvature of the electrode perimeter are consistent with the assumption of thin films underlying the entire development.

Equation [4] states the requirements for immobilization of the anion: a balance between concentration-diffusion, forced-diffusion, and convective fluxes. Simultaneous consideration of all three fluxes is difficult because it requires detailed knowledge of water transport across the gas-liquid interface. For the present, when it is only desired to obtain a semi-quantitative understanding of system behavior, a simpler approach seems in order, and two limiting cases are considered for this purpose:

1. No water transport across the liquid-gas interface: $v_w = v_{x^-} = 0$; $v^* - x_H + v_{H^+}$. Under these conditions convection is of minor importance, and the primary mechanism of immobilization is concentration polarization.

2. No resistance to water transport: $dc_{H^+}/dz = dc_{H^+}/dy = 0$. Under these conditions anion immobilization is entirely by convection. Since this requires a very substantial solution velocity, large amounts of water will have to condense into the liquid film and be transported downward by gravitational action, or else there will have to be very substantial spontaneous mixing. Real behavior should be intermediate between predictions for these two limiting situations.

For the case of no water transport across the gas-liquid interface and no spontaneous mixing, *i.e.*, negligible convection, Eq. [3] and [4] reduce to

$$I_z = -2FP\delta(z)\mathcal{D}_{H^+ m} c_{H^+} \frac{d\Psi}{dz} \text{ (negligible convection)} \quad [5]$$

$$\frac{dc_{H^+}}{dz} = c_{H^+} \frac{d\Psi}{dz} \text{ (negligible convection)} \quad [6]$$

Equation [6] may be readily integrated and the result substituted into Eq. [5] to obtain[2]

[2] Other available analyses taking concentration polarization into account include (2-4).

$$I_z = -2FP\delta(z)\, c_{H^+ \infty} \mathcal{D}_{H^+ m} e^{(\Psi - \Psi_\infty)} \frac{d\Psi}{dz} \text{ (negligible convection)} \quad [7]$$

Then, for conditions of negligible convection the effective conductivity of the film is a function of applied voltage, through the dependence on Ψ_z, the potential at large z.

When fluid convection prevents the development of appreciable concentration gradients, Eq. [4] reduces to

$$v^* = -\mathcal{D}_{x^- m} \frac{d\Psi}{dz} \text{ (convection dominant)} \quad [8]$$

This may be put into Eq. [3] to obtain

$$I = -P\delta(z)\{Fc_{H^+}(\mathcal{D}_{H^+ m} + \mathcal{D}_{x^- m})\} \frac{d\Psi}{dz} \text{ (convection dominant)} \quad [9]$$

The expression in braces is defined as $\kappa = KRT/F$ where K is the conductance of the electrolyte, mhos/cm. We may then write

$$I = -P\delta(z)\,\kappa \frac{d\Psi}{dz} \text{ (convection dominant)} \quad [10]$$

This is the expression used by Will, and it is, therefore, important to recognize both the restrictions on it and its physical significance:

(*i*) *Restrictions.*—Equation [10] is valid only when concentration gradients are substantially eliminated by convective mechanisms. This implies a substantial flow of solvent down the film, either because of effective equilibriation with the gas phase, natural convection, or the action of surface forces. These requirements clearly imply a sensitivity to geometry, scale factors, and orientation with respect to gravitational fields.

(*ii*) *Physical significance.*—The effect of convection is to oppose electrodiffusion of X^- and to reinforce that of H^+, in each case by exactly the same amount. Since its effect on X^- must exactly cancel out the corresponding electrodiffusion, its contribution to H^+ movement, *i.e.*, to the electrolytic current, is exactly that of electrodiffusion of X^- in an alternating voltage field.

It should also be noted that $\mathcal{D}_{X^- m}$ is always much smaller than $\mathcal{D}_{H^+ m}$. It follows that effective electrolyte resistance for conditions of negligible convection is only about half that for conditions of negligible concentration polarization, even at quite low applied voltages. At higher voltages the differences are even larger.

Then for the one-one electrolyte considered here, it should not be hard to determine from experimental data whether convection or concentration polarization is primarily responsible for immobilization of electrochemically inactive ions. This can be seen rather clearly by rewriting Eq. [7] and [10] in the common form

$$\boxed{I = -P\delta(z)\,\kappa_\infty \alpha \frac{d\Psi}{dz}} \quad [11]$$

with

$$\alpha = 1 \text{ (convection dominant)} \quad [12]$$

$$\alpha = 2 \exp[\Psi(z) - \Psi(\infty)] / \left(1 + \frac{\mathcal{D}_{x^- m}}{\mathcal{D}_{H^+ m}}\right) \text{ (convection negligible)} \quad [13]$$

Equations [2] and [11] through [13] summarize the useful continuity relations for this system. It should be kept in mind, however, that the situation is much more complicated for partially dissociated electrolytes.

Development of Current-Voltage Relations for Thin Films

Here, the hydrogen concentration $c_{H_2}(0, z)$ will be eliminated from Eq. [2] through use of Kirchoff's law and a modification of the Nernst equation, in a manner similar to that used by Will. In this way it may be shown that

$$\Psi_0 - \Psi_1 \doteq \ln \left[\frac{(c_{H^+})_1}{(c_{H^+})_0} \sqrt{\frac{(c_{H_2})_0}{(c_{H_2})_1}} \right] + \frac{F}{RT} (\eta_1 - \eta_0) \quad [14]$$

In the present analysis overvoltage η will be assumed constant. This is a major assumption which may result in serious error for many electrochemical reactions of practical interest. It should however be acceptable for our present limited purposes, for hydrogen oxidation. Variation in overvoltage, but not hydrodynamic flow, is treated by Grens, Turner, and Katan (4). We may thus rewrite Eq. [14] as

$$\frac{(c_{H_2})_1}{(c_{H_2})_0} = e^{-\beta(\Psi_0 - \Psi_1)} \quad [15]$$

with

$$\beta = 2 \text{ (convection dominant)} \quad [16]$$

$$\beta = 4 \text{ (convection negligible)} \quad [17]$$

Equation [15] may be rewritten more conveniently as

$$\boxed{c_{H_2}/c_{H_2}{}^o = \exp\left[-\beta\psi + (\beta - 2)\psi_\infty\right]} \quad [18]$$

with

$$\psi = \Psi_e - \Psi \quad [19]$$

Here Ψ_e is the solution potential for $c_{H_2} = c_{H_2}{}^o$ and $c_{H^+} = (c_{H^+})_\infty$. Equations [2] and [18] can now be combined to eliminate concentration and the result put in dimensionless form for convenience. The result is

$$\frac{dH}{d\zeta} = 1 - e^{-\beta\psi + (\beta - 2)\psi_\infty} \quad [20]$$

where the dimensionless current H and position ζ are defined as in the nomenclature list. The corresponding form of Eq. [11] is

$$H = \frac{1}{2} \epsilon\alpha \frac{d\psi}{d\zeta} \quad [21]$$

where ϵ is also defined in the nomenclature list. These two equations may now be combined and integrated to yield the desired current-voltage relations

$$H = \sqrt{\epsilon} \sqrt{\psi - \frac{1}{2}(1 - e^{-2\psi})} \quad \text{(convection dominant)} \quad [22]$$

$$H = \sqrt{\frac{2\epsilon}{1 + (\mathcal{D}_{x-m}/\mathcal{D}_{H+m})}} \sqrt{\frac{4}{5} e^{\psi_\infty/2} + \frac{1}{5} e^{-5\psi + 3\psi_\infty} - e^{-\psi + \psi_\infty}} \quad [23]$$

convection negligible

To evaluate the integration constants in these two expressions use was made of the fact that $H = 0$ when $c_{H_2} = c_{H_2}{}^o$. Note that the total applied voltage can be defined as ψ_∞ and that the total current is H_∞. Therefore, to obtain an expression for total electrode performance from Eq. [22] or [23], it is only necessary to replace ψ by ψ_∞ and H by H_∞.

It may be noted that:

1. Both relations are completely independent of film shape, provided only that the film is thin enough to provide mutually perpendicular gas and ion diffusion, and, of course, that $\gamma(\eta_0 - \eta_1)$ be zero.
2. The current-voltage relation at intermediate points in the film is dependent on total applied voltage when concentration polarization is appreciable, but not otherwise.
3. Current-voltage characteristics are quite different for the two limiting cases considered, so that it may be possible to determine the relative importance of convection and concentration polarization from experimental measurements. For acid hydrogen anodes, as considered here, greater currents are obtained when concentration polarization is appreciable. For alkaline hydrogen anodes or acid oxygen cathodes the reverse should, of course, be true.

The last of these points is the most important for our present purposes, and is worth considering in more detail.

To facilitate comparison of Eq. [22] and [23] we define r as the ratio of potentials for convection negligible and dominant

$$r \doteq 2/[1 + (\mathcal{D}_{x-m}/\mathcal{D}_{H+m})]^{1/2} \qquad (\text{Limit}, \psi_\infty \to 0)$$

For a rather typical value of 0.2 for $(\mathcal{D}_{X-m}/\mathcal{D}_{H+m})$ one thus obtains a value of the order of 2 for r, at low applied voltages. Since $RT/F \doteq 0.025$v at normal temperature, this expression would only be expected to be valid for applied potentials of about 10 mv or lower. At very high applied voltages

$$r \doteq \sqrt{\frac{8}{5} \frac{\exp(\psi_\infty/2)}{\left(1 + \frac{\mathcal{D}_{x-m}}{\mathcal{D}_{H+}}\right)\left(\psi_\infty - \frac{1}{2}\right)}} \quad [25]$$

so that r rapidly becomes large.

Comparison of Predicted Behavior with Available Data

The most complete available data directly applicable to the above analysis appear to be the experimental results of Will for cylindrical platinum electrodes immersed in 1*N* and 8*N* H_2SO_4 at 25°C. Representative results are reproduced in Fig. 2 and 3, along with predictions for the assumption of convection dominant in immobilization of the anions. Calculated results for the assumption of concentration polarization dominance are not shown because they are not directly applicable to a partially dissociated dibasic acid such as H_2SO_4.

At very low applied voltages (see Fig. 2) experimental results are in fair agreement with the assumption of convection dominance, although the experimental currents are slightly lower than predicted for the case of 8*N* acid. This result may be a consequence of activation polarization or inaccuracies in the assumed values of physical properties. The dif-

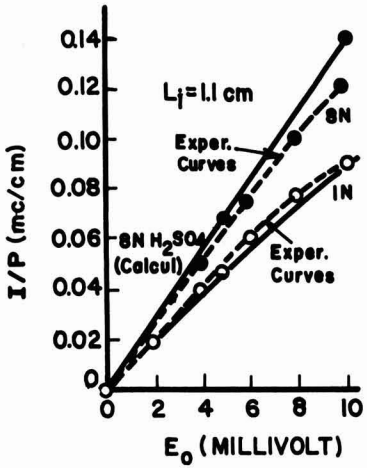

Fig. 2. Total current *vs.* applied potential [data of F. G. Will, ref. (1)].

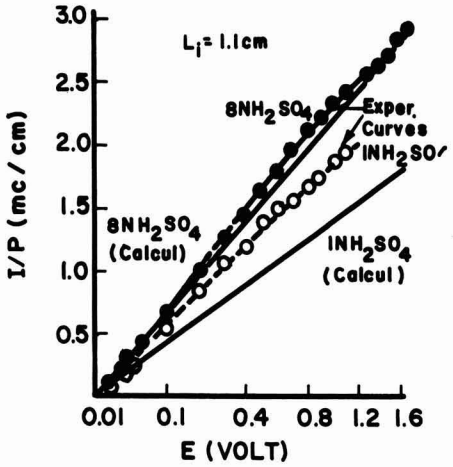

Fig. 3. Total current vs. applied potential [data of F. G. Will, ref. (1)].

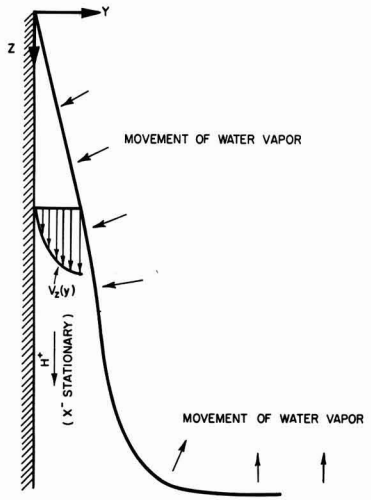

Fig. 4. Convection in film by vapor recirculation mechanism

fusivity of dissolved hydrogen, for example, is not accurately known. However, it may also be a result of concentration polarization superimposed on convection since 8*N* is very nearly the concentration of maximum sulfuric acid conductivity.

At higher applied voltages experimental currents for 1*N* acid are about 1/3 higher than those predicted, and, as previously stated by Will, this is an indication of concentration polarization. The magnitude of this effect is, however, far lower than can be explained by the above analysis for a 1-1 electrolyte with negligible convection. It would appear then, either that convection is important here, or that the effect of concentration polarization is markedly reduced, either by the partial dissociation of the acid, or by kinetic limitations. It is the opinion of the author that convection is important, but the complexities of sulfuric acid dissociation make a convincing analysis impossible at present. For 8*N* acid there is almost complete agreement with the assumption of convection dominance, but once again caution is indicated. At this rather high acid concentration diffusional interaction between the ions and between these and the undissociated acid must also be considered. This is impossible at present, and it is clear that sulfuric acid is too complex an electrolyte to permit meaningful interpretation of experimental results.

In summary then it appears reasonable to agree with Will that concentration polarization plays only a minor role in these experiments, but this is by no means certain.

It is also important to note that Will found strong indirect evidence of a liquid film, approximately 1μ in thickness, above the equilibrium meniscus, and that an appreciable fraction of the hydrogen oxidation took place in this super-meniscus region. The existence of such films has since been demonstrated experimentally by Muller (5, 6), using interferometric techniques, during reduction of oxygen on nickel cathodes partially immersed in aqueous sodium hydroxide. Muller found his films to be stable during the passage of the current, and that they increased in thickness with current density. The existence of such a film during this reaction was later used by Bennion and Tobias (2, 3) in their analysis of electrode behavior.

To date no convincing explanation for stable super-meniscus films with thickness of the order of microns has been offered for equilibrium conditions, *i.e.*, in the absence of a current. Their presence requires an appreciable charge density in the bulk of liquid in the film, or other equivalent repulsive force. Such forces have been observed, for example, in soap films (7), but it is easily shown (8) that they are not large enough to stabilize 1μ films under conditions being considered here.

Such films can be explained qualitatively in the presence of a current by water-condensation and gravitational flow, as explained above for hydrogen oxidation in an acid electrolyte. This is also true for oxygen reduction in a basic reaction, in spite of water consumption in the electrochemical reaction, and for the same reasons. It remains to determine if such an explanation is quantitatively appealing. This is the purpose of the next section.

Tentative Analysis of Convection

From the above analysis and the experimental observations of Will (1) and of Muller (5, 6) substantial fluid motion in the film-meniscus system appears quite possible. There are at least three possible causes of such motion, each basically dependent on the concentration polarization which must accompany a direct electrolyte current. These are: (*a*) surface-tension gradients, which must be considered in combination with density gradients; (*b*) natural convection; and (*c*) recirculation of water through the gas phase driven by differences in equilibrium water vapor pressure.

All of these should be considered, and it is planned ultimately to do so, but only the third is treated here. This is in part because it produces the simplest and most believable type of fluid motion, closely analogous to the classic Nusselt condensed-steam film. Natural convection or surface-tension driven flows, on the other hand, require both rising and descending currents in the same thin film.

The goal of the following analysis is then a simple and restricted one: to determine whether the falling film required to immobilize anions at an acid hydrogen anode has characteristics consistent with our knowledge of electrode reactions in film-meniscus systems. The acid hydrogen anode is used not only because it is the best understood, but also because convection is downward. Thus, a first approximate description can be attempted without detailed knowledge of surface forces. The procedure then will be first to relate film thickness to the mass average velocity in the film and then to relate this velocity to the total current.

Since the film will be thin and the Reynolds number of the flow in it extremely small the integrated equation of motion may be written down directly in the form

$$v = \rho g \delta^2 / 3\mu \quad [26]$$

where v is the flow-average value of the mass-average velocity in the axial direction. Next Eq. [3] is rewritten in the form

$$I = P \delta c_{H+} v_{H+} \quad [27]$$

where v_{H+} is the flow-average velocity of the hydrogen ion. Next the velocity of water in the film is related to that of hydrogen through combination of Eq. [8], [9], and [27].

$$v^* = x_{H+} v_{H+} + x_w v_w = v_{H+} \Big/ \left[1 + \frac{\mathcal{D}_{H+m}}{\mathcal{D}_{x-m}} \right] \quad [28]$$

where v^* is again a flow-average value. Note that to write Eq. [28] in flow-average terms it is necessary to neglect changes in species velocity ratios across the film. Since $x_w = 1 - 2x_{H+}$ it follows that

$$v_w = v_{H+} \left[\frac{1 - \left(1 + \frac{\mathcal{D}_{H+m}}{\mathcal{D}_{x-m}} \right) x_{H+}}{(1 - 2x_{H+}) \left(1 + \frac{\mathcal{D}_{H+m}}{\mathcal{D}_{x-m}} \right)} \right] \quad [29]$$

and, therefore, that the mass-average velocity

$$v = w_{H+} v_{H+} + w_w v_w = A v_{H+} \quad [30]$$

with

$$A = w_{H+} + w_w \left[\frac{1 - \left(1 + \frac{\mathcal{D}_{H+m}}{\mathcal{D}_{x-m}} \right) x_{H+}}{(1 - 2x_{H+}) \left(1 + \frac{\mathcal{D}_{H+m}}{\mathcal{D}_{x-m}} \right)} \right] \quad [31]$$

Equations [27] and [31] may now be combined to yield

$$I = P \delta c_{H+} v / A \quad [32]$$

or, introducing Eq. [26]

$$I = \frac{\mathcal{F} P \rho g c_{H+} \delta^3}{3\mu A}; \quad H = \left(\frac{\rho g \delta^3}{6\mu A \mathcal{D}_{H2m}} \frac{c_{H+\infty}}{c_{H_2}^{\circ}} \right) \quad [33\text{-a, b}]$$

Then, within the limits of this development, film thickness is simply related to local current in a way strongly reminiscent of the Nusselt condensate films. This expression is, however, only useful in the upper region of the meniscus, and there only if the calculated δ is much greater than the film thickness in absence of a current. It is not applicable at all to systems in which ion flow is upward. With all these limitations, however, Eq. [33] does permit an estimate of the contribution of convection to film thickness.

Consider then as an illustrative example the following hypothetical, but reasonable, conditions

$$I/P = 0.05 \text{ ma/cm}$$
$$c_{H+} = 10^{-3} \text{ eqts/cm}^3$$
$$\mu/\rho = 10^{-2} \text{ cm}^2/\text{sec}$$
$$\mathcal{D}_{H+m}/\mathcal{D}_{x-m} = 4.5$$

Then

$$A \doteq 0.001 + 0.999 \left[\frac{1 - \frac{(1 + 4.5)}{55}}{\left(1 - \frac{2}{55} \right)(1 + 4.5)} \right] \quad [34]$$

$$= 0.17$$

$$\delta = \left[\frac{(0.17) \left(5 \times 10^{-5} \frac{\text{coulombs}}{\text{sec cm}} \right) (3) \left(10^{-2} \frac{\text{cm}^2}{\text{sec}} \right)}{\left(980 \frac{\text{cm}}{\text{sec}^2} \right) \left(9.65 \times 10^4 \frac{\text{coulombs}}{\text{equivalent}} \right) \left(10^{-3} \frac{\text{eqts}}{\text{cm}^3} \right)} \right]^{1/3} = 1.4\mu \quad [35]$$

This corresponds remarkably well with the estimated thickness of 1.5μ suggested by Will for very similar conditions but a somewhat different physical model. While this degree of agreement must be considered coincidental, it is nevertheless encouraging.

Film height can also be determined readily. For the low current of the above numerical example acceptable results may be obtained quite readily. Here

$$H \doteq \sqrt{\epsilon}\, \psi \quad [36]$$

and

$$\frac{dH}{d\zeta} = \delta \frac{dH}{dz} \doteq 2\psi \doteq 2H/\sqrt{\epsilon} \quad [37]$$

Combining this result with Eq. [33] yields the desired relation for film shape

$$\frac{d\delta}{dz} = \frac{2}{3\sqrt{\epsilon}} \quad [38]$$

Then $L/\delta = 3/2\sqrt{\epsilon}$ where L is distance from top of film to level at which thickness is δ. For sulfuric acid at 25°C

$$\mathcal{F}/RT = 39.0 \text{ volt}^{-1}$$

$$c_{H_2}^{\circ} = 7.67 \times 10^{-7} \frac{\text{moles}}{\text{cm}^3} \; (1N \; H_2SO_4); \quad 7.17 \times 10^{-7} \; (8N)$$

$$\mathcal{D}_{H2m} = 3.1 \times 10^{-5} \frac{\text{cm}^2}{\text{sec}} \; (1N); \quad 2.2 \times 10^{-5} \; (8N)$$

$$K = 0.215 \text{ mhos/cm } (1N); \quad 0.826 \; (8N)$$

Then for these conditions $\epsilon = 2.40 \times 10^3$ and $(L/\delta) = 73.5$ ($1N$ H_2SO_4) or 118 ($8N$ H_2SO_4).

By way of contrast, Will found the electrochemically active region to extend about 100 to 200 film thickness above the visible meniscus. In view of the uncertainties, both in analysis and experiment, these predictions are in reasonable agreement with Will's data.

The only experimental evidence of meniscus thickening to date appears to be that of Muller for reduction of oxygen on a nickel tube in $3.5N$ KOH. Film thickness was found to increase with current density for this system, for example, thickening from about 0.3 to about 0.5μ at 15 mm above bulk liquid level, when the current was raised from 0.0047 to 0.047 ma/cm. This thickening was ascribed to electrocapillary effects, but without proof. It is not possible at present to say more than that this degree of thickening is of the order predicted by the above convective development. It is also important to note that Muller's films were thinner at higher elevations, and, in fact, that available data as reported in ref. (3) indicate the triangular cross section predicted by Eq. [38].

In summary then, both the thickness and height of the falling film required to immobilize the anions are consistent with experimental observation. In fact, the agreement between prediction and experiment is much better than would be expected in view of the many approximations made in this development. It would be unwise to neglect other mechanisms of diffusional stabilization or other sources of thin liquid films on the metal electrode surface. It is also too early to speculate on the specific effects of geometry and orienation on electrode performance.

Nevertheless, two facts seem to be demonstrated by this analysis:

1. Superficial treatment of the current-carrying diffusional and convective processes in meniscus-film systems preclude thorough understanding of electrode performance.
2. Convective processes are likely to prove important in many practical situations.

Failure to consider these points would make full practical utilization of Dr. Will's outstanding work on thin films very unlikely.

Manuscript received Jan. 7, 1965; revised manuscript received Jan. 8, 1966.

Any discussion of this paper will appear in a Discussion Section to be published in the December 1966 JOURNAL.

REFERENCES

1. F. G. Will, *This Journal*, **110**, 152 (1963).
2. D. N. Bennion and C. W. Tobias, Paper presented at the Washington, D. C. Meeting of the Society, October 1964
3. D. N. Bennion, "Phenomena at a Gas-Electrode-Electrolyte Interface," Ph.D. Thesis, Dept. of Chemical Engineering, University of California, Berkeley, California, June 1, 1964.
4. E. A. Grens, R. M. Turner, and T. Katan, *Advanced Energy Conversion*, **4**, 109 (1964).
5. R. H. Muller, Paper presented at the Toronto Meeting of the Society, May 1964.
6. R. H. Muller, Paper presented at the Washington Meeting of the Society, October 1964.
7. J. T. Davies and E. K. Rideal, "Interfacial Phenomena," Academic Press, New York (1961).
8. V. H. Ludviksson and E. N. Lightfoot, Unpublished calculations.

NOMENCLATURE

$$A = w_{H+} + w_w \left[\frac{1 - \left(1 + \frac{\mathcal{D}_{H+m}}{\mathcal{D}_{x-m}}\right) x_{H+}}{(1 - 2x_{H+})\left(1 + \frac{\mathcal{D}_{H+m}}{\mathcal{D}_{x-m}}\right)} \right]$$

c	total molar concentration
c_i	molar concentration of species i
$\mathcal{D}_{im}$	effective binary diffusivity of species i
E_o	standard electrode potential = 96,500 coulombs/equivalent, Faraday's constant
g	980 cm/sec^2, gravitational acceleration
H	$I/2PFc_{H_2}{}^o\mathcal{D}_{H2m}$, dimensionless (axial) current
I	(axial) current, amp
K	specific conductivity, mhos/cm
L	(total) film length
N_i	molar flux of species i relative to stationary coordinates, moles/area, time
P	electrode perimeter, normal to electrolytic current flow
R	international gas constant
T	absolute temperature
v	axial mass-average velocity, flow average value for film
v^*	(axial) molar average velocity, flow average for film
v_i	(axial) species velocity, flow average for film
x_i	mole fraction of species i
z	axial distance
α	dimensionless factor defined by Eq. [11]-[13]
β	dimensionless factor defined by Eq. [15]-[17]
γ	dimensionless factor defined by Eq. [15], [18], [19]
δ	film thickness in direction of dissolved hydrogen diffusion
ϵ	$= \kappa_x/c_{H_2}{}^o\mathcal{D}_{H2m}F$ (dimensionless)
ζ	$= z/\delta$
η	overvoltage
κ	$= KRT/F$
μ	viscosity
ρ	density
ϕ	electrostatic potential, volts
Ψ	$= \phi F/RT$, dimensionless potential
ψ	$= (\phi^o - \phi)F/RT$, dimensionless local applied potential relative to top of film
w_i	mass fraction of species i

Superscript

o	conditions at top of film

Subscripts

e	conditions for which $c_{H+} = (c_{H+})_e$ and $c_{H_2}(o,z) = c_{H_2}{}^o$
w	water
H^+	hydrogen ion
x^-	(unspecified) anion
∞	conditions at lower end of film-meniscus system

Technical Notes

Studies on the Oxygen Gradients in Oxidizing Metals

IV. Kinetics of the Oxidation of Hafnium at High Temperatures

J. P. Pemsler

Ledgemont Laboratory, Kennecott Copper Corporation, Lexington, Massachusetts

Like zirconium, hafnium dissolves significant quantities of oxygen during oxidation so that a metal zone rich in oxygen forms beneath the oxide layer. In a previous paper the author has shown that the oxygen gradient beneath the oxide film may be calculated with an appropriate diffusion equation and that the experimentally determined gradient is in good agreement with the theoretical expression (1). In addition, it was found that a remarkable anisotropy of the oxidation film growth occurred which persisted to the thick film region and that the effect was associated with a variation in the stoichiometry of the oxide film covering differently oriented grains (1). In previous studies of zirconium it has been shown that, while the oxygen solution obeys diffusion kinetics and remains parabolic for sufficiently thick samples, film growth does not obey normal rate laws (2).

It is the purpose of this paper to attempt to separate quantitatively the film growth and oxygen dissolution processes and to attempt to gain insight into the film growth mechanism.

Experimental

Hafnium in the form of ¾-in. rod was obtained from the Carborundum Metals Climax Company. The vendor's analysis lists Zr as 2.5 w/o and the following in ppm: Al < 80, Cu < 40, Nb < 50, Ta < 100, Ti < 20, Fe-475, and N-33. The purity of the oxygen used has been reported previously (3). Experimental details concerning the preparation of spherical sam-

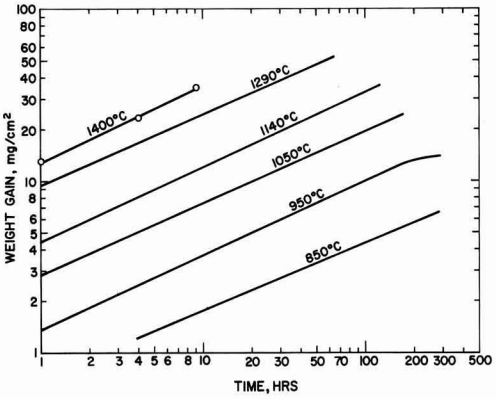

Fig. 1. Total weight gain of hafnium oxidized between 850° and 1400°C.

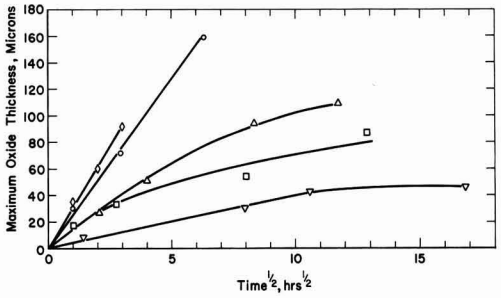

Fig. 2. Maximum oxide film thickness on oxidized hafnium. ○, 1293°C; △, 1140°C; □, 1050°C; ▽, 950°C; ◇, 1400°C.

ples, oxidation, and weight gain and film thickness measurements are similar to those used for zirconium (3).

Results

Total weight gain.—Data for the total weight gain between 850° and 1400°C are given in Fig. 1 in the form of a logarithmic plot. With the exception of the data at 1400°C where the separate data points are indicated, the results were obtained as a continuous weight gain record. The slopes of the log-log plots are about 0.42 and indicate a kinetic behavior between cubic and parabolic. Since the total weight gain is the sum of the film growth and oxygen solution and the latter two do not conform to the same kinetic behavior, no mechanistic interpretation of the total weight gain data can be made at this time.

Film thickness.—Examination of cross sections of the oxidized spheres indicate that at all times and temperatures there is a high degree of irregularity of the film thickness. This may be presumed to be associated with the high degree of anisotropy of oxide film formation on hafnium (1). In order to present the data it was found desirable to plot maximum, minimum, and average thicknesses of the film, and a parabolic plot of these data is shown in Fig. 2, 3, and 4. Data at the lowest temperature may be approximated as parabolic. At the intermediate temperatures the film growth is characterized by a continuously decreasing rate of higher power than parabolic. At the highest temperatures the film growth rate may again be approximated as parabolic.

During film formation grain growth occurs in the metal and becomes pronounced at high temperatures and long times. Oxygen in high concentration retards grain growth so that metal grains within the oxygen gradient may be smaller than those beyond the depth

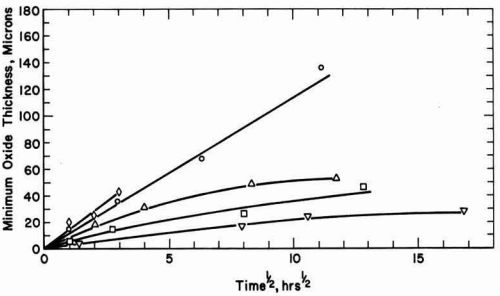

Fig. 3. Minimum oxide film thickness on oxidized hafnium. Symbols are the same as in Fig. 2.

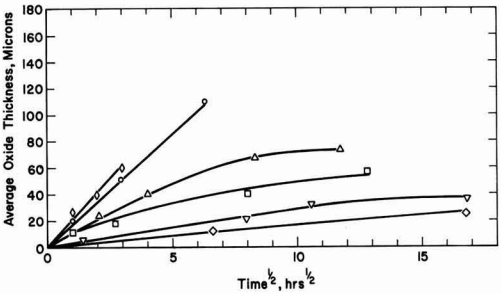

Fig. 4. Average oxide film thickness on oxidized hafnium. ○, 1293°C; △, 1140°C; □, 1050°C; ◇, 850°C; ▽, 950°C; ◇, 1400°C.

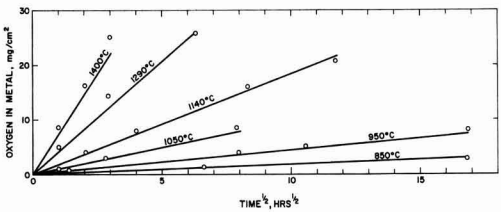

Fig. 5. Oxygen in solution in oxidized hafnium

of appreciable oxygen penetration. Since grain growth is apt to result in a preferred orientation, it is likely that grain growth coupled with the anisotropy of film formation might alter the film growth process. Thus, at the lowest temperatures grain growth is sufficiently slow so that the orientation of the different oxidizing grains is roughly constant. At intermediate temperatures grain growth becomes more pronounced, and the degree of preferred orientation is consequently altered, thereby altering the film growth. At the highest temperatures grain growth is exceedingly rapid, and the retarding effect of the oxygen gradient is absent, so that after a short time the characteristic grains develop which will be present for the remainder of the oxidation.

Oxygen in the metal.—A knowledge of the total weight gain and the measurement of the oxide film thickness enables computation of the quantity of oxygen dissolved in the metal substrate beneath the oxide film. Furthermore, the latter quantity can be calculated by equations previously given (3). Calculated and experimental data for oxygen dissolved in the metal are plotted as a function of a square root of time in Fig. 5. Here, the solid line represents calculated values, and the separate experimental points are indicated in the figure. Good agreement exists between calculated and observed oxygen content of

the metal and the data are parabolic as demanded by diffusion theory.

Discussion

During an investigation of the high-temperature oxidation of zirconium, it was postulated that there exists easy diffusion paths through the oxide which are not interconnected laterally (2). An hypothesis was also presented for the stabilization of the high-temperature tetragonal phase of zirconia at temperatures far below the normal transformation temperature and of different transport rates through the monoclinic and tetragonal oxides. It is possible that similar situations exist during the oxidation of hafnium. In order to understand the mechanism of film formation on hafnium, it is desirable to determine the contribution of nonlattice diffusion and tetragonal oxide to the film growth process. It is also necessary to determine the kinetics of film formation on single crystal material of well-defined orientations. This should give insight into the mechanism causing the pronounced anisotropy of film growth and yield meaningful film growth rates which are not affected by grain growth in the sample. The aforementioned investigations are being pursued in this laboratory.

Acknowledgment

It is a pleasure to acknowledge the valuable assistance and suggestions of J. K. Litchfield.

Manuscript received Dec. 2, 1965.

Any discussion of this paper will appear in a Discussion Section to be published in the December 1966 JOURNAL.

REFERENCES

1. J. P. Pemsler, *This Journal*, **111**, 1339 (1964).
2. J. P. Pemsler, *Electrochem. Technol.*, **4**, 128 (1966).
3. J. P. Pemsler, *This Journal* **112**, 477 (1965).

A Chemical Polish for Tin Telluride

Marriner K. Norr

United States Naval Ordnance Laboratory, White Oak, Silver Spring, Maryland

Until now there has been only one satisfactory method for chemically polishing SnTe (1, 2). It has had the disadvantage of frequently leaving a whitish haze (and sometimes dark stains) on the samples when they were polished for a long enough time (3-5 min) to remove the scratches formed by previous mechanical polishing (2).

This note describes a method of chemically polishing SnTe that gives a clean, somewhat flatter surface than (1, 2).

Procedure

The sample is mounted in a stainless steel jig assembly and ground flat on No. 600 grit SiC paper. It is then transferred to a polycarbonate jig assembly (to which it is attached with paraffin) and polished with Carborundum No. 50 grit Al_2O_3 optical finishing powder on a paraffin lap. Finally, it is polished with Linde A abrasive on a paraffin lap. Each of the abrasives is lubricated with a 1:1 solution of Joy detergent in ethanol. The sample, jig assembly, and hands should be thoroughly cleaned after each step of grinding and polishing.

The solution for chemical polishing is prepared by dissolving 0.35g I_2 in 40 ml ethanol (or methanol) and then adding 10 ml dist. H_2O and 4.0 ml 49% HF. A polyethylene beaker is used to avoid contamination from the container.

A piece of twill jean cloth[1] is stretched over a smooth Teflon plate and saturated with the solution at 25°C. It is recommended that the hands be protected from the solution with polyethylene gloves. The sample (still mounted in the polycarbonate jig assembly) is polished by lightly rubbing it over the wet twill jean cloth, using a figure eight motion, for 15-20 min. Periodically, additional solution must be added to keep the cloth saturated. The sample is then rinsed in a stream of methanol, followed by a stream of distilled water, and dried on lens paper. After demounting, it is soaked 2-3 times in fresh benzene to remove any adhering paraffin and dried on lens paper.

The SnTe crystals used in this work were grown by the Czochralski method. The polish produced a mirrorlike surface which has been used successfully for reflectivity measurements (3). Back-reflection Laue photographs, diffractometer measurements, and a Kossel photograph indicated that the surface was free of major strains.

[1] K. S. 2423 twill jean cloth, Exeter Manufacturing Company, Inc., Exeter, New Hampshire.

Acknowledgments

The author is indebted to Dr. Bland Houston for supplying the SnTe crystals and for helpful advice, to John V. Gilfrich for taking the Laue photographs and diffractometer measurements, and to Harvey Yakowitz for taking the Kossel photograph. The use of a cloth saturated with a chemical polishing solution was suggested to the author by a publication of Schmidt (4).

Manuscript received Feb. 28, 1966.

Any discussion of this paper will appear in a Discussion Section to be published in the December 1966 JOURNAL.

REFERENCES

1. J. W. Faust, Jr., and A. Sagar, Private communication through C. R. Martin.
2. M. K. Norr, "Polishes and Etches for Tin Telluride, Lead Sulfide, Lead Selenide, and Lead Telluride," NOLTR 63-156, U. S. Naval Ordnance Laboratory, White Oak, Maryland (1963).
3. R. F. Bis, *Solid State Commun.*, **2**, 161 (1964).
4. P. H. Schmidt, *This Journal*, **109**, 879 (1962).

Segregation Coefficients of Some Rare Earth Niobates in $SrMoO_4$

L. H. Brixner

Pigments Department, Experimental Station

E. I. du Pont de Nemours & Company, Incorporated, Wilmington, Delaware

The original laser experiments employing scheelite-type hosts were carried out with $CaWO_4$ (1). Other scheelites such as $SrMoO_4$ (2, 3), $CaMoO_4$ (4, 5), $PbMoO_4$ (4), and $SrWO_4$ (2) also have been used as host materials for lasers employing rare earth ions. Because low thresholds and ease of excitation, rods containing Nd^{+3} have been studied most intensively. However, rods containing other infrared emitting rare

Table I. Segregation coefficients for some $LnNbO_4$-type niobates in $SrMoO_4$

	% Deviation from Sr^{+2}	% Deviation from Ca^{+2}	Crystal color	k	c_s/c_n	Ln_2O_3: Nb_2O_5
Sc^{+3}	−27.7	−18.2	—	—	—	—
Y^{+3}	−17.8	−7.1	Colorless*	0.67	0.60	1:1.17 (T)
						1:1.05 (B)
La^{+3}	+1.8	+15.2	Colorless	1.04	1.01	1:0.91
						1:0.90
Ce^{+3}	−4.5	+8.1	Yellow	0.91	0.90	1:1.00
						1:0.97
Pr^{+3}	−5.3	+7.1	Green	0.96	0.97	1:0.95
						1:0.94
Nd^{+3}	−7.1	+5.1	Blue	0.93	0.95	1:0.90
						1:0.89
Sm^{+3}	−10.7	−1.0	Amber	0.88	0.83	1:1.07
						1:1.06
Eu^{+3}	−12.5	−1.0	Deep Red	0.93	0.89	1:0.88
						1:0.85
Gd^{+3}	−13.4	−2.0	Colorless	0.79	0.76	1:1.01
						1:0.99
Tb^{+3}	−16.9	−6.1	Colorless*	0.71	0.70	1:1.06
						1:1.05
Dy^{+3}	−17.8	−7.1	Light Yellow*	0.66	0.63	1:1.12
						1:1.04
Ho^{+3}	−18.7	−8.1	Light Brown*	0.62	0.59	1:1.00
						1:0.99
Er^{+3}	−20.5	−10.0	Pink*	0.48	0.50	1:1.11
						1:1.04
Tm^{+3}	−22.3	−12.1	—	—	—	—
Yb^{+3}	−23.2	−13.1	—	—	—	—
Lu^{+3}	−24.1	−14.1	—	—	—	—

* These crystals cracked on cooling.

earth ions such as Ho^{+3} and Tm^{+3} (4) also have been studied. The above papers describe mostly laser experiments; there have been few comprehensive studies of all rare earths in a given host with details on preparative and analytical procedures, as for instance in (5) and (6). Even here, no attempts have been made to correlate the observed segregation (or distribution) coefficients with the structural fit of the rare earth into the cation site of a scheelite.

In this note, we should like to point out some relationships between the ionic radii and the segregation coefficients for the $LnNbO_4$-type rare earth niobates in $SrMoO_4$. All single crystals were grown by the Czochralski technique as previously described (5). Conditions were maintained as uniform as possible with respect to pulling speed, rotation, shape, and weight of crystal. The starting mixture of all compositions was prepared according to the following stoichiometry:

$$0.99SrMoO_4 + 0.005Ln_2O_3 + 0.005Nb_2O_5 \rightarrow Sr_{0.99}Ln_{0.01}Mo_{0.99}Nb_{0.01}O_4,$$

where Ln = Y^{+3}, La^{+3}, Ce^{+3}, Pr^{+3}, Nd^{+3}, Sm^{+3}, Eu^{+3}, Gd^{+3}, Tb^{+3}, Dy^{+3}, Ho^{+3}, and Er^{+3}. This resulted in an activator concentration of 1% in the melt for all rare earth niobates, and it should be remembered at this point that k can also be a function of the concentration of the dopant.

Analysis and computation of k was done as described in (5). Table I summarizes the results. Crystals with Sc^{+3}, Tm^{+3}, Yb^{+3}, and Lu^{+3} were not grown, and the ionic radii deviations are merely included for completeness. For the purpose of a comparison we have also given the ionic radii deviation for Ca^{+2}. The most striking result is the fact that the segregation coefficient varies directly with the deviation of the rare earth ion size from that of Sr^{+2} as is evident in Fig. 1.

In the case of the examples marked with an asterisk no crack-free crystal could be grown on repeated attempts. It is particularly interesting to note that this transition from sound to cracked crystals occurred for a cation size difference of around 15%, the amount of deviation generally accepted as the limit of isomorphous substitution. That this is observable in single crystals at such low concentration is interesting; in the case of Y, six crystals grown from the melt cracked while being cooled to room temperature,

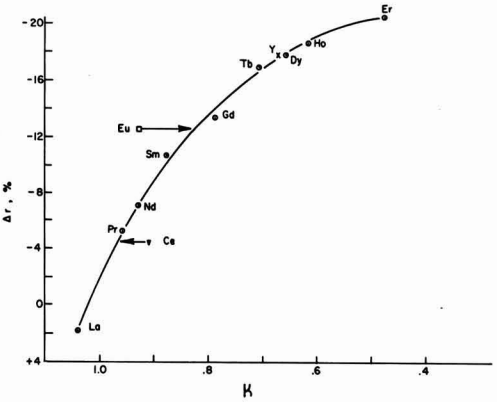

Fig. 1. Segregation coefficient k for $LnNbO_4$ in $SrMoO_4$ as a function of differential ionic radii ($r_{Ln+3} - r_{Sr+2}$).

indicating that true single crystalline solid solution are only stable at high temperature. There are two exceptions to the normal relationship, Ce^{+3} and Eu^{+3}; k for Ce seems too small and k for Eu^{+3}, too big. In the first case, we can only postulate that perhaps a small amount of Ce^{+4} causes this deviation as indicated by the intense yellow color, whereas in the Eu case we know that some Eu^{+2} enters the crystal, which has a deep red color. The better structural fit of Eu^{+2} in the Sr^{+2} site would account for the segregation coefficient nearer to unity. It is interesting to note that, contrary to the $CaMoO_4/EuNbO_4$ case, it was impossible to oxidize Eu^{+2} in $SrMoO_4$. After 100 hr under pure oxygen at 1400°C, the crystal was still deep red. A similar observation was made for $CaWO_4/Eu$ (6).

The column marked c_s/c_n gives the ratio of the concentration in the top of the crystal to the nominally charged concentration and in each case comes very close to k determined from analyses of top and bottom of the crystal. In the last column are the ratios of rare earth oxide to niobium pentoxide in top (T) and bottom (B) of crystal. Since the stoichiometric deviation is generally very small, it appears justified to treat the rare earth niobate in its entirety as we did for all computations. The general tendency is for this ratio to become smaller as the crystal grows, indicating somewhat stronger segregation of Nb_2O_5, but the change is certainly in no proportion to the change experienced by k itself. With the exception of Eu and Ce, a straightforward relationship between segregation coefficients and ionic radii has been established which permits the prediction of distribution coefficients from knowledge of the deviation of the substituted ion's size from that of the host ion. Failure to grow sound crystals with rare earths deviating more than 15% in size from that of Sr^{+2} indicates that these cannot be incorporated into the single crystalline $SrMoO_4$ lattice, at least not at this concentration and at room temperature. Compared to $SrMoO_4$, $CaMoO_4$ should be the better host for Nd^{+3}, although ultimately an appropriate solid solution of the two host compositions may be the best material, with essentially no segregation of the active constituent. This should also be possible for Ce and Pr, where the deviation of ionic radii in $CaMoO_4$ is opposite to the one in $SrMoO_4$.

Manuscript received Feb. 8, 1966.

Any discussion of this paper will appear in a Discussion Section to be published in the December 1966 JOURNAL.

REFERENCES

1. L. F. Johnson and K. Nassau, *Proc. IRE*, **49**, 1704 (1961).

2. L. F. Johnson and R. R. Soden, *J. Appl. Phys.*, **33**, 757 (1962).
3. P. A. Flournoy and L. H. Brixner, *This Journal*, **112**, 779 (1965).
4. L. F. Johnson, *J. Appl. Phys.*, **34**, 897 (1963).
5. L. H. Brixner, *This Journal*, **111**, 690 (1964).
6. K. Nassau and A. M. Broyer, *J. Appl. Phys.*, **33**, 3064 (1962).

Solubilities of Some II-VI Compounds in Bismuth

M. Rubenstein

Research Laboratories, Westinghouse Electric Corporation, Pittsburgh, Pennsylvania

Attention was first focussed on some of the larger band gap II-VI compounds, *i.e.*, ZnS, CdS, ZnSe, and CdSe, because of the interest in various optical properties such as luminescence. Much effort was and is still being expended to prepare powders of such materials in doped and undoped states. More recently other II-VI compounds (ZnTe and CdTe) have been studied because of possible uses in electroluminescence and in solar battery materials.

Since more attention is now being centered on trying to understand the observed phenomena exhibited by these materials and since some of the devices cannot utilize powders, there has been a greater effort in preparing single crystals in pure and doped states. Such single crystals have been grown from a vapor state and from a melt state. It is also possible to grow these II-VI compounds from a solution having an excess amount of the II or VI element, *i.e.*, one can grow single crystals of ZnTe by cooling a solution in which the initial charge is ZnTe and an excess of zinc. In order to grow such crystals a knowledge of the phase diagrams is of importance. Liquidus phase diagrams of ZnSe (1), ZnTe (2), CdS (3), CdSe (4, 5), and CdTe (6, 7) are already in the literature.

Solution growth must involve a solute and a solvent. A solution of a II-VI compound as the solute and the II element as the solvent has just been mentioned. ZnTe can also be grown by cooling a solution in which the initial charge is ZnTe and an excess of tellurium. One may also use solvents other than one of the constituent elements. For example, although GaP and GaAs crystals may be grown from solutions of gallium, they can also be grown from lead, bismuth, tin, indium, selenium, tellurium, and germanium (8, 9). BP can be grown from a solution of BP dissolved in nickel (10).

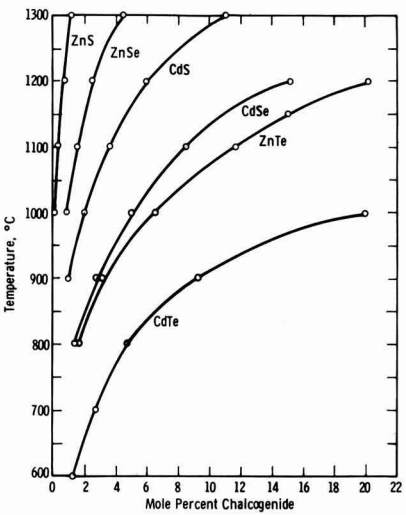

Fig. 1. Liquidus solubilities of ZnS, ZnSe, ZnTe, CdS, CdSe, CdTe as a function of temperature.

Data presented in this paper concern the liquidus solubilities of solutes ZnS, ZnSe, ZnTe, CdS, CdSe, and CdTe in a bismuth solvent.

The method used to obtain this data is the high-temperature filtration technique previously described (8). Temperature measurements were made using Pt-Pt 10% Rh thermocouples calibrated with the melting point of gold.

The bismuth used as the solvent was 99.999+% from ASARCO. The ZnS was RCA 33-Z-19 fired in H_2S at 1100°C, pressed into pellets, and fired in an evacuated tube (sealed off at a pressure less than 10^{-5} Torr) at 1100°-1200°C for 16 hr. The ZnSe was G.E. 118-8-3 purified by repeated sublimations in argon at 1300°C followed by a vapor transport (11) to produce either single crystals or masses with, at most, several crystals. The ZnTe was prepared from heating 99.999+% zinc and tellurium in argon to 500°C, and then the temperature was allowed to rise to 800°C. This material was heated in hydrogen at 600°C to remove excess tellurium. Single crystals were prepared using a vapor transport method (11). CdS was G.E. 118-8-2 material which was fired in H_2S at 1000°C followed by a vapor transport technique (11) to produce a sound mass of CdS. CdSe was prepared by sealing G.E. 118-8-4 material in a quartz tube at a pressure of less than 10^{-5} Torr and heating for several days at 950°C. The sintered material was removed from the tube and resealed at the same pressure and reheated for several days at 950°C. This yielded a hard sintered CdSe. The CdTe was prepared by heating 99.999+% cadmium and tellurium from ASARCO, sealed in a graphitized quartz ampule at a pressure less than 10^{-5} Torr, slowly to 1135°C and then slowly cooling this melt. Large single crystals were often prepared in this manner.

The mixtures of chalcogenide and bismuth were sealed in quartz tubes, maintained at temperature for 16 hr (the 1300°C experiments were maintained at temperature for 6 hr), filtered, and cooled. The filtrates and residues were separately weighed to the nearest 0.1 mg and treated with an excess of mercury at 150°C to remove the bismuth. The mercury-bismuth liquid solution was sucked off at 150°C using a small diameter tube, and finally small amounts of mercury were removed by heating the chalcogenide samples under vacuum. The chalcogenide samples were then separately weighed to the nearest 0.1 mg. Solubility measurements had a precision and accuracy of better than ±0.1 mole per cent for measurements in excess of 3 mole per cent chalcogenide and better than ±0.05 mole per cent for measurements less than 3 mole per cent chalcogenide.

The data obtained using this high-temperature filtration technique are shown in Fig. 1. It can easily be demonstrated, for the six chalcogenides, that solubility decreases as the molecular weight of the solute decreases and that solubility decreases as the sum of the tetrahedral covalent radii ($R^{II} + R^{VI}$) decreases. Needles of ZnS and platelets of the other five compounds were obtained from the filtrates.

Acknowledgments

The author would like to thank Dr. Willi Lehmann for preparing the samples of CdS, ZnSe, and ZnTe used in this paper. Also, thanks are extended to John

Burger for his assistance in the experimental phase of this work.

Manuscript received Feb. 15, 1966.

Any discussion of this paper will appear in a Discussion Section to be published in the December 1966 JOURNAL.

REFERENCES

1. A. G. Fischer, AFCRL-65-524, May 31, 1965, p. 16.
2. J. Carides and A. G. Fischer, *Solid State Communications*, **2**, 217 (1964).
3. H. H. Woodbury, *J. Phys. Chem. Solids*, **24**, 88 (1963).
4. M. Chikashige and R. Hitosaka, *Mem. Coll. Sci., Univ. Kyoto*, **2**, 239 (1917).
5. A. Reisman, M. Berkenblit, and M. Witzen, *J. Phys. Chem.*, **66**, 2210 (1962).
6. D. DeNobel, *Philips Research Repts.*, **14**, 488 (1959).
7. M. R. Lorenz, *J. Phys. Cehm. Solids*, **23**, 939 (1962).
8. M. Rubenstein, Extended Abstracts of the Electronics Div., **11**, 129, The Electrochemical Society Los Angeles Meeting, May 6-10, 1962.
9. M. Rubenstein, Extended Abstracts of the Electronics Div., **13**, 240, The Electrochemical Society Toronto Meeting, May 3-7, 1964.
10. B. Stone and D. Hill, *Phys. Rev. Letters*, **4**, 282 (1960).
11. W. W. Piper and S. J. Polich, *J. Appl. Phys.*, **32**, 1278 (1961).

Reaction Rates on Partially Blocked Rotating Disks–Effect of Chemical Kinetic Limitations

Daniel E. Rosner

AeroChem Research Laboratories, Inc., Subsidiary of Ritter Pfaudler Corporation, Princeton, New Jersey

Gregory and Riddiford (1) noticed that a chemically inert center stud failed to appreciably alter the rate of dissolution of a zinc disk rotating in iodine solutions, despite the fact that the inert area comprised some 4% of the working surface of the disk. Pursuing this further, these authors reported data (2) on the effect of progressively blocking off the center of rotating copper disks in H_2SO_4 solutions. In a discussion of this work, Ibl (3) correctly pointed out that, if the reaction on the unblocked disk was completely diffusion controlled, then the relation between the fractional reduction in reaction rate, J/J_0, and the fractional area blockage, $f \equiv (r_0/R)^2$ (see Fig. 1), would be

$$(J/J_0)_{\text{diff}} = (1 - f^{3/2})^{2/3} \qquad [1]$$

This relation is a straightforward consequence of Levich's result for species transport to a rotating disk (4, 5), as generalized by Zaidel (4) to include the effect of an inert central region ("patch"). The resulting blockage effect is considerably different from the simple result

$$(J/J_0)_{\text{chem}} = 1 - f \qquad [2]$$

(expected if the reaction were chemically controlled) since in the partially blocked diffusion-controlled case the reduction of active area is partially compensated for by greatly improved local conditions of convective diffusion (initially thin diffusion boundary layer) in the active region.

Objective.—Clearly, Eq. [1] and [2] represent two limiting cases of a more general relation governing reactions which (in the unblocked case) are neither reaction rate controlled nor diffusion controlled. Indeed, if this more general relation were known, such measurements could offer an attractive new method for inferring the extent of diffusion control, and hence true rate constants for rapid heterogeneous reactions. The purpose of this note is to outline how this more general relation can be obtained exactly[1] and to present graphically the pertinent results. For a detailed account of the theory of partially blocked rotating disks and their interesting relation to short tubular reactors, the reader is referred to ref. (6). An excellent critical review of the now extensive use of the rotating disk system in electrochemical investigations is provided in ref. (7).

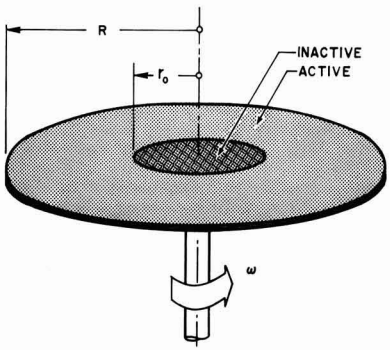

Fig. 1. Partially blocked rotating disk configuration

Outline of the analysis.—In the general case of species diffusion to a partially blocked reactive surface, outside of the nonreactive region a steady-state distribution of reactant concentration is established such that the local rate of diffusional transfer to the active disk surface is everywhere equal to that demanded by the concentration dependence of the surface reaction. While the reactant concentration (mass fraction) far from the surface, c_e, is uniform, a radial distribution of reactant concentration $c_w(r)$ is established along the surface in the region $R \geq r \geq r_0$. Both the local rate of convective diffusion and the local reaction rate depend on $c_w(r)$; hence, equating these two rates provides an equation for $c_w(r)$, from which all other quantities of interest can be obtained.

If δ_0 is the effective diffusion layer thickness as obtained from the Levich solution for the unblocked case,[2] then it can be shown (6) that the local mass rate of diffusional transport $-j''(r)$ to the active surface is related to the (as yet unknown) concentration distribution $c_w(r)$ by

$$-j''(r) = \frac{-D\rho}{\delta_0} \int_{\xi=r_0}^{\xi=r} \left[1 - \left(\frac{\xi}{r}\right)^3\right]^{-1/3} d[c_e - c_w(\xi)] \qquad [3]$$

At every $r > r_0$ this flux must be identically equal to the kinetic consumption rate, $-\mathcal{R}''$ independently expressible in terms of the local reactant concentration at the interface. In the special case of a first-order heterogeneous reaction $-\mathcal{R}''$ is given by $k_w \rho c_w$; hence, the reactant conservation equation at the interface

[1] *i.e.*, making no approximations other than those underlying the original Levich-Zaidel relation; *viz.* steady, laminar flow; constant physical properties (density, ρ, kinematic viscosity, ν, and Fick diffusivity, D); diffusional Prandtl (Schmidt) number $Pr (\equiv \nu/D) >> 1$; and negligible interfacial velocity.

[2] *i.e.*, $\delta_0 = [0.62048(Pr)^{1/3}(\omega/\nu)^{1/2}]^{-1}$, where ω is the disk speed.

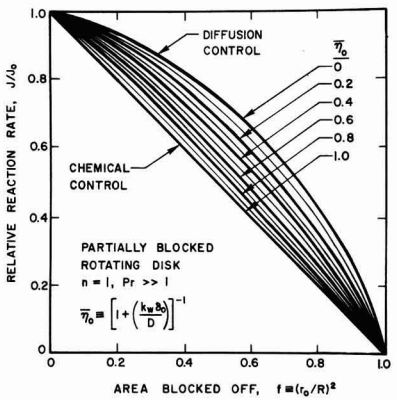

Fig. 2. Normalized reaction rate *vs.* fractional area blocked; first-order heterogeneous reaction.

takes the form of a linear, singular integral equation of the Volterra type[3]

$$k_w c_w(r) = \frac{-D}{\delta_0} \cdot \int_{\xi=r_0}^{\xi=r} \left[1-\left(\frac{\xi}{r}\right)^3 \right]^{-1/3} \frac{dc_w}{d\xi} \cdot d\xi \qquad [4]$$

Results

While local solutions to the dimensionless form of this equation can be obtained analytically, results over the entire $(k_w\delta_0/D)\,[(r/r_0)^3 - 1]^{1/3}$ range of interest are most readily obtained by numerical means on a digital computer. This has been done (6) and the results used to obtain the total reaction rate

$$-J \equiv k_w \rho \int_{r_0}^{R} c_w(r)\; 2\pi r\, dr \qquad [5]$$

from which the effects of partial blockage follow immediately. As expected, it is found that the reduction in reaction rate, J/J_0, depends not only on the fractional area blocked, $f \equiv (r_0/R)^2$ but also on the dimensionless chemical kinetic parameter $k_w\delta_0/D$. Equation [1] is recovered only when the unblocked reaction is diffusion controlled (*i.e.*, when $k_w\delta_0/D \to \infty$). Alternatively, Eq. [2] is recovered only when the unblocked reaction is chemically controlled (*i.e.*, when $k_w\delta_0/D \to 0$). Hence, by comparing the experimentally observed (J/J_0) *vs.* f relation with that predicted from Eq. [4], [5] (see Fig. 2),[4] one can infer the value of $k_w\delta_0/D$. However, rather than $k_w\delta_0/D$, we have chosen $\bar{\eta}_0$ as the parameter in Fig. 2, where

$$\bar{\eta}_0 \equiv [1 + (k_w\delta_0/D)]^{-1} \qquad (0 \leq \bar{\eta}_0 \leq 1) \qquad [6]$$

since this is the ratio of the actual reaction rate on the unblocked disk to the chemically controlled reaction rate on the same disk (5). Equivalently, $\bar{\eta}_0$ is the ratio of the apparent rate constant, $k_{w,a}$, to the true rate constant k_w. Thus, it now appears that diffusion corrections to apparent rate constants can be obtained directly[5] from careful reaction rate measurements on partially blocked disks.

It should be remarked that near the extreme of complete blockage (f near 1)[6] simple rational approximations can be obtained.[7] Thus, provided $\bar{\eta}_0$ is not too small, a first approximation to $\bar{\eta}_0$ (written $\bar{\eta}_0^{(0)}$) can be computed from

$$\bar{\eta}_0^{(0)} = (1-f)/(J/J_0)_{\text{observed}} \qquad [7]$$

which overestimates the true value of $\bar{\eta}_0$ with a relative error of about

$$\tfrac{3}{4}\,(0.8269934)\,[(1-\bar{\eta}_0^{(0)})/\bar{\eta}_0^{(0)}]\,(1-f)^{1/3} \qquad [8]$$

It is hoped that the present results, and similar exact "blockage effect" calculations under way for other flow reactor configurations, will provide the basis for a useful approach to the experimental inference of diffusion corrections and kinetic constants for rapid heterogeneous reactions.

Acknowledgments

It is a pleasure to acknowledge G. D. Bleich for programming the solution of Eq. [4] and A. Crossley for her assistance in presenting the results.

Manuscript received Feb. 10, 1966. The work on this paper was supported by the U. S. Air Force Office of Scientific Research, Propulsion Division, under Contract No. AF 49(638)1654.

Any discussion of this paper will appear in a Discussion Section to be published in the December 1966 JOURNAL.

REFERENCES

1. D. P. Gregory and A. C. Riddiford, *J. Chem. Soc.* **731**, 3756 (1956).
2. D. P. Gregory and A. C. Riddiford, *This Journal*, **107**, 950 (1960).
3. N. Ibl, *This Journal*, **108**, 610 (1961).
4. V. G. Levich, "Physicochemical Hydrodynamics," 2nd ed., Prentice Hall, New Jersey (1962).
5. D. E. Rosner, *AIAA J.*, **2**, 593 (1964).
6. D. E. Rosner, In preparation.
7. A. C. Riddiford, "The Rotating Disk System," in "Advances in Electrochemistry and Electrochemical Engineering," Vol. 4 (in press).
8. D. E. Rosner, *Int. J. Heat Mass Transfer*, In press.

[3] An identical equation governs the finite rate dissolution problem. In that case the local dissolution rate, $\mathcal{R}''$, is expressible in the form $k_w\rho \cdot (c_{w,eq} - c_w)$, where $c_{w,eq}$ is the equilibrium (or "saturation") value of the transferred species mass fraction at the wall. The equation governing the ratio $(c_{w,eq} - c_w)/(c_{w,eq} - c_e)$ is the same as Eq. [4], and the results presented below for the total normalized reaction rate, J/J_0, therefore apply to the case of dissolution as well. It should be reiterated that the present results are exact only in the absence of appreciable interfacial velocities. As discussed in ref. (8), this implies that the condition $(c_{w,eq} - c_e) << (1 - c_{w,eq})$ must be satisfied.

[4] A full-scale plot of these results is available from the author on request.

[5] Incidentally, on treating the 25°C data of ref. (2) in this way (allowing for some experimental scatter) we estimate that $\bar{\eta}_0$ was between 0.1 and 0.2, corresponding to a nearly diffusion-controlled dissolution.

[6] This corresponds to the use of a "ring" (electrode or active surface) of width $\Delta r << r_0$ in which case $1 - f$ may be identified with $2(\Delta r/r_0)$.

[7] Perhaps the simplest function that can be constructed to approximate the exact J/J_0 *vs.* f relation over the entire range of f and $\bar{\eta}_0$ is

$$J/J_0 \approx \{[\bar{\eta}_0/(J/J_0)_{\text{chem}}] + [(1-\bar{\eta}_0)/(J/J_0)_{\text{diff}}]\}^{-1}$$

However, this relation is found to be inadequate for inferring accurate values of $\bar{\eta}_0$ from experimental rate *vs.* area blockage data.

Brief Communications

The Pseudobinary System Ge-GaAs

M. B. Panish

Bell Telephone Laboratories, Incorporated, Murray Hill, New Jersey

Recently, several papers in which the liquid-solid equilibria in the Ge-GaAs pseudobinary system was discussed have appeared in the literature (1-3). Although there is agreement that the system is essentially simple binary eutectic in nature, there is considerable disagreement as to the position of the liquidus curve and the temperature and composition of the eutectic.

During studies of the Ga-As-Ge ternary system (4), this author determined the liquidus and eutectic temperatures at several compositions along the Ge-GaAs pseudobinary. These data, along with the previously reported data, are shown in Fig. 1.

It should be noted that Glazov and Malyutina (1), Takeda *et al.* (2), and this author agree quite well as to the eutectic composition (~ 16 mole % GaAs), while Lieth and Heyligers (3), Takeda *et al.* and this author agree very well on the eutectic temperature (663° ± 3°C). The major discrepancies are the liquidus and eutectic temperatures of Glazov and Malyutina, and the liquidus curve and eutectic composition of Lieth and Heyligers (3). The liquidus and eutectic temperatures of Takeda and this author are in fair agreement.

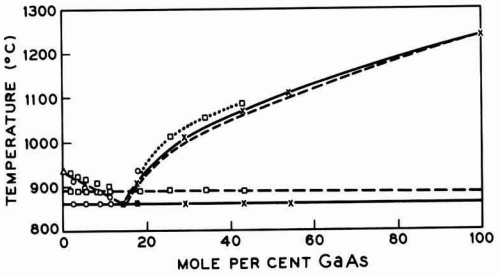

Fig. 1. GaAs-Ge pseudobinary phase diagram; symbols: □ (1), — — — (2), X this work, ○ (5), △ (6).

If the latter data are taken as essentially correct, the higher temperatures of Glazov and Malyutina may be ascribed to a thermometric discrepancy. It is more difficult to account for the data of Leith and Heyligers. The agreement between the eutectic temperatures eliminates any serious thermometric error or the possibility of serious component contamination by impurities. It is possible that the discrepancy between their data and that of Takeda and this author arises from an error in the way composition was reported. The assumption can be made that Lieth and Heyligers reported as mole per cent GaAs a quantity which was actually weight per cent GaAs. Their revised data (5) are shown in Fig. 1 and, except for one point, are in good agreement with the data of Takeda and this author.

Acknowledgment

Helpful discussions with C. D. Thurmond are gratefully acknowledged.

Manuscript received March 10, 1966.

Any discussion of this paper will appear in a Discussion Section to be published in the December 1966 JOURNAL.

REFERENCES

1. V. M. Glazov and G. L. Malyutina, *Russ. J. Inorg. Chem.*, **8**, 1000 (1963).
2. Y. Takeda, H. Hirai, and H. Hirao, *This Journal*, **112**, 363 (1965).
3. R. M. A. Lieth and H. J. M. Heyligers, *ibid.*, **113**, 96 (1966).
4. M. B. Panish, *J. Less Common Metals*, **10**, 416 (1966).
5. R. M. A. Lieth and H. J. M. Heyligers, Private communication.
6. F. X. Hassion, C. D. Thurmond, and F. A. Trumbore, *J. Phys. Chem.*, **59**, 1076 (1955).

Adsorption of Perchlorate Ions on Gold

J. D. Goodrich and G. M. Schmid

Department of Chemistry, University of Florida, Gainesville, Florida

In the course of a previous study of the differential capacity of the electrical double layer on a gold electrode in 1.0-0.01M perchloric acid solution (1) a hump in the capacity-potential curve at 0.4-0.8v *vs.* a standard hydrogen electrode (SHE) was ascribed to the adsorption of perchlorate ions on the electrode. To obtain experimental support for this assumption we attempted to measure the depletion of perchlorate ions from a very dilute solution in contact with gold foil polarized to various points in the indicated potential range.

Gold foil (fine gold, Engelhard Industries, Inc.) of 40 cm^2 apparent area was shaped into a tube and embedded at the bottom into Kel F-100 wax in a Pyrex cell. Electrical contact was provided by a gold wire welded to the foil. This test electrode was concentric to a polarizing electrode made of gold wire of about 1 cm^2 area. The reference electrode was a hydrogen saturated palladium wire (+ 50 mv *vs* SHE) (2). The volume of the cell was approximately 10 ml.

The test electrode was etched in aqua regia, cleaned in sulfuric acid-dichromate solution, and soaked in triple distilled water for several days. Helium, saturated with water vapor, was passed over the system for several hours prior to and during a run. The cell was polarized with a Sensitive Research Instrument model PV potentiometer; the potential was monitored with a Keithley model 610B electrometer.

Perchlorate ions, in 10 ml of solution, before and after a run, were determined spectrophotometrically after extraction with methylene blue according to Iwaski, Utsumi, and Kang (3) in the range 0.04-1.00

Table I. Polarization data: gold in perchloric acid

Concentration, M × 10^6	Potential, v *vs.* SHE	Time polarized, hr
2.072	0.50	2.5
2.072	0.25	6
1.036	0.30	3

ppm. By weighing all solutions to 0.01 mg and keeping the ambient temperature to 23° ± 1° the average deviation of the method could be kept to ±0.01 ppm (28 determinations).

Table I gives a sample of the perchloric acid concentrations used, the polarizing potentials, and the duration of polarization. No concentration change was noted in any of the experiments. With the method of determination used a concentration change of 0.01 ppm in 10 ml, or 6 x 10^{14} perchlorate ions, should have been detected. The coverage of the test electrode under the conditions employed here is therefore less than about 10^{13} perchlorate ions/cm^2 of apparent area, or less than about 1 % of a monolayer, not taking into account a roughness factor which is certainly greater than unity.

It should be pointed out that these results do not invalidate the assumption of perchlorate adsorption on gold made previously (1). The perchlorate ion adsorption we failed to detect here would be for a system in equilibrium with 10^{-6}M perchloric acid, whereas the assumption was originally based on work with 1.0-0.01M solutions.

Acknowledgment

Thanks are due to the National Science Foundation for financial support of this work under Grant No. 4228, and for a Summer Research Fellowship for one of us (J.D.G.).

Manuscript received Dec. 30, 1965.

Any discussion of this paper will appear in a Discussion Section to be published in the December 1966 JOURNAL.

REFERENCES

1. G. M. Schmid and Norman Hackerman, *This Journal*, **109**, 243 (1962).
2. D. Ives and G. Janz, "Reference Electrodes," Academic Press, New York (1961).
3. I. Iwasaki, S. Utsumi, and C. Kang, *Bull. Chem. Soc. Japan*, **36**, 325 (1963).

Discussion Section

This Discussion Section includes discussion of papers appearing in the JOURNAL of the Electrochemical Society, Vol. 112, No. 1, 6, 7, 8, 9, 10, 11, and 12 (January and June to December 1965). Discussion not available for this issue will appear in the Discussion Section of the December 1966 JOURNAL.

Catalytic Decomposition of Aqueous Formic Acid on Platinum Electrodes

D. R. Rhodes and E. F. Steigelmann (pp. 16-21, Vol. 112, No. 1)

W. Vielstich and U. Vogel[1]: In a series of publications it has been shown by different investigators that during the anodic oxidation of formic acid in acid electrolytes an intermediate product is formed which blocks the surface in a certain potential region. Anodic potential scans show three current peaks (at 0.5, 0.8, and 1.3v *vs.* H_2 electrode). In the region of the first peak the intermediate is formed; at the potential of the second peak the intermediate is oxidized to CO_2.

Rhodes and Steigelmann assume that the intermediate product is carbon monoxide formed by catalytic decomposition of HCOOH into CO and H_2O. Potential scan diagrams with HCOOH and CO are performed in order to prove this hypothesis.

In their experiments the authors observe a small difference (30 mv at a sweep rate of 1.2 v/sec, see their Table I) between the potential of the peak for CO and the potential of the second formic acid peak, especially during the first sweep, their Fig. 1 and 3. Nevertheless Rhodes and Steigelmann suggest that two peaks are caused by the oxidation of the same species.

In our laboratory we have repeated the above mentioned experiment,[2] recording the current/potential diagrams (corresponding to their Fig. 1 and 3) on the same figure. This diagram (our Fig. 1) clearly shows: (*a*) the difference in potential between the two peaks is very pronounced and amounts to about 60 mv; (*b*) the rising part of the CO peak is so sharp that due to adsorbed carbon monoxide only a very small current should be possible in the region of the formic acid peak.

In addition to the different shape of the current/potential diagrams there exists another strong argument against the assumption of carbon monoxide as intermediate product. Johnson and Kuhn[3] have made a simultaneous determination of the number of coulombs and the number of chemical equivalents of reduced CO_2; these species are identical with the intermediate product of formic acid oxidation.[4,5] Instead of the number of 2 electrons per particle stated in the paper[3] one of the authors recently informed us that, due to an error in calculation, the true number is one electron per particle.[5a]

Therefore, the results of Johnson and Kuhn[3, 5a] are in agreement with our own conclusion[4,5] that the intermediate product should be a formate radical, probably of the form 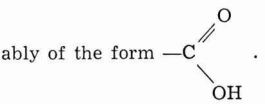 .

D. R. Rhodes and E. F. Steigelmann: The figure presented by Vielstich and Vogel does clearly show a

[1] Institut fuer Physikalische Chemie der Universitaet Bonn, Wegelerstrasse 12, Bonn, Germany.

[2] W. Vielstich and U. Vogel, Unpublished results.

[3] P. R. Johnson and A. T. Kuhn, *This Journal*, **112**, 599 (1965).

[4] W. Vielstich and U. Vogel, *Ber. Bunsen Ges. Physikal. Chem.*, **68**, 688 (1964).

[5] W. Vielstich, "Brennstoffelemente—Moderne Verfahren zur elektrochemischen Energiegewinnung," Verl. Chemie, Weinheim 1965.

[5a] A. T. Kuhn, private communication.

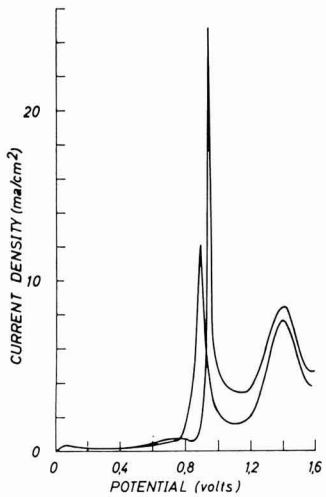

Fig. 1. First sweep of 0.085M HCOOH in 1*N* H_2SO_4 at 30°C on 1 cm^2 smooth Pt, sweep rate of 260 mv/sec; (*a*) N_2 stirring; (*b*) CO stirring.

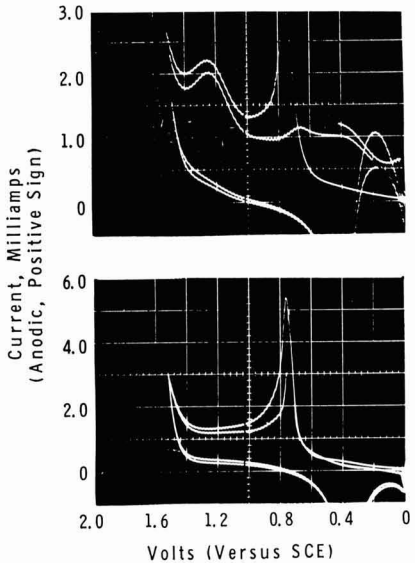

Fig. 1. First and third consecutive sweeps of 0.085M HCO_2H (top) and saturated CO (bottom) in 1*N* H_2SO_4 at 30°C on a platinum disk electrode rotating at 600 rpm; 0.97 cm^2 real surface area; sweep rate of 1.2 v/sec.

difference of 60 mv between the peaks for the first sweep of formic acid and carbon monoxide. Therefore, we have reexamined our curves from similar experiments.

One set of such curves is given in this discussion. These were used to sketch the figures given in our original article. They were obtained at a sweep rate of 1.2 v/sec and at a starting potential of 0.0v *vs.* SCE. The first sweep in each photograph is represented by the tallest peak at about +0.7v. The third sweep in each photograph, which was obtained by closing the camera shutter during the second sweep, shows that the peaks at about +0.7v have shifted slightly in the negative direction for both formic acid and CO. This effect was discussed in the original article.

Our figures show that we obtained a difference of 30 ± 10 mv between the formic acid and CO peak at about 0.7v during the first sweep. A check of the rest of our original data given in the article in Table I for the various sweep rates showed that the differences listed were accurate to ± 10 mv. Because we might have made some error during this series of experiments, we examined another set of similar data taken several days earlier. Once again the data fit to within ± 10 mv. We had also recorded sweeps of CO and formic acid oxidation on a recorder at sweep rates equal to 0.13 v/sec and lower. In each case the corresponding *dv/dt* curve had been recorded. At 0.13 v/sec the difference between the two peaks during the first sweeps was 20 ± 10 mv.

From the above discussion we conclude that the difference in peak voltages listed in Table I of the original article is a real effect and not an experimental error. Therefore, the difference between our results and that by Vielstich and Vogel must be a difference in experimental parameters. One obvious difference is that we started our sweeps at 0.0v *vs.* SCE (0.245v *vs.* NHE); whereas, they started their sweeps at 0.0v *vs.* NHE, which is well within the hydrogen region. It is known that the type of adsorption of CO affects the potential where it is oxidized [our figure here and Ref. (6)]. Perhaps the results by Vielstich and Vogel reflect the effect of hydrogen on CO oxidation and/or formic acid adsorption.

Perhaps the most important point brought out by Vielstich and Vogel is that Johnson and Kuhn[7] have changed from two electrons per particle to one electron per particle for the intermediate product of formic acid oxidation. We do not feel like making any comment on this change until it is made public.

On the Potential/pH Diagrams of the Cu-NH_3-H_2O and Zn-NH_3-H_2O Systems

H. E. Johnson and J. Leja (pp. 638-641, Vol. 112, No. 6)

F. Letowski and J. Niemiec[8]: The potential/pH diagrams given by Johnson and Leja as well as the potential/pH diagrams discussed by them and developed by Mattsson[9] enabled the authors to interpret the results of studies on the corrosion of brass in aqueous ammonia and ammonium salts solutions. Johnson and Leja disputed in their paper the correctness of the position of the stability ranges of Cu_2O and CuO oxides as well as those of the basic cupric sulfate $Cu(SO_4)_{0.25}(OH)_{1.5}$ on the potential/pH diagrams given by Mattsson. According to Johnson and Leja the oxides CuO_2 and CuO are stable, in 0.05M solution of Cu and 1.0M of NH_3 and NH_4^+ at *p*H values exceeding 11, but these compounds are not stable in the *p*H range 3-7.5 determined by Mattsson. In the discussion below it is shown, on the basis of the equilibria determined by Johnson and Leja and Mattsson,[9] that the solid phases in question are also stable in both of the *p*H ranges discussed.

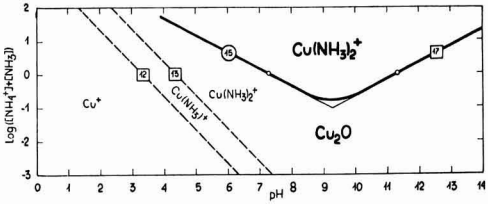

Fig. 1. Influence of *p*H and total $NH_3 + NH_4^+$ activities on the solubility ranges of Cu_2O at 25°C (total dissolved Cu = 0.05M; □—equilibria according to Johnson and Leja; ○—according to Mattsson).

According to Johnson and Leja the equilibrium of their reaction [17], dissolution of Cu_2O in ammonia solution,

$$Cu_2O + 4NH_3 + 2H^+ = 2Cu(NH_3)_2^+ + H_2O \quad [17]$$

is described by

$$pH = 9.99 + 2\log[NH_3] - \log[Cu(NH_3)_2^+]$$

The equilibrium [17] is shown in the plot of log ($[NH_3 + NH_4^+]$) *vs.* *p*H at Cu activity 0.05M in Fig. 1. It is valid merely within the range of NH_3 predominance, *i.e.*, at *p*H values higher than 9.26. At *p*H values lower than 9.26 the NH_4^+ ions prevail and equilibrium [17] (Johnson and Leja) becomes senseless. As determined by Mattsson for the reaction

$$0.5Cu_2O + 2NH_4^+ = Cu(NH_3)_2^+ + H^+ + 0.5H_2O$$

the equilibrium

$$pH \quad 8.56 - 2\log[NH_4^+] + \log[Cu(NH_3)_2^+] \quad [15]$$

becomes valid in this region. A plot of this equilibrium is shown in Fig. 1 at Cu activity 0.05M. Near *p*H 9.26 the NH_3 and NH_4^+ concentration (or activities) change with *p*H logarithmically; in Eq. [17] and our [15] their sum $[NH_3] + [NH_4^+]$ should be taken into account instead of the individual $[NH_3]$ and $[NH_4^+]$ activities. A gently transition of equilibrium [17] into [15] is thus obtained and, for *p*H 9.26, the logarithm of the sum of activities at which the solution over Cu_2O is saturated with $Cu(NH_3)_2^+$ is equal to —0.7. The ordinate values of the points situated in equilibrium curves [17] and [15] (Fig. 1) at a total $[NH_3] + [NH_4^+] = 1.0M$ should define the positions of these equilibria on the potential/pH diagrams of a Cu-NH_3-H_2O system; the first one extends toward the right from pH 11.29 (Johnson and Leja) and the second one toward the left from *p*H 7.26 (Mattsson).

By plotting the CuO and $Cu(SO_4)_{0.25}(OH)_{1.5}$ dissolution equilibria as log ($[NH_3] + [NH_4^+]$) against *p*H (Fig. 2) one obtains evidence that the stability

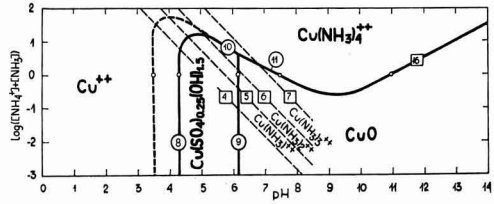

Fig. 2. Influence of *p*H and total $NH_3 + HN_4^+$ activities on the solubility ranges of CuO and $Cu(SO_4)_{0.25}(OH)_{1.5}$ at 25°C (total dissolved Cu = 0.05M; □—equilibria according to Johnson and Leja; ○—according to Mattsson; --- according to Bustorff and Muylder, and Letowski and Niemiec).

[6] S. Gilman, *J. Phys. Chem.*, 66, 2657 (1962).

[7] P. R. Johnson and A. T. Kuhn, *This Journal*, 112, 599 (1965).

[8] Institute of Inorganic Chemistry and Metallurgy of Rare Elements, Technical University, Wroclaw, Wybrzeze Wyspianskiego 27, Poland.

[9] E. Mattsson, *Electrochim. Acta*, 3, 279 (1961).

ranges of these solid phases were correctly placed by Johnson and Leja in the range of pH values higher than 10.95 and by Mattsson in the pH range 4.28-7.46. In conclusion, a correct image of the Cu-NH_3-H_2O system equilibria, based on thermodynamic data used by Johnson and Leja, and Mattsson, is obtained by superimposing their potential/pH diagrams [*This Journal*, **112**, 629, Fig. 2a and 2b]. The solubility limits of the basic cupric sulfate $Cu(SO_4)_{0.25}(OH)_{1.5}$ also seem to be controversial. Therefore, these limits in a 0.05M copper solution and 1.0M total ammonia and ammonium ions solution were also indicated in Fig. 2 by a dotted line, according to the potential/pH equilibria of the Cu-H_2O-H_2SO_4 system developed by Bustorff and Van Muylder[10] as well as the Cu-H_2O-NH_3-H_2SO_4 system developed by Letowski and Niemiec.[11] These differences in the solubility ranges of the basic cupric sulfate result from differences between the thermodynamic data used for elaboration of these systems.

Johnson and Leja have also argued the occurrence of the $Zn(OH)_2$ stability range in the potential/pH diagram of the Zn-NH_3-H_2O system made by Mattsson.[9] It follows, however, from the dissolution equilibria of zinc hydroxide shown in Fig. 3 that the presence of the $Zn(OH)_2$ stability range in the potential/pH diagram of the Zn-NH_3-H_2O system made by Mattsson is not in contradiction with the equilibria given by Johnson and Leja [*This Journal*, **112**, 640, Fig. 3a and 3b], as these diagrams are made for different zinc activities in solution (Mattsson, 0.01M; Johnson and Leja, 0.001M). The positions of the equilibria in Fig. 3 at $[NH_3] + [NH_4^+] = 1.0M$ are denoted by the points. The ordinate values of these points define the pH values at which the ZnO hydrat dissolution equilibria should be placed in the potential/pH diagram. For Zn activity = 0.01M (Mattsson), two stability ranges of zinc hydroxide should appear; the first one is comprised of the pH range 6.54-7.48 defined by equilibria [18] and [19] according to Mattsson[9]; the second one should be in the pH range from 11.19 to 13.89 limited by the equilibria of the reactions

$$Zn(NH_3)_4^{++} + H_2O = ZnO + 4NH_3 + 2H^+$$

$$pH = 10.19 + 2 \log [NH_3] - 0.5 \log [Zn(NH_3)_4^{++}]$$

according to the authors of the present discussion and

$$ZnO + H_2O = ZnO_2^{--} + 2H^+$$

$$pH = 14.89 + 0.5 \log [ZnO_2^{--}]$$

according to Pourbaix.[12] For Zn activity = 0.001M (Johnson and Leja) there should be only one ZnO hydrat stability region in the pH range from 11.69 to 13.39 which is determined by the above two equilibria.

Plotting of equilibria [21] and [22] in the potential/pH diagram of the Zn-NH_3-H_2O system of Johnson and Leja [*This Journal*, **112**, 640, Fig. 3b] does not seem to be justified. According to the Pourbaix's definition[12] these equilibria should separate the relative predominance ranges of Zn^{++} from those of $Zn(NH_3)_3^{++}$ and $Zn(NH_3)_3^{++}$ from $Zn(NH_3)_4^{++}$. However, because of the close positions of these equilibria such a situation never occurs. In Fig. 3 a dependence of pH and percentage contents of a more basic form in 1.0M total $NH_3 + NH_4^+$ solution is shown. The $Zn(NH_3)_3^{++}$ ions will never occur in concentrations equal to those of the neighboring ions. The maximum contents of the $Zn(NH_3)_3^{++}$ ions do not exceed 14%, so in the whole pH range in question the Zn^{++} or $Zn(NH_3)_4^{++}$ ions prevail.

The argument for the localization of oxide phases made by Johnson and Leja on the basis of ΔG^o values as well as their questioning of the stability ranges of solid phases defined by Mattsson, seem to be unnecessary; ΔG^o depends on the stability constants according to $\Delta G^o = -RT \ln K$, and the effect of the thermodynamic potential on equilibria is manifested in the equilibrium constants themselves which, on the other hand, determine the position of equilibria on the potential/pH diagram.

H. E. Johnson and J. Leja: We are grateful to Messrs. Letowski and Niemiec for their contribution which helped us to pin-point the source of error in the issue under discussion.

The attempt of theirs to strike a compromise between Mattsson's and our evaluation does not agree with our limited evidence that the system copper-ammonia does not show the development of Cu_2O tarnish in the pH range indicated by Mattsson (if precautions are taken to eliminate CO_2). Secondly, it seems inconceivable that the domains of stability of $Cu(NH_3)_2^+$ and Cu_2O, Fig. 1 of Letowski and Niemiec, can be separated by two lines thus endowing the same two species with an alternately reversed acid-basic characteristics.

We cannot agree that reaction [17] "becomes senseless" at pH values below 9.26 where NH_4^+ ions outnumber NH_3 groups; analogous reasoning would lead to the conclusion that reactions involving hydrogen ions are senseless at pH values above 7.0 where they are outnumbered by their hydroxyl ion counterparts. The crux of the present problem is the seeming inconsistency of Eq. [17] and [15]. Letowski and Niemiec have suggested a compromise which involves the sum of the $[NH_3]$ and $[NH_4^+]$ activities; it is interesting to note that a third modification of equations [17] and [15] can be written to express the dissolution of Cu_2O in terms of both NH_3 and NH_4^+ as follows

$$Cu_2O + 2NH_4^+ + 2NH_3 = 2\,Cu(NH_3)_2^+ + H_2O$$

Note that since this equation involves neither redox reactions no hydrogen ions it cannot be represented on a potential/pH diagram. Equation [17], on the other hand, considers the ligand rather than the undissociated ion, NH_4^+, and seems to represent the actual experimental observations.

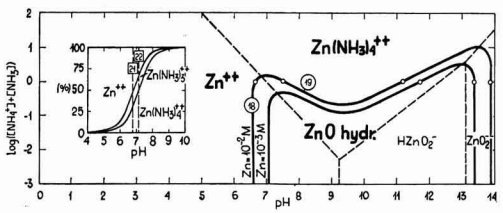

Fig. 3. Influence of pH and total $NH_3 + NH_4^+$ activities on the solubility of ZnO hydr. and the influence of pH on the percentage contents of Zn^{++}, $Zn(NH_3)_3^{++}$ and $Zn(NH_3)_4^{++}$ in 1.0M solution of $NH_3 + NH_4^+$ (□—equilibria according to Johnson and Leja; ○—according to Mattsson).

Hydrogen Peroxide Reactions on Gold Electrodes

A. K. M. S. Huq and A. C. Makrides (pp. 756-757, Vol. 112, No.7)

G. Bianchi, F. Mazza, and T. Mussini[13]: As far as gold in acid solutions of hydrogen peroxide is concerned, the reaction which determines the rest potential and the reaction which gives support to significant currents should be taken into account distinctly. In fact,

[10] A. Bustorff and J. Van Muylder, *Electrochim. Acta*, 9, 607 (1964).

[11] F. Letowski and J. Niemiec, *Roczniki Chem.*, 40, [7-8] (1966).

[12] M. Pourbaix, "Atlas d'Equilibres Electrochimiques a 25°C," Gauthier-Villars, Paris (1963).

[13] Laboratory of Electrochemistry and Metallurgy, University of Milan, Milan, Italy.

the reaction which determines the rest potential of gold has a very low exchange current, and cannot support currents significant and constant in the time.[14]

In our papers cited by Huq and Makrides, in a prior one,[15] and in a subsequent one[16] dealing explicitly with the process of oxygen and hydrogen peroxide on gold electrodes, we proposed the mechanism

$$H_2O_2 + 2H_{ads} \rightarrow 2H_2O$$

to explain the cathodic process at current densities ranging from 5×10^{-5} to 10^{-3} amp/cm^2. The range of electrode potentials corresponding to this range of current densities is + 0.4 to — 0.1v (NHE) and is not incompatible with the mechanism cited above, if the preceding reaction is rapid and no H_{ads} accumulation on the gold surface takes place.

As for the slope of the Tafel's line, the values one can draw from the Huq and Makrides' graph in the case of 10^{-3} m H_2O_2 solutions are 0.18 for increasing current densities and 0.30 for decreasing ones, respectively. Within the same range of current densities as above, we found a 0.18 slope in agreement with the previous results of Akopyan[17] who also made a distinction of processes occurring at currents either higher or lower than 5×10^{-5} amp/cm^2. Setting aside the question of the reaction which determines the rest potential of gold, as it is the subject of a next paper, we think that at present there is no argument to make inapplicable the mechanism we proposed for the cathodic reduction of hydrogen peroxide on gold at significant currents ranging from $5 \cdot 10^{-5}$ to 10^{-3} amp/cm^2.

As concerns the anodic reaction, we proposed a mechanism involving an adsorbed surface oxide and not the gold bulk oxide, the reactivity of the latter besides being the lower as the nobler is its anodic potential of formation.[17] The fact that at the + 1.4v (NHE) potential an anodic inhibition takes place, due to a beginning occurrence of the gold bulk oxide,[18] is not an argument against that mechanism since we proposed it in terms of a H_2O_2 anodic oxidation by reaction with an adsorbed surface oxide which forms within + 1.0 and + 1.4v (NHE), in the case of gold.

The Absorption of Electrolytically Generated Hydrogen

F. Matsuda and T. C. Franklin (pp. 767-771, Vol. 112, No. 8)

G. Dubpernell[19]: It is not believed that hydrogen can diffuse through solid iron at room temperature,[20] but rather that any diffusion is associated with pores or defects in the structure of the metal. It is noted that the iron membranes were prepared by etching shim steel sheet with 1M nitric acid, and that the membrane in Fig. 12 was 3.0×10^{-3} cm thick (0.0012 in.) and in Fig. 13, 2.5×10^{-3} (0.001 in.) thick.

It would be of interest to know how long the membranes were etched, and what was their original thickness. Was the loss in weight determined? How was the final thickness measured? Was any effort made to check whether or not the membranes had any pores or holes in them?

F. Matsuda and T. C. Franklin: The two membranes studied in this article were prepared from commercially available shim steel. The 3×10^{-3} cm membrane was prepared by severe etching of a sheet 0.003 in. thick in 1M nitric acid, while the 2.5×10^{-3} cm membrane was obtained by dipping a 0.001 in. sheet briefly in acid and immediately removing and rinsing. Thus the thinnest membrane was (as indicated by a micrometer caliper) essentially unetched 0.001 in. shim steel. In view of the fact that the results on the two membranes (prepared from different samples of starting material, etched in one case severely and in the other case negligibly, and having different final thickness) gave, when corrected for thickness, almost identical rate constants (4.3×10^{-5} and 4.8×10^{-5} cm/min) strongly indicates that migration could not have occurred by something so haphazard as holes.

In addition it should be pointed out that an iron membrane with a thickness of 0.003 in. (7.5×10^{-3} cm) (after degreasing and dipping briefly in nitric acid) was used in some early experiments. The results obtained were qualitatively the same as those indicated in the paper. This membrane was not used for quantitative runs because the increased thickness extended the time for a complete run beyond a convenient value. It is difficult to imagine pores in a membrane this thick.

In order to further check on this question two other experiments were run: (A) A new iron crucible with a wall thickness of 0.08 cm, after degreasing and a momentary dip in 1M nitric acid, was filled with 2*N* sodium hydroxide containing some potassium permanganate. Hydrogen was generated electrolytically on the exterior of the crucible immersed in 2*N* sodium hydroxide solution. The color of the permanganate solution was compared with that of a blank run, identical in every respect, except for the fact that hydrogen was not generated on the exterior wall of the crucible. Although the permanganate undergoes some decomposition on its own and there is some reduction by the iron, it was obvious after 1 hr, even to the naked eye, that the rate of reduction in the crucible acting as a hydrogen membrane was much greater than the rate of reaction in the blank. This increased reduction rate could only be caused by hydrogen passing through the iron crucible. Again, it is difficult to visualize the presence of pores in a new iron crucible. (B) Some measurements were made on the amount of hydrogen codeposited in the electrolytic deposition of iron. The plating bath consisted of 213g of ferrous sulfate ($FeSO_4 \cdot 7H_2O$) in one liter of solution with the pH maintained at 2.8-3.5 with sulfuric acid. The bath temperature was 45°C and the current density was 17.3 ma/cm^2. The cathode and the anode were prepared from Baker Analyzed Reagent Grade iron wire. The cathodes (21 cm long) were degreased in kerosine, rinsed in distilled water, dipped in 1-1 nitric acid and rinsed in distilled water. After plating, the amount of hydrogen codeposited with the iron was measured by the coulometric technique described in this paper and in the paper by Franklin and Goodwin.[21]

The amount of hydrogen found codeposited in iron by the coulometric method should increase linearly with increasing thickness of the deposit. However, at some thickness this increase should begin to depart from linearity because the method can only analyze for the amount of hydrogen that can diffuse to the surface during the time that the voltage sweeps through the hydrogen region. (Approximately 3 min.) Figure 1 shows the results obtained in a series of runs. It can be seen that the data is linear throughout the range covered by these experiments. Using the density of iron the largest deposit was calculated to be 2.3×10^{-3} cm thick. To explain this linear graph by migration only through pores or defects would require that such pores or defects be continuous throughout the deposit. Although possible, this does not seem probable. Migration along grain boundaries seems to

[14] J. P. Hoare, *This Journal*, 110, 245 (1963).

[15] G. Bianchi, *Corrosion et Anticorrosion*, 5, 146 (1957).

[16] G. Bianchi, F. Mazza, and T. Mussini, "Oxygen and Hydrogen Peroxide Electrochemical Behavior on Gold Electrodes," AFOSR-TN 2054, December 1961.

[17] A. U. Akopyan, *Zhur. Fiz. Khim.*, 33, 1625 (1959).

[18] S. B. Brummer and A. C. Makrides, *This Journal*, 111, 1122 (1964).

[19] M&T Chemicals Inc., Detroit 20, Michigan.

[20] G. Dubpernell, *This Journal*, 112, 646 (1965).

[21] T. C. Franklin and J. R. Goodwyn, *This Journal*, 109, 288 (1962).

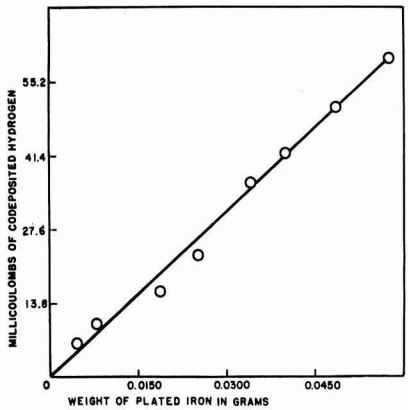

Fig. 1. The amount of hydrogen codeposited with iron

best explain the majority of data taken in our laboratory.

We wish to thank the Robert A. Welch Foundation of Houston for their support of this study.

Oxygen Overvoltage Measurements on Bright Pt in Acid Solutions, III. Nitric Acid Passivated Bright Platinum

J. P. Hoare (pp. 849-853, Vol. 112, No. 8)

J. A. Shropshire[22]: In reading the author's analysis of the effect of concentrated HNO_3 on the oxygen reduction in acid solution, I was disappointed that he failed to mention possible effects other than formation of a complex oxide structure. It is well known, for instance, that a platinum electrode in H_2SO_4 solution containing HNO_3 can exhibit extremely noble potentials, comparable to those for reversible oxygen, as a result of the complex NO, HNO_2, *etc.*, equilibrium.[23,24] It would appear that much of the transient behavior reported in this work, both cathodic and anodic to the reversible oxygen potential could be explained in terms of strongly adsorbed NO, HNO_2, species which can be removed by severe cathodization or anodization. The reduction of adsorbed HNO_2 coupled with an oxygen regeneration of the reduced product *in situ* might well support the observed cathodic currents. The efficient function of an adsorbed molybdate species in just this fashion is known in the oxidation of HCHO and CH_3OH at a platinum electrode in H_2SO_4.[25]

Although no coulombic data are available from the paper it would be interesting to see if the quantity of anodic coulombs consumed in the initial anodic transition shown in, *e.g.*, Fig. 4 in the paper corresponds to oxidation of monolayer quantities of material. As mentioned previously, I think it would be desirable to have the author recognize and comment on these possibilities.

J. P. Hoare: The comments of Dr. Shropshire are well taken and were a source of some concern as pointed out earlier.[26] However, it was noted that the high anodic potentials (about 1.28v) were observed by Vetter[27] when the nitric acid concentration ranged from 7 to 14.5N. Nitric acid concentrations studied by Shropshire and Tarmy[28] extended from 0.2 to 1M. Since the nitric acid treated electrodes used in these polarization studies[29] and referred to as Pt-O-alloy electrodes[30] were soaked in triply distilled water for at least one-half hour with at least five changes of water before being plunged into O_2-saturated, H_2O_2-free, 2N H_2SO_4 solution, it was considered safe to assume that a NO_2/NO couple was not potential-determining.[26] The concentration of HNO_3 in this case is minuscule.

In some recent studies,[31] treated and untreated samples of Pt were examined with x-ray diffraction techniques. The results show that only Pt diffraction lines were obtained in both cases except that the lines were slightly shifted in the treated case. From the results of vacuum fusion studies, the treated samples in every case not only contained more oxygen but also contained the same or even less nitrogen than the untreated samples.

It is concluded[31] that the treatment of Pt with HNO_3[26] permits more oxygen to be dissolved in the surface layers of the metal. This oxygen exists as an alloy of Pt and O atoms in these surface layers. Finally, this skin of Pt-O alloy is a better catalyst for many electrode reactions[29,32] than bare Pt. It must be remembered that the presence of adsorbed oxygen on the metal surface may inhibit the reduction of oxygen[33,34] but oxygen dissolved in the metal accelerates the reduction of oxygen.[29]

Consequently, explanations for the electrochemical behavior of the Pt-O-alloy electrode involving adsorbed NO, HNO_2, and the like must be rejected.

Electrochemical Studies of NO^+ and NO_2^+ in Concentrated H_2SO_4

L. E. Topol, R. A. Osteryoung, and J. H. Christie (pp. 861-864, Vol. 112, No. 8)

G. Bianchi and T. Mussini[35]: As concerns reaction [i] $NO^+ + e \rightarrow NO$ with subsequent stage [ii] $2NO + 2H^+ + 2e \rightarrow H_2N_2O_2$ or the possible alternative stage [iii] $NO + 3e + 4H^+ \rightarrow NH_2OH_2^+$ depending on the appearance of hydroxylamine as a final product of reaction, it is to be pointed out that results obtained with mercury electrodes cannot apply validly to the case of platinum, apart from the fact that platinum can exert a catalytic intervention[36,37] in the reaction [iv] $4NH_2OH_2^+ \rightarrow 2NH_4^+ + H_2N_2O_2 + 2H_2O + 2H^+$. Moreover, reaction [v] $NH_2OH + NO^+ \rightarrow H_2N_2O_2 + H^+$ (or else $NH_2OH + HNO_2 \rightarrow N_2O + 2H_2O$) can take place[38,39]; this is very rapid in the intermediate concentration range of H_2SO_4 (from 4 to 14M). The results obtained by Masek and Przewlocka[40] working with a platinum vibration electrode show a wave at the + 0.43v (SCE) half-wave potential, very near the + 0.70v (NHE) potential we proposed for reaction [i].[41] On mercury the half-wave

[22] Esso Research & Engineering Company, P. O. Box 121, Linden, New Jersey 07036.

[23] J. A. Shropshire and B. L. Tarmy, "The Nitric Acid-Oxygen Redox Electrode in Acid Electrolyte" in "Advances in Chemistry," No. 47, p. 153, ACS (1965).

[24] K. Vetter, *Z. Physik. Chem.*, 194, 199 (1950).

[25] J. A. Shropshire, *This Journal*, 112, 465 (1965).

[26] J. P. Hoare, *This Journal*, 110, 1091 (1963).

[27] K. J. Vetter, *Z. Anorg. Chem.*, 260, 242 (1949).

[28] J. A. Shropshire and B. L. Tarmy, "Advances in Chemistry," No. 47, p. 153, ACS (1965).

[29] J. P. Hoare, *This Journal*, 112, 849 (1965).

[30] J. P. Hoare, *Nature*, 204, 71 (1964).

[31] J. P. Hoare, S. G. Meibuhr, and R. Thacker, *This Journal*, To be submitted.

[32] J. P. Hoare, *J. Electroanal. Chem.*, In Press.

[33] M. W. Breiter, *Electrochim. Acta.*, 9, 441 (1965).

[34] W. Vielstich, *Z. Instrumkde.*, 71, 29 (1963).

[35] Laboratory of Electrochemistry and Metallurgy of the University of Milan, Milan, Italy.

[36] P. Pascal, "Nouveau Traité de Chimie Minérale," Vol. X, p. 277, Masson, Paris (1956).

[37] J. W. Mellor, "A Comprehensive Treatise on Inorganic and Theoretical Chemistry," Vol. VIII, pp. 286-287, Longmans & Green, London (1928).

[38] J. W. Mellor, cited p. 283.

[39] J. Masek and H. Przewlocka, *Coll. Czech. Chem. Commun.*, 28, 682 (1963).

[40] J. Masek and H. Przewlocka, *Coll. Czech. Chem. Commun.*, 28, 677 (1963).

[41] G. Bianchi, T. Mussini, and C. Traini, *Chem. e Ind.*, 45, 1333 (1963).

potentials are[42] about 0.0v (SCE) for reaction [i] and about −1.0v (SCE) for reaction [iii].

As for the anodic process of NO^+ oxidation to N_2O_4 and the rapid disproportionation of N_2O_4 in 96% w/w H_2SO_4, it is to be pointed out that the N_2O_4 disproportionation is very rapid at low H_2SO_4 concentrations (< 58% w/w): $N_2O_4 + H_2O \rightarrow HNO_3 + HNO_2$; and also at higher H_2SO_4 concentrations (> 85% w/w): $N_2O_4 + H_2SO_4 \rightarrow HO{\cdot}SO_2{\cdot}NO_2 + HNO_3$. At intermediate concentrations of H_2SO_4, corresponding to the field where we observed the anodic wave of NO^+ oxidation to N_2O_4, the velocity of N_2O_4 disproportionation may verify a minimum.[43] In a recent paper[44] the results obtained with the rotating-disk electrode method proved that the process $2NO^+ + 2H_2O - 2e \rightarrow N_2O_4 + 4H^+$ is a first-order reaction, whose standard potential is $E^o = +1.25$v (NHE).

In our opinion platinum exerts a catalytic action on the processes of nitrogen oxides. The results, particularly anodic curves, may be really affected by the surface state of the electrode, as it has been shown also in the work under discussion. For analogy with order cases[45] we consider the degassing of platinum electrodes *in vacuo* at 500°C to be essential. No direct comparison is possible with results obtained working with different metals, like gold or mercury.

L. E. Topol, R. A. Osteryoung, and J. H. Christie: In regard to Bianchi and Mussini's comment on the formation of $H_2N_2O_2$ or $NH_2OH_2^+$ we would like to point out that the dispute actually concerns them and Masek[46,47] and Przewlocka.[47] We did not work in the acid concentration range where the occurrence of the above electrode reaction products were reported.

As for the oxidation of NO^+ to N_2O_4, even if the disproportionation of N_2O_4 is slow in intermediate acid concentrations as claimed, we did not see any sign of NO_2^+ in the 96% solution. The reported formation[48] of N_2O_4 in this solution with its rapid subsequent disproportionation would yield NO_2^+ as well as NO^+ and the NO_2^+ should be detected in our studies.

Preferential Vaporization of Carbon from Hafnium Carbide

R. L. Hansler (p. 881, Vol. 112, No. 8)

Charles P. Kempter[49]: Dr. Hansler has cited only one reference relating the lattice parameter of hafnium carbide to composition and no references relating the electrical resistivity to lattice parameter and/or composition. In addition to Avarbe *et al.*, Cotter and Kohn,[50] Krikorian, Witteman, and Bowman,[51] Goretzki,[52] Bittner and Goretzki,[53] Nowotny, Benesovsky, and Rudy,[54] Krikorian, Wallace, and Anderson,[55] Adams and Beall,[56] Zhelankin and Kutsev,[57] Houska,[58] and Sara[59] have studied the lattice parameters of known compositions of hafnium carbide. A plot of all of these data indicates that the lattice parameter of stoichiometric HfC, if it exists, is ~4.641Å. The value of 4.6450 ± 0.0005Å reported by Hansler is very high and might be explained by the presence of a significant percentage of zirconium carbide in solid solution with the hafnium monocarbide. A spectrographic analysis of the filament would have been advisable. The room temperature specific electrical resistivities, lattice parameters, and combined carbon contents reported by Goretzki[52] are 172, 200, 230, 242, 245 microohm-cm, 4.638, 4.637, 4.634, 4.632, 4.625Å, and 47.4, 46.5, 45.1, 43.8, 41.3 a/o, respectively. $Hf_{0.901}$ corresponds to 47.4 a/o combined carbon. According to Paderno[60] the specific electrical resistivity of $HfC_{0.999}$ is 45.0 microohm-cm at room temperature. Other resistivity values have been reported for "HfC," but the stoichiometry was not stated.

According to Lyon,[61] "hafnium carbide has a congruently vaporizing composition at a carbon concentration slightly less than stoichiometric." Since Goretzki's measurements show that the specific electrical resistivity increases markedly with decreasing carbon content, Hansler's results are not in disagreement with those reported by Lyon.

R. L. Hansler: I wish to thank Dr. Kempter for his discussion.

Theory of Organic Corrosion Inhibitors—Adsorption and Linear Free Energy Relationships

F. M. Donahue and K. Nobe (pp. 886-891, Vol. 112, No. 9)

R. R. Annand[62]: When I first saw this paper I enthusiastically thought that now we might have a workable relationship to use for seeking inhibitor structure correlations. I was particularly favorably impressed with the arguments and derivations which tend toward developments of a specific set of sigma values for inhibitor or adsorption situations. On further study, however, it seems to me that before a reliable set of specialized sigma values can be developed it will be necessary to establish better experimentally a point that is assumed by the authors.

Usual LFER theory applies to organic reactions in which the mesomeric demands during the course of the reaction result in a highly localized electron distribution at the reaction center [for a brief but lucid discussion see ref. (63)]. Indeed, from his data showing a linear relationship between substituent constants and the energy of adsorption (reproduced in Fig. 1 of Donahue and Nobe's paper), Snyder concluded that he was observing charge localization at the nitrogen atom in his compounds during adsorption onto alumina from a highly nonpolar solvent.[64]

Donahue and Nobe have taken charge localization at a specific atom as an assumption, and as a necessary part of their theory. It seems to me that this

[42] J. Masek and H. Przewlocka, *Coll. Czech. Chem. Commun.*, 28, 673, 680 (1963).

[43] J. W. Mellor, cited, p. 701.

[44] T. Mussini and G. Casarini, *Chem. e Ind.*, 47, 600 (1965).

[45] G. Bianchi and T. Mussini, *Electrochim. Acta.*, 10, 445 (1965).

[46] J. Masek, "Advances in Polarography," I. S. Longmuir, Editor, Vol. I, p. 340, Pergamon Press, New York (1960).

[47] J. Masek and H. Przewlocka, *Coll. Czech. Chem. Commun.*, 28, 670 (1963).

[48] G. Bianchi, T. Mussini, and C. Traini, *Chim. Ind.*, 45, 1333 (1963).

[49] Los Alamos Scientific Laboratory, University of California, Los Alamos, New Mexico.

[50] P. G. Cotter and J. A. Kohn, *J. Am. Ceram. Soc.*, 37, 415 (1954).

[51] N. H. Krikorian, W. G. Witteman, and M. G. Bowman, *This Journal*, 110, 560 (1963).

[52] H. Goretzki, Doctoral dissertation, University of Vienna, 1963.

[53] H. Bittner and H. Goretzki, *Monatsh. Chem.*, 93, 1000 (1962).

[54] H. Nowotny, F. Benesovsky, and E. Rudy, *Monatsh. Chem.*, 91, 348 (1960).

[55] N. H. Krikorian, T. C. Wallace, and J. L. Anderson, *This Journal*, 110, 587 (1963).

[56] R. P. Adams and R. A. Beall, U. S. Bureau of Mine Rpt. Invest. 6304, 1963.

[57] V. I. Zhelankin and V. S. Kutsev, *Zhur. Strukt. Khim.*, 4, 865 (1963).

[58] C. R. Houska, *J. Amer. Ceram. Soc.*, 47, 310 (1964).

[59] R. V. Sara, Tech. Doc. Rpt. WADD TDR-60-143, Part V, 1964.

[60] V. N. Paderno, Izv. Akad. Nauk SSSR, Otd. Tekhn. Nauk, Met. i Toplivo, p. 176, 1962.

[61] T. F. Lyon, "Condensat. and Evap. of Solids," E. Rutner, P. Goldfinger, and J. P. Hirth, Editors, Gordon and Breach, New York (1964).

[62] Petrolite Corporation, 369 Marshall Avenue, St. Louis, Missouri 63119.

[63] J. F. Bunnett, "Technique of Organic Chemistry," Vol. 8, S. L. Friess, E. S. Luwis, and A. Weissberger, Editors, pp. 210-220, Interscience Publishers, Inc., New York, (1961).

[64] L. R. Snyder, *J. Phys. Chem.*, 67, 2344 (1963).

assumption is sufficiently challenged by previously reported work that its validity will have to be solidly confirmed before reliable substituent constants can be developed for inhibitor situations. In adsorption (particularly at metal surfaces where proton acidity is not possible) or in inhibition, there is no *a priori* reason why electron localization should occur at a specific atom in an aromatic molecule.

Among the literature references which challenge the charge-localization assumption, the following are typical: Bockris and co-workers have found that when aromatic molecules adsorb to metal surfaces from solutions of electrolytes, the electrons in the conjugated system participate in the bonding.[65] Furthermore, they have found that the contribution to the free energy of adsorption of a hydrocarbon radical is greater by about 6 kcal/mole for the naphthyl radical than for the butyl radical.[66] Indeed, they have found that naphthalene itself will adsorb to metal surfaces in the flat position.[67] Finally, in every adsorption investigation of which I am aware where the configuration of the aromatic amine was examined critically, it was found that the aromatic molecules preferentially adsorbed parallel to the plane of the metal surface.[68-70] All of this body of evidence supports the thesis that participation is predominantly by the electron cloud of the conjugated system, not by electron localization at an individual atom.

In fact, interaction of the electron cloud of double bonds (without localization at one of the atoms connected by the bond) is observed in a rather wide range of circumstances including: olefins with metal ions[71]; olefins with metal surfaces from the gas phase[72]; and even with an acidic hydrogen as in hydrogen bonding.[73, 74]

In view of this background, indicating that the electron cloud of the conjugate bonds of an aromatic system also participate in the adsorption of molecules at metal surfaces, it is disappointing when a large portion of the author's data points do not fall on the theoretical line supporting the single atom anchoring group hypothesis, and when in large measure the arguments revolve around reasons why the anomalous points do not fit the theoretical line. For example, in Fig. 2 it is argued that only four out of the eight points should fall on the theoretical line. It seems to me certainly possible that the theoretical line is not correct either when one can draw a straight line through six out of eight of the points, if the last six points are used instead of the first four.

To put this theory into a category worthy of working into inhibitor function correlations, or other aspects of inhibitor research, a carefully selected group of compounds should be critically examined to establish the statistical fit of the points to a line. Ideally there should be the widest spread possible, both on the inhibition axis and on the substituent constant axis. It should be possible to take these data relatively simply under controlled conditions of concentration, volume of acid, temperature and corroding time so that (*a*) the rate of corrosion is constant throughout the corroding period; (*b*) reproducibility is at least ± 10%; and (*c*) the effects from the poorer compounds are sufficiently different from the better ones that they can be reliably differentiated. Complex equipment and procedures are not necessary for this purpose; a judicious choice of compounds which are then reliably examined under identical experimental conditions is necessary.

I think this attempt to formalize the general approach to the structure-inhibition problem is possibly a useful one. It would be a great deal more useful if a reasonable amount of confidence could be found in experimental support for the approach. I hope this support will be put forth in the near future and that it will bear out the reliability of the theory.

Francis M. Donahue[75] and Ken Nobe: The authors wish to express their gratitude for Dr. Annand's interest in our work and his comments. However, we feel that he has not completely understood our intent.

We are not attempting to develop "a specific set of sigma values for inhibitor or adsorption situations." On the contrary, it is our intent to utilize the existing sigma values which are found in the literature (we cited four such references in the paper under discussion).

It appears that Dr. Annand has misread Snyder's[76] and our work concerning the correlation of the free energy of adsorption (Snyder's data) and substituent constants. The $\Delta\Delta G_{ads}$ data plotted in Fig. 1 of our paper were the differences between the "ΔF_p average" values of the substituted pyridine compounds and the ΔF_p average value of pyridine in Snyder's Table III.[76] On the other hand, in his LFER correlation, Snyder[76] plotted the $\Delta\Delta F_p$ values tabulated in his Table III. These values were the differences in the ΔF_p average (experimental results) and the ΔF_p calculated from his Eq. [5].[76] According to Snyder,[76] this equation accounts for contributions to the free energy of adsorption from all adsorbate groups within the molecule as well as the strongly adsorbing groups, but does not account for the electronic effects of the substituent on the strongly adsorbing groups (*e.g.*, the nitrogen in pyridine). Thus, the $\Delta\Delta F_p$ values in Snyder's Table III are a measure of the latter effects. He achieved a correlation for all his adsorbates (excluding the O-substituents).

Although Snyder's results showed that the nitrogen atom of the pyridines, pyrroles and anilines was strongly adsorbed, thus substantiating the anchoring group concept, he concluded that these compounds were all adsorbed parallel to the adsorbent surface. It is evident that adsorption at the anchoring group and parallel adsorption are not as mutually exclusive as Dr. Annand seems to imply.

Dr. Snyder[77] has pointed out that the method of plotting Fig. 1 in our paper assumes there is no contribution to the adsorption energy from the substituent group; results of other types of compounds show that the substituent groups could contribute to the adsorption energy. Therefore, according to Snyder,[77] our interpretation of the points in group B of Fig. 1 in our paper appears incorrect since the adsorption energies due to the substituents were not considered.

The concept of charge localization has indeed been utilized in the initial developments of LFER theory by organic chemists studying homogeneous reaction kinetics. However, in the opening paragraph we state "the assumption that the electron density at the 'anchoring group' uniquely determines the adsorbability still allows the possibility of π-interactions *provided* (emphasis added) that such interactions are assumed to vary in the same qualitative manner as the electron density at the functional group under consideration." Since the function group (nitrogen) in the pyridines is part of the conjugated system, it is not an outland-

[65] E. Blomgren and J. O'M. Bockris, *J. Phys. Chem.*, **63**, 1475 (1959).

[66] E. Blomgren, J. O'M. Bockris, and C. Jesch, *J. Phys. Chem.*, **65**, 2000 (1961).

[67] J. O'M. Bockris, M. Green, and D. A. J. Swinkels, *This Journal*, **111**, 743 (1964).

[68] Yu Yao Yung-Fang, *J. Phys. Chem.*, **68**, 101 (1964).

[69] B. H. Claussen, *This Journal*, **111**, 646 (1964).

[70] R. R. Annand, R. M. Hurd, and N. Hackerman, *This Journal*, **112**, 138 (1965).

[71] R. G. Guy and B. L. Shaw, "Advances in Inorganic Chemistry and Radio Chemistry," H. J. Emeléus and A. G. Sharpe, Editors, pp. 79-81, Academic Press, Inc., New York (1960).

[72] L. H. Little, N. Sheppard, and D. J. C. Yates, *Proc. Roy. Soc.*, **A-259**, 242 (1960).

[73] A. W. Baker and A. T. Shulgin, *J. Am. Chem. Soc.*, **80**, 5358 (1958).

[74] M. R. Basila, E. L. Saier, and L. R. Cousins, *J. Am. Chem. Soc.*, **87**, 1665 (1965).

[75] Present address: Department of Chemical and Metallurgical Engineering, University of Michigan, Ann Arbor, Michigan.

[76] L. R. Snyder, *J. Phys. Chem.*, **67**, 2344 (1963).

[77] L. R. Snyder, Private communication.

ish assumption to suggest that the electron densities in the conjugated system are coupled to that at the nitrogen.

Annand's allegation notwithstanding, there is an *a priori* reason why there should be electron localization at specific atoms in an aromatic molecule provided that one defines electron localization in terms of the electronic charge densities which may be calculated based on Molecular Orbital Theory.[78,79]

Correlations have been obtained by us[80-82] utilizing the data of Blomgren and Bockris.[83] The latter showed rather conclusively, as Annand has pointed out, that the orientation is parallel to the surface. Such a correlation by us merely underlines the validity of the proviso which we added to the original premise and have enumerated above.

Annand suggests that Fig. 2 is a rather weak argument for the correlation since he feels that more collinear points are obtained by ignoring, among other things, the parent compound. Such an attempt is justified only if one is attempting to fit data. It was our intent that we test the extent of the theory. On the basis of the theory, four of the points were required to fall on the line. The others were not. We frankly admitted, however, that one of those points did and we likewise surmised that, on the basis of Fig. 2, we could not make a firm statement concerning the orientation of the pyridines on iron. It should be noted that Hackerman and Ayers[84] were likewise at a loss to choose whether the orientation was parallel or not on the basis of their data.

As Annand has pointed out, to verify the suggested relationships it will be necessary to study systems where the extent of inhibition is large as well as the range of sigma values. We have addressed ourselves to this problem in the past[80-82] and are currently extending the initial studies.[85]

It was not our intent in the paper under discussion to present a panacea to the problem of the structure-inhibition relationship. It was instead an attempt at formalizing an approach to inhibition in a manner which has been hinted by previous authors, but which has not been structured such that it could be tested quantitatively. We feel that this paper was, at best, a first approximation, but it is felt that it is a significant starting place.

The Effect of Electrode Pretreatment on the Oxygen Reduction on Platinum in Perchloric Acid

Y. L. Sandler and E. A. Pantier (pp. 928-931, Vol. 112, No. 9)

G. Bianchi and T. Mussini[86]: In a recent paper on cathodic reduction of oxygen on smooth platinum electrodes in acid solutions,[87] phenomena of platinum poisoning during the cathodic reduction of oxygen in acid solution (0.5M H_2SO_4) have been put in evidence. Such a poisoning can be destroyed either by a cathodic polarization at potentials lower than + 0.2v, NHE, or by an anodic polarization at potentials higher than + 1.2v, NHE. In our opinion, such a poisoning is not due merely to oxygen strongly embedded in the surface, but to an intermediate species reducible or oxidizable which we deduced to be the HO_2 radical stabilized on the platinum surface. In a previous paper on catalytic decomposition of acid hydrogen peroxide solutions on platinum, iridium, palladium, and gold surfaces,[88] of which the authors seem to be unaware, we showed that an anodic or a cathodic treatment of the platinum surface does not change the catalytic activity of platinum for the decomposition of hydrogen peroxide, provided such treatments (anodic or cathodic) are made for short times and with moderate overpotentials, so that significant amounts of hydrogen or oxygen are neither evolved nor absorbed on platinum. On the contrary, an increasing catalytic activity of platinum treated with hydrogen may result from the destruction of the oxygen embedded in the surface (or better, in our opinion, of the adsorbed HO_2 radical) by hydrogen diffusing from the bulk of platinum. For this reason we thing it is necessary to degas platinum *in vacuo* at 500°C in order to obtain reproducible and reliable results when studying the cathodic reduction of oxygen. Another important point to be taken into due account is that some impurities, like chloride ions (and halide ions in general), can poison the platinum surface and strongly affect the catalytic decomposition of hydrogen peroxide.

Y. L. Sandler and E. A. Pantier: We cannot express a definite opinion as to the reason for the very strong poisoning observed by Bianchi and Mussini in their experiments. It may be connected with the particular experimental methods used.

The main point in our paper was the demonstration of the effect of the existence of different modes of oxygen chemisorption on the characteristics of the platinum oxygen electrode. This possibility is not considered and no evidence for it is found in Bianchi's work. In our experiments, the very strongly bound oxygen was formed either by thermal pretreatment of the electrode with oxygen at a high-temperature (and transfer to the cell in a closed system) or by pretreatment *in situ* at a high anodic potential.

Bianchi and Mussini's argument that short term variations in potential (between +0.6 and 1.1v, Bianchi and Mussini's Ref. 88) do not essentially influence the catalytic activity, is not in disagreement with our results and presumably means that the strong oxygen chemisorption is not affected under these conditions.

Our samples, after hydrogen pretreatment, were flushed with pure helium at 600°C for about 10 min before cooling very slowly in helium. It is unlikely that this treatment is less effective in removing the hydrogen than Bianchi and Mussini's treatment *in vacuo* at 500°C for 3 hr; it is also unlikely that any remaining hydrogen could support a sufficient flux to the surface at room temperature for continuous removal of HO_2 radicals which Bianchi and Mussini consider to be the poisoning species.

Any difference in the results must be due to differences in the purity of the system and electrode pretreatment. Bianchi and Mussini's standard pretreatment consists of grinding the electrode with quartz powder while exposed to laboratory air. No sensitivity to oxygen pretreatment is found by these authors. They come to the conclusion that their pretreatment simply makes the platinum surface really bare (Bianchi and Mussini's ref. 87, p. 447). We find this hard to believe and suggest that this result merely emphasizes again the need for very careful control of purity in this type of research.

[78] "Molecular Orbital Calculations," by J. D. Roberts, Benjamin, New York (1962).

[79] A. Streitwieser, "Molecular Orbital Theory for Organic Chemists," John Wiley & Sons, Inc., New York (1962).

[80] F. M. Donahue, Ph.D. Thesis, University of California (1965).

[81] F. M. Donahue, A. Akiyama, and K. Nobe, To be published.

[82] F. M. Donahue and K. Nobe, Paper presented at the Buffalo Meeting of The Electrochemical Society, October 10-14, 1965. Abstract 57.

[83] E. Blomgren and J. O'M. Bockris, *J. Phys. Chem.*, 63, 1475 (1959).

[84] R. C. Ayers, Jr., and N. Hackerman, *This Journal*, 110, 507 (1963).

[85] A. Akiyama and K. Nobe, Unpublished results.

[86] Laboratory of Electrochemistry and Metallurgy, University of Milan, Milan, Italy.

[87] G. Bianchi and T. Mussini, *Electrochim. Acta.*, 10, 445 (1965).

[88] G. Bianchi and T. Mussini, *Electrochim. Acta.*, 7, 457 (1962).

The Indous Ion: an Intermediate in the Electrochemical Oxidation of Indium Metal

R. E. Visco (pp. 932-937, Vol. 112, No. 9)

M. E. Straumanis[89]: Although it is known that In(I) ions exist even in aqueous solutions, nevertheless, there are observations which are not in accord with the electrochemical mechanism proposed, postulating that the irreversible electrochemical step is associated with the further oxidation of In(I) to In(III).

Davidson and Jiric[90] could not prove the presence of In^+ ions during the dissolution of the metal in acids; therefore they assumed, in order to explain the deviation from Faraday's law, that a secondary reaction occurs in acidic solutions with high speed

$$In^+ + 2H^+ \rightarrow In^{3+} + H_2 \qquad [1]$$

Stubbs[91] doubts whether there are In^+ and In^{2+} at all in form of oxides.

Straumanis and Martin[92] concluded from coulometric measurements that In (from an amalgam) goes into solution quantitatively (within the limits of error) only in the form of In^{3+}. Therefore, the first step is

$$In^o \rightarrow In^{3+} + 3e \qquad [2]$$

and there seems to be no justification for step 3:

$$In^o \rightarrow In^+ + e \qquad [3]$$

What might have happened in the experiments of Dr. Visco was the anodic partial disintegration of In. Already Davidson and Jirik[90] saw that, while the current was flowing, fine particles separated from the In anode and accumulated at the bottom of the vessel. This observation could be confirmed later.[92] Figure 1 shows such metallic In particles.

That the particles could not originate in a disproportionation process

$$3In^+ \rightarrow 2In + In^{3+} \qquad [4]$$

follows from the coulometric measurements, as no In^+ ions were formed.

Therefore, what is swept away from the In anode are not In^+ ions but very fine metallic In particles originating from the partially disintegrating anode. However, since small amounts of In^+ were detected polarographically, it might be that reaction [4] is slightly reversible: some In^{3+} are reduced by the fine

[89] University of Missouri at Rolla, Graduate Center for Materials Research, Rolla, Missouri.

[90] A. W. Davidson and F. Jirik, *J. Am. Chem. Soc.*, 72, 1700 (1950).

[91] M. F. Stubbs, *J. Am. Chem. Soc.*, 74, 6201 (1952).

[92] M. E. Straumanis and R. L. Martin, *Z. anorg. u. allgem. Chem.*, 334, 321 (1964).

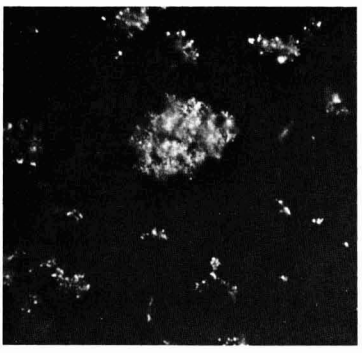

Fig. 1. In particles obtained by the anodic disintegration of the metal; single particles and clusters of them; current density, 70 ma/cm². 1430X, oil immersion.

In^o particles to In^+. The In-amalgam may act in the same manner. In fact the reducing ability of In metal or particles was even used by Dr. Visco to have In(I) in solution[93]:

$$In(III) + 2In(0) \rightleftharpoons 3In(I) \qquad [5]$$

Naturally, In(I) must then be found polarographically, if In(0) is present. Since finest In particles are formed continuously during anodic dissolution (at 70 ma/cm^{-2} streams of them can be detected already with the bare eye), a large surface of In metal is available for reaction [5]. Now the necessity of stirring becomes evident: it increases the outcome of In(I). This outcome also depends on the current density (see abstract) because the degree of surface disintegration of the anode changes with it.

Thus, Dr. Visco showed only that unstable In(I) is formed (in a secondary reaction) but not at all that the formation of In(I) is the first step in the dissolution of In(0) which also would be in contradiction to the coulometric measurements.[92]

Robert E. Visco: The observation by Professor Straumanis that an indium anode disintegrates when it is shorted to a large platinum cathode is doubtless quite real; but under these conditions, the initial current density is large (easily the order of $1A/cm^2$) and it seems likely that preferential attack along grain boundaries could occur, thereby altering the anode surface and providing a mechanism for easy particle formation. One of the points of my paper was to investigate in a controlled way the low current density region in the anodic dissolution of indium metal where gross attack is less likely. I wished to determine

(*a*) If measurable quantities of In^+ can be detected, and (*b*) if In^+ is formed, does it account for the apparent deviations from Faraday's law (based on an assumed 3 equivalents/mole for the oxidation of In).

The answer to both questions is yes; In^+ can be found by polarography in the anolyte, and the quantity of In^+ formed as determined either independently by polarography or coulometry agree and they show that sufficient In^+ is formed to explain the apparent deviations from Faraday's law.

Further, I went on to point out in this and an earlier paper[93] that since indium electrodes do not corrode at an appreciable rate in In^{+++} solutions containing only $HClO_4$, the equilibrium:

$$In^{+++} + 2In \rightleftharpoons 3In^+$$

is difficult to achieve in acid solution containing no complexing anions and, further, it must lie far to the left. How then does one explain large quantities of In^+ observed on anodic dissolution? The simplest and I think the most rational explanation is to say that In oxidation occurs in unit steps to give In^+, then In^{+2}, and finally In^{+3} and that the reason In^+ can be observed in the dissolution is because the rate-determining step in the above sequence is after In^+ formation. Thus, In^+ can be transported away from the anode. Recently Losev[94] has reached the same conclusions, based on an entirely different set of experiments and procedures. These experiments, in effect, measured the same quantities which I have reported.

The above results were confirmed by studies of the anodic dissolution of dilute amalgams. Recent unpublished calculations indicate that the quantity of In^+ formed from metal and amalgam anodes seems to be dependent only on the activity of indium in the amalgam relative to that in the metal. This suggests that the initial unit step in the anodic dissolution, that is

$$In \rightleftharpoons In^+ + e^-$$

[93] R. E. Visco, *J. Phys. Chem.*, 69, 202 (1965).

[94] A. P. Pchelnikov and V. V. Losev, *Protection of Metals*, 1, 482 (1965).

is at equilibrium for both liquid and solid indium electrodes and that the rate-determining step is later in the sequence of unit steps which lead to In^{+++}.

The Hydrogen Evolution Kinetics and Hydrogen Entry into α-Iron

J. O'M. Bockris, J. McBreen, and L. Nanis (pp. 1025-1030, Vol. 112, No. 10)

F. E. DeBoer[95]: In the first part of the discussion section, the authors say that two simultaneous reactions are occurring: reaction A (the hydrogen evolution reaction), and reaction B (hydrogen permeation). According to the data, reaction B is 1% of the total. It seems unreasonable that from the characteristics of this very minor reaction one can make definite conclusions about the mechanism of the major reaction, as the authors have done.

Complicating matters is the fact that they have taken no account of the complex nature of their membrane; that is, α-iron was treated as a perfect membrane for hydrogen permeation. It is the hydrogen that has permeated the iron that is measured, and these measurements are used to make conclusions about the hydrogen that has not even entered the iron; no account at all is taken of the hydrogen that has entered the iron and has not come out (*i.e.*, the hydrogen atoms might combine at internal discontinuities, and so forth). It is feasible that the amount of internal hydrogen is far greater than that which is measured.

The fact that the single crystal data are similar to the polycrystalline data does not invalidate this criticism, since atoms can be rendered immobile inside the iron at sites other than crystal boundaries.

J. O'M. Bockris, J. McBreen, and L. Nanis: In Eq. [3] and [9] of our paper, we give the relationship between the H permeation rate, the coverage (θ), and the rate of H evolution. The only major assumption here is that the adsorbed H intermediate is the same for H entry into the metal and for H gas evolution. The fraction of H which passes through the metal is related to the diffusion coefficient, the membrane thickness, and the ratio of the rate constants of the surface to bulk reactions. For the membrane thickness used, the potential range covered, and the temperature of the investigation, it turns out that the rates are such that the H which permeates the metal is of the order 1% of the total H which is discharged per unit time. Variation in the permeation rate with potential for constant inhibitor concentration reflects changes in θ, *i.e.*, of the adsorbed intermediate concentration. However, $\partial\theta/\partial\eta$ is a function if the mechanism assumed for the evolution reaction and theoretical relations are known which principal mechanisms. Hence the permeation-potential relation gives evidence concerning the mechanism of the evolution reaction which runs parallel to the permeation.

The consistence of our results support the assumption of identical intermediates for both reactions. The fact that the permeation rate happens to be about 1% of the total discharge rate in our system is not directly relevant to a discussion of mechanism.

The matters concerning H in the metal are dealt with in detail in a paper by Beck, Bockris, McBreen, and Nanis* which will be published shortly. In the potential region referred to for mechanism indications, it was found that no trapping of H occurred in the metal. Such trapping did occur if the potential was made more negative than a certain value. Data obtained in this region were not used to deduce mechanism: hence the termination of the permeation potential plots at about −0.5v with respect to NHE.

U. R. Evans[97]: The research provides valuable information about the entry and movement of hydrogen, and is greatly to be welcomed. The picture of the mechanism in absence of "poisons" appears acceptable, particularly the idea that the adsorbed state assumed before entry into metal as atoms is the same as that assumed before evolution as molecular gas (p. 1027). I am not equally happy about the idea (p. 1030) that poisons directly favor entry by loosening the H-metal bond; most earlier theories have pictured the poison as interfering with H_2 gas formation, and thus indirectly favoring the alternative reaction, the entry into the metal as atoms. Such a view appears to me more probable.

If adsorbed anions loosen the M-H_{ads} bond, then doubtless, provided that nothing else happens, the number of H atoms passing from an external (adsorbed) site to an internal (absorbed) site will be increased, say from n to $n + \Delta n$, so that the proportionate increase in hydrogen entry would be $\Delta n/n$. But the same loosening will surely increase the number of hydrogen pairs joining to form molecular (gaseous) H_2, say from N to $N + \Delta N$; since we are now dealing with pairs, the difference between squares must be taken and, if nothing else happens, the proportionate outward movement as H_2 gas will be

$$\frac{(N + \Delta N)^2 - N^2}{N^2} = \frac{2\Delta N}{N}, \text{ approximately}$$

Unless there is reason to think that $\Delta n/n$ is greater than $2\Delta N/N$, there is no reason to expect, on these grounds, that adsorption of CN or I will increase the entry of atomic hydrogen into the metal.

A more probable explanation, involving no *ad hoc* assumptions about bond loosening, is based on the fact that where a process involves two adjacent atoms, it will be more affected by coverage with a poison than a process involving only one atom. If α is the fraction of the surface not covered with poison (CN or I), then the rate of entry of atomic hydrogen (in absence of rival process) would be $k_1\alpha$, where k_1 is a constant, but the rate of evolution of *molecular* hydrogen would be

$$k_2\alpha p_{\alpha c}$$

where $p_{\alpha c}$ is the probability that a neighboring site is uncovered with a poison atom, which depends, not only on α, but also on c, the coordination number defining the number of "neighbors." Since two sites are involved in the H_2-evolution, it may be expected that

$$\frac{\text{Entry of atomic H}}{\text{Evolution of molecular } H_2} = \frac{k_1\alpha}{\frac{1}{2}k_2\alpha p_{\alpha c}} = \frac{2k_1/k_2}{p_{\alpha c}}$$

If c were known, $p_{\alpha c}$ could be calculated from simple probability theory. However, whatever the value of c, $p_{\alpha c}$ must decline as α declines, and immediately we reach the conclusion that, in absence of further complications, an increase of contamination with CN or I will diminish the fraction of hydrogen evolved as gas and increase that entering the metal as atoms.

This is only true of substances adsorbed as small ions or atomic groups. If the substance adsorbed consists of large molecules of irregular shape, there will be irregular gaps between the covered areas which, being left uncovered, will offer the same facilities for H-entry and H_2-evolution as a surface which is completely uncontaminated. Since the coverage of a large fraction of the area will, at constant potential, reduce the total current flowing, it follows that both H-entry and H_2-evolution will be reduced.

This seems to explain why CN and I favor the entry of hydrogen into metal, while organic nitriles diminish it. The effect of naphthalene is not so easily explained. It may be that single H atoms can enter the metal

[95] Corrosion Research Laboratory, Continental Can Company, Incorporated, 7622 South Racine Avenue, Chicago, Illinois.

[96] W. Beck, J. O'M. Bockris, J. McBreen, and L. Nanis, *Proc. Roy. Soc.*, in press.

[97] 19 Manor Court, Grange Road, Cambridge, England.

through the centers of the hexagonal rings, but that the points of entry are too much isolated from one another to allow union as H_2; this picture may seem rather fanciful, but it is difficult to think of an alternative.

J. O'M. Bockris, J. McBreen, and L. Nanis: Dr. Evans' view that additives effect the permeation rate of H through Fe by reduction of the rate of combination of H to H_2 is certainly a possible suggestion for such phenomena. However, it would only be tenable if the rate-detemining step (r. d. s.) in the hydrogen evolution reaction were combination; or is, in the sequence $2H^+ + 2e \rightarrow 2H_{ads} \rightarrow H_2$, the latter step were in equilibrium. In fact, the relation of the permeation rate to current density on the polarization side of the membrane

$$\partial P/\partial \ln J = 4\,RT/F$$

suggests strongly that $H^+ + e \rightarrow H_{ads}$ is the r. d. s. and is coupled to the following H combination reaction, with the reaction velocity $H_2 \rightarrow 2H_{ads}$ being negligible.

The most important of the points of experimental evidence in favor of this concerns the change of reaction rate associated with a change of permeation rate. As the r. d. s. for the over-all evolution reaction is not combination, the change reaction rate following additive additions (with constant mechanism) must arise from the effect of the adsorbed additive on bond strength. Thus, a decrease of the M-H bond strength would be consistent with an increase in overpotential for the same total current density,† but this would also lead to a corresponding increase of the permeation rate, as observed with CN^- and I^-.

We do not think that Dr. Evans' hypothesis is consistent with both the linked increase of over-potential and permeation and with the r. d. s. consistent with the $V/\log J$ relation.

In addition, the observations on the change of β with additions of additives has to be interpreted. Qualitatively, this arises from our model, for β depends on $\partial U/\partial x$, the slope of the potential energy-distance relation in stretching of the metal-hydrogen bond. It is easy to show that this coefficient is proportional to the bond strength. Finally, it may be noted that the interpretation given here to the permeation results in not a special theory but an application of independent interpretations previously made in respect to so-called "poisons" on the velocity of the hydrogen evolution reaction.

Electrode Potentials in Fused Systems, IX. Liquid Junction Potentials in the AgCl-AgBr System

K. Stern (pp. 1049-1050, Vol. 112, No. 10)

A. J. Easteal[98]: For the experimental cell

$$\mathrm{Ag}\,\Big|\,\underset{\text{(electrolyte I)}}{\mathrm{AgCl}(x_1),\,\mathrm{AgBr}(x_2)}\;\Big\|\;\underset{\text{(electrolyte II)}}{\mathrm{AgCl}(x_1'),\,\mathrm{AgBr}(x_2')}\,\Big|\,\mathrm{Ag}$$

where ‖ represents a liquid junction, Stern states: "In this cell any nonzero emf is a liquid junction potential and must arise from differences in the anion mobilities and transport numbers."

It is not true however that $(E_t - \epsilon) = 0$, where E_t is the cell emf and ϵ the liquid junction potential, except in certain limiting conditions. Assuming that the electrolytes I and II are completely dissociated into the simple ions Ag^+, Cl^-, and Br^-, and setting z_i equal to the electrovalency of the ions ($z_i > 0$ for cations, $z_i < 0$ for anions), the emf of the cell is given by the relationship[99]

$$E_t = -(RT/F)\int_{\mathrm{I}}^{\mathrm{II}} \sum_i t_i \left(-\frac{1}{z_i}\, d\ln a_i + \frac{1}{z_{Ag^+}}\, d\ln a_{Ag^+} \right) \quad [1]$$

and the liquid junction potential by

$$\epsilon = -(RT/F)\int_{\mathrm{I}}^{\mathrm{II}} \sum_i t_i \left(-\frac{1}{z_i}\, d\ln a_i \right) \quad [2]$$

By Eq. [1] and [2]

$$E_t - \epsilon = -(RT/F)\int_{\mathrm{I}}^{\mathrm{II}} d\ln a_{Ag^+} = -(RT/F)\ln\left(a_{Ag^+}{}^{\mathrm{II}}/a_{Ag^+}{}^{\mathrm{I}}\right) \quad [3]$$

where $a_{Ag^+}{}^{\mathrm{I}}$ and $a_{Ag^+}{}^{\mathrm{II}}$ denote the activities of Ag^+ ions in electrolytes I and II, respectively. According to Eq. [3], $E_t = \epsilon$ only if the activity of Ag^+ ions is the same in the two electrolytes. The fact that the concentration of Ag^+ is the same in the two electrolytes does not necessarily imply that no difference in a_{Ag^+} exists. If the system AgCl + AgBr were thermodynamically ideal in the sense

$$\left.\begin{array}{l}\gamma_{AgCl} = \gamma_{AgBr} = 1, \text{ for all values of } x \\ \text{such that } x_1 \geq x_{AgCl} \geq x_1'\end{array}\right\} \quad [4]$$

(where γ denotes activity coefficient) then it would be reasonable to assume that

$$\left.\begin{array}{l}\gamma_{Ag^+} = 1 \\ x_1 \geq x_{AgCl} \geq x_1'\end{array}\right\} \quad [5]$$

However proposition [4] is not valid,[100] at least for mixtures whose composition is such that

$$0.60 \geq x_{AgCl} \geq 0.30$$

It is therefore not possible to assess the difference in the activity of Ag^+ ions in the two electrolytes. Consequently it may not be true that the whole of the cell emf arises from the liquid junction potential.

Stern also states that the cell emf can be zero only if $t_{Cl^-} = x_1$, $t_{Br^-} = x_2$. That this is not a necessary condition for vanishing cell emf, is shown by the following considerations: E_t is zero if and only if

$$-(RT/F)\int_{\mathrm{I}}^{\mathrm{II}} \{(t_{Cl^-}\cdot x_{AgBr} - t_{Br^-}\cdot x_{AgCl})/x_{AgBr}\}\, d\ln a_{AgCl} = 0 \quad [6]$$

Since $d\ln a_{AgCl} \neq 0$, a sufficient condition for $E_t = 0$ is, therefore

$$\left.\begin{array}{l}t_{Cl^-}/t_{Br^-} = x_{AgCl}/x_{AgBr} \\ \text{for all values of } x \text{ such that} \\ x_1 \geq x_{AgCl} \geq x_1'\end{array}\right\} \quad [7]$$

A particular circumstance for which this condition is fulfilled is

$$\left.\begin{array}{l}t_{Cl^-} = x_{AgCl} \\ t_{Br^-} = x_{AgBr} \\ x_1 \geq x_{AgCl} \geq x_1'\end{array}\right\} \quad [8]$$

The conditions expressed by Eq. [7] (and its special case, Eq. [8]), are not however, necessary conditions for $E_t = 0$.

K. H. Stern: Dr. Easteal has raised two points. The first of these is the old question of single-ion activity again. In essence the question is: "what is the single ion activity of Ag^+ in a AgCl-AgBr mixture," or "is the activity of Ag^+ in AgCl and AgBr the same?"

Now we certainly know the activities of the thermodynamic components AgCl and AgBr in AgCl-AgBr

† We refer to "the same" current density for hydrogen evolution because the fraction of H which passes through the membrane is about 1% of the total H discharged, so that, if the total current density is constant, the current used by hydrogen evolution is constant to better than 1%.

[98] Chemistry Department, University of Auckland, Auckland, New Zealand.

[99] This equation is readily derived by the method of E. A. Guggenheim, "Thermodynamics," p. 396 *et seq.*, North-Holland Publishing Co., Amsterdam (1959).

[100] I. G. Murgulescu and D. I. Marchidan, *Zh. Fiz. Khim*, 34, 2534 (1960).

mixtures. The activities of the pure components are unity if a Raoult's law standard state is used. But the difficulty is that we do not know how to split up $a_{AgCl} = a_{Ag^+}\, a_{Cl^-}$ into single ion activities either for the pure compound or for AgCl in the mixture.

For example, Dr. Easteal's Eq. [3] contains two unknowns, the liquid junction potential ϵ and the ratio $(a_{Ag^+}{}^{II}/a_{Ag^+}{}^{I})$. In order to evaluate one we must make some assumption about the other. The usual way out of this dilemma is to assign a value of unity to the activity ratio and to interpret the cell emf only in terms of events at the liquid junctions.[101] If Dr. Easteal has a better suggestion it does not appear in his comments.

His second point concerns Eq. [6]. Since $d \ln a_{AgCl} \neq 0$ and $X_{AgBr} \neq 0$ $E_t = 0$ if and only if $t_{Cl^-} - X_{AgBr} - t_{Br^-} - X_{AgCl} = 0$.

Now, since t_{Cl^-} and t_{Br^-} are transport numbers relative to t_{Ag^+}, $(t_{Cl^-} + t_{Br^-}) = 1$ and also $X_{AgBr} + X_{AgCl} = 1$ from which his Eq. [7] and [8] follow immediately. Thus these equations are not only sufficient but also necessary.

The Voltage Sweep Method—Electronic Device for Producing Triangle Pulse and Ramps

F. G. Will (pp. 1157-1159, Vol. 112, No. 11)

N. S. Clayton[102]: The paper by Will deals with a circuit to produce a slow linear voltage sweep. A solid-state circuit Fig. 1, which has identical functions is in

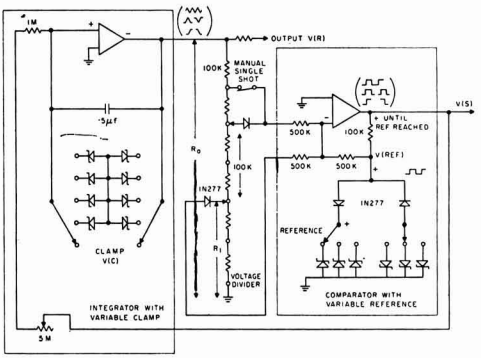

use here in conjunction with work on metal-oxide-silicon capacitors. Two operational amplifiers are used for integration and comparison, respectively. This allows the circuit to be constructed and modified simply and quickly.

Consider first the case with clamp switch open circuited. When the constant input to the integrator is positive, the output $V(R)$ ramps negative at a rate varied by the 5MΩ pot. R_1/R_0 of $V(R)$ is fed to the comparator.

The comparator operates in the noninverting mode in the sense that when the reference voltage V(ref) is reached the comparator switches to the same polarity as the input.[103] The sign of the feedback to the integrator $V(S)$ changes polarity causing the ramp to change direction. Note, $V(S)$ is always locked in positive or negative saturation due to positive feedback and thus provides a well-regulated input voltage to the integrator, while V(ref) is always clamped at the appropriate reference voltage.

$V(R)_m = (R_0/R_1)\ V$(ref), the height of wave form, is independently variable in each direction, provided the back biased diode on R_0 does not have significant leakage to the summing point.

It is now a simple matter to obtain single pulses or ramps starting from a prefixed voltage. A selection of back to back reference diodes may be switched in across the integrating capacitor which will clamp $V(R)$, *i.e.*, if $V(C) < (R_0/R_1)\ V$(ref). To unclamp or commence, a push button switch momentarily increases R_1 to change the state of the comparator.

The system is relatively insensitive to modifications: for example, the integrator feedback and interconnecting network have been varied by one or more orders of magnitude with no noticeable deterioration in performance. The integrating amplifier should be high quality, and the feedback network should allow little leakage current. The comparator amplifier is less critical. A high current amplifier (10 ma) is used to signal a stepping relay which automatically selects the next sample after one or half a cycle, as required.

F. G. Will: It is readily agreed that there are alternate methods of producing triangle pulses and ramps. It is the purpose of the original note to show how this can be done by a simple modification of commercial function generators that produce periodic waveforms. Dr. Clayton describes how operational amplifiers can be used to build a function generator as outlined in Textronix Manual 070-323. The addition of the back-to-back Zener diodes to clamp the integrator to several selected voltage levels is indeed a simple way of producing single pulses and ramps. It can be applied in cases where a continuous variation of clamping voltage levels is not required.

Logarithmic Oxidation Kinetics of Zinc

V. O. Nwoko and H. H. Uhlig (pp. 1181-1185, Vol. 112, No. 12)

F. E. DeBoer[104]: At the beginning of the paper, the authors say that the kinetics of this reaction have been described as parabolic as well as logarithmic. However, subsequently, they do not again refer to the possibility of parabolic behavior. On the contrary, they assert positively that they have proved that a two-stage logarithmic equation is obeyed. This is faulty on two counts: (*i*) the fact that a few points on semilog paper fit reasonably well on a straight line does not prove a logarithmic kinetic law. This is especially true when these points are closely bunched. Further, when it takes two straight lines to describe the form of these points, the possibility that this is indeed not a logarithmic relationship is high. (*ii*) The authors apparently did not test the parabolic law. In order to try this roughly, I used the curve labeled 206° of Fig. 2 and found that there was almost a perfect fit to a straight line described by $d = 2.35\ t^{1/2}$ (where d is oxide thickness in angstroms and t is time in minutes). Admittedly, it is difficult to determine data from a plot of the size presented (the other curves of Fig. 2 would be even harder to work with), but the fit was very good. Before assuming a two-stage logarithmic process, the authors should, at the least, show how well their original data fit when plotted in other ways, especially parabolically in this case.

A. Winterbottom in a discussion following Vernon's paper[105] pointed out that some of his low-temperature data would fit well on a parabolic plot. These were in the lower half of the temperature range discussed in the present paper. In view of this and the distinct possibility that the data discussed here conform to a parabolic law, it is probable that the oxidation is parabolic below 225° and logarithmic above 225° (see Vernon).

U. R. Evans[106]: The authors have done a service in showing that the oxidation of zinc shows the same

[101] K. H. Stern, *J. Phys. Chem.*, 63, 741 (1959).

[102] Molecular Electronics, Research and Development Laboratories, Canadian Westinghouse Company, Limited, P.O. Box 510, Hamilton, Ontario, Canada.

[103] Operational Amplifiers and Their Applications, Tetronix Manual.

[104] Corrosion Research Laboratory, Continental Can Company, Incorporated, 7622 S. Racine Avenue, Chicago, Illinois 60620.

[105] W. Vernon, E. Akeroyd, and E. Stroud, *J. Inst. Metals*, 65, 301 (1939).

[106] 19 Manor Court, Grange Road, Cambridge, England.

sudden breaks as does that of copper, nickel, cobalt, and iron. If the activation energy is almost the same for the two stages, that would suggest that the oxidation-mechanism is similar.

Figure 3 and Table I may convey the idea that oxidation is more rapid in the second stage than in the first. This is due to the fact that the time-scale in Fig. 3 is much more "open" for the first stage than for the second. The following table gives rough measurements of the time t_1 needed to produce the thickness L at which the second stage starts, and the additional time t_2 needed to produce an additional thickness equal to L (making $2L$ in all). Accurate measurements are impossible on any small-scale diagram, and the authors may care to provide a more accurate table. If they confirm that t_2 is greater than t_1, the conclusion will be that the second stage is the slower.*

Temperature, °C	L	t_1	t_2
125	4.5	95	245
157 (0.763 mm)	11	105	290
175	12	95	145
206	24	130	275

"Breakdowns," leading to spurts of renewed oxidation, are not confined to metal obeying the logarithmic law. Often there are several successive breakdowns; about 40 years ago, Pilling and Bedworth,[107] studying copper, published curves with about four breakdowns. Curves showing repeated breakdowns have also been published by Vernon,[108] by Tylecote,[109] and by Caplan and Cohen,[110] studying aluminum, copper, and iron-chromium alloys, respectively.

The rational explanation of breakdown is springing a leak of the film where it has become unsupported through the outward movement of cations, leaving vacancies. The same outward movement provides a simple explanation of the logarithmic growth law. At high temperature, these vacancies generally coalesce to form cavities, which are visible under the microscope, so that their existence is not in doubt. That, however, involves diffusion of vacancies over considerable distances; Dunnington, Beck, and Fontana[111] record cases where vacancies have diffused right through a sheet, so that its scale has become loose on one side while remaining adherent to the other side. Where there is coalescence of many vacancies into a few big cavities, the area where oxide is out of contact with metal is small, and the oxidation-rate will not be greatly effected. At low temperatures, diffusion of vacancies can only occur over small distances; some vacancies are doubtless annihilated at dislocations or other "sinks," others by atoms subsiding into them from the film, but some will remain at the interface. The effect will be to impede movement across the interface. When the gap between metal and oxide becomes at some places sufficiently broad to prevent crossing altogether, the area available for the passage of metal into oxide will diminish with time.†

It has been shown[112] that this leads, according to the assumption made regarding the growth law which would be obeyed if the whole area remained available for passage, either to the classical logarithmic equation

$$W = k \log (at + 1)$$

or to a "new" logarithmic equation

$$W = k \log (at^{1/2} + 1)$$

There are, of course, numerous examples of conformity to the classical equation, but when first I arrived at the "new" equation,[113] no experimentally established example was available. Shortly afterwards, T. Mills, studying the oxidation of copper, brought me results which failed to accord with the classical equation. I suggested that he tried the new equation, with which he was then unacquainted; the results fitted.[114]

If the falling off, much faster than the parabolic law would predict, is due to an increasing area of "no contact" between metal and oxide, a time will come when the "roof" will collapse or start to leak, and oxidation will be resumed, over the areas in question, at roughly the original pace. If the breakdown does not occur until conditions of "no contact" have spread over the whole area, the scale will flake off intact. If it remains adherent (as on zinc), that is proof that the "no contact" condition has not been established everywhere, and the renewed oxidation-rate of the specimen as a whole will be less than at the start of the first stage—which appears to be the case.

The discussion between the authors and Fromhold shows that they are strongly attached to interpretations based on space charges. This comment is addressed to those who prefer an explanation which, without *ad hoc* assumptions, offers an interpretation of the known facts up to the breakdown; after the breakdown, the geometry becomes complicated and the kinetics difficult. The simplicity of the interpretation may be an advantage, since, if there is a flaw in the argument, no reader can fail to detect it.

H. H. Uhlig: To prove whether a single equation fits a given set of data requires experimental points over a sufficient time interval; otherwise more than one equation may fit the points. One of the traditional difficulties of treating thin film oxidation data is that the time interval over which thin films exist is relatively limited. Therefore, the suggestion has sometimes been made, as F. De Boer mentions, that the parabolic as well as the logarithmic equation applies. If still fewer points than those presented in our Fig. 2 had been taken, it could also be demonstrated that the linear equation fits the data. However, several investigators have previously demonstrated that the logarithmic equation is commonly the only equation which fits thin film oxidation data when the data are carried out over a sufficient length of time so as to leave no doubt about the matter. Lustman and Mehl[116] showed that the data they obtained on oxidation of copper single crystals could be represented only by the logarithmic equation and the same conclusion is reached from low-temperature data by Tylcote,[117] and from our own measurements on copper. Kubaschewski and Hopkins[118] conclude that most thin film oxidation data for metals conform to the logarithmic equation or inverse logarithmic equation, with distinction between the two being difficult.

* The reason why Table I shows a higher value for the rate constant (k'_1) of the second stage than for that of the fast stage (k_1) is that τ' is much larger (110-140 min) than τ (5.5-7 min). The equations are $y = k_1 \log (t/\tau + 1)$ and $y = k'_1 \log (t/\tau' + 1)$. Clearly a time of, say, 10 min will only slightly increase $(t/\tau' + 1)$ above unity, but will greatly increase $(t/\tau + 1)$. Thus, even supposing that the oxidation rates were the same in both stages, k'_1 would need to be much larger than k_1, if the same value of t (10 min) is to produce the same increase of thickness, y.

† A small amount of oxidation can develop gradually even at the areas of "no contact" by the mechanism proposed by Dravnieks and McDonald.[115]

[107] N. B. Pilling and R. E. Bedworth, *J. Inst. Metals*, 29, 529 (1923).

[108] W. H. J. Vernon, *Trans. Faraday Soc.*, 23, 152 (1927).

[109] R. F. Tylecote, *J. Inst. Metals*, 81, 681 (1952).

[110] D. Caplan and M. Cohen, *J. Metals*, 4, 1057 (1952); *Corrosion*, 15, 141 (1959).

[111] B. W. Dunnington, F. H. Beck, and M. G. Fontana, *Corrosion*, 8, 2 (1952).

[112] U. R. Evans, "Introduction to Metallic Corrosion," 2nd Ed., pp. 192-195. Arnold (1963).

[113] U. R. Evans, "Reviews of Pure and Applied Chemistry," 5, 1 (1955).

[114] T. Mills and U. R. Evans, *J. Chem. Soc.*, p. 2182 (1956).

[115] A. Dravnieks and H. J. McDonald, *This Journal*, 94, 139 (1948).

[116] B. Lustman and R. Mehl, *Trans. AIME*, 143, 246 (1941).

[117] R. Tylecote, *J. Inst. Metals*, 78, 327 (1950-1951).

[118] O. Kubaschewski and B. Hopkins, "Oxidation of Metals and Alloys," p. 37-39, Academic Press, New York (1962).

It was our intent, therefore, to show that our data for zinc obtained over a limited time interval are consistent with the logarithmic equation in accord with most thin film oxidation data. This we have done. In particular, our data are consistent with two-stage logarithmic kinetics, also found by other investigators, the theoretical significance of which is outlined.

Dr. Evans' comments deal first with the characteristics of any logarithmic relation. It is, of course, true that growth of oxides following the logarithmic equation decreases markedly as time proceeds. In fact, early investigators suggested that the oxide completely stopped growing after a given time, whereas it is now considered more likely that the oxide continues growing and that it is only the peculiar relation of oxide thickness to logarithm of time which makes it appear as if oxide growth ceases. In the two-stage logarithmic oxidation process, the important consideration is that the value of the reaction rate constant k'_1 in the relation $y - L = k'_1 \log(t/\tau' + 1)$ for second-stage oxidation is demonstrably greater than the corresponding value of k_1 during first-stage oxidation. The greater value of k'_1 compared to k_1 means that the corresponding thickness of oxide at any time beyond L is greater than it would otherwise have been had oxidation continued in accord with first-stage kinetics. This conclusion is clearly evident by examining our Fig. 3.

Dr. Evans is correct, of course, in pointing out that discontinuities in the oxidation rate have various causes. Most of the instances he cites are for relatively thick films where spalling and cracking of the oxide is the common cause. An example of discontinuous oxidation rate can also be seen in the data of Heindlhofer and Larsen for oxidation of iron at 700°C reproduced in the "Corrosion Handbook" on p. 633. However, spalling, blistering and cracking are not as likely to occur in thin film oxidation (100-10,000Å), and in fact we have never observed evidence for it in any of our numerous experiments on oxidation of copper, nickel, and chromium-iron alloys. Consideration should also be given to the fact that the beginning of second-stage logarithmic oxidation tends to be more reproducible than one would expect if accidental spalling and cracking, caused in part by thermal fluctuations, were the cause. The fact that second-stage logarithmic oxidation begins at about the same time and thickness for a given temperature of oxidation suggests that its cause lies in a different source. Our work on Volta potentials of growing thin oxide films suggested to us that space charge may enter as the important factor, and subsequent exploration of this possibility led to the conclusions that are outlined in our present and previous papers.

It is of some interest that Tylecote's data on oxidation of copper, cited as reference by Dr. Evans, lends support to our viewpoint. Tylecote found that the parabolic equation fitted his data only at high temperatures (615°-908°C) whereas the logarithmic equation fitted his data in the lower temperature range (350°-550°C) especially during the first stages of oxidation (thin films). The transition between logarithmic and parabolic kinetics is not sharply defined, but significantly Tylecote points out that the thickness at which the transition occurs is in the order of 10^5Å which he states is "the same order as the 'barrier layer' on copper/copper oxide rectifiers as determined by measurements of electrical capacity; this correspondence appears to support the contention of Campbell and Thomas[119] that the departure from the parabolic relationship at low temperatures is a consequence of the peculiar electrical conditions in these thin films." The maximum thickness of oxide, equal to 10^5Å, for which logarithmic oxidation kinetics apply, corresponds to our maximum thickness of space charge including both the constant density and diffuse space charge layers. Tylecote goes on to say that "the logarithmic curve appears to be in two portions" corresponding, of course, to our described first- and second-stage logarithmic kinetics.

I think it unlikely that any model of thin film oxidation based on movement of atoms or ions through an oxide lattice as the controlling mechanism can hope for much success in describing the facts as we now know them. For example, there is a marked effect of Curie temperature, crystal face and lattice type on the thin film oxidation rate. In general, any of these factors within the metal would not be expected to have an effect on rate of migration of species such as ions or vacancies in the oxide phase. For this reason, I believe that the work function of the metal which is affected by Curie temperature, crystal face and lattice type, plus a growing space charge in the thickening oxide (confirmed by Volta potential measurements) enter as the more important determining factors accounting for observed logarithmic oxidation kinetics.

[119] W. Campbell and U. Thomas, *Trans. Electrochem. Soc.*, 91, 623 (1947).

On the Use of Galvanostatic Transients for the Study of Fuel Adsorption on Platinum

M. W. Breiter (pp. 1244-1245, Vol. 112, No. 12)

S. B. Brummer[120]: In a previous paper[121] a novel current-reversal method of estimating fuel adsorption on Pt was described. In this method, which was used both for HCOOH adsorption[121] and CO adsorption,[122] an anodic pulse is applied to strip the adsorbate partially (charge Q). Then a cathodic pulse is applied to determine how much of Q has gone toward electrode oxidation ($Q_{o,cath}$ in Breiter's terminology) and how much has gone toward cleaning the adsorbate off the electrode. The latter is determined as the fraction of the electrode available for H-atom deposition (θ_H). In the paper under discussion, the general point about this method is made that it has rarely been found that $Q_{o,an}$ (charge in oxidizing Pt) is the same as the charge found in reducing the oxide ($Q_{o,cath}$). This point was appreciated in the application of the current-reversal method and was fully discussed both for HCOOH[123] and for CO.[122] In the latter case, $Q_{o,cath}/Q_{o,an}$ $(= \theta_H)$ was found to be unity. This would remove the substance of the objection. For HCOOH, as indicated by Breiter, the extent of electrode oxidation is small until almost all the adsorbate has been oxidized. (However it is not zero; the importance of which will be shown later.)

In the case of other adsorbates, one would certainly have to know the value of θ_o. In this connection, one may note that in two rather careful recent studies by Bold and Breiter[124] and Gilman[125] θ_o has been found to be unity although the reduction of the Pt(O) is rather irreversible.[125] This irreversibility could pose a problem since it might mean that some oxide reduction is pushed into the H-atom deposition region. Since the oxide reduction is much more reversible when electrode oxidation is small, as it is in the application of the current-reversal technique, there is no interference due to oxide reduction in the H-atom deposition region. It is very likely that the reason θ_o is often found as < 1[126,127] is due to the presence of impurities in the solution. These impurities would adsorb on the Pt and their oxidation during the anodic pulse makes

[120] Tyco Laboratories, Incorporated, Bear Hill, Waltham, Massachusetts.

[121] S. B. Brummer, *J. Phys. Chem.*, 69, 562 (1965).

[122] S. B. Brummer and J. I. Ford, *J. Phys. Chem.*, 69, 1355 (1965).

[123] Tech. memo. no. 13 on Contract Nonr-3765(00), Aug. 1964.

[124] W. Bold and M. Breiter, *Electrochim. Acta*, 5, 145 (1961).

[125] S. Gilman, *Electrochim. Acta*, 9, 1025 (1964).

[126] K. J. Vetter and D. Berndt, *Z. Electrochem.*, 62, 378 (1958).

[127] S. W. Feldberg, C. G. Enke, and C. E. Bricker, *This Journal*, 110, 826 (1963).

an additional contribution to $Q_{o,an}$. If this were so, θ_o would always be unity when a strongly adsorbing fuel is available to adsorb on the electrode since this would prevent the adsorption of the impurities. This was found for CO adsorption.[122]

The paper also makes a number of specific points about the comparison between earlier results for HCOOH adsorption[128] and those obtained with the current-reversal method. It was reported[128] that θ_H decreases linearly with increase of θ_F during adsorption of HCOOH up to about 0.5 in θ_F (θ_F = $HCOOH_{ads}$ coverage/maximum $HCOOH_{ads}$ coverage). Thereafter, a curvature convex to the θ_F axis (curve b of Fig. 1) was found. Using the current-reversal method, θ_H and θ_F were found to be completely linear (curve a of Fig. 1). Breiter claims that there is in fact curvature at high θ_H in Fig. 5 and 6 of ref. (121). This is most evident he says in Fig. 6. No curvature, within the significance of the data, is evident to me in Fig. 5 of ref. (121). In Fig. 6, it should be noted that the data is uncorrected for electrode oxidation and for oxidation of material in the solution during the anodic transient. Both of these are discussed in ref. (121) (p. 569). The former is the more important in this case, and the dotted region of curve a at high θ_H in Fig. 1 is just the region when electrode oxidation is not zero. When this correction is made, the points at high θ_H of Fig. 6 of ref. (121) fall right on the line and θ_H is completely linear in θ_F over the whole range of coverage. There is another important point in this connection. Breiter appears to assume that curvature at high θ_H in Fig. 5 and 6 of ref. (121) would improve the agreement between curves a and b of Fig. 1. This is not so. If this curvature were real, it would lead to curve c in Fig. 1. This is concave to the θ_F axis and curved at the low θ_F end.

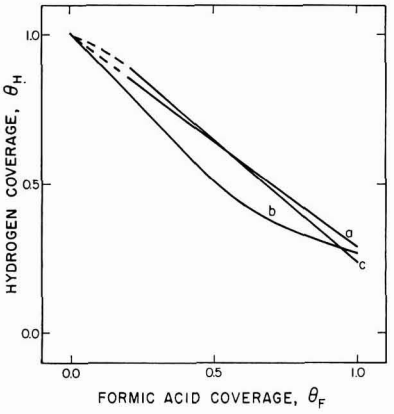

Fig. 1. Curve a, based on data of ref. (121) such that Q_{HCOOH}^{max} = 285 μcoul/real cm^2 and θ_H goes from 1.0 to ~0.28. Dotted region at low θ_H is omitted as described in ref. (121). Curve b, from paper under discussion, based on ref. (128). Curve c, based on ref. (1). Includes curvature suggested in paper under discussion, Q_{HCOOH}^{max} is taken as 356 μcoul/real cm^2.

The paper attempts to show that the estimate of Q_{HCOOH}^{max} in ref. (121) is too low, to improve agreement with data of ref. (128). Actually this would lead to further disagreement since the value of ref. (121) (285 μcoul/210 μcoul of H-atom charge, *i.e.*, per real cm^2) is already higher than that of (128) (260 μcoul/real cm^2). The agreement between these two values determined by two methods (10%) is already excellent considering that the comparison is based on 4 or 3 separate charge determinations, respectively, none of which is better than ± 1-2%.

The disagreement between curves a and b of Fig. 1 could arise as follows: Curve a represents the desorption of material adsorbed at a single potential: the slope gives the number of electrons released per site on oxidation of the adsorbate [~ 2, see ref (121)]. Curve b, on the other hand, represents the relationship between θ_F and θ_H when the HCOOH is adsorbed at various potentials. Specifically, the high θ_F end refers to material adsorbed at the lowest potentials. There is a considerable view growing that $HCOOH_{ads}$ is not HCOOH itself but some other species.[121,129,130,131] If this were so, we might not be surprised to find a more reduced species tending to accumulate on Pt during the last stages of HCOOH adsorption at low potentials. The slope of curve b at low θ_H is about 4 electrons per site, and this may represent evidence that some of the adsorbate at low potentials differs from that at higher potentials.[132]

M. W. Breiter: As stated in my paper, it was not mentioned in the fundamental paper[133] that the applicability of the technique depends upon the fulfillment of the condition $Q_{o,an}/Q_{o,cath}$ = 1. After this requirement was pointed out by me in the oral discussions at the Washington Meeting of the Electrochemical Society, it was dealt with in a subsequent paper[134] sent in for publication after the meeting. Reference (123) in Brummer's comments is not a publication. It is not clear why the above condition which represents a restriction of the technique was not discussed in the first paper[133] if it was known to its author. In the absence of fuel, the experimental result $Q_{o,an}/Q_{o,cath} \geq 1$ is due to a superposition of several effects: oxidation of adsorbed organic impurities, diffusion of oxygen atoms into the platinum, and O_2 evolution. It is not possible at present to separate the contributions of these processes.

With respect to the shape of the curves a and b in Fig. 1 of my paper, it should be pointed out that a straight curve implies that all the sites used for adsorption of H atoms are also used for the adsorption of HCOOH molecules or intermediates (COOH for instance). This assumption is not very likely. The specific points raised in Brummer's comments involve small corrections and extrapolations. The validity of the arguments falls in the realm of subjective judgment. The question of the nature of the adsorbed species has not been settled.

[128] M. W. Breiter, *Electrochim. Acta*, **8**, 447 (1963).

[129] S. B. Brummer and A. C. Makrides, *J. Phys. Chem.*, **68**, 1448 (1964).

[130] J. Giner, *Electrochim. Acta*, **8**, 857 (1963).

[131] J. Giner, *Electrochim. Acta*, **9**, 63 (1964).

[132] Data presented for adsorption of HCOOH at 0.2v [M. W. Breiter, Electrochim. Acta, **10**, 503 (1965)] show a higher value for Q_{HCOOH} than that found in ref. (128). This may also be evidence for this point.

[133] S. B. Brummer, *J. Phys. Chem.*, **69**, 562 (1965).

[134] S. B. Brummer and J. I. Ford, *J. Phys. Chem.*, **69**, 1355 (1965).

Electrochemical
NEWS
June
1966

• Section News •

Boston Section

The fifty-fourth meeting of the Boston Section was held at the Ashdown House, M.I.T., Cambridge, Mass., on March 22, 1966. The meeting was preceded by an informal social hour and a dinner. Dr. Jose D. Giner, Tyco Laboratories, Inc., Waltham, Mass., presented an excellent talk on "Fuel Cells and Electrocatalysis." Dr. Giner explained that in the last few years, fuel cells have been developed to the point where they can now be regarded as practical electrical power supplies for space and military applications as demonstrated by recent Gemini flights. The first limited commercial applications are expected in the near future. The present status of fuel cell technology was reviewed with special emphasis on the electrocatalysis research necessary to keep up with the engineering development. Criteria for the study and selection of electrocatalysis were discussed and results obtained from the study of oxygen electrodes were reported.

Mario D. Banus,
Secretary

Chicago Section

On April 14, 1966 the Chicago Section held a meeting at the Chicago Engineers Club. Guest speaker for the meeting was Dr. Rudolf E. Thun, Manager of Components Development at the IBM Electronics Systems Center, Owego, N. Y., who spoke on "Recent Developments in Integrated Circuit Technology." Dr. Thun presented a comparison of various microelectronic technologies emphasizing the differences in packing densities and component characteristics achievable with thick films, thin films and monolithic circuits. This was followed by a description of the modern planar fabrication process for silicon monolithic circuits. After a discussion of present development trends and problem areas, a few examples of typical monolithic circuits were described. Finally, he suggested likely future developments in the monolithic circuit field.

R. H. Hausler,
Secretary

National Capitol Section

The following officers were elected to serve for the 1966-1967 season:

Chairman—Frederic Bowers, U.S. Naval Ordnance Laboratory, White Oak, Md.

1st Vice-Chairman—Galen R. Frysinger, Electric Power Branch, Electrical Dept., U.S. Army Research and Development Laboratories, Ft. Belvoir, Va.

2nd Vice-Chairman—Kurt H. Stern, National Bureau of Standards, Washington, D. C.

Secretary—Robert T. Foley, Department of Chemistry, American University, Washington, D. C.

Treasurer—Clarence M. Shepherd, U.S. Naval Research Laboratory, Washington, D. C.

Councilors—Fielding Ogburn, Metallurgy Division, National Bureau of Standards, Washington, D. C., and Gwendolyn Wood, National Bureau of Standards, Washington, D. C.

Charles B. Kenahan,
Chairman

Ontario-Quebec Section

On March 18 a joint meeting of the Ontario-Quebec Section of the Society and the Toronto Section of the National Association of Corrosion Engineers was held at the Skyline Hotel in Toronto. Fifty-three people attended the meeting.

Abstracts of the five papers presented are given below.

The Purpose, Planning and Interpretation of Laboratory Tests

H. R. Copson, International Nickel Co., Suffern, N. Y.

Emphasis is placed on defining the objective of corrosion tests and in reproducing the form of corrosion of interest. Examples are given of tests in natural environment, such as atmosphere and sea water, and also laboratory environments. The purpose of these tests may be to choose the best existing materials, or to develop information on control of the environment. All special tests are discussed and conclusions drawn.

Accelerated Tests as a Means of Predicting Service Corrosion

F. G. Bush, Ford Motor Co., Detroit, Mich.

In a program involving more than 50,000 test specimens and approximately 2,000 variables, Ford Motor Co. compared various laboratory tests with service corrosion. No test has been found which can accurately predict the influence of material and process variations on the order of merit determined by actual service exposer.

Corrosion Testing of Water Cooled Nuclear Reactions

J. E. LeSurf, Atomic Energy of Canada, Chalk River, Ont., Canada

Nuclear reactors require materials which minimize neutron losses and the spread of activity outside the core. The paper describes some of the corrosion tests used to select materials for both the core region and heat transport circuits of water-cooled reactors. Quality control tests are also described and related to experience in operating reactors.

Corrosion Testing Experiments Under Operating Conditions

J. Greenblatt, Naval Research Establishment, Halifax, Canada

There are a number of factors that degrade laboratory performance of materials in actual operating situations. Field tests do not always sort out these factors properly with the result that in many cases as much time and effort can be spent in trying to achieve the optimum results of the laboratory as went into the original research. Examples are given of such experiences and some of the problems of running controlled experiments under actual operating conditions are described. Experience has shown that approximate simple criteria which show trends coupled with protective measures designed to cure symptomatically provide the best approach to corrosion control in many cases.

Some Corrosion Problems in an Electric Utility

R. C. Jacobsen, Hydro Electric Power Commission of Ontario, Toronto, Canada

The paper discusses work, largely on testing but some on development, carried on by the Ontario Hydro in combatting corrosion of underground cables, pipes and tower footings, of hot water tanks, and of structures both underwater and exposed to atmospheric attack. The usual tools of cathodic protection, wrapping, and coatings are used and it is the latter field with which most laboratory tests are concerned.

C. B. Camplong,
Secretary-Treasurer

Pacific Northwest Section

As a result of the recent election, the following officers for 1966 are:

Chairman—Dr. R. E. Meredith, Department of Chemical Engineering, Oregon State University, Corvallis, Ore. 97331

Vice-Chairman—C. M. Botchek, 15603 Ambaum Rd. S.W. #12, Seattle, Wash. 98166

Secretary-Treasurer—Dr. J. R. Divine, 1704 K Building, Battelle-Northwest, P. O. Box 999, Richland Wash. 99352

Councilor—Dr. T. R. Beck, 10035 31 Ave., N.E., Seattle, Wash. 98125

A. L. Crittenden
Secretary-Treasurer

Pittsburgh Section

The Pittsburgh Section of the Society held a joint meeting with the Pittsburgh Branch of the American Electroplaters' Society on April 13 at the Hotel Webster Hall in Pittsburgh. Guest speaker for the meeting was Dr. Harold J. Read, Professor of Metallurgy, Pennsylvania State University and 1st Vice-President of the Society, who spoke on Metallurgy and the Electroplater.

Dr. Read stated that although electroplating is still to some extent a black art, much progress has been made in the last two decades in transforming it to an engineering process susceptible of scientific control. A part of this development has been an increasing awareness that the metallurgical properties of the deposit are much affected by the kind of solution employed and the operating conditions during deposition. Both structure and properties are involved and they form the principal subject matter of the talk.

Thomas J. Butler,
Secretary-Treasurer

1967 Palladium Medal Award, ECS

The eighth Palladium Medal of The Electrochemical Society will be awarded at the Fall Meeting of the Society to be held in Chicago, Ill., October 8-13, 1967. The medal was established in 1951 by the Corrosion Division.

The candidate shall be distinguished for his original contributions to theoretical electrochemistry or to fundamental scientific knowledge of corrosion processes. He need not be a member of the Society. There shall be no restrictions or reservations made regarding his citizenship, age, or sex.

To be eligible, the candidate shall agree to receive the award in person at the designated national meeting of the Society. He shall also agree to present a general lecture before the Society, at the above designated national meeting, to be called the Palladium Medal Address. This address will in general describe some area of the candidate's researches, and will be presented at a time and place during the meeting to be specified in each instance by the Board of Directors.

Previous medalists have been: Carl Wagner, Max Planck Institut fur Physikalische Chemie; N. H. Furman, Princeton University; U. R. Evans, Cambridge University; K. F. Bonhoeffer, Max Planck Institut fur Physikalische Chemie (posthumous award); A. N. Frumkin, Electrochemical Institute of the USSR; H. H. Uhlig, Massachusetts Institute of Technology; and Norman Hackerman, University of Texas.

Sections, Divisions, and members of the Society are invited to send suggestions for candidates, accompanied by supporting information, to Mr. Ernest G. Enck, Executive Secretary, The Electrochemical Society, 30 East 42 St., New York, N. Y. 10017, for forwarding to the Committee Chairman. Deadline for submission of suggestions is December 31, 1966.

People

Donald M. Alstadt has been elected executive vice-president, a newly created post, of Lord Corp., Erie, Pa. As a scientist, Mr. Alstadt forsaw that a strong commitment to basic research was a key to future growth. He was instrumental in the establishment of a Central Research activity at Lord. His personal contribution in basic research resulted in the development of a totally new kind of rubber-metal adhesive that is now widely used.

Robert J. Cox has been appointed manager of Metallurgical Fluorspar Sales of Pennsalt Chemicals Corp., Philadelphia, Pa. Prior to his new appointment he had been assistant to the general manager of the Industrial Chemicals Division-East. Mr. Cox joined Pennsalt in 1949 as a production supervisor at the Calvert City Works in Kentucky. From 1950 until 1965 he was manager of production at Pennsalt's Wyandotte Works in Wyandotte, Mich.

Walter J. Hamer, chief of the Electrochemistry Section of the National Bureau of Standards, received the honorary degree of Doctor of Science from Juniata College at the Dedication Ceremonies of its new $2,750,000 Science Center on April 16, in Huntingdon, Pa. Dr. Hamer, an alumnus of the College, was cited for his creativity in research and administrative leadership.

Dr. Hamer has been chief of the Electrochemistry Section at NBS since 1950. He received his Ph.D. from Yale in 1932, served as research associate at M.I.T. in 1934-35, and has done research on electrolytes, hydrogen-ion concentration, counter-current electrolysis, lead-acid storage batteries, dry cells, thermal cells, standard cells, fused salts, and with his associates has redetermined the value of the faraday directly in terms of the national standards of electromotive force, resistance, and frequency. He received a Superior Accomplishments Award from the U.S. Department of Commerce in 1954 and the Gold Medal Exceptional Service Award for Distinguished Achievement in the Federal Service in 1965.

He is Editor of the Society's monograph on "The Structure of Electrolytic Solutions," a member of the Advisory Board of a number of books on electrochemistry, and was President of The Electrochemical Society during 1963-64.

Frank X. McGarvey has recently been appointed research director of the Barnstead Still & Sterilizer Co., Boston, Mass. Prior to joining Barnstead, Mr. McGarvey was associated with Rohm & Haas where he served 20 years in the field of ion-exchange technology. His ion-exchange experience extended to the recovery of uranium and rare metals from earth, sugar refining; water purification; and pioneer work in pharmaceutical manufacturing. In addition he has held positions in export operations and in the field of paper industry chemicals.

Erwin A. Schumacher, group leader, Electrodes and Cells, has retired from the Research Laboratory, Consumer Products Division on April 30, 1966 culminating a distinguished career of 42 years with the Research and Development Laboratories of Union Carbide Corp. Except for the period 1955-62 during which he was assistant manager for Special Projects of the Electrochemical Development Laboratory, his entire career was in research.

Mr. Schumacher joined the corporation at its Central Research on Long Island shortly after graduation from Brooklyn Polytechnic Institute in 1924. He moved to Cleveland with the National Carbon Division in 1925. His research activities have been largely in the electrochemistry of gas electrodes including early work and continuing contributions to oxygen depolarized electrode theory and practice in "Air Cells," the Sodium Amalgam Battery, and fuel cells. Much of his research was in close association with G. W. Heise with whom he did the first "Air Cell" work, and he undertook in the early thirties the first fuel cell work utilizing (low-temperature) oxygen-depolarized carbon electrodes. Other projects include railway signal cells, chlorine depolarized batteries, electrolytic iron, catalytic carbon, and alkaline MnO_2-zinc batteries. More recently he has been responsible for exploratory work on new systems including organic depolarizers and the use of electrochem-

ical cells to measure and control oxygen content in closed systems.

Mr. Schumacher's work led to a number of publications in electrochemical fields and to 36 patents in battery technology and related areas.

He has been an active member of The Electrochemical Society, Cleveland Section, for thirty years, and received in recognition of his contributions to the Section, its George W. Heise award presented in 1963. He is a charter member of the Battery Division of the Society, and has served on the Constitution and Executive Committees, and as Membership Chairman for this division. He is the author of the section on Alkaline Cells in the forthcoming book on Primary Batteries sponsored by the Battery Division.

C. Dean Starr, technical director, Wilbur B. Driver Co., will be presented with the Sam Tour Award by the American Society for Testing and Materials at the Awards luncheon, June 29, during ASTM's 69th annual meeting at Chalfonte-Haddon Hall, Atlantic City. The award is presented to the author of a technical paper, published by the Society, of outstanding merit on research on the improvements and evaluation of corrosion testing methods. Dr. Starr's award-winning paper "Methods of Testing Nickel-Chromium Alloys Used for Heating Elements," was published in the 1964 ASTM "Proceedings."

New Members

It is a pleasure to announce the following new members to The Electrochemical Society as recommended by the Admissions Committee and approved by the Board of Directors for March 1966.

Active Members

Berry, R. M., Dallas, Texas
Coulthard, J. J., Peabody, Mass.
Darnell, James R., Dallas, Texas
Dyer, L. D., Richardson, Texas
Goldner, R. B., Lexington, Mass.
Leatherman, Allen, Columbus, Ohio
Litchtenberg, L. R., Bloomington, Ill.
Newman, Gordon, Bay Shore, N. Y.
Pearl, I. A., Appleton, Wis.
Ruggiero, E. M., Dallas, Texas
Snow, G. A., Urbana, Ill.
Swette, L. L., Lexington, Mass.
Tillis, W. J., King of Prussia, Pa.

Student Associate Members

Ieumwananonthachai, Ieum, Ann Arbor, Mich.
Kostiner, Edward, Brooklyn, N. Y.
Parkash Mukheja, Om, Kingston, Ont., Canada

Reinstatement to Active Membership

Esbitt, A. S., New York, N. Y.

Transfer to Active Membership

Leonard, R. B., Kokomo, Ind.

New Book in ECS Series

The Electrochemical Society announces the availability of a new book in the ECS Series.

The Electron Microprobe, Edited by T. D. McKinley, K. F. J. Heinrich, and D. B. Wittry, [Published by John Wiley & Sons, Inc., New York, March 8, 1966. 1035 pages; $27.50.]

The latest addition to the ESC Series contains the proceedings of the Symposium sponsored by the Electrothermics and Metallurgy Division of the Society, held in Washington, D. C., October 1964.

The book presents the proceedings of the first national symposium dedicated exclusively to this field and contains contributions from the most prominent investigators in the Western world. It is a comprehensive survey of recent developments in electron probe theory, instrumentation, techniques, and applications. The book represents the largest collection of papers and the most comprehensive treatise on the electron microprobe to be included in any single volume. All the material is new and has not been previously published. Both theory and applications are covered and controversial matters are considered from many points of view.

Among the contents are recently developed techniques for soft x-ray detection. Several new contributions to quantitative analysis are included. Of major importance are detailed new tables for use in corrections for mass adsorption and fluorescence. They will permit fast and simple performance of the most important corrections to be applied in quantitative electron probe microanalysis. In particular, the Heinrich tables probably provide the most reliable data on mass adsorption coefficients to be found anywhere. Every laboratory engaged in electron microprobe work will find the book indispensable because these tables will be used virtually every time it is necessary to obtain quantitative results or interpret raw data.

News Items

AIME Has New Secretary

Jack V. Richard has been named secretary of The Metallurgical Society of AIME, replacing Robert W. Shearman, who left AIME after 11 years of service to become administrative secretary of the American Society of Quality Control in Milwaukee.

Mr. Richard, at the time of his appointment, was serving as meetings manager of the American Society of Metals.

Societies Plan Joint Meeting

The Optical Society of America will hold its 51st annual meeting October 17-19, and the Northern California Society for Spectroscopy and the American Chemical Society will hold their Western Regional Meetings October 19-21. The joint meeting (and equipment exhibit) will be held at the Jack Tar Hotel in San Francisco. Programs may be obtained by writing to Mr. John B. Mooney, Publicity Chairman, Varian Associates, 611 Hansen Way, Box K-217, Palo Alto, Calif.

ECS of India

The ECS of India was formed in March 1963 in place of the India Section of The Electrochemical Society, Inc., 30 East 42 St., New York, N. Y., as a professional body of scientists, technologists, and engineers interested in the field of electrochemistry, electrometallurgy, and allied fields.

The Journal of the ECS of India was started in January 1964, in continuation of the Bulletin of the India Section. Enquiries concerning membership should be addressed to Dr. S. Krishnamurthy, Secretary-Treasurer, The Electrochemical Society of India, Dept. of Inorganic and Physical Chemistry, India Institute of Science, Bangalore-12, India.

Book Review

"An Introduction to Fuel Cells," Edited by Keith R. Williams. Published by Elsevier Publishing Co., New York, 1966. 329 pages; $15.00.

This book succeeds admirably in its stated aim of introducing the uninitiated to fuel cells. Beginning with a brief historical survey of fuel cell concepts, each succeeding chapter leads us, progressively, towards a consideration of the current state of the art. Besides having gained insight into a technically sophisticated field, the reader has followed the step-wise development of a concept through the research stages and into the present systems engineering phase. This, in itself is an interesting experience and even the fuel cell expect will enjoy it and perhaps learn something new.

Following a chapter on the historical background of fuel cells and one on the concepts of electrode potentials and conversion efficiency are two chapters on kinetic effects, including a description of some current experimental techniques. The next five chapters describe, respectively, the H_2-O_2 cells; the methanol, hydrazine, and ammonia cells; molten carbonate cells; solid oxide cells, and finally hydrocarbon fuel cells. Somewhat more speculative fuel cell systems such as bio-

logical, regenerative, and amalgam cells are treated briefly in one chapter. A brief chapter outlines battery engineering fundamentals and a final summary chapter deals with the current status of fuel cell development and speculates on the probable development and applications.

Editor Keith R. Williams has done a commendable job in his choice of material and in contributors to this fine book. The style of each chapter is uniformly good, with many references for anyone wishing to delve deeper into any particular area. Printing and figures are attractive.

Ralf Koslow
Lessona Moos Labs

Letter to the Editor

The Discovery of Electroluminescence in Silicon Carbide

In the literature, the writer[1] and other workers[2] have repeatedly stated that electroluminescence in silicon carbide was first observed in Russia in 1923 by Lossew[3].

Recently, Mr. A. R. Peaker of the Manchester College of Science and Technology in England was kind enough to send me a photocopy of a letter from Mr. H. J. Round,[4] of New York City, to the Editor of "Electrical World" in 1907. This is reprinted below in its entirety.

"A Note on Carborundum

Sirs: During an investigation of the unsymmetrical passage of current through a contact of Carborundum and other substances a curious phenomenon was noted. On applying a potential of 10v between two points on a crystal of Carborundum, the crystal gave out a yellowish light. Only one or two specimens could be found which gave a bright glow on such a low voltage, but with 110v a large number could be found to glow. In some crystals only edges gave the light and others gave instead of a yellowish light green, orange, or blue. In all cases tested the glow appears to come from the negative pole, a bright blue-green spark appearing at the positive pole. In a single crystal, if contact is made near the center with the negative pole, and the positive pole is put in contact at any other place, only one section of the crystal will glow and that the same section whenever the positive pole is placed.

"There seems to be some connection between the above effect and the emf produced by a junction of Carborundum and another conductor when heated by a direct or alternating current; but the connection may only be secondary as an obvious explanation of the emf effect is the thermoelectric one. The writer would be glad of references to

any published account of an investigation of this or any allied phenomena.

New York, New York H. J. Round"

These observations clearly refer to electroluminescence in silicon carbide and are at the moment the earliest known reference to such an effect. The work of Round in this area predates that of Lossew by 16 years.

Henry F. Ivey
Westinghouse Research Labs.
Pittsburgh, Pa.

References

[1] G. Destriau and H. F. Ivey, Proc. IRE, 43, 1911 (1955); H. F. Ivey, This Journal, 104, 740 (1957); H. F. Ivey, "Electroluminescence and Related Effects" (Academic Press, New York, 1963).

[2] H. K. Henisch, "Electroluminescence" (Pergamon/Macmillan, New York, 1962); and also articles by A. G. Fischer, R. E. Shrader, and S. Larach (p. 1) and E. E. Loebner (p. 276) in "Photoelectronic Materials and Devices" (S. Larach, Ed.) (Van Nostrand, New York, 1965).

[3] O. W. Lossew, Telegrafia i Telefonia No. 18, p. 61 (1923); Wireless World, 15, 93 (1924); Phil. Mag. 6, 1024 (1928).

[4] H. J. Round, Elec. World, 49, No. 6, p. 308 (1907).

New Books

"Tables of Laplace Transforms," G. E. Roberts and H. Kaufman. Published by W. B. Saunders Co., Philadelphia, 1966. 367 pages; $6.75.

An up-to-date listing of approximately 3100 transform pairs. Separate tables are presented for locating direct and inverse transforms which are indexed for quick use.

"Advances in Chromatography," Vol. 1, Edited by J. C. Giddings and R. A. Keller. Published by Marcel Dekker, Inc., New York, 1966. 329 pages; $14.50.

This is volume 1 of a series covering selected topics in chromatography. The most interesting feature of this projected series is the editors' statement ". . . we have encouraged controversy . . ." in order to stimulate research and discussion. The only question that comes to mind is who is going to be the impartial mediator.

Advertiser's Index

The Electrochemical Society

INSTRUCTIONS TO AUTHORS OF PAPERS

(Revised as of 5/1/65)

Address all correspondence to the Editor, JOURNAL OF THE ELECTROCHEMICAL SOCIETY, 30 East 42 St., New York, N. Y., 10017

GENERAL

Manuscripts must be submitted in triplicate to expedite review. They should be typewritten, double-spaced, with 2½-4 cm margins.

Title should be brief, followed by the author's name and professional connection. Authors should be as brief as is consistent with clarity and should omit introductory or explanatory material which may be regarded as familiar to specialists in the particular field. Proprietary and trade names should be avoided if possible; if used, they should be capitalized to protect the owners' rights.

Authors are encouraged to suggest qualified reviewers for their manuscripts, the Editor reserving the right of final choice. It is very helpful if the author tells which ECS *Division* would be most interested in his paper.

TYPES OF ARTICLES

Technical Articles must describe original research of basic nature and must have adequate scientific depth. Articles of wide diversity of interest are acceptable, but subjects primarily covered in other specialized journals (*e.g.*, analytical or nuclear chemistry) are not considered appropriate. An ***Abstract*** of about 100 words should state the scope of the paper and summarize its results. Suitable headings and subheadings should be included, but sections should not be numbered. Articles in recent issues of the JOURNAL should be consulted for current style.

Technical Notes are used for reporting briefer research, developmental work, process technology; new or improved devices, materials, techniques, or processes which do not involve more extensive basic scientific study. No abstract is required.

Brief Communications are used only to report new information of scientific or technological importance which warrants rapid dissemination.

ILLUSTRATIONS

Drawings and ***Graphs*** ordinarily will be reduced to column width, 8.3 cm, and after such reduction should have lettering no less than 0.15 cm high. Lettering must be of letter-guide quality. India ink on tracing cloth or paper is preferred, but India ink on coordinate paper with blue ruling is acceptable. The sample graph shown on the reverse page conforms to suggestions of the American Standards Association (ASA Report Y15.1-1959).

Photographs should be used sparingly, must be glossy prints, and should be mailed with protection against folding. ***Micrographs*** should have a labeled length unit drawn or pasted on the picture. ***Captions*** for figures (including photographs) must be included on a separate sheet. Captions and figure numbers must *not* appear in the body of the figure; they will be removed if they do. ***Numerical Data*** should not be duplicated in tables and figures.

EQUATIONS

Mathematical Equations should be written on a single line if possible, and parentheses, brackets, the solidus (/), negative exponents, etc., may be used freely for this purpose. Authors are urged to consult Chapter VI of the "Style Manual" of the American Institute of Physics (available for $1.00 at American Institute of Physics, 57 East 55 St., New York, N. Y., 10022) and to follow the patterns described there.

SYMBOLS

If more than a few ***Symbols*** are used, they should be defined in a list at the end of the paper, with units given. For example:

$a, b \ldots =$ empirical constants of Brown equation

$f_i^\circ =$ fugacity of pure ith component, atm

$D_v =$ volume diffusion coefficient, cm²/sec

ABBREVIATIONS UNITS

The AIP "Style Manual" referred to here gives a suitable list of common ***Abbreviations.*** Units usually will be abbreviated without periods throughout the text, as sec, min, hr, cm, mm, etc. **Metric Units** should be used throughout, unless English units are clearly more appropriate in the area of discussion.

POTENTIAL SIGNS

Electrode Potentials: Authors are urged to state and make use of the polarity of test electrodes with respect to the reference electrode used, *i.e.,* Zn is normally negative, Cu normally positive with respect to the standard hydrogen electrode. The sign for the emf of a cell should conform to the free energy change of the chemical reaction as written or implied, in accordance with the definition $\Delta G = -nFE$. These suggestions agree with the IUPAC conventions adopted in 1953.

REFERENCES

Literature References should be listed on a separate sheet at the end of the paper in the order in which they are cited in the text. Authors' initials must be given, and the style and abbreviations adopted by *Chemical Abstracts* should be used. Any recent issue of the JOURNAL may be consulted.

PUBLICATION CHARGE

A charge of $35* per printed page is made for publication of technical material in THIS JOURNAL. A 10% reduction is allowed if at least one author of an article is an ECS member or an employee of a Patron or Sustaining Member firm. However, acceptance of a manuscript is in no way dependent on such payment, and the charge may be waived in individual cases.

* See Editorial page 135C, June 1966 JOURNAL.

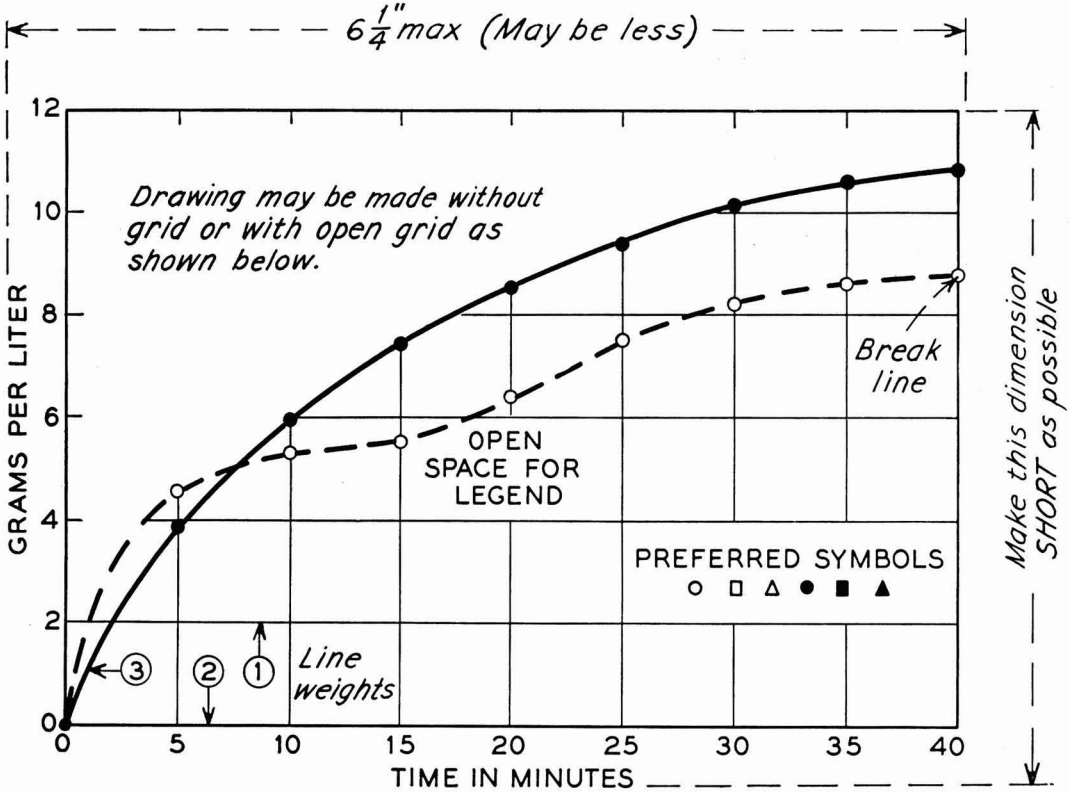

Remarks: Line weight 2 is used for borders and zero lines. When several curves are shown, each may be numbered and described in the caption. Lettering shown is approximately ⅛ in. In plotting current or potential as ordinate, increasing negative values should go down.

SAMPLE CURVE DRAWING FOR REDUCTION TO ½ SIZE

Patron and Sustaining Members of THE ELECTROCHEMICAL SOCIETY

Patron Members

Aluminum Co. of Canada, Ltd., Montreal, Que., Canada

Dow Chemical Co.
Chemicals Dept., Midland, Mich.
Metals Dept., Midland, Mich.

International Nickel Co., Inc., New York, N. Y.

General Electric Co.
Capacitor Dept., Hudson Falls, N. Y.
Chemical Laboratory, Knolls Atomic Power Laboratory, Schenectady, N. Y.
Chemical Systems and Processes Laboratory, Research and Development Center, Schenectady, N. Y. (3 memberships)
Direct Energy Conversion Operation, West Lynn, Mass
Lamp Division, Cleveland, Ohio
Materials & Processes Laboratory, Large Steam Turbine-Generator Dept., Schenectady, N. Y.

Olin Mathieson Chemical Corp.
Chemicals Division, Research Dept., New Haven, Conn.

Union Carbide Corp.
Divisions:
Carbon Products Division, New York, N. Y
Consumer Products Division, New York, N. Y.

Westinghouse Electric Corp.
Electronic Tube Division, Elmira, N. Y.
Lamp Division, Bloomfield, N. J.
Molecular Electronics Division, Elkridge, Md.
Semiconductor Division, Youngwood, Pa.
Research Laboratories, Pittsburgh, Pa.

Sustaining Members

Air Reduction Co., Inc., New York, N. Y.

Allen-Bradley Co., Milwaukee, Wis.

Allied Chemical Corp.
General Chemical Div., Morristown, N. J.

Aluminum Co. of America, New Kensington, Pa.

American Metal Climax, Inc., New York, N. Y.

American Potash & Chemical Corp., Los Angeles, Calif

American Smelting and Refining Co.,
South Plainfield, N. J.

American Zinc Co. of Illinois, East St. Louis, Ill.

American Zinc, Lead & Smelting Co., St. Louis, Mo.

M. Ames Chemical Works, Inc., Glens Falls, N. Y.

Ampex Corp., Redwood City, Calif.

Armco Steel Corp., Middletown, Ohio

Basic Inc., Bettsville, Ohio

Bell Telephone Laboratories, Inc., New York, N. Y. (2 memberships)

Bethlehem Steel Co., Bethlehem, Pa. (2 memberships)

Boeing Co., Seattle, Wash.

Burgess Battery Co., Freeport, Ill. (2 memberships)

Burndy Corp., Norwalk, Conn.

Canadian Industries Ltd., Montreal, Que., Canada

Carborundum Co., Niagara Falls, N. Y.

Chrysler Corp., Detroit, Mich.

Consolidated Mining & Smelting Co. of Canada, Ltd., Trail, B. C., Canada (2 memberships)

Continental Can Co., Inc., Chicago, Ill.

Corning Glass Works, Corning, N. Y.

Diamond Alkali Co., Painesville, Ohio

Wilbur B. Driver Co., Newark, N. J. (2 memberships)

E. I. du Pont de Nemours & Co., Inc., Wilmington, Del

Eagle-Picher Co., Chemical and Metals Div., Joplin, Mo.

Eastman Kodak Co., Rochester, N. Y.

Eltra Corp.
Prestolite Div., Toledo, Ohio
C&D Batteries, Conshohocken, Pa.

Electric Storage Battery Co., Philadelphia, Pa. (2 memberships)

Engelhard Industries, Inc., Newark, N. J.

The Eppley Laboratory, Inc., Newport, R. I

Esso Research and Engineering Co.
Engineering Technology Div., Florham Park, N. J.

Exmet Corp., Bridgeport, Conn.

Fairchild Semiconductor Corp., Palo Alto, Calif.

FMC Corp.
Inorganic Chemical Div., Buffalo, N. Y.
Inorganic Chemicals Div., South Charleston, W. Va.

Foote Mineral Co., Exton, Pa.

Ford Motor Co., Dearborn, Mich.

General Motors Corp.
Allison Div., Indianapolis, Ind.
Delco-Remy Div., Anderson, Ind.
Research Laboratories Div., Warren, Mich.

General Telephone & Electronics Laboratories, Inc., Bayside, N. Y. (2 memberships)

Globe-Union, Inc., Milwaukee, Wis.

Sustaining Members (cont'd)

B. F. Goodrich Chemical Co., Cleveland, Ohio

Gould-National Batteries, Inc., Minneapolis, Minn.

Great Lakes Carbon Corp., New York, N. Y.

Harshaw Chemical Co., Cleveland, Ohio (2 memberships)

Hercules Powder Co., Wilmington, Del.

Hill Cross Co., Inc., West New York, N. J.

Hoffman Electronics Corp., Semiconductor Division, El Monte, Calif.

Honeywell, Inc., Minneapolis, Minn.

Hooker Chemical Corp., Niagara Falls, N. Y. (3 memberships)

HP Associates, Palo Alto, Calif.

Hughes Research Laboratories, Div. of Hughes Aircraft Co., Malibu, Calif.

International Business Machines Corp., New York, N. Y.

International Minerals & Chemical Corp., Skokie, Ill.

International Resistance Co., Philadelphia, Pa.

ITT Federal Laboratories, Div. of International Telephone & Telegraph Corp., Nutley, N. J.

Jones & Laughlin Steel Corp., Pittsburgh, Pa.

K. W. Battery Co., Skokie, Ill.

Kaiser Aluminum & Chemical Corp.
Metals Division Research, Permanente, Calif.
Div. of Metallurgical Research, Spokane, Wash.

Kawecki Chemical Co., Boyertown, Pa.

Kennecott Copper Corp., New York, N. Y.

Leesona Moos Laboratories, Div. of Leesona Corp., Great Neck, N. Y.

Arthur D. Little, Inc., Cambridge, Mass.

Lockheed Aircraft Corp., Missiles & Space Div., Sunnyvale, Calif.

Mallinckrodt Chemical Works, St. Louis, Mo.

Metal Pumping Services, Inc., Cleveland, Ohio

P. R. Mallory & Co., Indianapolis, Ind.

Melpar, Inc., Falls Church, Va.

Miles Chemical Co., Div. of Miles Laboratories, Inc., Elkhart, Ind.

Monsanto Chemical Co., St. Louis, Mo.

M&T Chemicals Inc., Detroit, Mich.

Nalco Chemical Co., Chicago, Ill.

National Cash Register Co., Dayton, Ohio

National Lead Co., New York, N. Y.

National Steel Corp., Weirton, W. Va.

North American Aviation, Inc., El Segundo, Calif.

Northern Electric Co., Montreal, Que., Canada

Norton Co., Worcester, Mass.

Owens-Illinois Glass Co., Toledo, Ohio

Pennsalt Chemicals Corp., Philadelphia, Pa.

Phelps Dodge Refining Corp., Maspeth, N. Y.

Philco Corp., Research Div., Blue Bell, Pa.

Philips Laboratories, Inc., Briarcliff Manor, N. Y.

Pittsburgh Plate Glass Co., Chemical Div., Pittsburgh, Pa.

Potash Co. of America, Carlsbad, N. Mex.

Radio Corp. of America
Electronic Components and Devices, Lancaster, Pa.
RCA Victor Record Div., Indianapolis, Ind.

Republic Foil Inc., Danbury, Conn.

Reynolds Metals Co., Richmond, Va.

Shawinigan Chemicals Ltd., Montreal, Que., Canada

Socony Mobil Oil Co., Inc., Dallas, Texas

Speer Carbon Co.
International Graphite & Electrode Div., St. Marys, Pa.

Sprague Electric Co., North Adams, Mass.

Stackpole Carbon Co., St. Marys, Pa.

The Standard Oil Company of Ohio, Cleveland, Ohio

Stauffer Chemical Co., Dobbs Ferry, N. Y.

Texas Instruments, Inc., Dallas, Texas
Metals and Controls Corp., Attleboro, Mass.

3M Company, St. Paul, Minn.

Titanium Metals Corp. of America, Henderson, Nev.

Tyco Laboratories, Inc., Waltham, Mass.

Udylite Corp., Detroit, Mich. (4 memberships)

United States Borax & Chemical Corp., Los Angeles, Calif.

United States Steel Corp., Pittsburgh, Pa.

Univac, Div. of Sperry Rand Corp., New York, N. Y.

Universal-Cyclops Steel Corp., Bridgeville, Pa.

Upjohn Co., Kalamazoo, Mich.

Varian Associates, Palo Alto, Calif.

Western Electric Co., Inc., Chicago, Ill.

Wyandotte Chemicals Corp., Wyandotte, Mich.

Yardney Electric Corp., New York, N. Y.